WIND AND RAIN INTERACTION IN EROSION

2004

Tropical Resource Management Papers, No. 50 (2004). ISBN 90-6754-843X
ISSN: 0926-9495

Financial support for the organisation of the course titeled: "Wind and Water Erosion: Modelling and Measurements" was obtained from the C.T. de Wit graduate school PE & RC, Wageningen, The Netherlands. Financial support for the printing of this publication was obtained from the Stichting "Fonds Landbouw Export-Bureau 1916/1918", Wageningen, The Netherlands.

WIND AND RAIN INTERACTION IN EROSION

Saskia M. Visser and Wim M. Cornelis (eds.)

Acknowledgements

The idea for organizing a combined wind and water erosion course was born while I visited the Wind Erosion Unit (Manhattan, Kansas) and the National Soil Erosion Laboratory (Purdue, Indiana) as part of my thesis-work. Back in the Netherlands, Ghent University was contacted and preparations started. Thanks to financing of the C.T. de Wit graduate School PE & RC (Wageningen, The Netherlands), the course "Wind and Water Erosion: Modelling ad Measurement" started in September 2003. Young (PhD) researchers with 9 different nationalities came together to discuss and learn more about the interaction between wind and water erosion.

I would like to thank Ghent University and the Erosion and Soil & Water Conservation Group of Wageningen University for hosting the course. Special thanks for their contribution to the course goes to the lectures: Ed Skidmore (WERU, Kansas University), Dennis Flanagan (NSEL, Purdue University), Donald Gabriels (Ghent University), Leo Stroosnijder (ESW, Wageningen University), Gunay Erpul, (Soil Department, University of Ankara), Wim Cornelis (Ghent University), Michel Riksen (ESW, Wageningen University) and Geert Sterk (ESW, Wageningen University).

At the end of the course the idea came up to combine the experiences and ideas of this group of researchers in this special edition of TRMP, for which financing for printing was obtained from the Stichting "Fonds Landbouw Export-Bureau 1916/1918", Wageningen, The Netherlands. Last but not last I want to thank all authors who contributed to this 50th edition of Tropical Resource Mangement Papers.

Saskia Faye-Visser

Table of Contents

Chapter 1

Introduction

L. Stroosnijder & D. Gabriels
[1]Wageningen University, Erosion and Soil & Water Conservation Group, Nieuwe Kanaal 11, 6709 PA Wageningen; Email: Leo.Stroosnijder@wur.nl
[2]Dept. Soil Management and Soil Care, International Centre for Eremology, Ghent University, Coupure links 653, B-9000 Gent, Belgium; Email:Donald.Gabriels@Ugent.be

Introduction

The 'Tropical Resources Management Papers' (TRMP) series is published by Wageningen UR to disseminate the results obtained by past and present researchers and graduate students in Wageningen research projects on managing tropical and subtropical resources. This 50th publication in the TRMP series is special because it brings together wind and water erosion, students and staff from Ghent and Wageningen universities, and American modeling experts from The National Soil Erosion Laboratory (NSEL), Purdue University, Indiana, USA (WEPP; Water Erosion Prediction Project) and the Wind Erosion Unit (WERU) at Manhattan, Kansas, USA (WEPS; Wind Erosion Prediction System).

The classic paradigm is that water and wind erosion have little in common; they occur in different climates at different moments of the year, with water erosion confined to the humid zones during the rainy season and wind erosion to the more arid zones during the dry season. However, at the onset of the rainy season in semi-arid environments, high intensity rainfall is often preceded by strong convective winds and the processes of wind and water erosion occur almost simultaneously at the same location. Further, there is growing evidence of interaction between the two processes. In Australia and the West African Sahel, rivers draining inland towards desert regions bring vast amounts of sediment to semi-arid regions; when dry, these sediments may be vulnerable to wind erosion. In this way, water erosion of soils in the more humid margins of deserts is an important source of sediment for dust storms in semi-arid areas (McTainsh et al., 1992). On a smaller scale, the processes of wind and water erosion control crust formation and the dynamics of the fine particles. Under the influence of water, specific crusts that mitigate wind erosion are formed. Cultivated fields are the source of fine particles that will be eroded by wind and deposited elsewhere, where they result in more crust development and, in turn, in more runoff and erosion. So, the interaction between wind and water erosion plays an important role in fertility management in traditional agrosystems (Rajot and Valentin, 2001; Visser, 2004).

The interaction between wind and water erosion also affects mass transport. Though wind is a factor that has important roles in water erosion processes, very few studies have been done on the effect of wind on raindrops and overflow characteristics (Erpul et al., 2004). In wind-driven rains, the wind velocity and direction are expected to affect not only the energy input of the rains, but also the shallow flow hydraulics, because impacting raindrops induce changes in micro relief. Significant aspects of the erosion processes in situations where wind and rain occur simultaneously are still imperfectly understood. In his wind tunnel study, Cornelis (2002) showed that the particles transported due to wind-driven rain traveled higher and longer than particles saltating in rainless wind.

Despite the many differences in the processes of wind and water erosion, there are also many similarities. Air and water are both fluids and thus air behaves in many ways like water. Sediments are detached by the same lift forces and so both fluids have to overcome the same resistances to stress. Sediment transport, whether by wind or by water, is dependent on the transport capacity of the fluid. When the flow is hindered by obstacles, this capacity decreases and selective deposition will occur: the coarser sediment is deposited first, and the finest sediment last. The similarities between the processes result in commonalities in the models describing the processes of wind and water erosion.

There has been substantial effort in research and development of models of water erosion, and since the 1980s the number of publications on wind erosion has been rising sharply. However, so far the interrelationship between wind and water erosion has not attracted much interest, even though these interactions are an important component of the continuous land degradation in semi-arid environments. Furthermore, despite the clear commonalities, so far there has not been a single model that describes/predicts both the processes of wind and water erosion; neither has there been worldwide collaboration between the experts in the two research fields. To redress this, the idea was born to bring together Ph.D. students interested in the commonalities between wind and water erosion in a 2-week postgraduate course under supervision of the Wageningen 'Production Ecology and Resource Conservation' Graduate School. The long-standing collaboration between the universities of Ghent and Wageningen made it easy to assemble a team of Dutch and Belgian students. The lecturers from Ghent and Wageningen were augmented by lecturers from Purdue and Kansas State universities. One week of the course was in Ghent and one in Wageningen. The students contributed their recent research experience in the form of case studies, and the lecturers contributed results from previous projects. The course was so successful that at its conclusion it was decided to combine all the experience and ideas into this special 50th TRMP publication.

The book starts with a discussion in chapter 2 on the commonalities of WEPP and WEPS, two physically based models on water and wind respectively, developed in the USA. Their applicability outside the USA is discussed in chapter 3 and the possibilities for upscaling field-scale models to the region scale are described in chapter 4. Chapters 5 through 9 highlight the various aspects of the interrelationship between wind and water. How African farmers recognize the presence of wind and water erosion is described in chapter 10. Chapter 11 discusses the various techniques for measuring wind and water erosion separately, and chapter 12 describes the use of a wind tunnel to investigate water and wind interaction. The book concludes with the outlook for future research on wind and water erosion.

Leo Stroosnijder and Donald Gabriels

References

Cornelis, W., 2002. Erosion Processes of dry and wet sediment induced by wind and wind-driven rain: a wind-tunnel study. Doctoral thesis, Applied Biological Sciences, Option Land management and Forestry. Ghent University, Ghent, Belgium.

Erpul, G., Gabriels, D., and Norton, L.D., 2004. Wind effects on sediment transport by raindrop-impacted shallow flow: a wind-tunnel study. Earth Surface Processes and Landforms, 29, 955-967.

McTainsh, G.H., Rose, C.W., Okwach, G.E. and Palis, R.G., 1992. Water and Wind Erosion: Similarities and Differences. In: H. Hurni and K. Tato (ed), *Erosion Conservation and Small-scale Farming.* Walsworth Publ. Co., Marceline, MS. pp: 107-119.

Rajot, J.L. and Valentin, C., 2001. Wind eroded versus deposited mineral dust: a mass budget for a Sahelian village land unit in Niger. In: J.C. Ascough and D.C. Flanagan (ed), *Soil Erosion Research for the 21st Century.* Proceedings of the international Symposium, Honolulu, USA January 3-5, 2001. American Society of Agricultural Engineers (ASAE), USA. pp: 404-407.

Visser, S.M., 2004. Modeling Nutrient Losses by Wind and Water Erosion in northern Burkina Faso. Doctoral thesis, Environmental Sciences, Erosion and Soil & Water Conservation Group. Wageningen-UR, Wageningen, The Netherlands. 169 pp.

Chapter 2

Commonalities in WEPP and WEPS and Efforts Towards a Single Erosion Process Model

D.C. Flanagan[1] & S.M. Visser[2]

[1] Agricultural Engineer & WEPP Leader USDA - Agricultural Research Service & Adjunct Professor, Department of Agricultural & Biological Engineering Purdue University National Soil Erosion Research Laboratory 275 S. Russell Street West Lafayette, Indiana 47907 USA; Email: Flanagan@ecn.purdue.edu

[2]Erosion and Soil & Water Conservation Group, Department of Environmental Sciences, Wageningen University, Nieuwe Kanaal 11, NL-6709 PA Wageningen, the Netherlands; Email: Saskia.Faye-Visser@wur.nl

Commonalities in WEPP and WEPS and Efforts Towards a Single Erosion Process Model

Abstract
Since the late 1980's, the Agricultural Research Service (ARS) of the United States Department of Agriculture (USDA) has been developing process-based erosion models to predict water erosion and wind erosion. During much of that time, the development efforts of the Water Erosion Prediction Project (WEPP) and the Wind Erosion Prediction System (WEPS) were independent of each other. However, many of the same physical processes important in erosion by wind and erosion by water are modeled by WEPS and WEPP in similar ways. This paper discusses the WEPP and WEPS models, their differences and commonalities, and current and future work towards creation of a single process-based erosion model that would allow prediction of erosion by wind and/or water.

Introduction

The Water Erosion Prediction Project (WEPP) was conceived in 1985, and initiated in 1986, as part of efforts to revise and replace the empirical Universal Soil Loss Equation (USLE, Wischmeier and Smith, 1978). While USLE was a very important and practical tool, it lacked the ability to predict sediment deposition, sediment delivery from fields, and temporal and spatial estimates of soil erosion by water. A national Core Team of initially eight scientists was formed in 1985-1986 to develop the various prediction model components as well as conduct necessary laboratory and field experiments to allow for parameterization and database development. A complete and validated WEPP hillslope and watershed model was released in 1995, and updates are made to the model, interfaces and databases on an approximately annual basis via the WEPP web site at the USDA- National Soil Erosion Research Laboratory (NSERL).

The Wind Erosion Prediction System (WEPS) was initiated by ARS in 1987 and was meant to be a replacement for the Wind Erosion Equation (WEQ, Woodruff and Siddoway, 1965). WEPS development has been by a national, multidisciplinary team of scientists from ARS and several other federal agencies. Leadership of WEPS has been through the Wind Erosion Research Unit (WERU) located in Manhattan, Kansas. WEPS version 1.0 is slated for delivery in January 2005 for ultimate implementation in USDA Natural Resources Conservation Service (NRCS) offices.

Water Erosion Prediction Project (WEPP) Model

WEPP is a process-based, distributed parameter, continuous simulation model that predicts erosion by overland water flow, due to rainfall excess, snowmelt, or irrigation. The model can simulate soil detachment by raindrops (interrill erosion) and by flowing water in rills (rill erosion), as well as sediment transport and sediment deposition in rills. Additionally, erosion in larger channels (ephemeral gullies, earthen channels, grass waterways, etc.) can also be modeled. WEPP is meant to be applied to field-sized (similar to USLE) and farm-sized (small watersheds) areas, where the dominant processes are sheet, rill and small channel detachment due to overland flow. Typically size of watershed areas (Figure 1) modeled will be less than 260 ha (Flanagan et al., 1995).

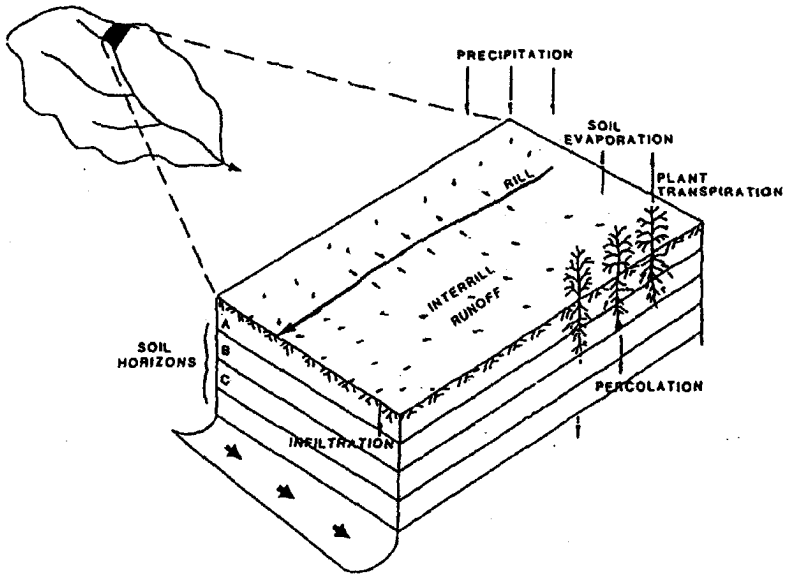

Figure 1. Hydrology processes simulated on a WEPP hillslope profile that may be part of a small watershed, as shown here (after Savabi and Williams, 1995).

Critically important parts of WEPP include the hydrology and water balance components that simulate infiltration, percolation, soil evaporation, plant transpiration, depressional storage and surface runoff. If rainfall (or irrigation or snowmelt) occurs on a day, and then if runoff is predicted, soil loss calculations are subsequently made. The four main parameters that must be calculated in the hydrology component and passed to the erosion component are the duration of rainfall excess, effective rainfall intensity, runoff depth, and peak runoff rate. During a modeled rain storm event, WEPP uses a Green-Ampt Mein-Larson model (Mein and Larson, 1973) modified for unsteady rainfall (Chu, 1978) to determine infiltration depth. Surface depressional storage is modeled as a function of random roughness, which will decrease runoff. Rainfall in excess of infiltration and depressional storage becomes part of cumulative runoff. Peak runoff rate is calculated using a semi-analytical solution (or an approximation) of the kinematic wave model (Stone et al., 1992, 1995). The effective duration of runoff is computed by dividing the total runoff depth by the peak runoff rate, while the duration of rainfall excess is the time period over which rainfall rate exceeds the infiltration rate (and storage capacity is exceeded). In addition to providing the values to estimate event soil loss, any water predicted to infiltrate is used to update the soil moisture content in a continuous simulation.

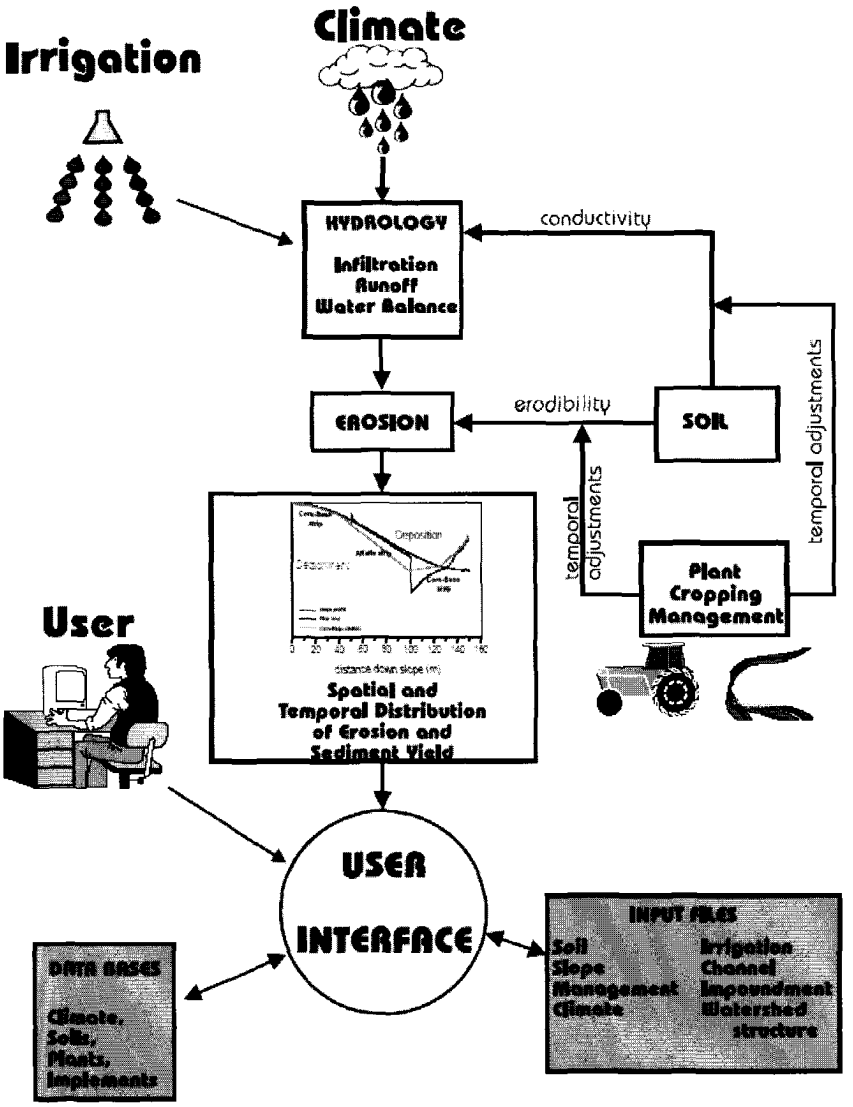

Figure 2. Model flow chart for the WEPP model (from Flanagan et al., 1995).

The erosion component of WEPP uses a steady-state sediment continuity equation, in which the change in sediment load with distance down a slope profile is the sum of the rill detachment (or deposition) rate and the interrill sediment delivery rate (to the rill). Interrill sediment delivery to a rill is a function of rainfall intensity, runoff rate, slope, and adjusted erodibility (Foster et al., 1995). Rill detachment is a function of excess flow shear stress, and is predicted to occur if the sediment load in the flow is below the transport capacity and the shear stress of the flow acting on the soil exceeds the critical shear stress (Nearing et al., 1989). If the sediment load in the flow exceeds the transport capacity, then deposition will be predicted to occur (Foster et al., 1995).

The model tracks the cumulative totals of rainfall, runoff, soil loss and sediment yield, then can provide output reports by individual storm event, by month, by year, or on an average annual basis over the entire simulation period. Net predicted soil loss (detachment) or gain (deposition) is predicted at a minimum of 100 points down a slope profile, and the WEPP model interface programs allow users to easily and rapidly view both the spatial soil loss estimates. Additionally, there are a large number of other outputs available, including a graphical output viewer for examining temporal changes in model outputs or internal variables (e.g. canopy cover) during the simulation period.

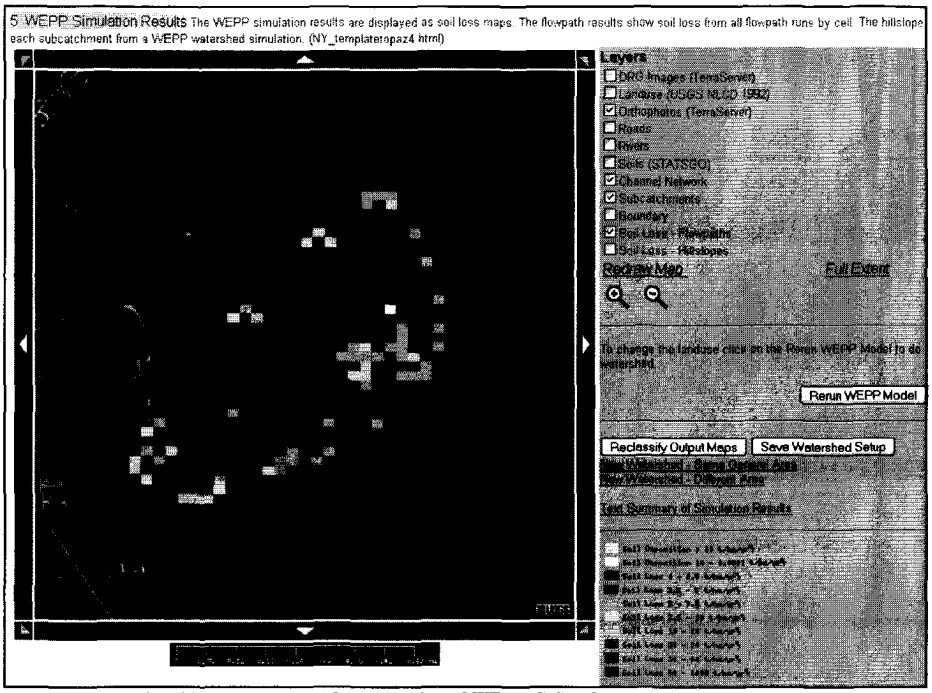

Figure 3. Spatial soil loss estimates with the web-based WEPP GIS software.

In simulations of small watersheds, users can combine multiple hillslopes, channels and impoundments to represent their watershed configuration. The same water balance, plant growth and residue decomposition components as in a hillslope simulation are applied to channel reaches in a watershed. Additional model inputs are needed to provide specific channel and impoundment parameters for a simulation.

In watershed channels, erosion is again modeled utilizing a steady-state sediment continuity equation (Ascough et al., 1997). The change in sediment load with distance down a channel is the sum of the rate of lateral inflow to the channel (from hillslopes) plus the channel detachment or deposition rate. Detachment is again a function of excess flow shear stress. In channel situations, a nonerodible layer can be specified, so if detachment will decrease if the channel incises to that layer.

A variety of graphical user interfaces exist for application of the WEPP model for both hillslope and watershed simulations. A Windows interface is available for download from the WEPP internet site that contains all of the U.S. climate and soils database files, and allows users to access and modify any of the model inputs (http://topsoil.nserl.purdue.edu/nserlweb/weppmain). Prototype web-based interfaces

are also available (http://milford.nserl.purdue.edu) that allow for simple model simulations using existing database values. An ArcView GIS extension called GeoWEPP is also available (Renschler et al., 2002), and current work at the NSERL is focused on completion of a web-based WEPP GIS system (Flanagan et al., 2004), shown in Figure 3.

Wind Erosion Prediction System (WEPS)

The Wind Erosion Prediction System (WEPS) was developed with the intention to replace the empirical Wind Erosion Equation (WEQ) (Woodruff and Siddoway, 1965) with a physically based model. WEPS is a process-based, daily time-step computer model that predicts soil erosion through simulation of the physical processes that control wind erosion (Hagen, 1991), and is intended primarily for soil conservation and environmental planning. WEPS 1.0 is the first implementation of WEPS intended for use by the Natural Resources Conservation Service. The graphical user interface allows the user to easily select climate stations, specify field site dimensions, pick a predominant soil type, and describe any field wind barriers and management practices applied to an agricultural field (Fig. 4). This interface allows the user to quickly assess a site's susceptibility to wind erosion and evaluate the impacts that alternate practices and conditions might have on reducing that susceptibility. Features and capabilities of the WEPS 1.0 user interface include 1) the ability to define wind barrier characteristics and their location on the boundaries of the simulation region, 2) selection of soils obtained from the NRCS National Soil Information System (NASIS) soil database, and 3) detailed specification of actual management practices employed by land managers. Display of output information regarding soil loss by transport mode, direction, and size (saltation/creep, suspension, PM10) is also available.

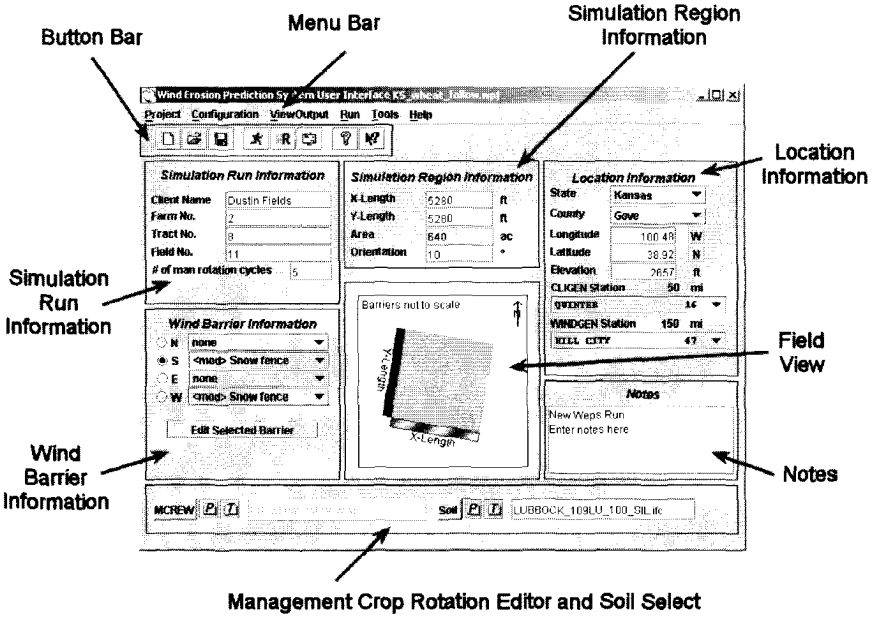

Figure 4. WEPS graphical user interface

The model has a modular structure that includes a daily weather simulator along with an hourly wind speed simulator. Five additional submodels simulate crop growth, residue decomposition, hydrology, soil status and management (Figure 5). All of these submodels provide the required information for the erosion submodel, which determines when friction velocity exceeds the threshold and then simulates soil loss and deposition over the simulation region on a subhourly basis (Hagen et al., 1999). The erosion submodel considers the simulation area to be a rectangular field and composed of one or more subregions with different surface conditions for soil, management or cropping. The simulation region is divided into grid cells and soil loss/deposition is simulated at grid points over the entire area. This allows the users to see spatial variation in erosion/deposition over the simulation area. Though WEPS is designed to predict erosion on larger time-scales, the model calculates on a daily basis, and users can obtain outputs ranging from single storms to multiple years.

Wind erosion is initiated when wind speed exceeds the saltation threshold velocity for a given soil and biomass condition. After initiation, the duration and intensity of the erosion event depends on the wind speed distribution and the evolution of the surface condition. Since WEPS is a continuous model, it does not only simulate the basic wind erosion processes, but the processes that modify the soil's erodibility are simulated as well. So in WEPS the weather changes the temporal properties of the field surface. Hence in wet years e.g. the soil roughness is reduced faster than average and in dry years e.g. the biomass development is reduced.

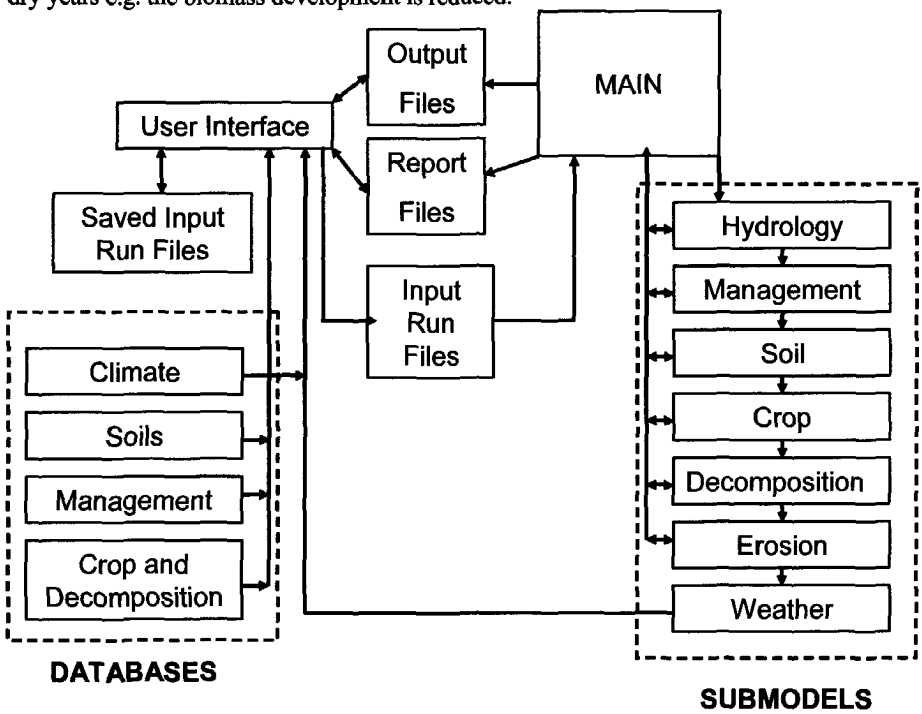

Figure 5. Structure of the WEPS model (after Hagen, 1996)

The modeling techniques that are used to simulate processes in WEPS vary (Hagen, 1996). The WEATHER submodel generates stochastic simulated weather variables. Mechanical and statistical relations are generally used to represent processes in the other sub-models.

The WEPS model is currently being tested and continually being improved with periodic updates. The model can free of charge being downloaded from ftp.weru.edu. Latest documentation and an users manual can be downloaded from: http://www.weru.ksu.edu.

Common processes modeled by WEPP and WEPS

Though different in density and viscosity, wind and water are both fluids and therefore their response to stress is similar in many ways; e.g. when a fluid's velocity is reduced, the transport capacity of the fluid (either wind or water) decreases and selective deposition commences. So, many of the processes that control wind erosion also control water erosion; e.g. soil cover increases the soils resistance to stress and therefore reduces both wind and water detachment. Many processes that are described in WEPP are described in WEPS as well and vice versa. This section gives an overview of the various physical process and submodels that are common in WEPP and WEPS and how simulations are conducted.

Climate

Both WEPP and WEPS require daily climate information for process simulations in their components, and both models make use of the CLIGEN stochastic weather generator (Nicks et al., 1995). CLIGEN was developed for the WEPP type of erosion models (Nicks et al., 1987), and predicts storm depth, duration, peak intensity & time of peak occurrence, air temperatures, solar radiation and wind information. All this generated daily weather data is used as an input to WEPP and WEPS; additionally WEPS uses a simulator called WINDGEN for improved predictions of wind speed and direction.

Hydrology

Both WEPP and WEPS make use of one or more hydrology components. However the purpose of the components in the main models is different. In WEPS, the main purpose of the hydrology component is to obtain a value for the surface soil wetness at the soil atmosphere interface, whereas in WEPP the main purpose of the hydrology component is to provide the erosion component with the duration of rainfall excess, the rainfall intensity during this period of excess, the runoff volume and peak discharge rate. Both models require hydrologic calculations to provide the amount of water available for crop growth and residue decomposition rate computations, and for calculation of the total soil water balance.

The hydrology sub-model of WEPS maintains a continuous, daily soil water balance using eq. 1:

$$SWC = SWCI + (PRCP + DIRG) + SNOW - RUNOFF - ETA - DPRC \qquad [Eq. 1]$$

where SWC is the amount of water in the soil profile on any given day (mm), SWCI is the initial amount of water in the soil profile (mm), PRCP is the amount of daily precipitation (mm), DIRG is the amount of daily irrigation (mm), SNOW is the daily snow melt minus accumulation (mm), RUNOFF is the amount of daily surface runoff (mm), ETA is the amount of daily actual evapotranspiration (mm) and DPRC is the amount of daily deep percolation (Hagen, 1996). WEPP makes use of the same water

balance, but adds two more components: rain interception by vegetation and subsurface lateral flow (Savabi and Williams, 1995).

In WEPS, the infiltration of rain and irrigation water is calculated with the Darcy equation. Water that cannot infiltrate in the soil profile becomes runoff, but the overland flow of water is not simulated. In WEPP, infiltration is simulated using the Green and Ampt infiltration equation and the model uses kinematic wave routing to simulate the overland flow of runoff water. One of the main disadvantages of not routing runoff in WEPS is that no spatial variation in soil wetness due to differences in infiltration related to run on and stagnating water can be predicted. Knowing that the model is highly sensitive to a correct prediction of soil moisture suggests that adding routing of runoff in WEPS might substantially improve predictions.

Both models calculate percolation within the soil profile. In WEPS, the infiltration water is stored in the uppermost simulation layer, until its water content reaches field capacity. Any excess water is then added to the succeeding lower layer, where it is stored with the same maximum storage restriction. Any excess water that flows out from the lowermost simulation layer becomes part of deep percolation, which is estimated to be equal to the conductivity of the lower simulation layer, assuming a unit hydraulic gradient. WEPP also calculates percolation in excess of field capacity, but WEPP additionally simulates subsurface lateral flow and flow to drainage tile and ditches.

Potential evapotranspiration in WEPS is calculated using a revised version of Penman's combination method (Van Bavel, 1966). The total daily rate of potential evapotranspiration is then partitioned on the basis of the plant leaf area index into potential soil evaporation and potential plant transpiration and adjusted for plant residue effects. Finally daily potential rates are adjusted to actual evapotranspiration rate based on water availability. In WEPP, the evapotranspiration component is a modified version of Ritchie's model (Ritchie, 1972). Depending on the availability of meteorological data two options for calculating potential evapotranspiration are available. In the case that daily radiation, temperature, wind and dew point temperature or relative humidity data are available, the WEPP model uses the Penman (1963) equation. If only solar radiation and temperature data are available, then the model uses the Priestly-Taylor (1972) method.

Plant Growth and Residue Decomposition

A continuous erosion model requires the simulation of plant growth and residue decomposition to account for a plant's effect on the erosion process. WEPS' CROP submodel (Retta and Armbrust, 1995) was adapted from the Erosion Productivity Impact Calculator (EPIC) crop growth model (Williams et al., 1990). WEPP also uses EPIC concepts of phenological crop development as a basis for its plant growth sub-model (Arnold et al., 1995). From this common starting point, the modelers adapted each plant growth component to meet their individual needs when predicting the effects of a growing crop on wind or water erosion.

In WEPS, the component is adapted so that the model generates daily estimates of leaf and stem growth in mass and area. These additional capabilities were developed to meet the need for predicting the effects of a growing crop on wind erosion specifically. The CROP submodel also provides estimates of the amount of leaf, stem, grain and chaff mass produced on a daily basis to account for a differentiation in decomposition. Furthermore, the CROP submodel accounts for differences in cover due to initial plant density.

The purpose of the plant growth components that are used in WEPP is to predict temporal changes in plant and residue variables such as canopy cover, canopy height, root development and crop biomass production, which can be subsequently removed during a harvest operation or end up as surface residue material. In WEPP, crop growth for both annual and perennial plants can be simulated.

The residue decomposition models of both WEPP and WEPS calculate separately the decomposition of standing and flat residues as well as decomposition of the roots and buried residues. Furthermore, both models take the effect of land management on decomposition rates into account. Output of the two decomposition models is the horizontal and vertical residue cover.

Current Areas of WEPS and WEPP Model Commonality Work

The process based water (WEPP) and wind (WEPS) erosion models that have recently been developed are designed to replace older models that are currently in use (Retta et al., 2001). The Natural Resources Conservation Service of USDA and other agencies have requested WEPP and WEPS to be combined into a single model that simulates both wind and/or water erosion. Some of the advantages of a single model, compared to using two different models include: easier communication of simulation results to clients, consistency of model results, less computer code and databases to maintain, and lower training costs for agencies. Some steps that have been taken so far are described in this section.

Climate Generation

Climate generation is already being conducted using a common tool – the CLImate GENerator (CLIGEN) program (Nicks et al., 1995). This software is currently being maintained, tested, and enhanced by staff at the USDA-ARS National Soil Erosion Research Laboratory (http://horizon.nserl.purdue.edu/Cligen). Efforts are also underway to potentially utilize alternative climate simulation tools such as the GEM (Generation of weather Elements for Multiple applications) model (http://www.wcc.nrcs.usda.gov/climate/gem_fact.html) for WEPP and WEPS simulations in the future.

Common Plant Growth Component

WEPP and WEPS plant growth components use identical or nearly identical procedures to calculate the major processes of plant growth and development, and in places where there are some differences, they can easily be reconciled in most cases (Retta et al., 2001). However, some of the unique processes that are simulated in either one of the individual plant growth components will need to be included in any common model. The new common model should be as modular as possible to allow further developments. The ALMANAC model (Kiniry et al., 1992) has been used as the basis for a possible common crop growth model. ALMANAC can simulate both cropland and rangeland plant species, and multiple competing plant species. Therefore, the need for two different models for cropland and rangeland plant growth as is currently used in WEPP could be eliminated. Finally the new model will also need to include enhancements beyond the current WEPP and WEPS crop growth component, possibly including nutrient stresses. Description of plant partitioning and location of plants is also important, especially in wind erosion modeling and should be added to any new combined crop growth component. Furthermore a common method for user adjustment of crop yield will need to be determined.

Common Interface Screen Views and Functions
Currently the WEPP model and WEPS model share some common interface screen appearance and functionality. This is largely due to the MOSES (Modular Soil Erosion System) project efforts during 1997-2000 (Meyer et al., 2001). However, since the disintegration of the MOSES effort in 2001, commonality efforts on the individual Windows interfaces of WEPS and WEPP have drifted significantly apart. A new combined model would require new interface software, in order to handle all inputs and outputs to accommodate both wind and water erosion simulations.

Common Databases
WEPS and WEPP already share a large common database of 2600+ weather stations for use with CLIGEN within the United States. Additionally, both models can now utilize NRCS – NASIS soil database information to create the necessary soil inputs for their simulations. The largest area of work necessary to allow common application of both systems is in databases for representation of the wide range of cropping/management systems used across the U.S.

Future Plans for Common Process-based Wind and Water Erosion Models
In early 2004, the USDA-NRCS identified the development of a common physical process-based wind and water erosion model as one of their top priority requests of the Agricultural Research Service over the next 10 years. Approaches to accomplish this task are currently being evaluated by ARS scientists in West Lafayette, Indiana, Manhattan, Kansas, and Fort Collins, Colorado. One possible approach will be to disintegrate the current WEPP and WEPS models into unique standalone components (hillslope water erosion, wind erosion, infiltration, runoff routing, etc.), and then to incorporate these modules into the Object Modeling System (OMS). OMS is a model archiving, maintenance and development tool that is under development by the USDA-ARS Great Plains Systems Research Unit (GPSRU) and Colorado State University in Fort Collins, Colorado (Ahuja et al., 2004). It has the potential to greatly assist model developers in creation of new models from archived components. In the fall of 2004, the hillslope erosion component (Foster et al., 1995) from WEPP was extracted and made into a standalone software program, then incorporated into OMS. Plans are to incorporate additional components from WEPP, WEPS and other ARS models within OMS, and also to develop the necessary temporal and spatial looping descriptions to allow for satisfactory water and/or wind erosion simulations.
For a new common model, a new single graphical user interface will need to be developed that allows users to set up and run either a wind erosion simulation or a water erosion simulation. Also, possibly with enhancements to the science components it will likely be possible to predict the combined effects of wind and water detachment during a storm event, and output these new results. This should become much easier to do once a single common model exists. The new interface will need to allow for user access to all input parameters, and only request of the user those inputs necessary to run the type of simulation (water, wind, combined) requested.

Summary
WEPS and WEPP are physically-based erosion models that have a considerable number of commonalities in their science and databases. However, they are currently two separate software programs with some significant differences in their scientific components (water balance, hydrology, etc.), and spatial area delineated and modeled. Development of a combined wind and water process-based erosion prediction model is a

critical need, and will be the focus of considerable work within the United States over the next 5-10 years. Utilization of new modular software development tools as well as existing legacy code in the WEPP and WEPS models should allow for relatively rapid development of the new software. New model maintenance and enhancement should also be improved under the OMS system. Work on common cropping/management databases and new graphical user interfaces will also be required for the new model. In addition to allowing simulation of either erosion by water or erosion by wind separately (but maintaining a single water balance), the new model may also have the potential to simultaneously predict combined wind and water soil detachment, transport and deposition.

References

Ahuja, L.R., O. David and J.C. Ascough II. 2004. Developing natural resource models using the object modeling system: feasibility and challenges. Proceedings of International Environmental Modelling And Software Society (IEMSS) 2004 Conference - Complexity And Integrated Resources Management, Osnabruck, Germany. June 14-17, 2004. 6 pp.

Arnold, J.G., M.A. Weltz, E.E. Alberts and D.C. Flanagan. 1995. Chapter 8. Plant growth component. In (D.C. Flanagan and M.A. Nearing, eds.): *USDA-ARS Water Erosion Prediction Project (WEPP) Hillslope Profile and Watershed Model Documentation.* NSERL Report No. 10, National Soil Erosion Research Laboratory, USDA-Agricultural Research Service, West Lafayette, Indiana. 41 pp.

Ascough II, J.C., C. Baffaut, M.A. Nearing and B.Y. Liu. 1997. The WEPP watershed model: I. hydrology and erosion. Transactions of the ASAE 40:921-933.

Chu, S.T. 1978. Infiltration during an unsteady rain. *Water Resources Research* 14: 461-466.

Flanagan, D.C. and M.A. Nearing (eds.). 1995. *USDA-ARS Water Erosion Prediction Project (WEPP) Hillslope Profile and Watershed Model Documentation.* NSERL Report No. 10, National Soil Erosion Research Laboratory, USDA-Agricultural Research Service, West Lafayette, Indiana. 298 pp.

Flanagan, D.C. and S.J. Livingston (eds.). 1995. *Water Erosion Prediction Project (WEPP) Version 95.7 User Summary.* NSERL Report No. 11, National Soil Erosion Research Laboratory, USDA- Agricultural Research Service, West Lafayette, Indiana. 139 pp.

Flanagan, D.C., J.C. Ascough II, A.D. Nicks, M.A. Nearing and J.M. Laflen. 1995. Chapter 1. Overview of the WEPP erosion prediction model. In(D.C. Flanagan and M.A. Nearing, eds.): *USDA-ARS Water Erosion Prediction Project (WEPP) Hillslope Profile and Watershed Model Documentation.* NSERL Report No. 10, National Soil Erosion Research Laboratory, USDA-Agricultural Research Service, West Lafayette, Indiana. 12 pp.

Flanagan, D.C., J.R. Frankenberger and B.A. Engel. 2004. Web-based GIS application of the WEPP model. Paper No. 04-2024, American Society of Agricultural Engineers, St. Joseph, MI. 12pp.

Foster, G.R., D.C. Flanagan, M.A. Nearing, L.J. Lane, L.M. Risse and S.C. Finkner. 1995. Chapter 11. Hillslope erosion component. In: (D.C. Flanagan and M.A. Nearing, eds.): *USDA-Water Erosion Prediction Project: Hillslope Profile and Watershed Model Documentation*, NSERL Report No. 10, USDA-ARS National Soil Erosion Research Laboratory, West Lafayette, IN. 12 pp.

Hagen, L.J. 1991. A wind erosion prediction system to meet user needs. *Journal of Soil and Water Conservation* 46:106-111.

Hagen, L.J. (ed.). 1996. *WEPS, USDA Wind Erosion Prediction System, Technical Documentation.* Available on-line at http://www.weru.ksu.edu/weps/docs/weps_tech.pdf. 284 pp.

Hagen, L.J., L.E. Wagner, and E.L. Skidmore. 1999. Analytical solutions and sensitivity analyses for sediment transport in WEPS. *Transactions of the ASAE* 42: 1715-1721.

Kiniry, J.R., J.R. Williams, P.W. Gassman and P. Debaeke. 1992. A general, process-oricnted model for two competing plant species. *Transactions of the ASAE* 35: 801-810.

Mein, R.G. and C.L. Larson. 1973. Modeling infiltration during a steady rain. Water Resources Research 9: 384-394.

Meyer, C.R., L.E. Wagner, D.C. Yoder and D.C. Flanagan. 2001. The modular soil erosion system (MOSES). In (J.C. Ascough and D.C. Flanagan, eds.): *Soil Erosion Research for the 21st Century*, Proceedings of the International Symposium, 3-5 Jan. 2001, Honolulu, HI. American Society of Agricultural Engineers, St. Joseph, MI. pp. 358-361.

Nearing, M.A., G.R. Foster, L.J. Lane and S.C. Finkner. 1989. A process-based soil erosion model for USDA-water erosion prediction project technology. *Transactions of the ASAE* 32: 1587-1593.

Nicks, A.D., J.R. Williams, C.W. Richardson and L.J. Lane. 1987. Generating climatic data for a water erosion prediction model. Paper No. 87-2541, International Winter Meeting ASAE, December 15-18, Chicago, IL.

Nicks, A.D., L.J. Lane and G.A. Gander. 1995. Chapter 2. Weather generator. In: (D.C. Flanagan and M.A. Nearing, eds.): *USDA-Water Erosion Prediction Project: Hillslope Profile and Watershed Model Documentation*, NSERL Report No. 10, USDA-ARS National Soil Erosion Research Laboratory, West Lafayette, IN. 22 pp.

Penman, H.L. 1963. Vegetation and Hydrology. Tech. Com No. 53. Commonwealth Bureau of Sols. Harpenden England. 125 pp.

Priestly, C.H.B. and R.J. Taylor, 1972. On the assessment of surface heat flux and evaporation using large scale parameters. *Mon Weth Rev.* 100:81-92

Retta, A. and D.V. Armbrust. 1995. WEPS technical documentation: Crop sub-model. SWCS WEPP/WEPS Symposium. Ankeny, IA.

Retta, A., L.A. Deer-Ascough, L.W. Wagner, D.C. Flanagan and D.V. Armbrust. 2001. Common plant growth model for WEPP and WEPS. In (J.C. Ascough and D.C. Flanagan, eds.): *Soil Erosion Research for the 21st Century*, Proceedings of International Symposium, 3-5 Jan. 2001, Honolulu, HI. American Society of Agricultural Engineers, St. Joseph, MI. pp. 380-383.

Renschler, C.S., D.C. Flanagan, B.A. Engel and J.R. Frankenberger. 2002. GeoWEPP – the geo-spatial interface for the water erosion prediction project. Paper No. 02-2171, American Society of Agricultural Engineers, St. Joseph, MI. 10 pp.

Ritchie, J.T. 1972. A model for predicting evaporation from a row crop with incomplete cover. *Water Resources Research* 8(5):1204-1213.

Savabi, M.R. and J.R. Williams. 1995. Chapter 5. Water balance and percolation. In: (D.C. Flanagan and M.A. Nearing, eds.): *USDA-Water Erosion Prediction Project: Hillslope Profile and Watershed Model Documentation*, NSERL Report No. 10, USDA-ARS National Soil Erosion Research Laboratory, West Lafayette, IN. 14 pp.

Stone, J.J., L.J. Lane and E.D. Shirley. 1992. Infiltration and runoff simulation on a plane. *Transactions of the ASAE* 35(1):161-170.

Stone, J.J., L.J. Lane, E.D. Shirley and M. Hernandez. 1995. Chapter 4. Hillslope surface hydrology. In(D.C. Flanagan and M.A. Nearing, eds.): *USDA-Water Erosion Prediction Project: Hillslope Profile and Watershed Model Documentation*, NSERL Report No. 10, USDA-ARS National Soil Erosion Research Laboratory, West Lafayette, IN. 20 pp.

Van Bavel, C.H.M. 1966. Potential evapotranspiration: the combination concept and its experimental verification. *Water Resources Research.* 2:455-467

Williams, J.R., C.A. Jones and P.T. Dyke. 1990. The EPIC Model. An Erosion/Productivity Impact Calculator: I Model Documentation. A.N. Sharply and J.R. Williams (eds.) USDA Tech. Bulletin No. 1768.1. 235 pp.

Wischmeier, W.H. and D.D. Smith. 1978. *Predicting Rainfall Erosion Losses: A Guide to Conservation Planning.* USDA-Agriculture Handbook 537, Washington, D.C. 58 pp.

Woodruff, N.P. and F.H. Siddoway. 1965. A wind erosion equation. *Soil Science Society of America Proceedings* 29: 602-608.

Chapter 3

Application of WEPP and WEPS in the Benelux

M.J.P.M. Riksen[1], K. Verbist[2] W. Schiettecatte[2] & S.M. Visser[1]
[1]Erosion and Soil & Water Conservation Group, Department of Environmental Sciences, Wageningen University, Nieuwe Kanaal 11, NL-6709 PA Wageningen, the Netherlands; Email: Michel.Riksen@wur.nl
[2] Dept. Soil Management and Soil Care, International Centre for Eremology, Ghent University, Coupure links 653, B-9000 Gent, Belgium; Email: Koen.Verbist@UGent.be

Using WEPP for Single Rainfall Event Prediction in Belgium

Koen Verbist and Wouter Schiettecatte

Introduction

The WEPP model (Nearing et al., 1989) was created for assessing average soil losses on agricultural fields. Since it is physically based, it can be used on an event basis, if the boundary conditions can be delineated. This option can be particularly interesting when daily rainfall data with a high temporal resolution is available. Additionally, if runoff measurements are made on a daily basis, the WEPP model can be validated. Laflen et al. (2004) also noted that the emphasis in erosion modeling has shifted recently towards the prediction of individual storm events, since the protection of downstream water resources against catastrophic events has gained much importance.

Several researchers have used data sets to evaluate and validate the WEPP model since its launch in 1989. Yu and Rosewell (2001) found that WEPP generally over-predicts average annual runoff and soil losses. The CLIGEN module, responsible for generating the climatic input data, over-predicted peak rainfall intensity in comparison with measured rainfall data. Reyes et al. (2004) found that WEPP performed poor in predicting runoff amounts and soil losses on erosion plots with different tillage practices, which were monitored for a period of 17 months. They used literature data and estimated model input values to evaluate the overall performance of the model for uncalibrated conditions. These researchers therefore stressed the importance of model calibration to increase model prediction accuracy for specific situations. Bhuyan et al. (2002) applied WEPP both for individual rainfall events and to predict average annual soil losses. After extensive calibration, they found a good agreement between predicted and measured runoff volumes and soil losses for three different tillage practices. These studies show that model calibration plays an important role in physical based modeling and that parameter estimation should be done with great care. Nearing et al. (1994) pointed out that model validity should not be based on one or two data sets, since erosion measurements tend to show a very high variability. They also noted that storm-by-storm comparisons give more useful information for model accuracy assessment. Bowen et al. (1999) found WEPP sensitive for rainfall intensity and effective hydraulic conductivity, a parameter most often used to calibrate physically based erosion models. A good overview of WEPP calibration and validation studies at both the field and watershed scale is given by Laflen et al. (2004). They found WEPP giving more than satisfactory predictions for various tillage techniques and forest soils, whereas it performed poorly in situations with furrow irrigation.

In this chapter WEPP is applied on a hillslope at an experimental site in Nukerke Belgium, in order to investigate the effect of different buffer strip lengths. Runoff and sediment measurements are compared with uncalibrated WEPP model predictions for these conditions, using breakpoint rainfall data.

Materials and Methods

Field measurements

To evaluate the overall accuracy of WEPP to predict runoff volumes and soil losses for individual rainfall events, a set of field measurements was used. At the experimental site in Nukerke (Belgium), 16 field plots of 100 m length and 1 m wide were installed in January 2001. A series of buffer strips with varying length were

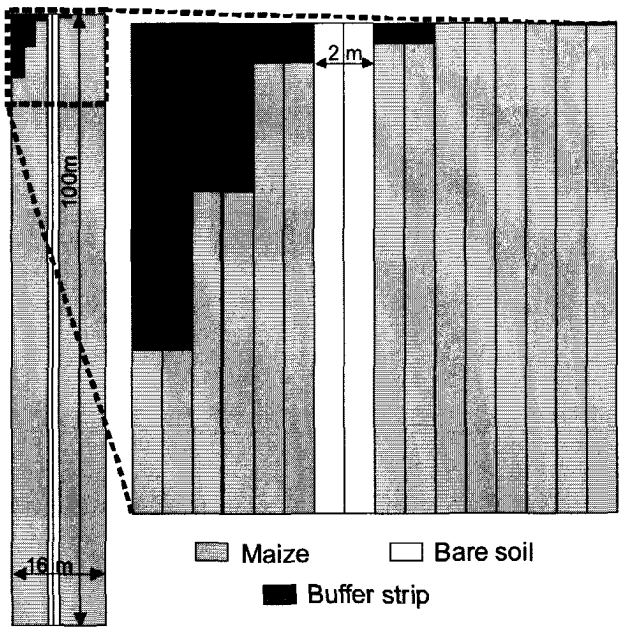

Figure 1. Field setup at the Nukerke experimental site

placed at the bottom of the field plots. Figure 1 shows the field setup and the orientation of the buffer strips of 1m, 2m, 5m and 10m long.

A rain gauge next to the field plots was used to measure the rainfall intensities during five minutes intervals. Runoff from the plots was guided towards a series of calibrated tipping buckets, with a volume between 1.6 and 2 l. The type of instrument used, bears close resemblance to the one described by Klik and Sokol (2001). The number of tips during every five minutes period was recorded using a data logger, resulting in a continuous measurement of discharge. Part of the runoff (2.5%) was collected in barrels. Prior to the installation, laboratory tests were performed to check if the sediment concentration collected in the barrels was representative for the average sediment concentration in the runoff. These tests revealed a linear relation between the average sediment concentration in runoff and the measured concentration in the sample, with zero intercept and a slope of one (r^2 = 0.95). Therefore, this method was found to be useful to determine the average sediment concentration of the runoff.

After every rainfall event of importance, data were downloaded from the logger and runoff samples where taken from the collection barrels of every field plot. The runoff samples were weighed and oven-dried at 105°C. After desiccation, the dried runoff samples were weighed again and the sediment concentration was calculated. The soil loss of the rainfall event was calculated by multiplying the total runoff amount with the sediment concentration.

To evaluate WEPP, all 28 rainfall events of 2001 were used. In Figure 2 the typical relation between runoff (mm) and soil loss (ton ha^{-1}) is shown for all events in 2001, as measured at the field plots without a buffer strip. These data show that relatively few events produce most of the runoff. This is consistent with data sets reported in literature, which are mostly characterized by their highly skewed nature (Nearing et al., 1994; Bowen et al., 1999).

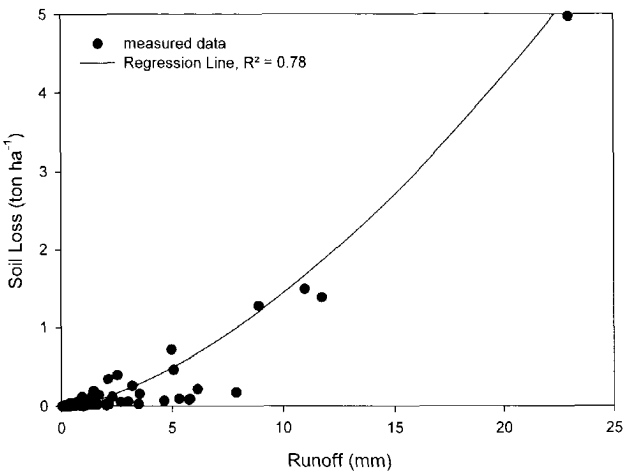

Figure 2. Relation between runoff and soil loss for the field plots without buffer strips and for all rainfall events

Model input

At present, three different types of climate input files are supported by the WEPP Windows Interface, allowing direct input of climate data from raw data. These are long term climatic data on one hand and two types of single storm data on the other hand. The latter are, however, difficult to use for comparison with measured data, since only the total amount of rainfall and peak intensity can be defined for the rain storm.

To allow the model to predict erosion for the rainfall events in 2001, the climate files have to be constructed by hand (Flanagan and Livingston, 1995). Zeleke et al. (1997) constructed a program, the Breakpoint Climate Data Generator (BPCDG), to facilitate the construction of these input files from standard precipitation data. Using this freeware, actually measured data can be imported in WEPP in the correct form, allowing the exact simulation of rainfall events. Using this methodology, a correct comparison can be made between measured and predicted runoff and soil loss for every single event.

The use of BPCDG in combination with WEPP has some drawbacks, however. The BPCDG program is designed to work with pre-defined formats for rainfall data, temperature, wind and other climatic data. So eventually, the problem of constructing your own climatic input files is narrowed down to constructing your own BPCDG input files, which can be cumbersome. Especially for storms that last various hours, the data input becomes difficult, since not more than 50 breakpoints per 24 hours are allowed in WEPP. This obliges the user to reduce the temporal resolution of the input data and to construct pluviophases with more or less the same rainfall intensity. Since this has to be done manually by the user, constructing input data files for the BPCDG still is time consuming. Apart from that, BPCDG is not perfectly aligned with CLIGEN requirements regarding the hour formatting, causing possible WEPP malfunction. So the use of breakpoint climatic data with WEPP still has some mayor flaws, which hopefully will be corrected in the near future.

Other necessary input is the soil data. The field at the Nukerke experimental site lies within the silt loam region of Belgium. The soil texture for every soil layer was determined by Steeman (2002), as well as most of the physical parameters of the soil. The input parameters interrill erodibilty, rill erodibility, critical shear stress and the effective hydraulic conductivity were not defined initially, but calculated by the WEPP model, using the pedotransfer functions described by Flanagan and Livingston (1995).

The slope input file was configured to reflect the complex slope profile at the experimental site, which was measured by Steeman (2002) with a high spatial resolution using topographic equipment.

Ultimately, the management input was adapted to the management situation at the field during 2001. A single crop monoculture of maize (*Zea Mays*) is applied at the site since 2000. During wintertime, only maize stubble remains on the field. All available information on crop characteristics and crop management were used to fine-tune the WEPP default 'maize' entry for the situation at the Nukerke experimental site. For the simulations of the grass strips, additional management sections of various lengths (1 to 10 m) were introduced on the lower end of the slope, to model the influence of these grass strips on runoff and sediment loss.

Model results and Discussion

WEPP was run for all buffer strip lengths and for all rainfall events of the year 2001, as monitored near the field plots. Both runoff volumes and soil losses for every event were produced by the program and this for the various buffer strip lengths. Since actually measured rainfall events were used as input rather than average climatic conditions, a comparison can easily be made between measured and predicted values.

The most notable difference between the WEPP model and the measured data set is the different number of rainfall events causing soil loss. Whereas 28 rainfall events from the data set were found to produce runoff and soil loss, the model only predicted runoff and soil loss for 8 events. A closer look at the data set revealed that all the largest events with more than 5 mm of runoff were found in the model output. As shown in Figure 2, these events also produce most of the soil loss. However, some of the rainfall events with less than 5 mm of runoff, and all events with less than 1 mm of rainfall resulted in zero runoff and soil loss. This discrepancy between measurement and prediction was negatively correlated to either rainfall amount, maximal kinetic energy of the rain storm and maximal 5-minute rainfall intensity. So it can be concluded that small rainfall events with small to moderate soil losses (<0.2 ton/ha) are not well modeled by WEPP. A similar result was found by Bowen et al. (1999), who considered the failure of the model to simulate smaller events as not being significant, because their rainfall input parameters were chosen less meticulously.

Since this section aims at investigating the capabilities of WEPP to predict runoff and soil loss, input selection was done with great care. This leaves only two options to explain discrepancies between model and measurement. First, the model is not capable to predict the complex natural phenomena, or needs site-specific calibration of some internal parameters. For some specific field management situations, Laflen et al. (2004) indicated that WEPP soil erodibility parameters need further improvement. Additionally, some researchers found that WEPP predictions could be improved significantly using a parameter optimizing technique (Bowen et al., 1999; Bhuyan et al., 2002; Larose et al., 2004; Reyes et al., 2004).

A second origin of errors can be found in the measurements itself. Especially the variability in soil loss data is a cause of model-measurement discrepancy. Nearing et al. (1999) found that the variance between replicates is highly dependent on the magnitude of the soil loss, indicating that the coefficient of variance is higher for small erosion events. This means that for low erosion rates more replications of field data are necessary to obtain the same level of confidence. Therefore, validating a model with small erosion events without abundant replications can be considered as less accurate. This is addressed further in this paper.

Model validation has been an important issue in erosion modeling literature over the past 20 years. Various techniques have been used to indicate model efficiency in predicting measured events. Especially the cumulative frequency distributions of the measured and predicted events were found to give an adequate indication on model over- or under-prediction (Nearing et al., 1994). This is shown in figure 3 for both runoff and soil loss. Two conclusions can be drawn from this figure. First, there is a clear indication that WEPP underestimates small runoff events, causing an even larger discrepancy in the cumulative soil loss graph. On the other hand, some events are over-predicted.

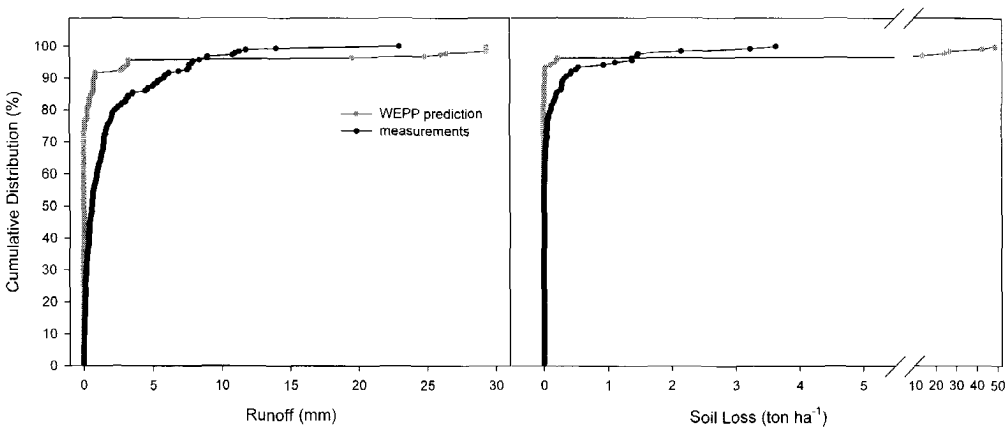

Figure 3. Cumulative frequency distributions of measured and predicted runoff volumes for all rainfall events and all plot treatments ($n_{measured}$: 194, n_{WEPP}: 56)

For one event, the model predicted 3 to 10 times more soil loss than the measured value. This model behaviour is difficult to improve by calibration, since a clear trend in model over- or under-prediction is not present. It was also found to be contradictory to some literature sources, who found that WEPP over-predicted small events and under-predicted large values (Bowen et al., 1999; Larose et al., 2004) and which was also explained theoretically by Nearing (1998).

To further investigate the model results, the eight rainfall events modeled by WEPP are compared to the measured values for both runoff (Fig. 4) and soil loss (Fig 5). The measurements are given as a range, indicating the minimum and maximum values observed. These figures indicate that there exists a large variation in measured runoff and soil loss values. This variation is not only encountered between treatments, but also within treatments, indicated as the range of the measurements. This variability is typical for erosion measurements (Nearing et al., 1999; Gómez et al., 2001). As a result, Nearing et al. (1994) posted that a large number of data sets should be evaluated in the attempt to estimate the model prediction capabilities.

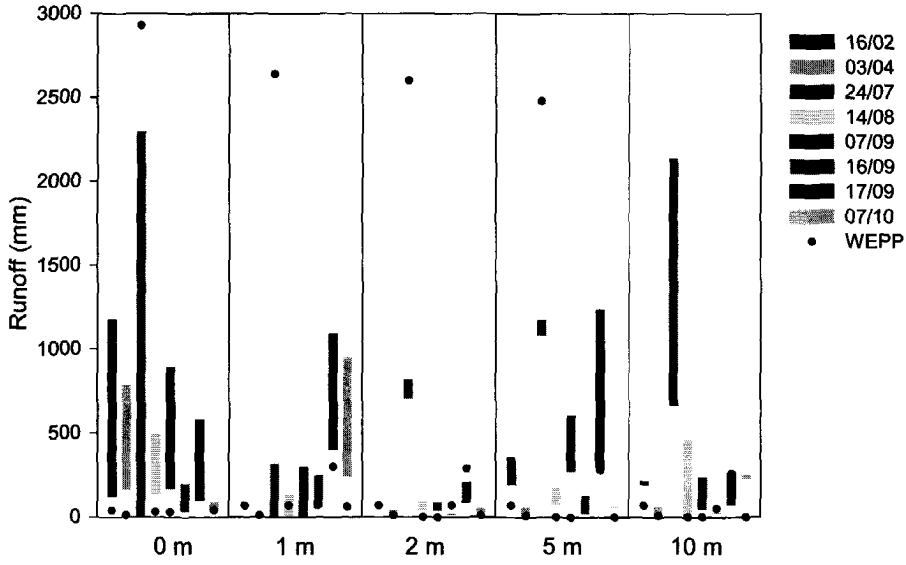

Figure 4. Comparison of the measured and simulated runoff amounts for the erosive rainfall events modeled by WEPP, for the different buffer strip lengths; The bars indicate the range of measured values (min/max)

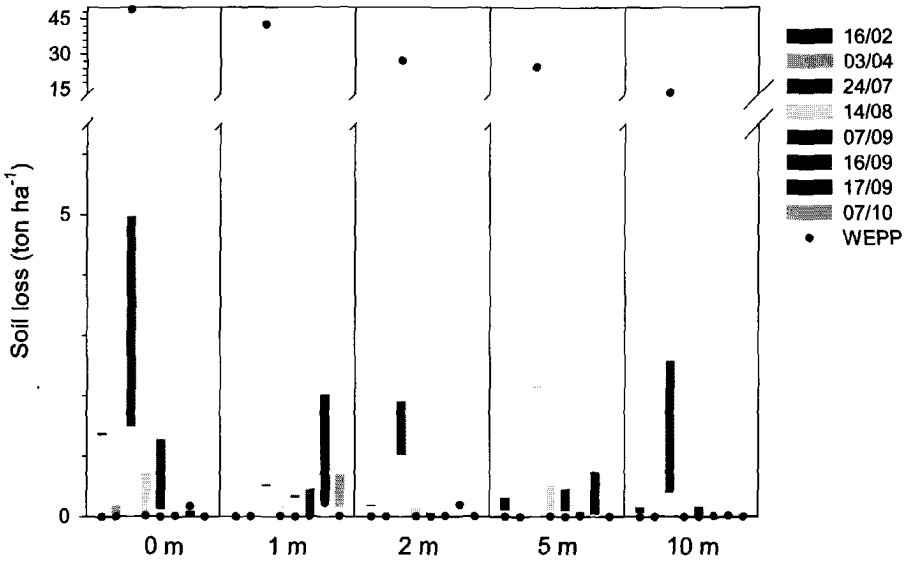

Figure 5. Comparison of the measured and simulated soil losses for the erosive rainfall events modeled by WEPP, for the different buffer strip lengths; The bars indicate the range of measured values (min/max)

In order to address this variability in our model efficiency evaluation, a methodology was used, described by Nearing et al. (1999) and discussed further by Laflen et al. (2004). Instead of using the measured soil loss data, the coefficient of variation (CV) is introduced. This coefficient is an assessment of the variability of the data, and can be calculated using the following relationship (Nearing et al., 1999);

$$CV = 0.73 \cdot M^{-0.306} \qquad \text{[Eq. 1]}$$

where M, the measured soil loss value, is expressed in ton ha^{-1}.

This coefficient of variation can be used to calculate the confidence interval (CI) on measured soil losses (Laflen et al., 2004);

$$CI_{95} = t_{\frac{\alpha+1}{2}} \cdot M \cdot CV = 1.43 \cdot M^{0.694} \qquad \text{[Eq. 2]}$$

where, t is the cumulative distribution value for $\frac{\alpha+1}{2}$ for an infinite number of points, and α is the probability selected (95% in this case).

Calculating both the upper and lower limit of the confidence interval on the measured soil loss values, a graphical representation of data variability can be plotted and compared with the model predictions. This assures that the model is not compared with measured values, whose exact nature is uncertain. Laflen et al. (2004) noted that an erosion model should not be expected to give better results than found when comparing replicated measurements.

In Figure 6 the measured and predicted soil losses for all (modeled) rainfall events and for all buffer strip lengths are compared, indicating the confidence interval on the measurements. Figure 6 reveals somewhat different information, compared to Figures 3-5. Clearly, a large range of values is observed between the upper and lower limit of the 95% confidence interval, converting the 1:1-line into a 'zone of reasonable agreement'. So rather than considering the Pearson correlation coefficient, the question is if the data points are within the appropriate range.

Most predicted values fall well within the upper and lower limit of the CI_{95}. For some events, however, the model predictions are extreme overestimations that can be considered as a model discrepancy in predicting the rainfall event correctly. The origin of this malfunction is however not yet identified. A possible reason could be the clustering of rainfall data in discrete pluviophases, to construct the breakpoint CLIGEN files used as input. This could possibly result in over-estimation of storm erosivity, if the clustering is done with a high temporal resolution.

Summary and Conclusions

This paper investigated the possibility of using WEPP for erosion prediction with individual rainfall events. It was found that WEPP indeed can be used for this type of simulations. For such applications, accurate data preparation and model input proved to be important conditions to produce meaningful results.

One of the aims of the study was to evaluate WEPP prediction capabilities compared to measured data. This revealed a low sensitivity of WEPP for small erosion events, resulting in a significant lower amount of rainfall events causing erosion. The importance of these unmodeled events compared to total measured soil loss was found to be rather limited.

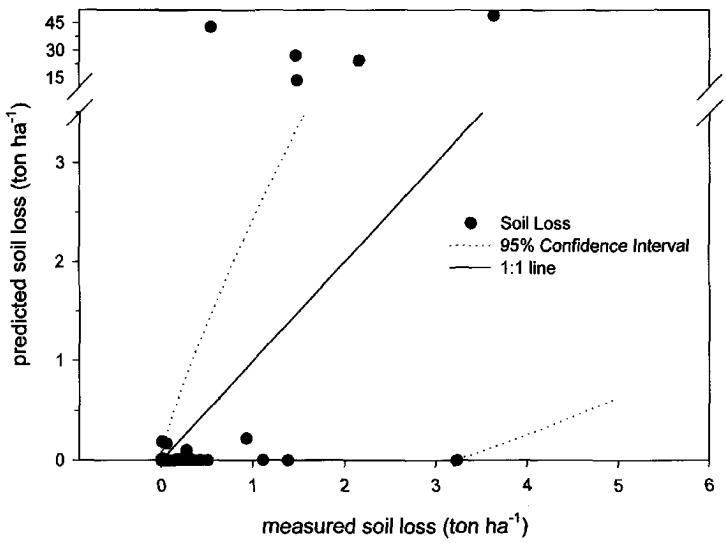

Figure 6. Comparison between measured and modeled sediment loss

Some rainfall events caused overestimations of soil loss of various magnitudes. The inability of the model to predict these losses correctly, was considered important, but could not be explained. More data sets, with more plot-year data, have to be used to confirm these results.

It should finally be noted that the simulations were carried out without calibrating the model. This would have most likely enhanced WEPP prediction capabilities.

References

Bhuyan, S.J., Prasanta, P.K., Janssen, K.A. and Barnes, P.L., 2002. Soil loss predictions with three erosion simulation models. *Environmental Modeling & Software*, 17: 137-146.

Bowen, W., Baigorria, G., Barrera, V. Cordova, J., Muck, P. and Pastor, R., 1999. A Process-based Model (WEPP) for Simulating Soil Erosion in the Andes. CIP Program Report 1997-1998. International Potato Center, Lima, Peru. p403-408.

Flanagan, D.C. and Livingston, S.J., 1995. USDA-Water Erosion Prediction Project: WEPP User Summary. NSERL Report No. 11, USDA-ARS National Soil Erosion Research Laboratory, West Lafayette, IN. 141p.

Gómez, J.A., Nearing, M.A., Giraldez, J.V. and Alberts, E.E., 2001. Analysis of sources of variability of runoff volume in a 40 plot experiment using a numerical model. *Journal of Hydrology*, 248: 183-197.

Jetten, V., De Roo, A. and Favis-Mortlock, D., 1999. Evaluation of field-scale and catchment-scale soil erosion models. *Catena*, 37: 521-541.

Klik, A. and Sokol, W., 2001. A New Measuring Device for Field Erosion Plots. In: American Society of Agricultural Engineers (Ed.): Proc. of the International Symposium: "Soil Erosion Research for the 21st Century", 234-236. January 2-5, 2001, Honolulu, Hawaii.

Laflen, J.M., Flanagan, D.C. and Engel, B.A., 2004. Soil erosion and sediment yield prediction accuracy using WEPP. *Journal of the American Water Resources Association*, 40(2): 289-297.

Larose, M., Oropeza-Moto, J.L., Norton, D., Turrent-Fernández, A., Martinez-Menes, M., Pedraza-Oropeza, J.A. and Francisco-Nicolás, N., 2004. Aplication of the WEPP model to hillside lands in the Tuxtlas, Veracruz, México. *Agrociencia*, 38, 155-164.

Nearing, M.A., 1998. Why soil erosion models over-predict small soil losses and under-predict large soil losses. *Catena*, 32: 15-22.

Nearing, M.A., Foster, G.R., Lane, L.J. and Finkner, S.C., 1989. A process-based soil erosion model for USDA-Water Erosion Prediction Project Technology. *Transactions of the ASAE*, 32(5): 1587-1593.

Nearing, M.A., L.J. Lane, and V.L. Lopes., 1994. Modeling soil erosion. In: Lal, R.(ed.). Soil erosion research methods. Second edition. St. Lucie Press and Soil and Water Conservation Society, St Lucie, FL, USA. 127-156.

Nearing, M.A., Govers, G. and Norton, L.D., 1999. *Soil Sience Society of America Journal*, 63: 1829-1835.

Reyes, M.R., Raczkowski, C.W., Gayle, G.A. and Reddy, G.B., 2004. Comparing the soil loss predictions of GLEAMS, RUSLE, EPIC, and WEPP. *Transactions of the ASAE*, 47(2): 489-493.

Steeman, G., 2002. De invloed van verslemping en bodemcompactie op infiltratie en percolatie van regenwater. MSc Thesis (in Dutch), University of Ghent, 194p.

Yu, B. and Rosewell, C.J., 2001. Evaluation of WEPP for runoff and soil loss prediction at Gunnedah, NSW, Australia. *Australian Journal of Soil Research*, 39: 1131-1145.

Zeleke, G., Winter, T. and Flannagan, D., 1999. BPCDG: Breakpoint Climate Data Generator for WEPP using observed climate standard weather data sets. In: WEPP 2002.7. CD-ROM presented at the "Wind & Water Erosion: Modelling and Measuresment International Workshop", September 30 – October 10, 2003. University of Ghent and Wageningen University. Available at: http://topsoil.nserl.purdue.edu/nserlweb/weppmain/BPCDG.html

Predicting the Effect of Tilling Practices on Wind Erosion Activity
Application of WEPS in Western Europe

Michel J. P.M. Riksen and Saskia M. Visser

Abstract
The inland drift sand areas in northern Europe are characterised by a rapid decline in both aeolian activity and area size. Much of the former drift sand surface has become immobilised by spontaneous or by man-induced colonisation by plants, or has been destroyed for agricultural, economic or societal reasons. The strong reduction of these areas automatically implies the disappearance of a unique ecosystem with a high natural and landscape value. Therefore, it is necessary to investigate how the drift sand areas can be preserved, and how their immobilisation by vegetation can be counteracted by introducing techniques that reactivate the aeolian processes. Four such techniques (rotary cultivator, beach sand cleaner, disk harrow and excavator) were evaluated during an 8-month experiment at Kootwijkerzand, Netherlands. The effectiveness of the techniques to reactivate the aeolian processes was measured by investigating their effect on the raising and lowering of the surface due to aeolian activity and the horizontal sediment transport flux. As field experiments under natural conditions can contain much noise caused by local variations in the terrain and unwanted border effects, the WEPS wind erosion model was used to do additional simulations for each tilling technique. Both, field experiment and model simulation showed that the most effective method is the beach sand cleaner, followed by the rotary cultivator. Unlike the field measurements the model did not simulate any mass transport on the plot tilled with the excavator. Here incoming sediment could have initiated mass transport. In case of the plot tilled with the disk harrow the model overestimated the transport. In case of the simulation it was assumed that the surface moisture content, which is known as an important variable controlling both entrainment and transport, is zero. In reality however a surface layer with a high random roughness shows big variation in moisture content in space and time resulting in lower mass transport.

Introduction
The active inland drift-sands in the Netherlands are unique in Western Europe. According to most authors, the strongly degraded landscape originated mainly in the Middle Ages (Schimmel, 1975, Koster 1978, Castel, 1991), but recent studies point to a much older period, presumably at least Iron age (van den Ancker and Jungerius, 2003). In almost all cases they owe their existence to the reactivation of late-glacial cover sands and river dunes. The European drift-sand areas reached their maximum size in the 19th century (Koster *et al.*, 1993): 200-300 km^2 in northern Belgium, approximately 950 km^2 in the Netherlands, 1400-2000 km^2 in northwestern Germany, and 450-550 km^2 in Denmark. In England, Koster *et al.* (1993) also mapped small drift-sand areas, particularly in East Anglia.

From the end of the 19th century until halfway the 20th century most drift-sand areas in Europe were successfully reforested. Due to the success of the reforestation programme, no more than 6,000 ha of the original drift-sand areas were preserved in the Netherlands in the mid 1960s (Bakker *et al.*, 2003; Jungerius, 2003). Today the open drift-sand landscape is especially appreciated because its vegetation shows patches of distinct stages in the natural succession, with typical pioneers such as *Corynephorus canescens*, *Spergula morisonii*, *Polytrichum piliferum*, lichen such as *Cladonia sp.*, and

Cladina sp. The combination of open land and vegetated patches creates the habitat for rare insects, birds and lizards.

However, since the 1960s the remaining active drift-sand areas have shown a rapid decline in size due to natural regeneration. This is attributed to the increased atmospheric nitrogen deposition, a corollary of the intensive bio-industrial activities on the sandy soils in most parts of the Netherlands (Bakker *et al.*, 2003). Of the 6,000 ha in 1960, only 4,000 ha were left around 1980 and no more than 1,500 ha in 2002 (Jungerius, 2003). Without human intervention, the active drift-sand areas, with their characteristic flora and fauna, will slowly regenerate and turn into forest.

In 1989 the Dutch government launched the 'Overlevingsplan Bos en Natuur (OBN, Survival Plan for Forests and Nature, Ommering 2002) to provide grants for measures to counteract the effects of N-deposition in the Netherlands. Since then, several projects have been launched to preserve the drift-sand landscape and to reactivate already stabilised drift-sand areas.

An active and adequate management, focusing on a restoration of the degradation-regeneration balance, is needed if European inland drift-sand areas are to be preserved for future generations. Until 1990, measures were mainly taken ad-hoc (Bakker *et al.*, 2003). They usually focused on removing vegetation or retarding its development, but did not, or not fully, take into account the physical process of wind erosion. This puts severe constraints on their efficiency, as optimum results will only be achieved when wind erosion, as a physical process, is sufficiently stimulated by these measures.

To get a better insight in the effect of the different tilling methods on the erodibility of the treated surfaces a field experiment has been carried out at the inland drift-sand area Kootwijkerzand, The Netherlands in 2003. The experiment showed clear differences in erosion activity as described in Riksen and Goossens (2004, submitted). However field conditions were far from ideal due to the heterogeneity in the landscape. Small differences in relief between the experimental plots could have influenced the local wind velocities at the surface, resulting in variations in mass transport. Also some material from outside the plots could have entered the plots causing increased transport on the plots. The non-erodible zone between the plots was too small resulting in the deposition of material origin from one plot in the northern part of the next plot. It was also not possible to repeat the experiment in the field. For a better explanation of the results of the field experiment a complementary research in which these uncertainties could be excluded was therefore preferable.

For this study the WEPS wind erosion model was used to simulate the different tilling practices. The effects of the different treatments on the surface conditions were translated into the input parameters of the WEPS model. For each treatment scenario the WEPS model was used to predict the erosion transport rate for storms with different wind velocities. The model outputs were then compared with the result of the field experiments.

Materials and Methods

Site description

The Kootwijkerzand nature reserve is located on the Veluwe, in the centre of the Netherlands, near the village of Kootwijk (52.12 N, 5.45 E). It is about 700 ha in size and consists of heath-land and drift-sand surrounded mainly by pine forest (Figure 1).

The foundation of the late Pleistocene deposits at Kootwijkerzand is of glacial origin (ground moraine) and dates from the Riss/Saale. During the Würm/Weichsel,

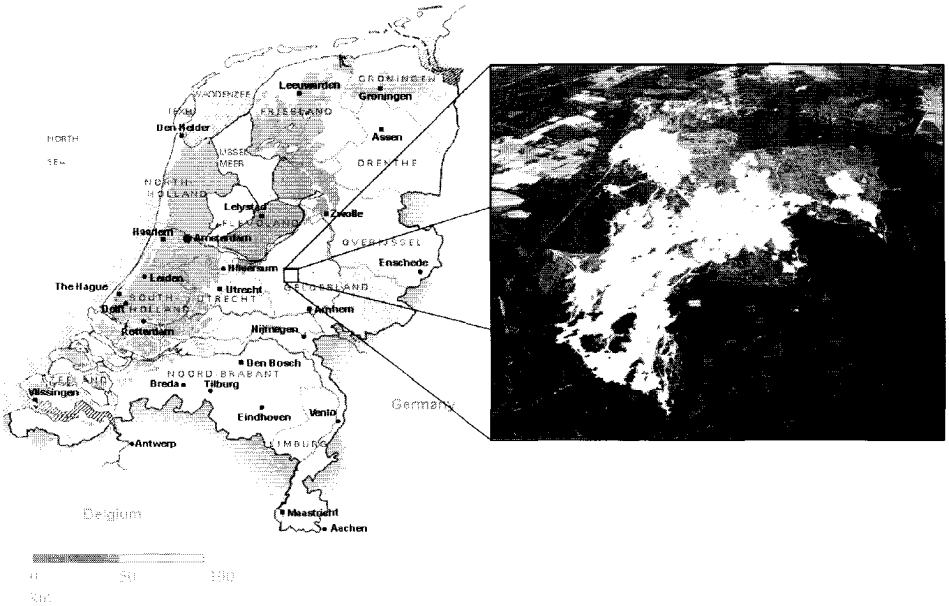

Figure 1. Drift-sand area Kootwijkerzand, Gelderland, The Netherlands.

winds transported large quantities of sand, which deposited all over the central Netherlands. This cover sand became prone to wind erosion at many places during the Holocene, and large areas changed into drift-sand areas. This drift sand has been described as the formation of Kootwijk (Stiboka, 1979). The Pleistocene cover sand occurs as large, often irregular ridges or as gently undulating plains. The drift-sand, by contrast, is characterised by isolated dunes and by blown-out plains. The dunes vary from 4 to up to 20 m in height. At Kootwijkerzand, a number of buttes occur in addition to the dunes and the blown-out plains. These buttes are several hundred m^2 in size and up to 10 m high. Their summit is usually covered by pine trees or by shrubs, protecting them from severe wind erosion. The main soil type in the region is an (albic) arenosol composed of fine, well-sorted and well-rounded quartz sand and without a clear A1 horizon. The drift-sand, which is mainly of local origin, is light yellow-greyish in colour. It is characterised by a relatively loose grain packing (Koster *et al.*, 1993). Vegetation at Kootwijkerzand is variable in space, depending on the stage of succession (Table 1). In 2003, 18 % of the area consisted of bare sand, whereas 15 % was covered by forest and 67 % was in one of the intermediate stages of succession (Riksen and Sweeris, 2003).

Tilling techniques

Four tilling techniques were evaluated to investigate their potential for reactivating aeolian erosion on stabilised drift-sand areas. The following contains a description of the equipment used in this experiment (Riksen and Goossens, 2004 submitted):

Technique 1: rotary cultivator

The rotary cultivator used has a tilling depth of 0.20 m (Figure 2A). L-shaped knifes rotate with a high speed, cutting up the vegetation and mixing the top layer. The treatment leaves a smooth, loosely packed surface.

Table 1. Succession stages of inland drift-sands in The Netherlands.

Succession stage	*Composition of the vegetation (main species)*	*Vegetation cover (%)*	*Soil profile*	*OM top soil (%)*	*pH KCl*
0	No vegetation	0	C	0.30	4.7
1	Patches of pioneer grasses: *C. canescens*, *Ammophila arenaria, Festuca rubra* sp. *commutate and Carex arenaria*	< 5	C	0.30	4.7
2	Mix of *C. canescens* and green algae	50 – 80*	C	0.34	4.6
3	Mix of pioneer grasses, algae crust and *P. piliferum* and *Spergularia morisonii*	40 – 75*	C	0.58	4.5
4	Carpet of *P. piliferum* covered by algae and lichens, and patches of *C. canescens*	70 - 100*	AC	0.79	3.5
5	Mix of *C. canescens*, mosses, grasses, lichens and *C. vulgaris*	90 - 100	AC	0.88	3.5
6	Mosaic vegetation of grass, mosses, lichen and *C. vulgaris* with seedlings of some trees	100	AC	1.37	3.5
7	Forest with grasses, mosses and some heather	100	A(B)C	-	-

**) Source: Ketner-Oostra, 1994*
-) no data available
The moss C. introflexus is an exotic moss species that has invaded inland drift-sands since the 1980s.
(Typology after: Masselink, 1994; Ketner-Oostra and Huijsman, 1998).

Technique 2: beach sand cleaner

This machine, also known as the "sod sieving machine", is shown in Figure 2B. The machine scrapes a layer approximately 0.1 m in thickness from the topsoil and puts it on a conveyor belt consisting of lamella 0.008 m distant from each other. The conveyor belt moves under an adjustable slope (during the test approximately 30 degrees) over a camshaft and acts as a sieve. Sand falls through the open space on a second identical conveyor belt. Plant residue left on the conveyor belts is dropped into a container at the rear of the machine. The cleaned sand is then dropped to the field surface. The result of the operation is a smooth, loosely packed topsoil devoid of any plant residue.

Technique 3: disk harrow

The disk harrow has a tilling depth of 0.20 m (Figure 2C). The harrow consists of two rows of 9 disks each. The disks are 0.65 m in diameter and are spaced at a distance of 0.2 m. They stand 30 degrees oblique to the direction of advancement. The operation results in a rough top layer with clods several cm in size, and with a relatively large amount of vegetation left.

Technique 4: excavator

The excavator is used to remove the upper 0.05-0.10 m of the topsoil including all vegetation (Figure 2D). The speed of the operation depends on the type and size of the machine. The result of the operation is a flat, slightly compacted sand surface devoid of any vegetation.

Experimental layout

A careful examination was made of the entire Kootwijkerzand area to find a place with an appropriate topography, vegetation cover and accessibility. To exclude topographic effects, a fairly flat, open terrain was selected well away from dunes and buttes. The vegetation consisted of scattered clumps of grey hair grass (*Coryneplorus canescens*)

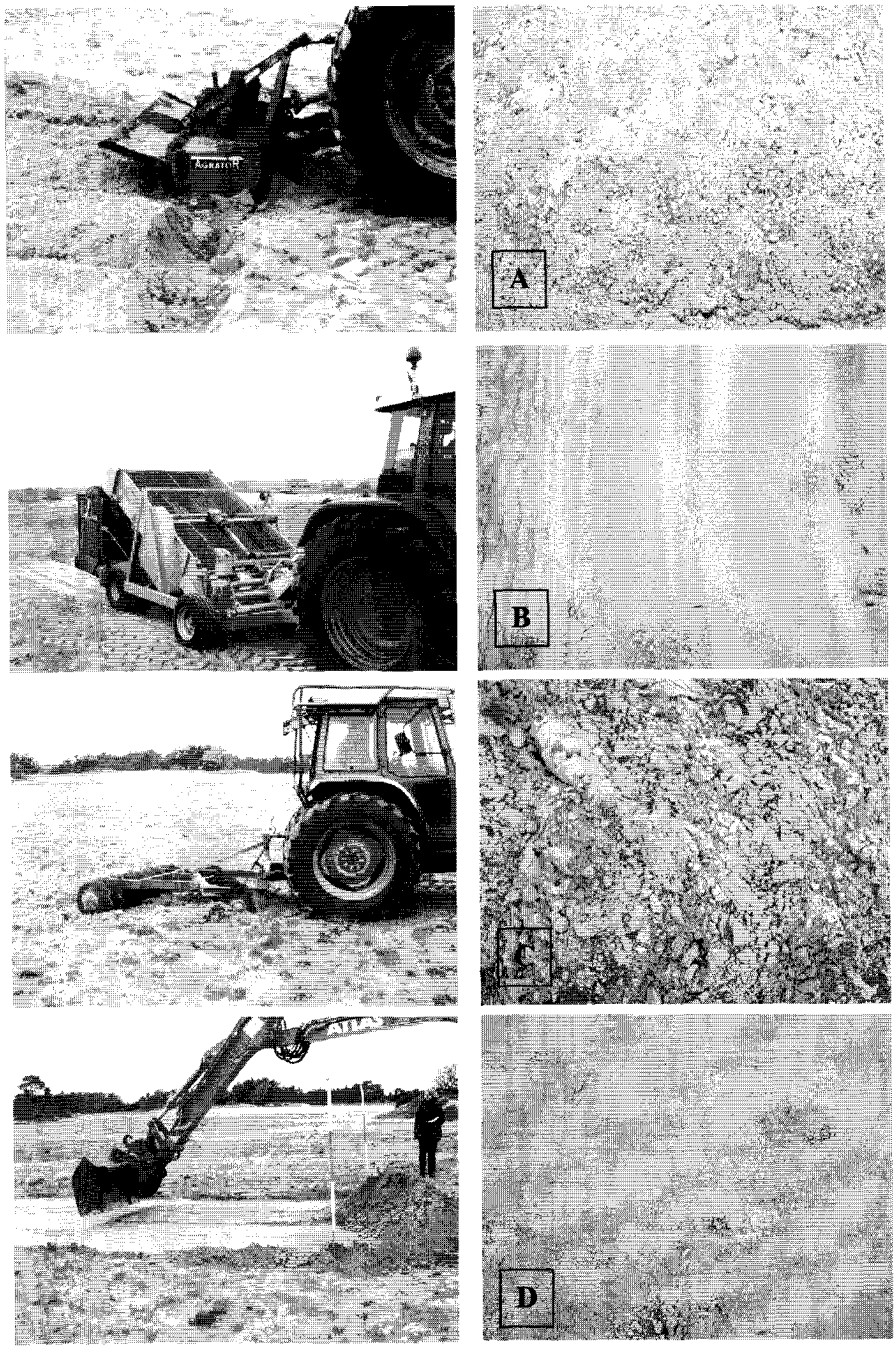

Figure 2. Surface after tilling with: A Rotary cultivator; B Beach sand cleaner; C Disk harrow; D Excavator. November 2002, Kootwijkerzand, The Netherlands.

with, in between, an initial development of algae crusts and some *Polytrichum piliferum* moss. Within the test area, five experimental plots of 4m wide and 30m in length were installed in the direction of the prevailing erosive wind with a 2m wide untreated strip between the plots (for a detailed description see Riksen and Goossens, 2004 Submitted). Plot No. 1 was prepared with the rotary cultivator, plot No. 2 with the beach sand cleaner, plot No. 4 with the disk harrow, and plot No. 5 with the excavator. Plot No. 3, located in the middle of the experimental area, was left untreated as a control area.

Surface characteristics after tilling

Grain size distribution was determined for the upper 5 cm for each plot. The plot samples were composed of 20 randomly taken sub-samples. Each sample was first sieved at 1 mm to exclude possible vegetation residue, and then analysed with a Malvern Mastersizer (type: S). As the samples showed nearly no aggregation, all analyses were done in water (not in air). The grain size distribution is almost identical at all plots. The median grain diameter is always between 167 and 176 µm (Table 2), and the proportion of silt and clay is negligibly small (< 1%). All plots also contain a small (< 5%) fraction of coarse sand grains between 0.5 and 2 mm in size. After tillage the vegetation cover and presence of crusts were determined and described (Table 2). And detailed photographs were taken to estimate the random Roughness (RR) factor according to Fryrear et al. (1998, p. 139-143).

Table 2. Surface conditions after tilling at Kootwijkerzand, The Netherlands.

	Tilling technique				
Parameter	**Rotary cultivator**	**Beach sand cleaner**	**Disk harrow**	**Excavator**	**Control**
Vegetation cover			*(% of total surface)*		
Grey hair grass	0	0	0	0	16
Algae (crust)	0	0	0	0	1
Polytrichum moss	0	0	0	0	traces
Plant residue	4	2	11	0	0
Surface roughness	Smooth uniform surface	Smooth uniform surface	Irregular surface consisting of clods.	Smooth uniform surface	Irregularities formed by small vegetated mounds
Random roughness (cm)	0.5	0.1	3.0	0.2	3.0
D50 (µm)	172	167	174	176	172
Bulk density (g cm^{-3})	1.55	1.56	1.55	1.60	1.59

Meteorological parameters.

A meteorological station was installed SW of the test plots. The following parameters were measured: wind speed (at 1 and 2 m height), wind direction (at 2 m), air temperature, relative air humidity and precipitation. Wind speed was measured with cup anemometers and precipitation with a tipping bucket (at 2 m above ground level). To record the periods of wind erosion, 3 saltiphones (Spaan and van den Abeele, 1991) were installed as well, at a height of 10 cm above the surface. Wind, temperature and humidity were stored as 10-min averages whereas the saltiphone data were stored as the total number of counts in 10 minutes.

Horizontal sediment flux.

Horizontal sediment transport (caused by wind erosion on the plots) was measured with Modified Wilson and Cooke (MWAC) catchers. Four vertical masts with seven MWAC catchers were installed on each plot. The technical description and calibration of the catchers are given in a paper by Goossens and Offer (2000). The bottles used at Kootwijkerzand were 9.4 cm long and 4.8 cm in diameter. For the wind erosion events investigated, the efficiency of the catchers was between 109 and 119 % for sand having a grain size similar to that at Kootwijkerzand (Goossens *et al.* 2000). All measured fluxes were corrected accordingly. The MWAC catchers were installed at the following height at each mast (values refer to the centre of the inlet tubes): 5, 12, 19, 26, 45, 70 and 100 cm. The exact values were checked every week, and any increase or decrease (due to erosion or accumulation near the masts) was taken into consideration when calculating the horizontal sediment fluxes. These fluxes were calculated by measuring the amount of sediment caught by the catchers and dividing these over the surface area of the catcher inlet (0.44 cm^2) and the total sampling time (usually 168 h, or 7 days). The total horizontal sediment flux at each mast was then calculated by vertically integrating the flux values for the first 100 cm above the surface. Since more than 99 % of the airborne sediment at Kootwijkerzand consists of sand (diameter > 63 μm), the amount of sediment transported outside these first 100 cm is negligibly small (Riksen and Goossens, 2004 Submitted).

Raising and lowering of the surface

The raising (due to aeolian accumulation) or lowering (due to aeolian erosion) of the surface in each experimental field was measured with erosion pins (De Ploey and Gabriels, 1980). Four transects of four erosion pins each were installed on each field. The pins were 50 cm long and had a diameter of 5 mm. All pins were checked weekly. They were read with a precision of 1 mm (0.5 mm when this appeared to be necessary). Because of the highly permeable sand soil, no runoff occurred on the fields, even during the heaviest rains. This ensures that all changes in surface elevation measured by the erosion pins were caused by aeolian activity only.

Scenario runs with the WEPS model in PC-raster

Visser et al. (2005) rewrote the erosion sub-model of the Wind Erosion Prediction System (WEPS) (Hagen, 1996) in the dynamic modelling language PCRaster (De Jong, 1997). WEPS is a process-based daily time step computer model that predicts soil erosion by simulating the physical processes that control wind erosion (Hagen, 1991).Translating the original WEPS code into PCRaster allows us to insert spatially varying parameters that control wind erosion e.g. vegetation cover, crust type, and soil roughness. The model calculates the friction velocities and the threshold friction velocities for each grid cell. When the friction velocity is larger than the threshold friction velocity sediment transport is possible, and the model calculates the soil loss or deposition for each grid cell and updates the surface parameters. The original erosion sub-model of WEPS was modified by:

- Allowing sediment to enter the field (no non-eroding boundaries),
- Allowing transport to occur when erosion is no longer possible (friction velocity is still larger than transport threshold but smaller than the erosion threshold) (due to the small grid size),
- Assuming the water content of the topsoil to be 0.

For a detailed description of the WEPS erosion sub-model and the adaptations made see Hagen (1996) and Visser et al. (2004).

Scenario runs

Table 3 shows the main input parameters and their values for the four tilling techniques and the untreated plot (control). The model was run for each tilling scenario for two different storms. In the first simulations the wind speed was set at an average of 6.5 ms^{-1} (at 2m height) varying between 4.5 and 8.5 ms^{-1}. During the second run the wind speed was set at an average of 8.5 ms^{-1} (at 2m height), varying between 6.5 and 10.5 ms^{-1}. The total duration of each run was set to 30 minutes.

Table 3. Model input parameters and values after tillage at Kootwijkerzand, The Netherlands.

	Tilling technique				
Parameter	**Rotary cultivator**	**Beach sand cleaner**	**Disk harrow**	**Excavator**	**Control**
RR	0.5	0.1	3.0	0.2	0.3
Slagm	0.172	0.167	0.174	0.176	0.172
Slags	3.85	4.09	3.98	4.0	3.83
SFcr	0	0	0	0	0.01
Bffcv	0.04	0.02	0.11	0	0
Brlai	0.04	0.02	0.11	0	0.16
Brsai	0	0	0	0	0.03
Bzht	1	1	1	0	5
Zom	6.0	4.0	8.0	5.0	13.0

RR = random roughness; Slagm = geometric mean aggregate distribution (mm); Slags = standard deviation aggregate distribution; Bffcv = biomass fraction flat coverage; Brlai = leaf area index; Brsai = stem area index; Bzht = height biomass (mm); Zom = roughness height (local).

Results

Meteorological parameters.

Figure 3 depicts the wind compass card at Kootwijkerzand for two cases: the complete compass card (all periods included) and the compass card during saltation activity only. At Kootwijkerzand the wind usually blows from the SW and NE directions, but the winds that generate saltation predominantly come from the SW. Therefore, at Kootwijkerzand, wind-eroded sediment is generally transported from the SW to the NE, and the experimental layout of the five test plots was based on this background.

During 81% of the time during the experiment there was no or little wind erosion activity (Table 4), 15% of the total time there was little to moderate erosion activity and 3% of the total time was classified as moderate to high erosion activity. The latter covered 48% of the recorded saltation. 11 Storms, together less than 1 % of the total period, were recorded with high to very high saltation activity covering 34% of the recorded saltation. There was much variety as to the wind speed during the experiment. Wind velocity was generally high in January 2003 and in April-May 2003, but there were many other weeks with high wind speed (Figure 4). Rainfall was extremely high in the second half of December 2002, with 135 mm rain in less than two weeks. It was also high at the end of January and in early February 2003, during the last week of April 2003, and in May 2003. There was little rainfall in February and March 2003.

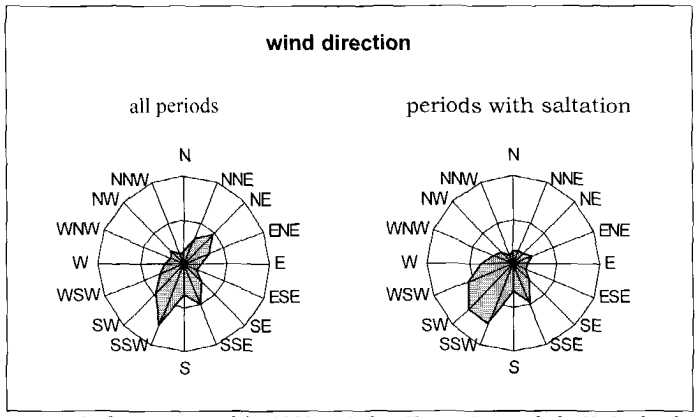

Figure 3. Wind compass card for 2002 - 2003 at Kootwijkerzand, the Netherlands.

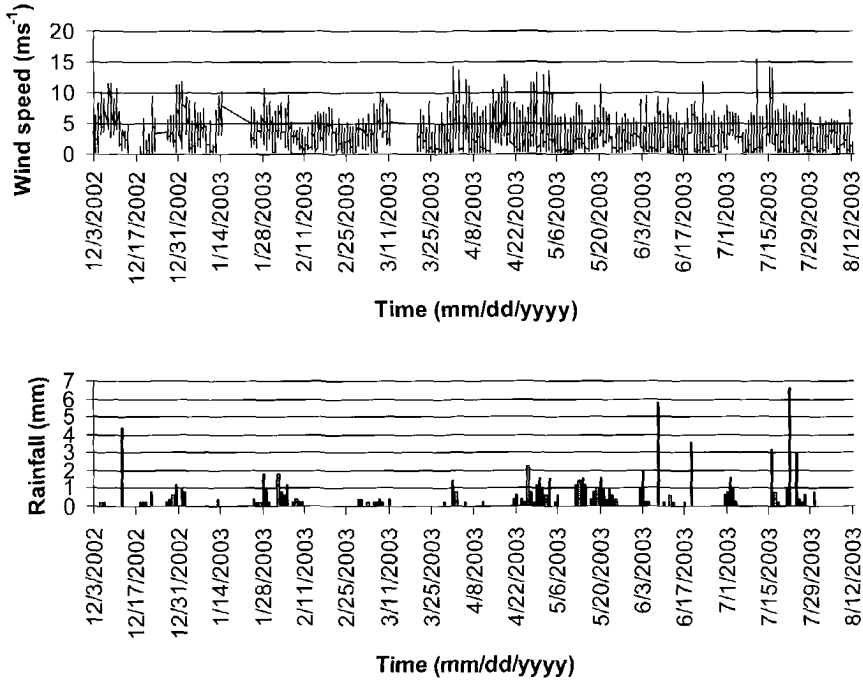

Figure 4. Weather conditions at Kootwijkerzand in the period 3/12/2002 – 14/08/2003.

Table 4. Wind erosion activity: duration and average wind speed at 2m height over the period 3/12/02 – 14/08/03 at Kootwijkerzand.

Average saltation flux (cts 10 min^{-1}) *	< 33	33 – 3333	3333 - 16666	> 16666
Description saltation activity	No	Little to moderate	Moderate to high	High to very high
Average wind speed (m s^{-1})	2.8	5.7	7.5	8.8
Duration (days)	177	31.7	7.5	1.8
% of total counts	0.2	17.8	48.1	33.8

* *Average of the three saltiphones.*

Horizontal sediment flux

The intensity of aeolian activity on the test plots is best described by the (airborne) horizontal sediment flux, which was measured by the MWAC catchers. Table 5 shows the average (in space and time) vertically integrated horizontal sediment flux over each of the five test plots during the experiment. Most transport occurred over plot No. 2 (beach sand cleaner), followed by plot No. 1 (rotary cultivator) and plot No. 5 (excavator). Aeolian transport over plot No. 4 (disk harrow) was smaller than over the untreated reference plot No. 3.

Table 5. Average (in space and time) vertically integrated horizontal sediment flux between 0m and 1m height (kg m^{-2} $week^{-1}$) over each of the five test plots during the experiment, 3/12/02 – 14/08/03, Kootwijkerzand, The Netherlands.

Average vertically integrated horizontal sediment flux	Tilling technique				
	Rotary cultivator	**Beach sand cleaner**	**Disk harrow**	**Excavator**	**Control**
(kg m^{-2} $week^{-1}$)	753	1179	170	437	298

Figure 5 shows a period with saltation activity under almost ideal circumstances with one main storm with wind speeds between 8 and 10 ms^{-1} and from an almost ideal SW wind direction varying between 200 – 250 degree, almost parallel to the longest plot side (220 degree). Table 6 shows the measured transport rates at the begin, in the middle and at the end of each plot during this period. In three cases most sediment transport was measured at the end of the plot (beach sand cleaner, disk harrow and control). In case of the rotary cultivator and the excavator, most sediment transport was measured at the centre.

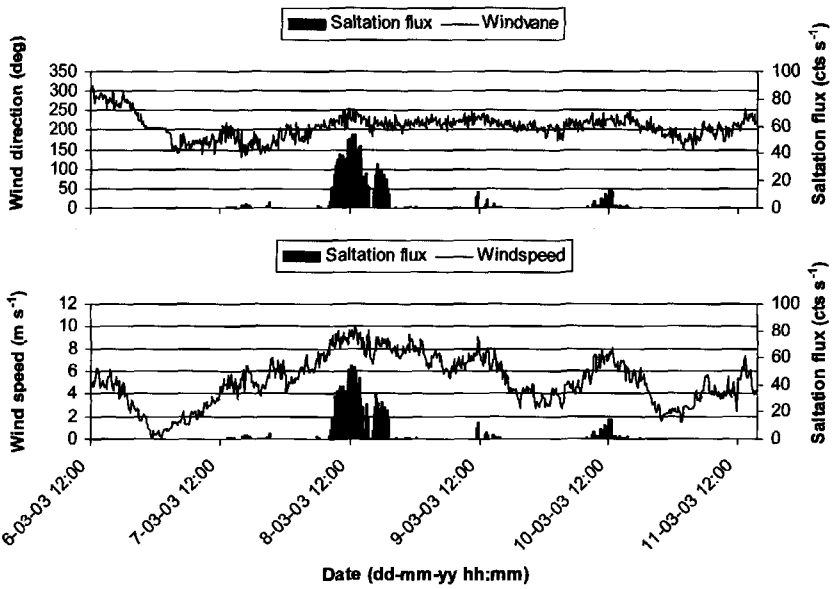

Figure 5. Saltation activity, wind speed at 2 m and wind direction for the period 6/03/03 – 11/03/03, at Kootwijkerzand, The Netherlands

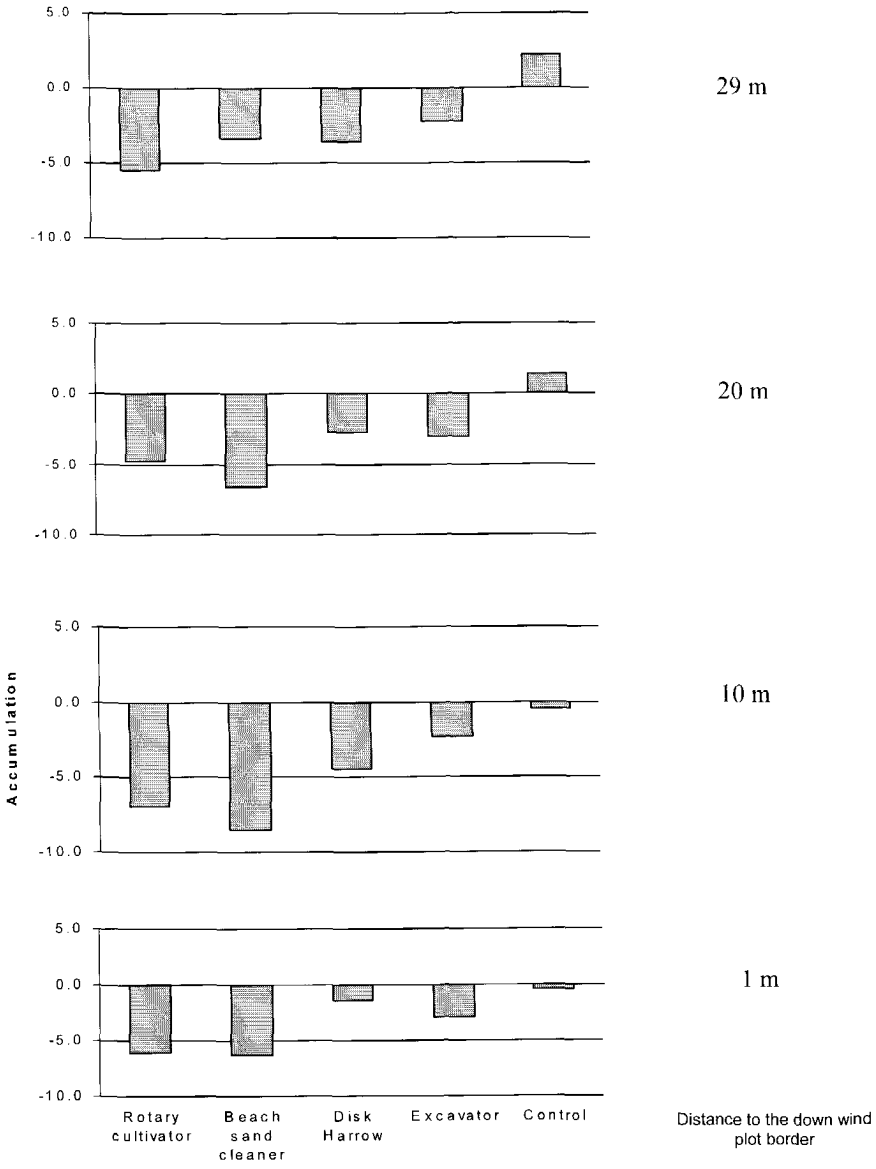

Figure 6. Net erosion (-), sedimentation (+), Kootwijkerzand, 3/12/02 – 14/08/03.

Table 6. Average vertically integrated horizontal sediment flux between 0m and 1m height (kg m^{-2}), 6/03/03 – 13/03/03, Kootwijkerzand, The Netherlands.

Wind direction	Location of the catcher in the plot	Tilling technique				
		Rotary Cultivator	Beach sand cleaner	Disk harrow	Excavator	Control
↓	Begin (1m)	2.3	4.0	0.6	0.3	0,4
	Centre. (15m)	108.3	17.7	1.6	111.9	1,9
	End (29m)	35.7	220.9	9.1	46.6	15,7

Raising and lowering of the surface

Figure 6 shows the average net erosion and sedimentation on each plot at the end of the experiment. Most material was lost from the plot tilled with the beach sand cleaner followed by the plot tilled with the rotary cultivator. The plot tilled with the disk harrow and excavator showed less losses. The control plot showed no erosion at all, but some deposition in the north-easterly half of the plot.

WEPS simulated horizontal sediment flux

Table 7 shows the results of the WEPS. The plot tilled with the beach sand cleaner showed most transport closely followed by the rotary cultivator. The transport on the plot treated with the disk harrow was much lower. The model results showed no transport for the plot tilled with the excavator and on the control plot. The simulation at a higher wind speed gives a more or less similar picture (Table 7). Only the plot tilled with the disk harrow showed relative higher transport rates.

Table 7. Simulated mass transport between 0 m and 1 m height (kg m^{-2}) for an event with a duration of 30 minutes and wind speed of respectively 6.5 ms^{-1} and 8.5 ms^{-1} (at 2m).

Wind speed (ms^{-1})	Location of the catcher in the plot	Tilling technique				
		Rotary Cultivator	Beach sand cleaner	Disk harrow	Excavator	Control
6.5	Begin (1m)	0.3	0.4	0.2	0	0
	Centre. (15m)	12.2	13.3	5.2	0	0
	End (29m)	22.5	24.2	9.69	0	0
8.5	Begin (1m)	0.95	1.07	0.57	0	0
	Centre (15m)	35.82	37.71	20.05	0	0
	End (29m)	67.07	69.62	37.44	0	0

Discussion

Measurements under field conditions can contain much noise influencing the measurements. Even small local variation in relief and soil moisture can have big consequences for local sediment transport. A clear example is given by table 6 where highest transport rates were found in the centre of plot tilled with the rotary cultivator and the plot tilled with the excavator.

For the field experiment and WEPS erosion simulations, it was found that the beach sand cleaner is most effective in reactivating wind erosion activity, closely followed by the rotary cultivator. This was expected as the surface conditions after tilling was more or less the same for both treatments, except for the amount of plant residue on and in the soil surface layer. That they yield most transport of all treatments can be explained by the fact that the sand grains were loosely packed as result of the used tilling technique, thus making the grains better available e.g. more exposed to wind erosion.

In theory the transport rate increases until the maximum carrying capacity of the wind is reached. The mass transport measured in the field showed more spatial variation then expected (Table 6). The WEPS erosion simulations (Table 7) showed a normal

spatial pattern of the mass transport rates; low at the begin and maximum or highest transport rates at the end of each plot. The spatial variation in the measured transport rated can be explained by the spatial variation in surface roughness, surface moisture and slope. The lower transport rates found at the end of the plots tilled with the rotary cultivator and excavator is mainly caused by an decrease in the windward slope at the second half of these plots causing a drop of the wind speed (e.g. carrying capacity) near the surface.

The presence of vegetation, clods or other large roughness elements is important to the entrainment process (Nickling, 1994). In case of the disk harrow and also the untreated plot, the increased random roughness, by vegetation and clods, is the main reason for the relative low sediment transport. As surface roughness increases, an increasing proportion of the wind shear stress is taken up by the larger elements (Lyles et al, 1974). However the model showed relatively (compared to transport rates found for the beach sand cleaner and rotary cultivator) significant more transport as measured in the field experiment. We assume that the simulation did overestimate the mass transport here. An explanation for this might be that we underestimated the random roughness. But it can also partly explained by the surface moisture. Field observations and wind tunnel studies have shown that surface moisture content is an extremely important variable controlling both the entrainment and transport of sediment by wind (Nickling, 1994). For the simulation it was assumed that the water content of the topsoil is zero. In reality however, the drying pattern of a surface with a high surface roughness is much more variable than for a smooth surface like of the plots tilled with the beach sand cleaner and rotary cultivator. Over time it means that a part of the surface is less erodible due to the higher surface moisture.

On the plot where the vegetation was removed by sod cutting with an excavator, the model simulation showed no transport at all. An explanation for this is that the surface is too smooth with a few projections subject to lift. Also the friction velocity is higher over a rough surface for the same ambient wind speed than over a smoother surface (Cooke et al., 1993). Unlike the WEPS simulation, the field experiment showed significant sediment transport as shown in Table 5 and 6. Figure 6 however, shows that the net erosion on this plot was the lowest of the four tilling techniques, indicating that a larger part of the measured sediment transport origins from outside the plot. Through the bombardment by the incoming particles it is possible that the transport process on this surface type continues. Reptation was hardly observed on this plot indicating that most energy remained for the transport of the incoming grain. Beside loose material along the border of this plot material was transported into the plot from the area northeast of the plot where the vegetation was destroyed by the driving with the excavator and dump truck used for this plot. Another explanation can be that sediment transport takes place at higher wind speeds than the simulated ones.

Conclusions

Simulations with a wind erosion model make it possible to exclude those factors that can causes noise in a field experiment, like small differences in relief, unwanted border effects causing an increase or decrease of sediment transport and sediment entering the plots from the neighbour plot or surrounding area. Therefore combining field experiments with additional information from the model simulations, can give a better insight of the on-site effect of the treatments. In this study both, field experiment and WEPS model simulations showed that the beach sand cleaner is most effective, followed by the rotary cultivator, for the reactivation of aeolian erosion on with grey hair grass stabilised drift sands.

Excluding incoming sediment on the plots in the simulation confirmed that the excavator result in a surface in which the particles act as one layer from which individual particles are more difficult entrained by the wind. If there is loose material available it is easily transported over such surface. The bombardment with particles from outside the plot is probably the main reason for the erosion e.g. lowering of the surface, measured in the field experiment. However erosion might also occur at higher wind speeds. In practice the excavator is the most appropriate method to remove the vegetation, for instance on steep slopes. To improve the effect of this method more simulations with higher wind speeds and incoming material are needed. In addition to this the use of an extra tilling, with a harrow for instance, should be further investigated.

Excluding the effect of parameters like soil moisture in the simulation can also lead to an overestimation of the mass transport. This seems to be the case for the simulated mass transport on the plot tilled with the disk harrow.

Acknowledgements

This study was carried out as part of the research project "Making use of Wind and Water Erosion Processes in Dutch Landscape Development", carried out by the Erosion and Soil & Water Conservation Group of Wageningen University, and was funded by the Dr. Ir. Cornelis Lely Foundation, the C.T. de Wit graduate school of Product Ecology and Resource Management (Wageningen University). The field experiments were realised in co-operation with the Dutch Forestry Foundation (Staatsbosbeheer), who provided the experimental terrain and assisted with the preparation of the experimental plots. Special thanks are expressed to Dirk Goossens, Huiberdien Sweeris and Piet Peters for their assistance during the field measurements and the laboratory work.

References

Ancker, J.A.M. van den and Jungerius P.D., 2003. *De ontwikkelingsmogelijkheden van stuifzanden op de Weerterheide/Boshoverheide.* Rapport Bureau G&L in opdracht van DGW&T, ministerie van Defensie.

Bakker, T., Everts, H., Jungerius, P.D., Ketner-Oostra, R., Kooijman, A., Turnhout, C. Esselink, H., 2003. *Preadvies Stuifzanden.* Report EC-LNV No. 2003/228-0. Expertisecentrum LNV, Ministerie van Landbouw, Natuur en Voedselkwaliteit, Ede/Wageningen, the Netherlands, 114 pp.

Castel, I.I.Y., 1991. *Late Holocene eolian drift sands in Drenthe* (the Netherlands). PhD thesis, Department of Geography, University of Utrecht, 157 pp.

Cooke, R., Warren, A. and Goudie, A., 1993. *Desert Geomorphology.* UCL Press, London, UK, 526 pp.

De Ploey, J., Gabriëls, D. (1980). Measuring soil loss and experimental studies. In: *Soil Erosion* (Eds. Kirkby, M.J. and Morgan, R.P.C.). Wiley, Chichester: 63-108.

Fryrear, D.W., Saleh, A., Bilbro, J.D., Schomberg, H.M., Stout, J.E. and Zobeck, T.M., 1998. *Revised Wind Erosion Equation.* United States Department of Agriculture, Agricultural research Service, Southern Plains Area Cropping Systems Research Laboratory, Wind Erosion and Water Conservation unit. Technical Bulletin No. 1.

Goossens, D., Offer, Z.Y., 2000. Wind tunnel and field calibration of six aeolian dust samplers. *Atm. Env.* 34, 1043-1057.

Goossens, D., Offer, Z.Y., London, G., 2000. Wind tunnel and field calibration of five aeolian sand traps. *Geomorphology* 35, 233-252.

Jong, K. de, 1997. PCRaster homepage; info, software and manuals, http://www.modelkinetix.com/modelmaker/.

Jungerius, P.D., 2003. De rol van de beheerder bij het behoud van actieve stuifzanden. *Vakblad Natuurbeheer LNV* 42, 43-45.

Hagen, L.J., 1991. A wind erosion prediction system to meet user needs. *Journal of Soil and Water Conservation*, 46: 106-111.

Hagen, L.J., 1996. WEPS, USDA Wind Erosion Prediction System. Technical documentation, USDA-ARS Wind erosion research unit, Kansas, USA.

Ketner-Oostra, R., Huijsman, W., 1998. Heeft het stuiflandschap in Nederland toekomst? *De Levende Natuur* 99/7, 272-277.

Koster, E.A., 1978. *The eolien drift sands of the Veluwe (Central Netherlands) : a physical geographical study* (De stuifzanden van de Veluwe; een fysisch-geografische studie). Thesis, University of Amsterdam, 195 pp.

Koster, E.A., Castel, I.I.Y. and Nap, R.L., 1993. Genesis and sedimentary structures of late Holocene aeolian drift sands in northwest Europe. In: Pye, K. (Ed.), *The Dynamics and Environmental Context of Aeolian Sedimentary Systems*. Geological Society Special Publications 72: 247-267.

Lyles, L., Schrandt, R.L and Schneidler, N.F., 1974. How aerodynamic roughness elements control sand movement. *Trans. Am. Soc. Agr. Engnrs,* 17: 134-139.

Nickling, W.G., 1994. Aeolian sediment transport and deposition. In: Pye, K. (Ed.), 1994. *Sediment Transport and Depositional Processes*. Blackwell Scientific Publications, pp. 293-349.

Ommering, G. van, 2002. *Handleiding Subsidie Effectgerichte Maatregelen 2003*. Rapport EC-LNV 2002/160-O, Ministerie LNV, Ede-Wageningen, the Netherlands.

Riksen, M.J.P.M. and Goossens, D., submitted. Tilling Techniques to Reactivate Aeolian Erosion on Inland Drift-Sand.

Riksen, M.J.P.M. and Sweeris, H., 2003. *Voortgangsrapport Erosieonderzoek Kootwijkerzand.* Erosion and Soil and Water Conservation Group, Wageningen University, Wageningen, 23 pp.

Schimmel, H., 1975. Atlantische woestijnen. De Veluwse zandverstuivingen. *Natuur en landschap* 29: 11-44.

Spaan, W.P. and Abeele, G.D. van den, 1991. Wind borne particle measurements with acoustic sensors. *Soil Technology* 4: 51-63.

Stiboka, 1979. Bodemkaart van Nederland, Blad 33, West Apeldoorn. Toelichting bij kaartblad 33. Stiboka, Wageningen.

Visser, S.M., Sterk, G. and Karssenberg, D., 2005. Wind erosion modelling in a Sahelian environment. *Journal of Environmental Modelling and Software.* 20: 69-84.

Chapter 4

Up-scaling Wind and Water Erosion Models Far from reality?

S.M. Visser[1] & J. Palma[2]

[1] Erosion and Soil & Water Conservation Group, Department of Environmental Sciences, Wageningen University, Nieuwe Kanaal 11, NL-6709 PA Wageningen, the Netherlands; Email: Saskia.Faye-Visser@wur.nl

[2]Agroscope Fal Reckenholz Ecological Controlling Research Group Reckenholzstrasse 191, 8046 Zurich Switzerland; Email: joaopalma@fastmail.fm

Upscaling Wind and Water Erosion Models
Far from reality?

Introduction

Modeling soil erosion either by wind or water can be performed at a large range of spatial and temporal scales depending on the interest of the model users. Farmers are interested in the amount of soil losses from their fields when fields are exposed to an intensive erosion event. Policy makers are more interested in the erosion problems of a whole region over a period of e.g. 10 years when they are confronted with the creation of rural development plans. It may be clear that the outcomes of the models simulating e.g. water erosion, even though working at different scales, should be in proportion.
The erosion process is complex and can best be investigated and modeled at the time scale of one event and at the smaller field scale (Visser, 2004). However, with the further development of modeling tools to solve problems posed by policy makers, advisers and farmers, the need for models that can function at a number of different scales increases.

The need to change the scale of a model is a general problem in modeling. Here we define changing the scale as a change to the resolution of any output values from the model. Changes in scale may therefore involve changes in spatial units (from field scale (pixel size of e.g. 30 x 30 cm) to catchment scale (pixel size of e.g. 5 x 5 m) to region scale (pixel size of e.g. 1 x 1 km) or changes in temporal units (from soil loss g s^{-1} to soil loss ton y^{-1}).

When a decision is made to change the scale of a model, one of the first problems arising is the scale of the processes; which processes have sufficient impact at the new scale to be included and which process can be discarded? Krikby et al. (1996) suggest that factors critical to the erosion process vary depending on spatial scale, with different processes dominant at each hierarchal spatial level. For example, at the scale of a single erosion plot initiation and volume of overland flow are critical, whereas at catchment scale, topography, land use and soil are more important. So the models at the coarser scale may simplify or integrate over processes which were dominant at the finer scale and may add new processes which are unique for the coarser scale.
Another problem that arises when small scale models are used at larger scales is the availability of the input data. Models defining systems using accurate scientific formulas (physically based models) often require large amounts of input data which is simply not available for the larger region. In such cases model users often use mean values as an input. However a heterogeneous variable as e.g. texture may only be characterized by the mean if the models response to the mean is the same as the mean of the model responses to all possible input (Smith 1999). Zobeck et al. (2000) showed that when using different soil maps as input for a field-scale wind erosion model applied at a region-scale in Terry Country, Texas, USA, the generalized soil map had over 26% greater erosion potential than did the detailed soil map. Clearly, the reliability of the model outcomes is closely related to the accurateness of the input data.

Finally, when a physically based field-scale model is applied to the larger region-scale simulation efficiency must be maximized in order to avoid extremely long calculation times. In addition data entry would be extremely time-consuming.

In this paper the problems arising with scaling-up wind and water erosion models will be discussed. Furthermore the authors aim to raise an awareness of careful interpretation of model results. First the processes on which the up-scaling will have most impact are discussed (we assume a base model with the temporal scale of one event and the spatial scale of a field) and then the applicability and accuracy of up-scaled model is discussed.

Processes

Wind Erosivity

When upscaling a wind erosion model, two components of the wind should be taken into account; the duration of a wind erosion event and the geographic spreading of the event. When scaling up a model that predicts total wind erosion after one event to a model that predicts total erosion in e.g. one year, a number of questions arise: How many wind erosion events occur in one year?, What is the duration of the events?, What is the intensity of the events? How are the events spread throughout the year? Models like the Revised Wind Erosion Equation (RWEQ) (Zobeck et al. 2001) and the Wind Erosion Prediction System (WEPS) (Hagen 1996) make use of a wind simulator to find the answers to these questions. The WEPS requires wind speed and direction to simulate the process of soil erosion by wind and WINDGEN is the program that simulates these parameters for WEPS (Skidmore and Tatarko 1990). WINDGEN was developed especially for the use with WEPS and stochastically simulates wind direction and maximum and minimum wind speeds on a daily basis. Whenever the maximum wind speed for the day exceeds a predetermined erosion threshold, sub-daily wind speeds will be calculated. So WINDGEN predicts the number of events in a year, and WEPS starts simulating these events at the temporal scale of one event, finally WEPS sums up the erosion after all events.

For the prediction of the erosion events, WINDGEN makes use of a large database containing wind speed measurements and WEIBULL parameters (Takle and Brown 1978). This database is also used by the wind simulator of RWEQ, and the Wind Erosion Stochastic Simulator (WESS) of EPIC (the Environmental Policy Integrated Climate model) also requires a large database containing 10 minute average wind speeds and stochastic wind speeds perturbation factors (Van Pelt et al. 2004). If these erosion models are to be applied outside the USA where no databases are available, new databases should be created and this is very expensive. Furthermore the question remains: can the local climate be characterized by e.g. the stochastic WEIBULL parameters? Is the WINDGEN model able to simulate both the windy days that occur in e.g. Texas and the turbulent events that may last 10-20 minutes that occur in the Sahel?

In the case that wind erosion models are scaled up from field- to region-scale, one of the main factors that should be accounted for is the distribution of the wind speeds over the region. Especially for events such as those that occur in the Sahel where convective thunderstorms move westward through the region. Within a fully developed thunderstorm, strong vertical downdrafts occur, causing a forward outflow of cold air that creates the typical dust storms of the Sahel (Sterk 2003). These events are usually short lived, may result in intense mass transport, but are also characterized by their large spatial variation. At relatively short distances (approximately 1000 m) intensity of sediment transport may vary from 0 to 170 kg m^{-1} (pers. obs., Visser 2001). This spatial variation is related to the relative position of a site compared to the centre of the storm. Close to the centre of the storm, highest wind speeds occur, whereas further from the centre lower wind speeds are measured (Magono 1980). Thus when scaling up a field scale model to the region scale, the model 1) requires a non-homogeneous wind field and 2) should simulate the movement of the event over the region.

Water Erosivity

In water erosion two active forces are the erosive agent; rain and streaming water. The forces of either the raindrop impact or the streaming water are responsible for sediment detachment and the subsequent erosion process. When upscaling a water erosion model

two characteristics of the active forces should be taken into account: 1) the temporal aspect of rainfall and streaming water and 2) the spatial distribution of the processes.

At small scales daily, eventually hourly precipitation data is used. At larger temporal scales, monthly, eventually yearly, precipitation data is used. To tackle temporal upscaling, attempts to relate erosivity to monthly and yearly precipitation data were made (Arnoldus 1980; Foster et al. 1981; Rogler and Schwertmann 1981; Renard and Freimund 1994; Gabriels 2001). When comparing the applicability of these estimations, it can be observed how upscaling time can be an important source of error. As an example, Tomás and Coutinho (1994) comparing Foster (1981) and Wishmeier (1978) equations found doubled values for the USLE rainfall factor for the same area.

At field scale erosion by streaming water occurs in two forms: interrill and rill erosion. Interrill erosion occurs more or less uniformly over a slope segment with uniform soil and cover characteristics. At places where the interrill flow converges, rill flow and so rill erosion occurs. Simulating rill erosion at larger temporal scales brings along problems due to the temporal character of rills. The position of rill development changes between erosion events or even during a single rainfall event depending on the development of the small scale topography. As a result even at the small temporal scale it becomes extremely difficult to determine if and where rill erosion occurs. At larger temporal scales for a given hill section often an average value for rill erosion will be simulated. This value might be an over- or underestimation depending on the actual development of rills.

Regarding spatial upscaling of the erosive forces of the rain, the problem consists in the extrapolation of point measured rain data (meteorological stations) to the landscape/region. Point collected climatic is usually "spread" to be used at higher scale when data of more than one climatic station is available. This procedure involves modelling techniques (e.g. Krigging, Iverse Distance Weight) which requires spatial autocorrelation for a good spatial extrapolation (Goodchild 1986). However this autocorrelation is frequently not observed due to lack of climatic stations, creating, as a consequence, erratic spatial distributions of rain. Besides the autocorrelation, there are also some trends (e.g. topography) that need to be taken into account as they influence the distribution of climatic variables (Zimmermann and Roberts 2001). Additionally, studies of wind driven rain (Erpul *et al.* 2003; Lima *et al.* 2003) already revealed that the dynamic behaviour of a storm, with or without significant wind driven rain, passing trough a landscape, have strong effect on erosivity, which leads us to ask 1) How much error is related to these factors and 2) How can this behaviour be modelled at landscape scale and consequently 3) How real are the erosion estimations at higher scales?

Erodibility

Vegetation plays a large role in wind and water erosion processes. Vegetation reduces the erodibility of the soil by holding the soil with roots. Furthermore vegetation protects the soil from the erosive force of the rain by avoiding direct impact of raindrops and from the erosive forces of the wind by reducing the wind speed at the soil surface. Due to its high impact on erosion processes it is important that the input parameters related to vegetation are correctly scaled up.

When an erosion model requires a temporal increase in scale, an automatic consequence for the vegetation is that vegetation/crop growth needs to be accounted for. Generally crop growth simulation models are used to account for crop growth. Besides information on crop type, these models often require information on soil type, management and weather and these parameters all need to be scaled up, by using a model, in turn. In the western world, and especially in the USA, sufficient data is

available for calibrating and validating these models, in third world countries however sufficient data is lacking. Further, if one wants to simulate in a natural environment, so far not much vegetation growth models are available that can be used within an erosion model. In Africa natural vegetation is found at farmers' fields and some researchers mention the parkland system, a system in which natural vegetation is spread over the area, might be successful in protecting the soil against wind erosion (Leenders 2005). Therefore, especially for African countries a natural vegetation growth model should be created.

Generally average values for vegetation/crop cover are used when the simulation area of an erosion model is scaled up. In western management systems this is often not a problem. With the automatic sowing machines the crops are regularly distributed over a field and e.g. crop density can be represented by an average. In areas where land management is not automated, large variations in e.g crop density or crop height can be found within a field. The variations are related to local variations in e.g. soil moisture content or soil fertility. A field may have an area without cover and an area with a high crop density. Due to this variation parts of the field are highly erodible and other parts are not erodible. If the vegetation cover in such a field is represented by an average value then the predictions for soil erosion will most probably be incorrect. In order to obtain sufficient input data on the distribution of vegetation in areas where agriculture is practiced without sophisticated machines large scale mapping of the vegetation distribution is required. This is a money and time consuming exercise. Therefore the authors suggest the development of statistical models that can predict the spatial distribution of crops but also of the natural vegetation that is scattered over the cultivated area.

Soil erodibility refers to the inherent susceptibility of soil particles or aggregates to the erosive forces above mentioned. Erodibility of a soil is usually estimated on particle size distribution, organic matter, soil structure and soil permeability (Terrence *et al.* 2002). Higher spatial scales assessments deal with erodibility in a form of a discrete spatial variable: a soil map. These maps are drawn based on analytical point collected data. When a certain soil area is represented by samples of soil cores, the soil analytical figures are representative means of those soil cores, having an error associated (variance). Furthermore, this point data is considered to be homogeneous trough a whole area constrained by map lines. This has error related to data extrapolation from point to an area and that the soils have transitional properties between them, not line delimited as in a map. In addition, soil moisture conditions (an important particle cohesive force) are known to be related to topography (Pachepsky *et al.* 2001; Klik *et al.* 2003). As topography is not a discrete variable trough the landscape the drawn lines of a soil map will be even more meaningless.

Decisions in upscaling

When changing the scale of a physically based model, decisions should be made in determining which processes will still be simulated and which will be either ignored or represented by a fixed value. For instance in wind erosion at field scale it might be interesting to simulate the wind flow around a vegetation stand, whereas at a regional scale the reduction in wind speed by vegetation may be represented by an average value for a specific site. The latter results in a less physically based model, but drastically increases model speed and reduces data requirement.

Furthermore, when scaling up a model the model builder is confronted with the different temporal scales of the processes; e.g. detachment of sediment occurs when a raindrop hits the soil surface (microseconds), transport of sediment is related to the

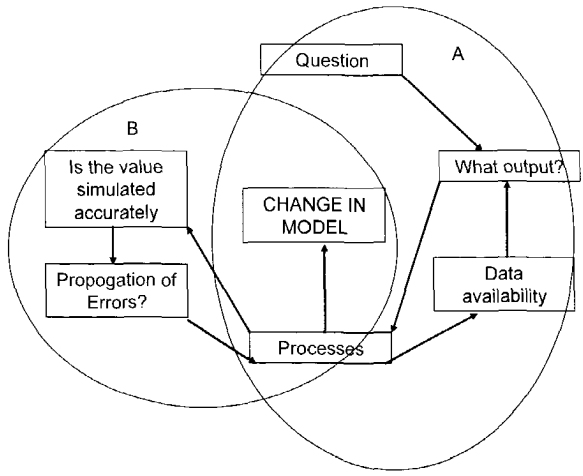

Figure 1. Procedure for determining the change in model related to a change in scale (after Smit, 1999)

stream velocity of the sediment (mm s^{-1} or m s^{-1}) and sedimentation is related to the fall velocity of the sediment (millisecond for larger particles and hours or days for suspended particles). So the following questions remain; What is the time step to be used in the upscaled-model?, and what are the consequences for the simulation of the processes that work on a larger or smaller temporal scale?

The procedure of changing the scale of a model should start with rising questions that are driving the change in scale (Fig. 1A) (Smith 1999). This results in a summation of the output values that are required to answer each question. Then all processes that provide the required information are marked. If any questions remain unanswered the model needs to be adapted to incorporate additional processes. Then two lists of 1) the available data and 2) the required data to drive the model are created. Input data that is not available is added to the list of model output values and must be produced by some parts of the model. Again the model is further adapted and this process continues until all required input values are included in the list of available data. Finally any process that influences none of the required output data represent an inefficient use of data and simulation time and can be omitted from the model.

The next stage in determining the change in model is to evaluate the accuracy of each identified output value simulated by the new model (Fig. 1B). Failure of the model can be due to error propagation through the model from the newly incorporated processes. Methods for determining the acceptable error are discussed by (Smith 1999). Having completed the sensitivity analysis the model is further optimized by omitting any processes that the sensitivity analysis suggests are redundant at the larger scale.

The above describe procedure, in which measured input data is replaced by simulated data often results in the addition of empirical relationships. These relationships make the new upscaled model less transferable, since the empirical relations may not be valuable in another region.

Applicability of up-scaled models

From the previous sections we can conclude that applying an upscaled model brings along a certain error. However, the error can be minimized if the upscaled model meets certain requirements.

First of al the user of the upscaled model should have information on the initial scale of the model and he should know what assumptions are made for upscaling the process. Second the user requires information on the input data, What is the measurement error?; At which scale are the measurements performed?; and if necessary How where the measurements upscaled?; Are the input data simulated and if so with what model and what is the measurement error of the model?

Further, information on the calibration of the upscaled model is necessary and finally a sensitivity analysis of the upscaled model should be performed. These last two procedures are important steps, though are often forgotten. However since the impact of the various processes is variable at different scales information on error propagation is required.

Uncertainty analysis of the application of an upscaled model is frequently disregarded, e.g.(Mongkolsawat et al. 1994; Van der Knijff et al. 2000) due to some simplicity of models associated with high temptation/need to apply these models to evaluate higher scales. Consequently the misuse of the correct scale for where the model was designed, leads to a careful interpretation of the quantitative results (Wischmeier 1976). However when comparing different scenarios in land use the relative results of an upscaled model are still a valuable source of information because, although the error is present, it is present in equal proportion in both (or more) scenarios and the final result can be comparable in its relative terms.

References

Arnoldus, H. (1980). An approximation of the rainfall factor in the Universal Soil Loss Equation. *Assessment of Erosion*. M. De Boodt, Gabriels, D. Chichester, John Wiley & Sons: 127-132.

Erpul, G., L. Norton, et al. (2003). "The effect on wind on raindrop impact and rainsplash detachment." *Transactions of the ASAE* 45: 51-62.

Foster, G., D. McCool, et al. (1981). "Coversion of the USLE to SI metric units." *Journal of Soil and Water Conservation* Nov-Dec: 355-359.

Gabriels, D. (2001). Rainfall erosivity in Europe. Third International Congress Man and Soil at the Third Millennium, Valencia, Spain, European Society for Soil Conservation.

Goodchild, M. F. (1986). *Spatial Autocorrelation*. Norwich, Catmog 47, Geo Books.

Hagen, L. J. (1996). WEPS, USDA Wind Erosion Prediction System. Technical documentation. Kansas, USA., USDA-ARS Wind erosion research unit.: http://www.weru.ksu.edu.

Klik, A., W. Jester, et al. (2003). Soil Hydrologic conditions along a hillslope and their effects on runoff and erosion. 25 Years of Assessment of Erosion - International Symposium, Ghent - Belgium, International Center for Eremology - University of Ghent.

Krikby , M. J., A. C. Imeson, et al. (1996). "Scaling up processes and models from the field plot to the watershed and regional areas." Journal of Soil and Water Conservation 51: 391-396.

Leenders, J. K. (2005). Wind erosion protection by dispersed trees and shrubs in the Sahelian zone of Burkina Faso. Erosion & Soil and Water Conservation. Wageningen, Wageninegn University.

Lima, J., V. Singh, et al. (2003). "The influence of storm movement on water erosion. Storm direction and velocity effects." Catena 52: 39-56.

Magono, C. (1980). *Thunderstorms*. Amsterdam, The Netherlands, Elsevier.

Mongkolsawat, C., P. Thirangoon, et al. (1994). Soil Erosion Mapping with Universal Soil Loss equation and GIS. 15th Asian Conference on Remote Sensing, Bangalore, India, Gisdevelopment.net.

Pachepsky, Y. A., D. Timlin, et al. (2001). "Soil water retention as related topographic variables." *Soil Science Society of America Journal* 65: 1787-1785.

Renard, K. G. and J. R. Freimund (1994). "Using Monthly Precipitation Data to Estimate the R-Factor in the Revised USLE." *Journal of Hydrology* 157: 287-306.

Rogler, H. and U. Schwertmann (1981). Erosivität der Niederschläage und Isoerodentenkarte Bayerns. *Zeitschrift für Kulturtechnik und Fluerbereinigung*. 22: 99-112.

Skidmore, E. L. and J. Tatarko (1990). "Stochastic wind simulation for erosion modelling." *Transactions of the ASAE* 33: 1893-1899.

Smith, J. U. (1999). Models and Scale: Up- and Down-Scaling. *Data and models in action*. F. W. T. Penning de Vries: 81-98.

Sterk, G. (2003). "Causes, consequences and control of wind erosion in Sahelian Africa: A review." *Land Degradation & Development* 14: 95-108.

Takle, E. S. and J. M. Brown (1978). "Note on the use of Weibull statistics to characterize wind speed data." *Journal of applied Meteorology* 17: 556-559.

Terrence, J., G. Foster, et al. (2002). Soil Erosion: Processes, Prediction, Measurement and Control. New York, John Wiley & Sons.

Tomás, P. and M. Coutinho (1994). Comparison of observed and computed soil loss, using USLE. *Conserving Soil Resources.* R. J. Rickson. Walingford, CAB International.

Van der Knijff, J. M., R. J. A. Jones, et al. (2000). Soil erosion Risk Assessment in Europe, European Commision. European Communities.

Van Pelt, R. S., T. M. Zobeck, et al. (2004). "Validation of the winderosion stochastic simulator (WESS) and the revised wind erosion equation (RWEQ) for single events." *Environmental Modelling and Software* 19: 191-198.

Visser, S.M., Sterk, G. and Snepvangers, J.J.C. 2004. Spatial variation in wind-blown sediment transport in geomorphic units in northern Burkina Faso using geostatistical mapping. *Geoderma* 120: 95-107.

Wischmeier, W. H. (1976). "Use and Misuse of Universal Soil Loss Equation." *Journal of Soil and Water Conservation* 31: 5-9.

Wishmeier, W. and D. Smith (1978). Predicting rainfall erosion losses - a guide to conservation planning. Agriculture Handbook No. 537, US Department of Agriculture.

Zimmermann, N. E. and D. W. Roberts (2001). Final report of the MLP climate and biophysical mapping project. Birmensdorf, Switzerland, WSL: 18.

Zobeck, T. M., N. C. Parker, et al. (2000). "Scaling up from field to region for wind erosion prediction using a field-scale wind erosion model and GIS." Agriculture, Ecosystems and Environment 82: 247-259.

Zobeck, T. M., S. Van Pelt, et al. (2001). Validation of the Revised Wind Erosion Equation. Soil Erosion Research for the 21st century, Honolulu, USA, American Society of Agricultural Engineers (ASAE).

Chapter 5

The Role of Crust Formation in the Interaction Between Wind and Water Erosion in the Sahel

S.M. Visser[1] & J.K. Leenders[1]
[1] Wageningen University, Erosion & Soil and Water Conservation Group
Nieuwe Kanaal 11, 6709PA Wageningen; Email: Saskia.Faye-Visser@wur.nl

The Role of Crust Formation in the Interaction Between Wind and Water Erosion in the Sahel

Abstract
Sahelian soils are characterized by their susceptibility to crust development. Crust type and structure are amongst others influenced by erosion and deposition of sediment by wind and water. But in return the development of surface crusts has a large effect on the processes of wind and water erosion.
First a description of the various crust types that occur in the Sahel is given. Then the roles of crust formation on wind and water erosion and vice versa are discussed. Finally it is concluded that given the large influence of soil crusting on the processes of wind and water erosion in the Sahel, these processes can only b e correctly simulated if the process of crust development is added to the erosion model. Parameters that should be incorporated in the crust submodel are: the availability of loose sediment, the change in infiltrability during the development of a soil crust, the changing distribution of the crust types and the change in crust thickness and crust strength.

Introduction

Crusting of soil surfaces under influence of (high intensity) rainfall is a worldwide phenomenon (e.g. Stolte *et al.*, 1997; Valentin and Bresson, 1992). The Sahelian soils are especially vulnerable for crust development due to their sandy or sandy-loam texture. Hence crusts and crust like features are omnipresent characteristics of Sahelian soils (D'Herbes and Valentin, 1997).

The type and structure of soil crusts are influenced by soil texture, kinetic energy of rain, erosion and deposition of sediment by wind and water and vegetation cover. The spatial distribution of the crusts is further controlled by terrain position, micro-relief and impact of wind. In the Sahel, processes starting with the formation of a soil crust are proceeded by reduced infiltration and water erosion followed by reduced plant cover and, in the case of agricultural land, reduced yields (Hoogmoed and Stroosnijder, 1984; Valentin, 1995b). Crust development has a large influence on the agricultural production potential in the Sahel and therefore it is important to correctly understand the processes related to crust formation.

Crusts are usually formed during the short rainy season (June-September) during which intensive rainfall is often preceded by wind erosion events. Further development of the crust occurs during the dry Harmattan season (October till May) under influence of the wind, termite activities and human activities (Graef and Stahr, 2000). At the onset of the following rainy season the crust is dry, has reached its optimal strength and has a minimal infiltration capacity (provided that it is not damaged by human or animals activities). The high intense rainfalls of the early rainy season can scarcely infiltrate and a large portion flows over the surface as runoff, causing erosion. Thus crust development has a major implication for runoff and hence on both soil moisture and soil material distribution on field- and watershed-scale (D'Herbes and Valentin, 1997). Furthermore, due to the effect of crust formation on the soil material distribution and the strength of the soil surface, crust formation directly affects the sediment availability for wind erosion.

Clear, crust formation changes the surface characteristics of the soil and so wind and water erosion in the Sahel are highly affected by the presence of a soil crust. So far an extended amount of research has been performed on the effect of one specific crust on either infiltration (Collinet and Valentin, 1985; Hoogmoed and

Stroosnijder, 1984), water erosion (Stolte *et al.*, 1997) or wind erosion (Chepil, 1953; Rajot *et al.*, 2003; Zobeck, 1991a). However, in the Sahel the processes of wind and water erosion both cause significant soil erosion and occur almost simultaneously at the same location (Visser *et al.*, 2004). Furthermore, crust formation does not only affect wind and water erosion; the processes of wind and water erosion affect the surface characteristics of the crust in return. Therefore, in the Sahel the role of crust formation on the interaction between wind and water erosion cannot be regarded without discussing the effect of the combined wind and water erosion processes on crust formation.

The aim of this paper is to describe the role of crust formation in the interaction between wind and water erosion and vice versa. The paper starts with a classification of the various types of crusts that are present in the Sahel. Then the role of wind and water erosion in the development of surface crusts and the effect of these crusts on the processes of wind and water are discussed. Based on the discussion we will finally define the consequences for soil erosion modeling.

Crust Classification

In an attempt to organize the knowledge of soil crusting processes and to group soil crusts on basis of common morphological features and physical properties Valentin and Bresson (1992) developed a classification system for surface crusts formed by rainfall on loamy sandy soils as are often found in the Sahel. Three main classes of crust were distinguished: Structural, erosion and depositional crust. Each of these classes is subdivided in subclasses. Here we will briefly describe the most important crust types that are common in the region of interest, according to the classification of Valentin and Bresson (1992).

Structural crust

Structural crusts are characterized by in situ rearrangement of particles without a distinct evidence of lateral movement. Four main subtypes are distinguished morphologically and named after their dominant forming process: slaking crust, infilling crust, coalescing crust and sieving crust. The sieving crust is the most common crust type in the sandy loamy soils of the Sahel (Fig. 1A). It consists of a layer of loose skeleton grains overlaying a plasmic layer. In its most advanced form it consists of three well-sorted layers. The upper layer is composed of loose, coarse grains, the middle one consists of fine densely packed grains with vesicular voids and the lower (plasmic) layer shows a high content of fine particles with considerably reduced porosity (Valentin and Bresson, 1992). Sieving crusts develop as a result of water drop impact and the downward translocation of the finest particles by the percolating water. The fine particles accumulate and form the plasmic layer at a depth which is related to the depth of reduced porosity due to compaction by raindrop impact (Valentin, 1991).

A particular form of the sieving crusts is the coarse pavement crust (Fig.1B). In this type of crust, coarse fragments are embedded in a crust, with a microstructure similar to sieving crust. Coarse pavement crusts commonly occur in arid and semi-arid areas (Figueira and Stoops, 1983), but so far little information is available on the processes involved in the formation of these crusts. Differences in texture between the top- and sub-soil suggest that surface material consists of wind deposited particles, which have subsequently been subjected to processes similar to those for the formation of sieving crusts (Valentin and Bresson, 1992).

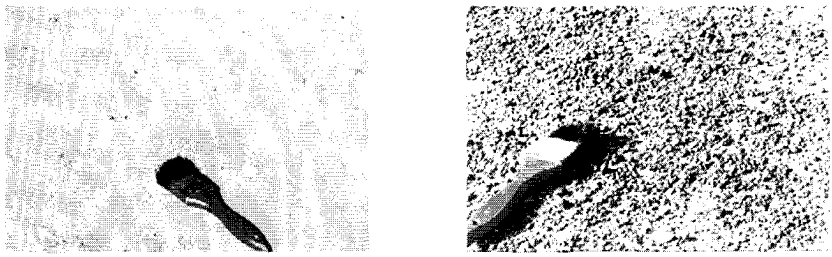

Figure 1. Two types of structural sieving crusts commonly found in the Sahel A) Structural sieving crust, B) Coarse pavement crust

Erosion crust

Erosion crusts consist of only one rigid, thin and smooth surface layer enriched in fine particles (Fig. 2). They result from erosion of slaking or sieving crusts and may be strengthened by certain algae or fungi. Due to the lack of pores and voids in the plasmic layer infiltrability is extremely low.

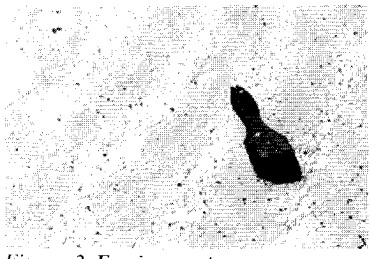

Figure 2. Erosion crust

Depositional crust

Depositional crusts are characterized by sediment sorting. Two types of depositional crusts exist: the runoff depositional crust (Fig. 3A) and the still depositional crust (Fig. 3B). Runoff depositional crusts form after a rainfall event whereby runoff occurs. They are characterized by a microbedded layer and often overlay structural crusts. Runoff transport-capacity and disjunction between fine and coarse particles induce alternating submillimetric microbeds which have a contrasting texture and are unconformable with the underlying layer (Valentin and Bresson, 1992).

Still depositional crusts develop in standing water, where surface flow is hindered. They consist of densely packed and well-sorted particles, with increasing size with depth. When dry, these crusts often break up into curled-up plates (Fig 3B). Still depositional crusts often form in puddles where the larger grains sink rapidly to the bottom and the finer grains deposit more slowly and form the top layer (Valentin and Bresson, 1992).

The role of wind and water erosion in crust formation

The effect of wind and water erosion on the process of crust formation varies with the texture of the soil, the local topography and the intensity of the erosion processes and is therefore not univocal. To obtain an impression of the possible impact of the erosion processes on crust formation we discuss here an example as described by Rajot and Valentin (2001). In the countryside of Niamey, Niger, the dynamics of the fine sediments play a key role in the distribution of fertility and crust formation in the traditional cultivation systems. The traditional cultivation system alternates periods

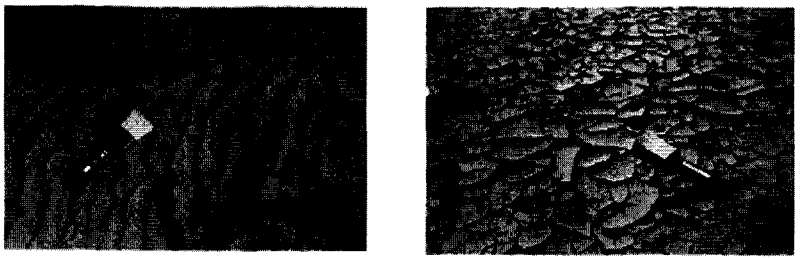

Figure 3. Two types of depositional crusts often found in the Sahel A) Runoff depositional crust B) A dry still depositional crust

with cultivation with periods of fallow. With an annual rainfall of approximately 500 mm, aeolian dynamics are closely related to the cultivation practices. Only the cultivated fields, stripped from their vegetation cover, are erodible. The fallow areas are generally sufficient covered so that no wind erosion, but deposition of wind-blown sediment takes place. Hence, the fields are a source of fine particles and the fallow areas are a sink (Rajot, 2001). Furthermore, the studied soils, which contain small amounts of silt and clay (approximately 3% at the top-soil), are extremely sensitive for small variations in fine particle content. With a small increase in fine particle content, the soils will undergo crust formation. First structural crusts will develop and infiltration will be reduced. So runoff percentages will increase and water erosion will occur, resulting in the development of erosion crust, runoff depositional crusts and still depositional crust. This process can be observed in the fallow areas (Ambouta *et al.*, 1996).

In the cultivated fields the opposite will occur. With a reduction of the fine particle contents, crust formation will no longer take place. This process is observed at fields, which have continuously been cultivated for a period longer than10 years. (De Rouw and Rajot, in press). This disappearance of soil crusts allows a better infiltration, but also involves a reduced soil fertility and lessivage. Furthermore, at the early rainy season, when most intense wind erosion events occur, the soil is no longer protected by the crust and so more vulnerable for wind erosion.

The effect of soil crusts on wind and water erosion

It is well known that soil crusting is a significant factor in the susceptibility of surface particles to be entrained by the wind (Lyons *et al.*, 1998). Chepil (1953) estimated that the erosion rate at a crusted soil is approximately 6-60% smaller than the erosion rate at freshly cultivated fields and Zobeck, (1991a) showed that crusted soils effectively reduce total soil erosion under various abrading circumstances. Belnap and Gillette (1998) showed that the threshold friction velocities for wind-blown sediment transport increased with a factor 10 on soils with a well-developed biological crust compared with a non-crusted sandy soil. However, (Rajot *et al.*, 2003) showed that a sieving crust formed at a soil with a fine-particle content lower than 3% does not protect agricultural soils from wind erosion.

The intensity of sediment transport by wind is generally highly variable even at the scale of one field (Sterk and Stein, 1997; Visser *et al.*, 2004). Visser *et al.* (2005) showed that in absence of a vegetation cover, the variation in sediment transport can be explained by the occurrence of the different crust types. Furthermore, Goossens, (2004) showed that in determining the effect of crusts in relation to wind erosion, crust strength is the most important parameter. The crust strength varies due

to the strong seasonal dynamics in crust formation at cultivated fields and therefore the impact of the different crust types on wind erosion is variable trough time.

In the Sahel, two distinct periods during which wind-blown sediment transport occurs can be distinguished. During the dry period (October till May) the northeastern Harmattan winds dominate. These winds originate from the Sahara desert and transport large amounts of fine sediments and nutrients. Though parts of the nutrient enriched sediment are deposited in the Sahel, Harmattan winds may result in moderate wind erosion (Michels *et al.*, 1995). After harvesting, the cultivated fields are generally covered with a structural crust and some mulch. During the dry season the mulch coverage is generally eaten by the free-roaming animals and the surface crusts dry and increase in strength. During the moderate-severe wind erosion events that occur in the Harmattan season, the loose sediment on top of the structural crusts is eroded and the plasmic layer is exposed. This type of crust is called erosion crust and increases in strength during the dry season. So during the Harmattan season sediment transport by wind becomes sediment limited due to the development of surface crusts. However, at soils with a fine-particle content < 3%, this exposure of the plasmic layer does not occur, as the strength of the plasmic layer in these soils is limited. When this plasmic layer is exposed to the scouring sand grains the layer is ruptured (Rajot *et al.*, 2003). Therefore crust development does not limit wind erosion at fields with a soil with a fine-particle content <3%. The only way to minimize nutrient losses from these soils is to limit saltation (e.g. by applying mulch).

At the onset of the rainy season, which is the second and most important wind erosion period, wind erosion at several fields is limited by sediment availability. In the early rainy season high intensity rainfall is often preceded by strong winds (Casenave and Valentin, 1989; Shao, 2000). These wind erosion events usually last from a few minutes up to one hour (Rajot, 2001; Sterk, 2003). After the first rainfalls farmers start sowing and approximately two weeks after sowing the surface crust is broken by cultivation practices. At this moment the soil is not yet sufficiently covered by the crop and the loose soil is extremely vulnerable for wind erosion at this moment. Depending on the intensity and the distribution of the rainfall, it takes 1 to 4 weeks for the crust to redevelop and even then the crust has not yet reached its maximum strength. The intense rainfall, which often directly follows the wind erosion event, causes partial deposition of the raised dust and limits further wind erosion, but may result in detachment of large amounts of sediment even from the freshly developed crusts. Due to the general low slopes in the Sahel, large amounts of the sediment detached by water erosion are locally deposited and become available for wind-blown sediment transport during the next wind erosion event (Visser *et al.*, 2004).

Several researchers have investigated the impact of soil crusting on water erosion (Hoogmoed and Stroosnijder, 1984, Boiffin and Bresson, 1987; Chow *et al.*, 1988; Govers, 1991; Graef and Stahr, 2000; Visser *et al.*, 2004). The formation of a seal or a crust at the soil surface alters the way water is partitioned at the soil surface, resulting in decreased infiltration and increased overland flow (Bristow *et al.*, 1994).

Despite all the research performed, uncertainties still exists on the behaviour of soil crusts and particularly on their effect on infiltration and runoff. Due to the fact that the various crust types develop under influence of a variety of processes e.g.1) the impact of raindrops, 2) the erosive forces of wind and water, 3) deposition processes and 4) the reorientation of particles induced by mechanical and/or chemical dispersion, soil crusts do not tend to form homogeneously over a specific soil unit. Therefore the hydraulic properties of the crusts vary in space, and under continuous development they vary in time as well. Therefore, the effect of a soil crust on runoff

generation and soil loss in a catchment may vary depending on the spatial distribution of crusted and non-crusted areas and the possible occurrence of shrinkage cracks within the crusted layer (Govers, 1991).

Generally it is believed that processes beginning with the formation of soil crusts precede to runoff and an increase in soil losses through erosion. However, the effect of crust formation on soil loss might be reversed, as the soil strength increases during soil crust formation.

The early rainy season is the period during which most water erosion occurs in the Sahel. At the onset of the rainy season, the soils of the cultivated fields are generally covered with a strong erosion crust. During the first minutes of the rainfall event, water erosion is thus limited by sediment availability. But the first rains of the season generally come with strong winds (Casenave and Valentin, 1989), which increase the kinetic energy of the raindrops and therefore the impact force (Pedersen and Hasholt, 1995). The raindrops smashing on the crust are able to detach sediment from the crust, which becomes available for transport. Due to the generally small slopes in the Sahel of western Africa, sediment transport by runoff is limited by the transport capacity. So a large percentage of the detached sediments are locally deposited and available for wind erosion (Visser *et al.*, 2004).

In the above described case, water erosion facilitates wind erosion and the combination of the two processes results in the loss of fertile soil and finally a reduced crop growth. However, in arid and semi-arid regions, crust formation and the following erosion processes are not necessary unprofitable for crop growth. Farmers in Burkina Faso, Cape Verde, Niger and Libya convey water from crusted areas to small basins made from earth mounds, with a height of a few tens of centimetres and shaped into a V or a half-circle (Bruins *et al.*, 1986). In these areas the fertile water eroded sediment is accumulated, water storage is increased and seedlings are protected against wind erosion by the earth mounds (Reij *et al.*, 1988).

Consequences for soil erosion modeling

Given the large influence of soil crusting on the processes of wind and water in the Sahel and vice versa, one can only conclude that the process of soil crusting should be accounted for in the various available wind and water erosion models. At the onset of soil erosion modeling, e.g. in the USLE or WEQ, crusts were not considered because they were transitory. Today however, soil erosion is often estimated on event base and detailed information is needed to run the model (Zobeck, 1991b). If soil crusts are considered in these event-based models, they are generally characterized by rigid values, whereas especially during a rainfall event, crust characteristics are subject to major changes (Visser *et al.*, 2004). Therefore wind and water erosion models should not only account for the crust characteristics of the present crust type, but these characteristics should be updated during the event simulation. This can be done by adding a crusting sub-model to the existing model. Several factors that should be incorporated in such a crust model are:

- The availability of loose sediment
- The changing infiltrability during the formation of a soil crust
- The changing distribution of the various crust types
- The changing crust thickness
- The increase in crust strength with the drying of the crust

In the Wind Erosion Prediction System (WEPS) (Hagen, 1991) some of these characteristics (availability of loose sediment and crust thickness) are updated after

each time step but other characteristics are not accounted for. The process of soil crusting can easily be added to erosion models that are currently available. If the crust type is defined the crust characteristics that are needed as model input are easily predicted from the crust types (Valentin, 1995a).

References

Ambouta, J.M.K., Valentin, C. and Laverdière, M.R., 1996. Jachères et croûtes d'érosion au Sahel. *Sécheresse*, 7: 269-275.

Belnap, J. and Gillette, D.A., 1998. Vulnerability of desert biological soil crusts to wind erosion: the influences of crust development, soil texture and disturbance. *Journal of Arid Environments*, 39: 133-142.

Boiffin, J. and Bresson, L.M., 1987. Dynamique de formation des croûtes superficielles: raport de l'analyse microscopique. In: N. Fedoroff, L.M. Bresson and M.A. Courty (Editors), *Micromorphologie des sols*. A.F.E.S., Plaisir, pp. 393-399.

Bristow, K.L., Smetten, K.R.J. and Ross, P.J., 1994. Water entry into sealing, crusting and hardsetting soils: A review and illustrative simulation study. In: H.B. So, G.D. Smith, S.R. Raine, B.M. Schafer and R.J. Loch (Editors), *Sealing, crusting and hardsetting soils: productivity and conservation*. Australian Society of Soil Science Inc., Brisbane, Australia., pp. 183-203.

Bruins, H.J., Evenari, M. and Nessler, U., 1986. rainwater harvesting agriculture for food production in arid zones: The callenge of the African famine. *Applied Geography*, 6: 13-33.

Casenave, A. and Valentin, C., 1989. Les États de surface de la zone Sahélienne: l'influence sur l'infiltration. Orstom, Paris, 229 pp.

Chepil, W.S., 1953. Factors that influence clods structure and erodibility of soil by wind: I Soil texture. *Soil Science*, 75: 473-483.

Chow, V.T., Maidment, D. and Mays, L.W., 1988. Applied hydrology. McGraw-Hill Book Co, Singapore, 571 pp.

Collinet, J. and Valentin, C., 1985. Evaluation of factors influencing water erosion in West Africa using rainfall simulation. Challenges in African Hydrology and water Resources.(IAHS publ. 144): 451-461.

De Rouw, A. and Rajot, J.L., in press. Soil organic matter, surface crusting and erosion in Sahelian farming systems based on manuring or fallowing. *Agriculture, Ecosystems, Environment*.

D'Herbes, J.M. and Valentin, C., 1997. Land surface conditions of the Niamey region:ecological and hydrological implications. *Journal of hydrology*, 188-189: 18-42.

Figueira, H. and Stoops, G., 1983. Application of micromorphometric techniques to the experimental study of vesicular layer formation. *Pedology*, 223: 77-89.

Goossens, D., 2004. Effect of soil crusting on the emission and transport of wind-eroded sediment: Field measurements on loamy sandy soil. *Geomorphology*, 58: 145-160.

Govers, G., 1991. A field study on topographical and topsoil effects on runoff generation. *Catena*, 18: 91-111.

Graef, F. and Stahr, K., 2000. Incidence of soil surface crust types in Semi-arid Niger. *Soil & Tillage research*, 55: 213-218.

Hagen, L.J., 1991. A wind erosion prediction system to meet user needs. *Journal of soil and water conservation*, 46: 106-111.

Hoogmoed, W.B. and Stroosnijder, L., 1984. Crust formation on sandy soils in the Sahel. *Soil Tillage Research*, 4: 5-23.

Lyons, W.F., Munro, R.K., Shao, Y. and Leslie, L.M., 1998. Broad scale wind erosion model for environmental assessment and management. *Advances in Ecological Sciences*, 1: 275-294.

Michels, K., Sivakumar, M.V.K. and Allison, B.E., 1995. Wind erosion control using crop residue I. Effects on soil flux and soil properties. *Field crops Research*, 40: 101-110.

Pedersen, H.S. and Hasholt, B., 1995. Influence of wind speed on rain splash erosion. *Catena*, 24: 39-54.

Rajot, J.L., 2001. Wind blown sediment mass transport of Sahelian village land units in Niger. *Bulletin de la Societé Géologique de France*, 172: 523-531.

Rajot, J.L., Afaro, S.C., Gomes, L. and Gaudichet, A., 2003. Soil crusting on sandy soils and its influence on wind erosion. *Catena* 53:6-19

Rajot, J.L. and Valentin, C., 2001. Wind eroded versus deposited mineral dust: a mass budget for a sahelian village land unit in Niger. In: J.C. Ascough and D.C. Flanagan (Editors), *Soil erosion research for the 21st century*. American Society of Agricultural Engineers (ASAE), Honolulu, USA., pp. 404-407.

Reij, C., Mulder, P. and Begermann, L., 1988. Water harvesting for plant production., World Bank, Technical paper, no 91.

Shao, Y., 2000. Physics and modelling of wind erosion. Kluwer Academic, Dordrecht, 393 pp.

Sterk, G., 2003. Causes, consequences and control of wind erosion in Sahelian Africa: A review. *Land Degradation & Development*, 14: 95-108.

Sterk, G. and Stein, A., 1997. Mapping wind-blown mass transport by modeling variability in space and time. *Soil science society of America journal*, 61(1): 232-239.

Stolte, J., Ritsema, C.J. and De Roo, A.P.J., 1997. Effects of crust and cracks on simulated catchment discharge and soil loss. *Journal of Hydrology*, 195: 279-290.

Valentin, C., 1995a. Links between wind and water erosion in semi-arid systems. In: U.E.P.A.E.r. Laboratory (Editor), Erosion under global change-GCTE, Corvallis, Oregon.

Valentin, C., 1995b. Sealing crusting and hardsetting soils in Sahelian agriculture. In: H.B. So (Editor), Sealing, crusting and hardsetting soils: Productivity and Conservation. Australian Society of Soil Sciences, Brisbane, Australia, pp. 53-76.

Valentin, C. and Bresson, L.M., 1992. Morphology, genesis and classification of surface crusts in loamy and sandy soils. *Geoderma*, 55: 225-245.

Visser, S.M., Sterk, G. and Karssenberg, D., 2004. Modelling water erosion in the Sahel; application of a physical model on a gentle sloping area. *Earth Surface Processes and Landform.* in press

Visser, S.M., Sterk, G. and Karssenberg, D., 2005. Wind erosion modelling in a Sahelian environment. *Journal of environmental modelling and software*. 20: 69-84

Visser, S.M., Sterk, G. and Ribolzi, O., 2004. Techniques for simultaneous quantification of wind and water erosion in semi-arid zones. *Journal of Arid Environments*.59: 699-717

Visser, S.M., Sterk, G. and Snepvangers, J.J.J.C., 2004. Spatial variation in wind-blown sediment transport in geomorphic units in northern Burkina Faso using geostatistical mapping. *Geoderma*, 120: 95-107.

Zobeck, T.M., 1991a. Abrasion of crusted soils: Influence of abrader flux and soil properties. *Soil science society of America journal*, 55: 1091-1097.

Zobeck, T.M., 1991b. Soil properties affecting wind erosion. *Journal of soil and water conservation*, 46(2): 112-118.

Chapter 6

Effect of Wind on Runoff

G. Erpul[1], D. Gabriels[2] & D. Norton[3]
[1] Faculty of Agriculture, Department of Soil Science, University of Ankara, 06110 Diskapi – Ankara, Turkey phone: + 90 (312) 317 0550; fax: + 90 (312) 317 8465; Email: erpul@agri.ankara.edu.tr
[2] Department of Soil Management and Soil Care, Ghent University, Coupure Links 653, B 9000 Ghent, Belgium.
[3] USDA – ARS National Soil Erosion Research Laboratory, 1196 SOIL Bldg., Purdue University, West Lafayette, IN, 47907 – 1196, USA.

Effect of Wind on Runoff

Abstract

By changing roughness induced by raindrop impacts with an angle on flow and the rainsplash trajectories of soil particles within flow, wind velocity and direction affects shallow flow hydraulics in wind-driven rains. A wind-tunnel study under wind-driven rains was performed to assess the effects of horizontal wind velocity and direction on sediment transport by the raindrop-impacted shallow flow. Windless rains and the rains driven by horizontal wind velocities of 6, 10, and 14 ms^{-1} were applied to three agricultural soils packed into a 20 by 55 cm soil pan placed both windward and leeward slopes of 7, 15, and 20%. During each rainfall application, sediment and runoff samples were collected at 5-min intervals at the bottom edge of the soil pan with wide-mouth bottles and were determined gravimetrically. Based on the interrill erosion mechanics, raindrop impact pressure (Γ) as a rainfall parameter and product of unit discharge and slope in the form of $q^b S_o^c$ as a flow parameter were used to explain the interactions between impact and flow parameters and sediment transport (q_s). Flow depth was calculated from the measured discharge and slope using the Darcy-Weishbach friction coefficient (f). The results of flow depth indicated that the ratios of mean drop size to the flow depth (d_{50}/y) were always greater than unity and ranged from 2.13 to 6.37 and from 1.89 to 11.86 for windward and leeward slopes, respectively. Although, within these ranges, soil detachment by shallow waterflow was assumed minimal, and a large raindrop effect on detachment was expected, statistical analysis of power law models showed that Γ had much smaller exponent values when compared to those of q and S_o, indicating that flow parameters better explained the variations in the sediment transport. Further analysis of the Pearson correlation coefficients between Γ and qS_o and q_s also showed that wind velocity and direction significantly affected the hydraulic roughness, and f, which didn't account for wind effects on roughness, resulted in unrealistic flow depth calculations in windward slopes where not only reverse within-flow particle trajectories but also reverse lateral raindrop stress with respect to the shallow flow direction occurred.

Introduction

The basic processes of raindrop-impacted shallow flow are detachment by raindrop impact and transport by overland flow. Given generally shallow depths of overland flow, detachment by the flow is often of minor importance for interrill erosion (Foster, 1982), and therefore, interrill detachment is considered to be mainly due to the raindrop impact. As a result of rainsplash of soil particles within shallow flow, raindrop-impacted overland flow can transport soil particles in the flow direction even if there is very thin flow. This process differs from the transport by both overland flow without raindrop impact and rill flow, which must attain a critical velocity to set soil particles in motion.

Overland flow under rainfall is governed by the laws of conservation of mass and momentum (Chow, 1959). The continuity equation of flow is derived from the condition that the net influx of mass through the control surface equals the rate of increase inside the control volume, and for the case of steady overland flow, it reduces to:

$$q = u_f y \qquad \text{[Eq. 1]}$$

where, q is the lateral inflow rate (unit discharge), y is the flow depth, and u_f is the mean flow velocity. Similarly, the kinematic wave approximation (momentum

equation), for steady-uniform flow, states that the friction slope (S_f) is the same as the channel bottom slope (S_0) or the soil surface slope:

$$S_o = S_f \qquad \text{[Eq. 2]}$$

By using the kinematic wave equation and existing open channel flow friction equations the sediment discharge (q_s) may be estimated by an empirical power function of the flow velocity, or the flow depth only:

$$q_s = \chi y^m \qquad \text{[Eq. 3]}$$

where χ and m are empirical constants whose values depend upon the sediment properties. The parameter m is related with type of flow, and χ will be given a physical interpretation reflecting the effects of surface slope, raindrop impact, wind and hydraulic roughness on the depth of flow.

The Darcy-Weisbach friction coefficient has been widely used to describe raindrop-induced flow resistance (Shen and Li, 1973; Julien and Simons, 1985; Gilley et al., 1985; Katz et al., 1995):

$$S_f = \frac{f}{8}\frac{u_f^2}{gy} \qquad \text{[Eq. 4]}$$

where, f is the Darcy-Weisbach friction coefficient, and g is the gravitational acceleration. By equation 2, equation 4 is solved for y:

$$y = \frac{f}{8}\frac{u_f^2}{gS_0} \qquad \text{[Eq. 5]}$$

The friction coefficient is a function of the Reynolds number (R_e) and the relative roughness for turbulent flows. R_e is defined as:

$$R_e = \frac{u_f y}{\nu_*} \qquad \text{[Eq. 6]}$$

where, ν_* is the kinematic viscosity of water. The friction factor for laminar flow is found to increase with increasing rainfall intensity and to decrease with increasing R_e (Shen and Li, 1973; Katz, et al., 1995). Generally, in laminar flows with raindrop impact, the f is assumed to be the sum of the friction coefficient due to raindrop impact (f_r) and the friction coefficient without rainfal 1 (f_0):

$$f = f_r + f_0 \qquad \text{[Eq. 7]}$$

where, $f_r = k_r/R_e$ and $f_0 = k_0/R_e$. Shen and Li (1973) developed the following equation for smooth surfaces from experiments on the effect of rainfall on k_r:

$$k_r = bI^c \qquad \text{[Eq. 8]}$$

where, I is the rainfall intensity and b and c are regression parameters. For laminar flow over smooth surfaces $k_0 = 24$ (Chow, 1959). When these assumptions are applicable, in flows with raindrop impact the friction factor can be expressed as:

$$f = \frac{k_o + bI^c}{R_e} \qquad \text{[Eq. 9]}$$

Shen and Li (1973) and Katz et al. (1995) determined values for the regression coefficients shown in equation 9. For rainfall intensities reported in mm h^{-1}, values of b and c are given as 7.21 and 0.41, respectively. Under steady state conditions with equation 1, the following relation of determining flow depth is obtained:

$$y = \left[\left(\frac{k_o + bI^c}{8gS_o}\right)\nu * q\right]^{1/3} \qquad \text{[Eq. 10]}$$

Julien and Simons (1985) investigated the applicability of several sediment transport equations under different hydraulic conditions and suggested the following equation for a general transport capacity:

$$q_s = \alpha S_o^{\beta} q^{\gamma} I^{\delta} \qquad \text{[Eq. 11]}$$

where, q_s is the mass of soil particles per unit length per unit time, which is transported by raindrop-impacted overland flow. Basically, Eq. [11] describes the relationship between the rainfall erosivity and the soil detachment and that between the unit discharge and bedslope and the soil transport. In an attempt of developing model equations for raindrop-impacted soil detachment and sediment transport capacity on interrill areas, Gilley et al. (1985) assumed that soil detachment by a single raindrop impact on a soil with a thin flow of water is a linear function of maximum impact pressure:

$$D = KI^{\prime} \qquad \text{[Eq. 12]}$$

where, K is the soil detachment factor and must be evaluated experimentally for each different soil. Impact pressure (Γ) is related to the normal component of raindrop velocity for inclined surfaces:

$$\Gamma = \rho_w v^2 \cos^2\theta \qquad \text{[Eq. 13]}$$

where, ρ_w is the raindrop density, v is the raindrop impact velocity, and θ is the slope gradient.

In order to include the effect of flow depth on the detachment, authors used the following empirical relation developed by Wang and Wenzel (1970) from experimental measurements of raindrop impact pressure for various raindrop sizes, impact velocities and water layer depths:

$$\Phi = 0.2\left(\frac{d}{y}\right)^{1.83} \quad \text{for } d/y < 1 \qquad \text{[Eq. 14]}$$

where, Φ is the dimensionless impact pressure at the bottom of the water layer directly under the raindrop impact point, and d is the raindrop size. Dimensionless impact pressure is also given by:

$$\Phi = \frac{\Gamma}{\rho_w v^2} \qquad \text{[Eq. 15]}$$

From equations 12, 14 and 15, the following relation for soil detachment by a raindrop impact on shallow flow is obtained:

$$D = 0.2K\rho_w v^2 \cos^2\theta \left(\frac{d}{y}\right)^{1.83} \qquad \text{[Eq. 16]}$$

As described previously in equation 11, flow transport capacity is chiefly related to the product of unit discharge and slope and rain intensity. In our case with wind-driven raindrops, raindrop impact pressure might be replaced with an intensity term of equation 11 to account for wind effects on the raindrop impact and impact velocity (Zhang et al., 1998). Therefore, sediment transport capacity of raindrop-induced overland flow under wind-driven rain can be described by:

$$q_s = f(\Gamma, q, S_o) \qquad \text{[Eq. 17]}$$

The objectives of this study are to evaluate the effects of wind on interrill transport process by raindrop-impacted shallow flow and to provide a better insight into the process under wind-driven raindrops.

Materials and methods

The study was conducted in a wind tunnel rainfall simulator facility at Ghent University, Belgium (Gabriels et al., 1997). Wind velocity profiles above wind tunnel floor are characterized by the following logarithmic equation:

$$u(z) = \left(\frac{u_*}{\kappa}\right) \ln\left(\frac{z}{z_o}\right) \text{ for } z > z_o \qquad \text{[Eq. 18]}$$

where, u(z) is the wind velocity at height z, z_o is the aerodynamic roughness height, u_* is the wind shear velocity, and κ is the von Karman's constant. Average wind velocity profiles regardless of slope gradient and aspect with a fixed roughness height of 0.0001 m for a bare and smoothed soil surface are $0.0001e^{1.1148u}$, $0.0001e^{0.7480u}$ and $0.0001e^{0.5142u}$, and the corresponding reference shear velocities (u_*) are 0.35, 0.53, and 0.77 ms^{-1} for the reference wind velocities of 6, 10, and 14 m s^{-1}, respectively. These are the profiles in the form of:

$$z = ae^{bu} \qquad \text{[Eq. 19]}$$

where, $a = z_o$ and $b = \kappa/u_*$. The logarithmic profile in the air-water interface introduces a flow resistance, which is related to the tangential wind shear stress (τ_w) exerted on the flow surface:

$$\tau_w = \rho_a u_*^2 \qquad \text{[Eq. 20]}$$

where, ρ_a is the air density. Since the wind disturbances on the flow will be much less than the flow resistance induced by the raindrop impacts in wind-driven rains (De Lima, 1989) and given the size of soil pan (20 by 55 cm), which has a very limited length to generate waves, we assumed a minor effect of wave-induced perturbations in our experiments.

All experiments are conducted in the working area, which is 1.20 m wide and 12 m long and with the ceiling adjustable in height from 1.80 m to 3.20 m. In this study, we used a continuous spraying system of ten downward-oriented nozzles installed at 2 m high and 1 m intervals. Nozzle pressure was kept at 1.50 bars. Erpul et al. (1998, 2000) gives a detailed description of the raindrop size distribution for the simulated rainfalls of the wind tunnel. The nozzles at 1.5 bar-operating pressure deliver a median raindrop size (d_{50}) of 1.00, 1.63, 1.53, and 1.55 mm for windless rain and the rains driven by 6, 10, and 14 m s^{-1}, respectively. The energy of simulated rainfalls was measured by a piezoelectric ceramic kinetic energy sensor (Sensit^{TM}, 2000). The functional relationship obtained by the kinetic energy sensor between the kinetic energy (KE) and the horizontal wind velocity (u) was in the form of:

$$KE = 6E-06e^{0.2184u} \qquad \text{[Eq. 21]}$$

where, KE in Joules, and u in ms^{-1}, and E notation shows "times 10 to the power". The calculated resultant impact velocities (v_r) of median drop sizes for the windless rains and the rains driven by the reference wind velocities of 6, 10, and 14 ms^{-1} were 4.38 ± 0.58, 4.64 ± 0.56, 7.64 ± 0.60, and 10.48 ± 0.57 ms^{-1}, respectively.

The intensity of simulated rains was directly measured with 5 small collectors on the inclined plane with respect to the prevailing wind direction. That is, the collectors were placed next to the soil pan with the same slope gradient and aspect as the soil pan during each run. In this way, the intensity measurements were made truly representative for each run without any need for correction due to the rain inclination gained from horizontal wind velocity and slope gradient and aspect (Sharon, 1980; De Lima, 1990). From the direct intensity measurements, the average angle of rain incidence between the wind vector and the plane of the surface $(\alpha \mp \theta)$ was calculated using the cosine law of spherical trigonometry (Sellers, 1965):

$$\varphi = \frac{I_a}{I} = \cos(\alpha \mp \theta) \qquad \text{[Eq. 22]}$$

where, ϕ is the impact efficiency of wind-driven raindrops, I_a is the actual intensity (mm h^{-1}), I is the rainfall intensity in respect to a plane normal to the rain vector (mm h^{-1}), α is the raindrop inclination from vertical (degree), and θ is the slope gradient (degree). The calculated average rain inclination was $53.0 \pm 11.5^{\circ}$, $68.2 \pm 7.6^{\circ}$, and $73.5 \pm 6.6^{\circ}$ for the rains driven by wind velocities of 6, 10, and 14 m s^{-1}, respectively (Fig. 1). The angles refer to the average values generalized over the raindrop size range, and the analysis of variance showed that at the level of $\alpha = 0.05$ the means were significantly different from each other.

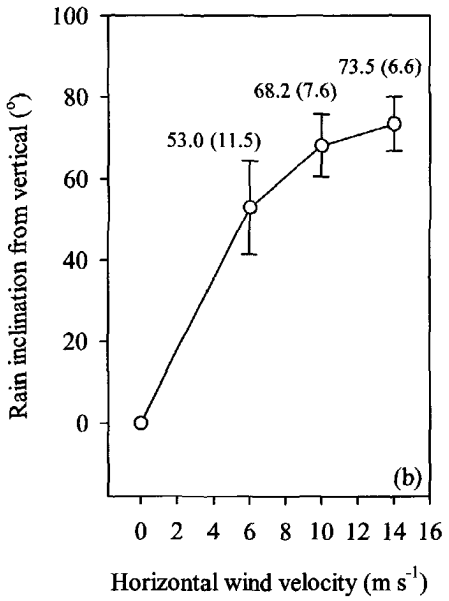

Figure 1. Mean rain inclination from vertical (α, degree) as a function of the horizontal wind velocity (u, m s^{-1}).

Three loess derived agricultural soils, Kemmel1 sandy loam (57.6% sand, 31.1% silt, and 11.3% clay) and Kemmel2 loam (37.8% sand, 44.5% silt, and 17.7% clay) from the Kemmelbeek watershed (Heuvelland, West Flanders, Belgium) and Nukerke silt loam (32.1% sand, 52.3% silt, and 15.6% clay) from the Maarkebeek watershed (Flemish Ardennes, East Flanders, Belgium) were used in this study. The soil samples were collected from the A_p horizon and air-dried prior to the experiment. Soil was sieved into three aggregate fractions: 1.00 - 2.75, 2.75 - 4.80, and 4.80 - 8.00 mm, and the weighing factors assigned to each fraction were 28, 32, and 40%, respectively to reconstitute the packing soil. A 5-kg soil sample was then packed loosely into a 55-cm-long and 20-cm-wide pan after the three fractions of aggregates were evenly mixed.

Windless rains and the rains driven by horizontal wind velocities of 6, 10, and 14 m s^{-1} were applied to the soil pan placed at both windward and leeward slopes of 7, 15, and 20%. For each soil and slope aspect, there were three replicates, or 36 runs for a total of 216 rainfall simulations.

In the present study, we assumed rainsplash detachment rate under inclined rain is related to the normal component of raindrop impact velocity (Heymann, 1967; Springer, 1976; Gilley et al., 1985; Gilley and Finkner, 1985). Accordingly, the total rain pressure (Γ, MPa) was described by:

$$\Gamma = 0.2\Xi\left(\rho_w v_r^2\right)\cos^2(\alpha \mp \theta)\left(\frac{d_{50}}{y}\right)^{1.83} \qquad \text{[Eq. 23]}$$

where, ρ_w is in kg m^{-3}, v in m s^{-1}, α and θ in degrees, d_{50} and y in m, and Ξ is the number of raindrops in # and calculated by:

$$\Xi = \frac{I_a A t}{\forall_{d50}} \qquad \text{[Eq. 24]}$$

where, I_a is in m s^{-1}, A is the surface area of soil pan (0.55 m × 0.20 m = 0.110 m^2), t is the time during which shallow flow-driven process occurred in s, and $\forall_{d_{50}}$ is the volume of median raindrop size in m^3. In order to include the effect of rainfall inclination, slope gradient and aspect on the normal component of raindrop impact velocity, we replaced the slope term $\left(\cos^2\theta\right)$ of equation 13 with the angle of rainfall incidence $\left(\cos^2(\alpha \mp \theta)\right)$ in equation 23.

Simulated rainfalls were conducted under freely drained conditions, and generally steady-state soil loss and runoff rates were attained within 45 min in windless rains and the wind-driven rains on windward slopes. However, particularly in the rains driven by wind velocities of 10 and 14 m s^{-1} on the leeward slopes of 15 and 20%, time to runoff changed greatly, and overland flow generation was retarded due to the lesser amount of rain interception. In these cases, an additional 45-min rainfall run was needed to be able to collect sediment and runoff samples at steady-state rates. During each rainfall application and after runoff started sediment and runoff samples were collected at 5-min intervals at the bottom edge of the pan using wide-mouth bottles and were determined gravimetrically. Total sediment and runoff values, and the total simulated rainfall duration were used in calculation of sediment transport capacity by rain-impacted thin flow (q_s). The following log-linear model (SAS, 1995) was analyzed for the sediment transport by rain-impacted thin flow based on interrill erosion mechanics (Julien and Simon, 1985; Gilley et al., 1985; Guy et al., 1987; Zhang et al., 1998; Parsons et al., 1998):

$$q_s = k\Gamma^a q^b S_o^c \qquad \text{[Eq. 25]}$$

where, k is soil transport parameter for the sediment transport by raindrop-impacted shallow flow and a, b, and c are regression coefficients to which total rain pressure, unit discharge and slope are raised, respectively.

Results and discussion

Measured rain intensities, angle of rain incidence, and total raindrop pressure for the windless rain and the rains driven by the reference wind velocities of 6, 10, and 14 ms^{-1} are presented in Table 1, and summary of the data used in evaluating sediment transport by the rain-impacted shallow flow for three soils is presented in Table 2 and 3. The statistical fit of equation 25, which is based on the interaction between raindrop impact and flow parameters, is shown in Table 4.

Table 1. Measured rainfall intensities (I_a), angle of rain incidence ($\alpha \pm \theta$), and total raindrop pressure (Γ) for the windless rains and the rains driven by the reference wind velocities of 6, 10, and 14 m s^{-1}.

u (m s^{-1})	v_r (m s^{-1})	d_{50} (mm)	α degree (°)	S_o (m m^{-1})	θ degree (°)	I_a mm h^{-1}	$\alpha \pm \theta$ Degree (°)	ϕ	Γ MPa
0 - ww	4.38 ± 0.58*	1.00 0.97 ≤ d_{50} ≤ 1.04†	-	0.07	4.0	142	4.0	0.9976	157.74
				0.15	8.5	140	8.5	0.9890	152.85
				0.20	11.3	134	11.3	0.9806	143.82
6 - ww	4.64 ± 0.56	1.63 1.38 ≤ d_{50} ≤ 1.84	53.0 ± 11.5*	0.07	4.0	90	49.0	0.6561	11.21
				0.15	8.5	100	44.5	0.7133	14.72
				0.20	11.3	106	41.7	0.7466	17.09
10 - ww	7.64 ± 0.60	1.53 1.50 ≤ d_{50} ≤ 1.57	68.2 ± 7.6	0.07	4.0	120	64.2	0.4352	21.55
				0.15	8.5	130	59.7	0.5045	31.37
				0.20	11.3	131	56.9	0.5461	37.04
14 - ww	10.48 ± 0.57	1.54 1.51 ≤ d_{50} ≤ 1.57	73.5 ± 6.6	0.07	4.0	90	69.5	0.3502	19.31
				0.15	8.5	103	65.0	0.4226	32.18
				0.20	11.3	112	62.2	0.4664	42.63
0 - lw	4.38 ± 0.58	1.00 0.97 ≤ d_{50} ≤ 1.04	-	0.07	4.0	165	4.0	0.9976	183.29
				0.15	8.5	172	8.5	0.9890	187.78
				0.20	11.3	179	11.3	0.9806	192.12
6 - lw	4.64 ± 0.56	1.63 1.38 ≤ d_{50} ≤ 1.84	53.0 ± 11.5	0.07	4.0	126	57.0	0.5446	10.81
				0.15	8.5	112	61.5	0.4772	7.38
				0.20	11.3	94	64.3	0.4337	5.11
10 - lw	7.64 ± 0.60	1.53 1.50 ≤ d_{50} ≤ 1.57	68.2 ± 7.6	0.07	4.0	92	72.2	0.3057	8.15
				0.15	8.5	61	76.4	0.2351	3.20
				0.20	11.3	51	79.5	0.1822	1.61
14 - lw	10.48 ± 0.57	1.54 1.51 ≤ d_{50} ≤ 1.57	73.5 ± 6.6	0.07	4.0	66	77.5	0.2164	5.41
				0.15	8.5	42	82.0	0.1392	1.42
				0.20	11.3	34	84.8	0.0906	0.49

u: horizontal wind velocity (ww: windward; lw: leeward); v_r: resultant raindrop impact velocity; d_{50}: median drop size; α: rain inclination from vertical; $\theta\alpha$ and S_o: slope gradient; ϕ: cosine of angle of rainfall incidence [= cos ($\alpha \pm \theta$)].

**Standard deviations of the resultant raindrop impact velocity and the rainfall inclination are given next to the mean value with ± sign.*

†95% confidence interval on mean values of d_{50}.

Table 2. (*) Summary of the data for main flow parameters used to evaluate the sediment transport capacity by raindrop-impacted shallow flow for three soils.

u ($m\ s^{-1}$)	S_o ($m\ m^{-1}$)	Nukerke			Kemmel1			Kemmel2			n
		q ($m^2\ s^{-1}$)	y (m)	d_{50}/y	q ($m^2\ s^{-1}$)	y (m)	d_{50}/y	q ($m^2\ s^{-1}$)	y (m)	d_{50}/y	
0 ww	0.07	6.463E-06	4.352E-04	2.30	8.225E-06	4.689E-04	2.13	5.405E-06	4.087E-04	2.45	3
	0.15	8.147E-06	3.649E-04	2.74	8.500E-06	3.692E-04	2.71	5.901E-06	3.277E-04	3.05	3
	0.20	8.230E-06	3.312E-04	3.02	8.729E-06	3.374E-04	2.96	6.386E-06	3.047E-04	3.28	3
6 ww	0.07	7.180E-06	4.344E-04	3.75	4.525E-06	3.711E-04	4.39	3.913E-06	3.535E-04	4.61	3
	0.15	9.102E-06	3.679E-04	4.43	6.282E-06	3.259E-04	5.00	3.370E-06	2.643E-04	6.17	3
	0.20	9.593E-06	3.427E-04	4.76	7.924E-06	3.225E-04	5.05	4.001E-06	2.558E-04	6.37	3
10 ww	0.07	9.805E-06	4.964E-04	3.08	9.161E-06	4.849E-04	3.16	4.270E-06	3.732E-04	4.10	3
	0.15	1.228E-05	4.149E-04	3.65	1.077E-05	3.998E-04	3.83	5.715E-06	3.219E-04	4.75	3
	0.20	1.321E-05	3.902E-04	3.92	1.241E-05	3.814E-04	4.01	5.780E-06	2.957E-04	5.17	3
14 ww	0.07	7.980E-06	4.516E-04	3.43	6.812E-06	4.269E-04	3.63	3.967E-06	3.559E-04	4.36	3
	0.15	8.730E-06	3.662E-04	4.23	8.615E-06	3.648E-04	4.25	4.600E-06	2.957E-04	5.24	3
	0.20	1.008E-05	3.504E-04	4.42	9.779E-06	3.472E-04	4.46	5.480E-06	2.865E-04	5.41	3
0 lw	0.07	1.116E-05	5.280E-04	1.89	1.015E-05	5.136E-04	1.95	8.875E-06	4.907E-04	2.04	3
	0.15	1.112E-05	4.087E-04	2.45	8.215E-06	3.734E-04	2.68	7.736E-06	3.659E-04	2.73	3
	0.20	1.381E-05	4.007E-04	2.50	9.923E-06	3.625E-04	2.76	1.092E-05	3.757E-04	2.66	3
6 lw	0.07	9.194E-06	4.854E-04	3.36	4.938E-06	3.937E-04	4.14	6.789E-06	4.367E-04	3.73	3
	0.15	7.307E-06	3.427E-04	4.76	3.697E-06	2.737E-04	5.96	3.687E-06	2.726E-04	5.98	3
	0.20	6.592E-06	2.989E-04	5.45	3.002E-06	2.297E-04	7.10	2.413E-06	2.127E-04	7.66	3
10 lw	0.07	6.498E-06	4.195E-04	3.65	3.165E-06	3.286E-04	4.66	3.238E-06	3.325E-04	4.60	3
	0.15	2.741E-06	2.351E-04	6.51	1.671E-06	1.995E-04	7.67	1.352E-06	1.866E-04	8.20	3
	0.20	2.271E-06	1.979E-04	7.73	1.154E-06	1.579E-04	9.69	7.590E-07	1.381E-04	11.08	3
14 lw	0.07	2.927E-06	3.122E-04	4.96	1.862E-06	2.691E-04	5.76	1.608E-06	2.550E-04	6.08	3
	0.15	1.383E-06	1.822E-04	8.51	8.880E-07	1.568E-04	9.88	1.045E-06	1.668E-04	9.29	3
	0.20	1.118E-06	1.533E-04	10.11	6.895E-07	1.307E-04	11.86	7.190E-07	1.332E-04	11.64	3

** Mean values are given in the table.*

u: horizontal wind velocity (ww: windward; lw: leeward); S_o: slope gradient or channel bottom slope; q: unit discharge; y: flow depth; d_{50}: median drop size; n: number of replicates.

Table 3. (*) Data for the sediment transport rates by raindrop-impacted shallow flow for three soils.

u ($m\ s^{-1}$)	S_o ($m\ m^{-1}$)	Nukerke q_s ($kg\ m^{-1}\ s^{-1}$)		Kemmel1 q_s ($kg\ m^{-1}\ s^{-1}$)		Kemmel2 q_s ($kg\ m^{-1}\ s^{-1}$)		n
		Mean	St. Dev	Mean	St. Dev	Mean	St. Dev	
0 ww	0.07	3.997E-04	4.023E-05	2.761E-04	9.030E-05	3.355E-04	1.398E-05	3
	0.15	4.992E-04	5.986E-05	6.399E-04	9.905E-05	3.793E-04	1.605E-05	3
	0.20	7.511E-04	6.675E-05	6.250E-04	3.056E-05	6.943E-04	3.527E-05	3
6 ww	0.07	1.892E-04	8.331E-06	8.911E-05	1.999E-06	1.333E-04	1.362E-05	3
	0.15	4.988E-04	5.227E-05	3.140E-04	1.512E-05	2.099E-04	3.400E-05	3
	0.20	7.565E-04	5.820E-05	5.528E-04	3.346E-05	3.723E-04	7.970E-05	3
10 ww	0.07	4.381E-04	2.026E-05	2.859E-04	2.728E-05	3.442E-04	7.550E-05	3
	0.15	1.115E-03	1.848E-04	1.032E-03	1.413E-04	6.419E-04	1.819E-04	3
	0.20	1.741E-03	1.408E-04	2.033E-03	9.967E-05	8.314E-04	4.423E-05	3
14 ww	0.07	3.566E-04	2.794E-05	2.497E-04	6.404E-05	1.915E-04	8.216E-06	3
	0.15	9.068E-04	2.542E-04	7.666E-04	1.012E-04	6.048E-04	9.569E-05	3
	0.20	1.351E-03	3.695E-04	1.537E-03	1.061E-04	9.291E-04	5.709E-05	3
0 lw	0.07	5.796E-04	4.780E-05	5.817E-04	7.610E-05	5.149E-04	2.136E-05	3
	0.15	6.599E-04	4.060E-05	8.247E-04	3.531E-05	5.079E-04	6.485E-05	3
	0.20	1.053E-03	5.107E-05	9.991E-04	9.593E-05	9.319E-04	1.205E-04	3
6 lw	0.07	2.397E-04	1.507E-05	1.635E-04	8.577E-06	2.404E-04	9.373E-06	3
	0.15	2.835E-04	1.315E-05	1.726E-04	9.808E-06	1.370E-04	4.674E-06	3
	0.20	3.283E-04	1.616E-05	1.376E-04	8.531E-06	9.312E-05	6.794E-06	3
10 lw	0.07	2.459E-04	5.530E-06	1.165E-04	6.414E-06	1.947E-04	1.136E-05	3
	0.15	1.384E-04	2.158E-05	5.382E-05	3.419E-06	7.531E-05	1.078E-05	3
	0.20	9.496E-05	5.970E-06	3.154E-05	2.112E-06	3.077E-05	4.614E-06	3
14 lw	0.07	1.656E-04	1.176E-05	9.598E-05	5.005E-06	1.360E-04	9.714E-06	3
	0.15	1.136E-04	1.672E-05	4.382E-05	2.059E-06	4.996E-05	4.141E-06	3
	0.20	8.294E-05	3.122E-06	1.723E-05	8.418E-07	2.999E-05	3.392E-06	3

**Mean values are given in the table; however, statistical analyses are performed with individual data points.*

u: horizontal wind velocity (ww: windward; lw: leeward); S_o: slope gradient or channel bottom slope; q_s: sediment transport rate.

Table 4. Statistical analyses for the equation of sediment transport by the raindrop- impacted shallow flow developed by log-linear regression technique for three soils.

Soil	$q_s = k\Gamma^a q^b S_o^c$								
	k	**Prob>|T|**	**a**	**Prob>|T|**	**b**	**Prob>|T|**	**c**	**Prob>|T|**	**R^2**
Nukerke	11.682	0.0408	0.16	0.0001	0.80	0.0001	0.62	0.0001	0.87
Kemmel1	3858.549	0.0001	0.09	0.0781	1.26	0.0009	0.69	0.0001	0.93
Kemmel2	25.611	0.1095	0.18	0.0053	0.91	0.0079	0.34	0.0014	0.87

The analysis of variance showed that the exponent a was significant at the level of $\alpha = 0.05$ for Nukerke and Kemmel2 but not for Kemmel1, and the soil transport parameter for shallow flow-driven process k was significant at the level of $\alpha = 0.05$ for Nukerke and Kemmel1 but not for Kemmel2. The exponent values to which the unit discharge and slope were raised (b and c, respectively) were significant at the level of $\alpha = 0.05$ for all cases. The power law models are, respectively for Nukerke silt loam, Kemmel1 sandy loam, and Kemmel2 loam, given by:

$$q_s = 11.682\Gamma^{0.16}q^{0.80}S_o^{0.62} \quad \text{[Eq. 26]}$$

$$q_s = 3858.549\Gamma^{0.09}q^{1.26}S_o^{0.69} \quad \text{[Eq. 27]}$$

$$q_s = 25.611\Gamma^{0.18}q^{0.91}S_o^{0.34} \quad \text{[Eq. 28]}$$

units of variables are as presented in Table 1, 2 and 3.

The ratios of flow depth to mean raindrop diameter (d_{50}/y) ranged from 1.89 to 11.86 for all data. In other terms, (d_{50}/y) was greater than unity in all cases (Table 2), and this suggested that soil detachment by shallow flow could be assumed minimal, and a large raindrop impact could be expected (Moss and Green, 1983, Guy et al., 1987). However, the statistical fits showed that of model parameters Γ had the lowest exponent values, which were 0.16, 0.09, 0.18 for Nukerke silt loam, Kemmel1 sandy loam, and Kemmel2 loam, respectively (Table 4). In contrast to the expectation of a large impact of raindrop from the values of (d_{50}/y), those values were surprisingly very small, implying a very slight contribution of raindrop impact to the sediment transport. Therefore, analysis of the Pearson correlation coefficient was done to provide a better picture of the interactions between impact and flow parameters and their effect on the process (Table 5). Partitioning of the data of wind-driven rains with respect to the slope aspects indicated that q_s had very poor correlation with Γ and much greater correlation with qS_o in windward slopes (-0.03 and 0.88, respectively), which indicated that flow parameters and not the impact parameter reasonably explained the variation in the sediment transport rate (Fig. 2).

On the other hand, Γ was as much in effect as qS_o for sediment transport in the leeward slopes, and correlation coefficient between Γ and q_s was 0.91 (Table 5). Evidently, a significant difference in flow hydraulics occurred with different aspects under the impacts of wind-driven raindrops. It was clear from the statistical analyses that the flow depth calculation using the empirical relation of equation 10 to some extent resulted in unrealistic values for windward slopes. This was ascribed to a roughness induced by the splash trajectories of particles by the inclined raindrop impact within the shallow flow and the contrary lateral stress of impacting raindrops to the direction of the shallow flow.

One would expect by instinct that three types of rainsplash courses within shallow flow appear to exist in our study. First, in the windless rains incident on a slope, particles splashed by raindrop impact within shallow flow move downslope or downslope particle movement is more important than the upslope particle movement irrespective of the slope aspect. In other words, the splash asymmetry of the detached soil particles occurs such that more momentum is transferred in the downslope direction and thus the difference between upslope and downslope transport increases

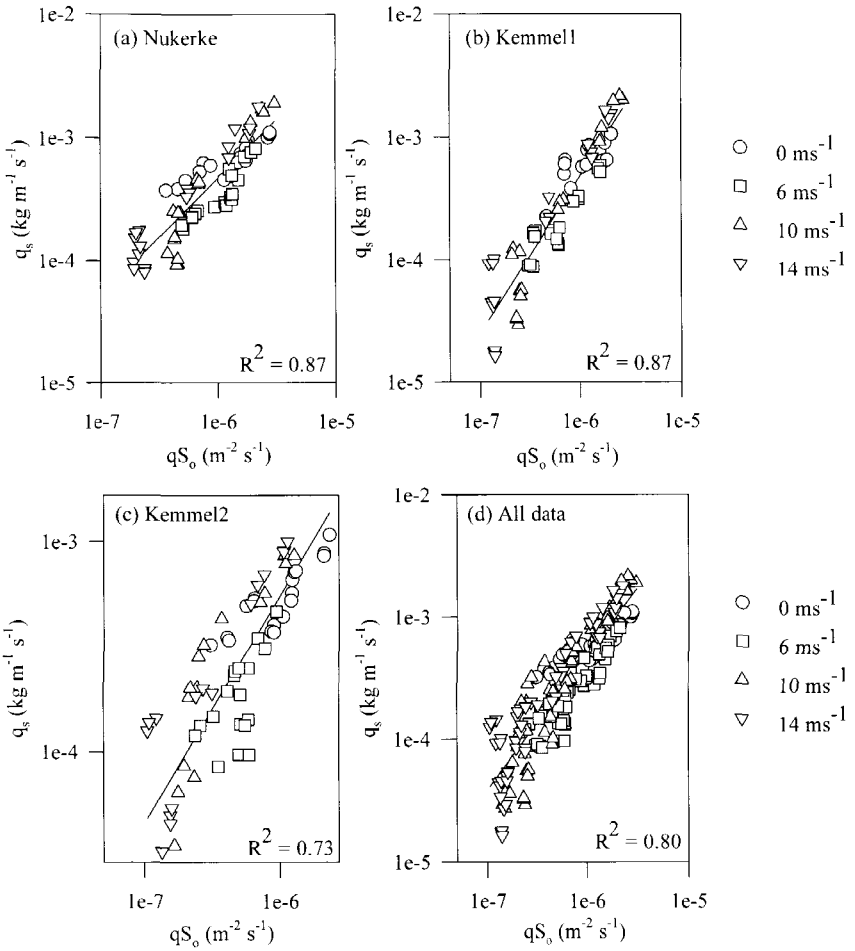

Figure 2. Sediment transport rate by raindrop-impacted shallow flow (q_s) as a power function of unit discharge×slope (qS_o) for Nukerke silt loam (a), Kemmel1 sandy loam (b), Kemmel2 loam (c), and for all data regardless of soil type (d).

as the slope gradient increases. In this case, lateral raindrop stress is also at the same direction as the shallow flow direction. In fact, raindrop-induced flow resistance estimated by equation 9 (Shen and Li, 1973; Katz et al., 1995) represents this condition of windless rain incident on a slope. Second, wind-driven rains incident on the windward slopes, the particles splashed by the inclined raindrops are directed upslope, and there is only upslope movement at threshold, and these particles are captured by the shallow flow running downslope. Clearly, reverse rainsplash courses at impact with respect to the shallow flow direction occur, and together with contrary lateral raindrop stress, which increases as the horizontal wind velocity increases, to the shallow flow direction this forms such raindrop-induced roughness that equation 9 is evidently unlikely to be suitable to explain. Third, in the wind-driven rains incident

Table 5. Pearson correlation coefficients among the total raindrop pressure, Γ (MPa) and the product of flow parameters in the form of qS_o and the sediment transport rate by the raindrop-impacted shallow flow, q_s (kg m^{-1} s^{-1}), using combined data from three soils.

Windless and wind-driven rains			
	Γ	**qS_o**	**q_s**
Γ	1.00 (0.0000)*	0.44 (0.0001)	0.38 (0.0001)
qS_o		1.00 (0.0000)	0.89 (0.0001)
q_s			1.00 (0.0000)
Wind-driven rains			
	Γ	**qS_o**	**q_s**
Γ	1.00 (0.0000)	0.75 (0.0001)	0.86 (0.0001)
qS_o		1.00 (0.0000)	0.92 (0.0001)
q_s			1.00 (0.0000)
Windward rains			
	Γ	**qS_o**	**q_s**
Γ	1.00 (0.0000)	0.04 (0.6890)	-0.03 (0.7520)
qS_o		1.00 (0.0000)	0.88 (0.0001)
q_s			1.00 (0.0000)
Leeward rains			
	Γ	**qS_o**	**q_s**
Γ	1.00 (0.0000)	0.74 (0.0001)	0.91 (0.0001)
qS_o		1.00 (0.0000)	0.91 (0.0001)
q_s			1.00 (0.0000)

** Numbers in parentheses are significance levels.*

on the leeward slopes, the particles splashed by the inclined raindrops are directed downslope and thus being at the same direction as shallow flow direction and similar to the first case, the lateral raindrop stress is also at the same direction as the shallow flow. Only difference from the first case is the unidirectional downslope particle movement without any upslope component of particle movement in this case.

As explained, different hydraulics of shallow flow might occur depending on wind velocity and direction. Our analysis of Pearson correlation coefficients (Table 5) appeared to reflect these differences. Γ was very poorly correlated with q_s, and qS_o tended to dominate as flow depth increased in the windward slopes, while Γ performed as equally well as qS_o in explaining more than 90% variation of q_s in the leeward slopes. The Darcy-Weisbach friction coefficient used to predict the raindrop-induced roughness (Shen and Li, 1973; Gilley et al., 1985; Katz et al., 1995) could not account for the variations in the roughness and flow resistance in windward slopes where reverse within-flow particle trajectories and lateral raindrop stress with respect to the shallow flow direction occurred. These two effects worked together to lead to more deepened flow in the windward slopes than that calculated by the Darcy-Weishbach friction coefficient, and accordingly giving rise to the decreased raindrop impact contribution to the sediment transport in these slopes.

Conclusions

Only experimental results directly taken on the wind effects on the sediment transport by the raindrop-impacted shallow flow have been given in this study, aiming to provide a better insight into the process under wind-driven rains. Based on the interrill erosion mechanics, raindrop impact pressure and unit discharge and slope were used to explain the interactions between the impact and flow parameters and the sediment transport. Flow depth was predicted from the measured discharge and slope along with the Darcy-Weishbach friction coefficient. Statistical analyses of power law models and the Pearson correlation coefficients showed that the friction coefficient

could not account for the variations in the roughness and flow resistance caused by wind velocity and direction. The reverse/advance rainsplash trajectories within shallow flow and the lateral stress of impacting raindrops at angle with respect to the shallow flow direction were concluded to have significant effects on the shallow flow hydraulics under wind-driven rains. However, there is a need for further experimentation to parameterize these roughness elements, and an understanding of these mechanisms should facilitate the development of robust models to assess the sediment transport by raindrop-impacted shallow flow under wind-driven rains.

References

Chow, V. T. 1959. Open-Channel Hydraulics. New York: McGraw-Hill Book Co. Inc.

De Lima, J. L. M. P., 1990. The effect of oblique rain on inclined surfaces: A nomograph for the rain-gauge correction factor. *Journal of Hydrology*, 115: 407-412.

De Lima, J. L. M. P., 1989. Overland flow under simulated wind-driven rain. Proceedings of the 11th International Congress on Agricultural Engineering, Dublin, 4 – 8 September, pp. 493-500.

Erpul, G., D. Gabriels, and D. Janssens. 1998. Assessing the drop size distribution of simulated rainfall in a wind tunnel. *Soil and Tillage Research*, 45: 455-463.

Erpul, G., D. Gabriels, and D. Janssens. 2000. The effect of wind on size and energy of small simulated raindrops: a wind tunnel study. *International Agrophysics*, 14: 1-7.

Foster, G. R. 1982. Modeling the soil erosion process. In: *Hydrologic Modeling of Small Watersheds*. Haan, C. T., H. P. Johnson and D. L. Brakensiek (eds.). ASAE Monograph No. 5. ASAE, St. Joseph, MI 49085, pp. 297-382.

Gabriels, D., W. Cornelis, I. Pollet, T. Van Coillie and M. Quessar. 1997. The I.C.E. wind tunnel for wind and water erosion studies. *Soil Technology*, 10: 1-8.

Gilley, J. E. and S. C. Finkner. 1985. Estimating soil detachment caused by raindrop impact. *Transactions of the ASAE* 28: 140-146.

Gilley, J. E., D. A. Woolhiser and D. B. McWhorter. 1985. Interrill soil erosion. Part I: Development of model equations. *Transactions of the ASAE* 28: 147-153 and 159.

Guy, B. T., W. T. Dickinson and R. P. Rudra. 1987. The roles of rainfall and runoff in the sediment transport capacity of interrill flow. *Transactions of the ASAE* 30: 1378-1386.

Heymann, F. J., 1967. A survey of clues to the relation between erosion rate and impact parameters, Second Rain Erosion Conference, 2, 683-760.

Julien, P. Y. and D. B. Simons. 1985. Sediment transport capacity of overland flow. *Transactions of the ASAE* 28: 755-762.

Katz, D. M., F. J. Watts and E. D. Burroughs. 1995. Effects of surface roughness and rainfall impact on overland flow. *Journal of Hydraulic Engineering* 121: 546-553.

Moss, A. J. and P. Green. 1983. Movement of solids in air and water by raindrop impact. Effects of drop-size and water-depth variations. *Aust. J. Soil Res.*, 21: 373-382.

Parsons, A. J., S. G. L. Stromberg and M. Greener. 1998. Sediment-transport competence of rain-impacted interrill overland flow. *Earth Surf. Processes and Landforms*, 23: 365-375.

SAS, 1995. SAS System for Elementary Statistical Analysis. SAS Inst. Inc., Cary, NC, USA, pp. 280-285.

Sellers, W. D. 1965. Physical Climatology. University of Chicago Press: Chicago.

Sensit™, 2000. Model V04, Kinetic Energy of Rain Sensor. Sensit Company, Portland, ND 58274-9607.

Sharon, D. 1980. The distribution of hydrologically effective rainfall incident on sloping ground. *Journal of Hydrology* 46: 165-188.

Shen, H. W. and R. W. Li. 1973. Rainfall effect on sheet flow over smooth surfaces. *J. Hydrology. Div. Amer. Soc. Civil Eng.* May: 771-792.

Springer, G. S., 1976. Erosion by liquid impact. John Wiley and Sons, Inc., New York.

Wang, R. C. T. and H. G. Wenzel. 1970. The mechanics of a drop after striking a stagnant water layer. Univ. of Illinois, Water Resources Center, Report No. 30, Urbana, 130 pp.

Zhang, X. C., M. A. Nearing, W. P. Miller, L. D. Norton and L. T. West. 1998. Modeling interrill sediment delivery. *Soil Sci. Soc. Am. J.* 62: 438-444.

Chapter 7

The Role of Wind and Water Erosion in Drift-Sand Areas in the Netherlands

M.J.P.M. Riksen[1], D. Goossens[1,2] & P.D. Jungerius[3]
[1] Erosion and Soil & Water Conservation Group, Department of Environmental Sciences, Wageningen University, Nieuwe Kanaal 11, NL-6709 PA Wageningen, the Netherlands; Email: Michel.Riksen@wur.nl
[2] Laboratory for Experimental Geomorphology, Katholicke Universiteit Leuven, Redingenstraat 16 bis, B-3000 Leuven, Belgium
[3] Bureau Geomorphology & Landscape Ecology (G&L), Oude Bennekomseweg 31, NL-6717LM Ede, the Netherlands

The Role of Wind and Water Erosion in Drift-Sand Areas in the Netherlands

Introduction

The active inland drift-sands (Fig.1) in the Netherlands are unique in Western Europe. According to most authors, the strongly degraded landscape originated mainly in the Middle Ages (Schimmel, 1975, Koster 1978, Castel, 1991), but recent studies point to a much older period, presumably at least Iron age (van den Ancker & Jungerius, 2003). In almost all cases they owe their existence to the reactivation of late-glacial cover sands and river dunes. The reactivation is attributed to the increase in population and the related heavy demand of natural resources, such as wood and agricultural land (Schimmel, 1975; Castel, 1991, Koster *et al.* 1993, Bakker *et al.*, 2003). This and new technologies led to a more intensive land-use by farming systems such as the "potstal" system. Heath sods were brought in from the heath, which was communal land. They were used in stables to produce organic manure, which was later spread on the arable fields. For one hectare of arable field, up to 30 hectares of heath land were needed to produce sufficient heath sods (Bakker *et al.*, 2003). Regular burning of the land and the drift of sheep also led to a drop of the protective vegetation cover. Where the vegetation disappeared, the highly erodible outcropping coversands became exposed to the wind. Once started, the wind erosion process was difficult to stop. Because of the lack of economic alternatives there was no incentive for farmers to change their practices on the communal land. As a consequence, small wind-eroded spots could easily merge into larger entities. This ultimately resulted in the creation of drift-sand areas covering several thousands of hectares. Destruction of the vegetation in and along roads and paths also created drift-sand areas, especially in Germany.

The European drift-sand areas reached their maximum size in the 19th century (Koster *et al.*, 1993): 200-300 km^2 in northern Belgium, approximately 950 km^2 in the Netherlands, 1400-2000 km^2 in northwestern Germany, and 450-550 km^2 in Denmark. In England, Koster *et al.* (1993) also mapped small drift-sand areas, particularly in East Anglia. In some cases the sands formed an increasing threat to farmland, farms and community properties such as roads. People started to plant trees to protect their properties. But it was only since the collapse of the wool industry and the introduction of fertilizers on one hand, and the increasing demand for wood for the growing coal mine industry on the other, that it became attractive to reforest communal lands. From the end of the 19th century until halfway the 20th century most drift-sand areas in Europe were successfully reforested. Only fossil sand dunes remind us of the times when wind erosion was a major factor in shaping the North-European landscape.

To date, drift-sand processes and drift-sand formation can still be studied in the Netherlands. Several areas were not replanted with trees to preserve them as a nature reserve, or for military purposes. Because of their limited size, and because most of them were surrounded by forest, they were no longer considered a threat to the neighbouring land.

Due to the success of the reforestation programme, no more than 6,000 ha of the original drift-sand areas were preserved in the Netherlands in the mid 1960s (Bakker *et al.*, 2003; Jungerius, 2003). During the reforestation, nature conservationists like Jac. P. Thijsse convinced the policymakers of the values active drift-sand areas add to nature. The open drift-sand landscape was especially appreciated because its vegetation shows patches of distinct stages in the natural succession, with typical pioneers such as *Corynephorus canescens, Spergula*

Figure 1. Active drift-sand areas are protected in the Netherlands because of their high nature, geomorphologic and culture-historical value. A: Lichen; B: sand earwig; C: side view of a plateau-dune at Wekeromse Zand, showing a buried profile; D Polytrichum piliferum; E: ripples and shadow dunes are common erosion features at Kootwijkerzand, pointing to recent wind erosion activity; F exposed roots of Pinus silvestis; and G: Kootwijkerzand, the largest still active inland drift-sand area of Western Europe.

morisonii, Polytrichum piliferum, lichen such as *Cladonia sp.*, and *Cladina sp.* The combination of open land and vegetated patches creates the habitat for rare insects (Fig. 1), birds and lizards.

Since the 1960s the remaining active drift-sand areas have shown a rapid decline in size due to natural regeneration. This is attributed to the increased atmospheric nitrogen deposition, a corollary of the intensive bio-industrial activities on the sandy soils in most parts of the Netherlands (Bakker *et al.*, 2003). Of the 6,000 ha in 1960, only 4,000 ha were left
around 1980 and no more than 1,500 ha in 2002 (Jungerius, 2003). Without human intervention, the active drift-sand areas, with their characteristic flora and fauna, will slowly regenerate and turn into forest.

In 1989 the Dutch government launched the 'Overlevingsplan Bos en Natuur (OBN, Survival Plan for Forests and Nature, Ommering 2002) to provide grants for measures to counteract the effects of N-deposition in the Netherlands. Since then, several projects have been launched to preserve the drift-sand landscape and to reactivate already stabilised drift-sand areas. So far most measures were taken *ad hoc* and did not always show the expected results (Ketner-Oostra and Huijsman, 1998; Bakker *et al*, 2003). For a more effective and efficient management of the drift-sands in the future, more knowledge is needed about the landscape differentiating processes and their role in drift-sand ecology.

In the last decades, however, most research focused on the origin of the drift-sands (central Netherlands: Koster, 1978; Province of Drenthe: Castel, 1991; southern

part of the country: van Mourik, 1988a, 1988b). Many detailed studies of the fauna and vegetation of inland drift-sands were also conducted, among them Ketner-Oostra (1994, 1996) on drift-sand lichen and vegetation, Pluis (1993) on algae crust formation in blowouts, Goede et al. (1993) on changes in nematode community structure in a primary succession of blown-out areas, and Deuzeman (2003) on birds and small wildlife.

So far little attention has been paid to the role of the different processes of erosion in the remaining active drift-sand areas. Literature often refers to the positive effects of wind erosion on the characteristic vegetation types in these areas (Ketner-Oostra and Huijsman, 1998). In practice, however, wind erosion vanishes in the first few metres of a vegetated area adjacent to open sand unless the event is extremely strong and/or its duration is sufficiently long. The role of splash drift in transporting fine sand further into the vegetation is usually disregarded. Also, the consequences of the redistribution of sand and organic matter by slope wash have not been sufficiently examined. For a successful implementation of landscape-restoration measures and techniques, it is necessary to understand the various erosion processes that occur in a drift-sand landscape, and to know more about their extent, their intensity, and the role they play in drift-sand ecology.

In this paper we focus on the most relevant erosion processes prevailing on the inland drift-sands in the Netherlands: wind erosion, (wind driven) splash erosion and water erosion. For each process we describe the controlling factors and the role the process plays in the landscape. The study comprises literature research, field observations and field measurements of erosion activity.

The Inland Drift-Sand Landscape

The Dutch drift-sand areas consist of various ecotopes. The main parameters determining these ecotopes are relief and, to a lesser degree, vegetation.

Relief

Topographically, the following landscape units can be distinguished in Dutch drift-sand areas (Castel, 1991):

- Blown-out areas: the original surface of the cover sand with its podzolic soil profile has been largely removed by deflation. The area is generally fairly flat, and gravel may appear at the surface. This gravel represents the coarse (fluvio-periglacial) material that occurs below the cover sand, or is a desert pavement formed by the concentration of scattered gravel in the cover sand over the course of time.
- Low drift-sand dunes (< 1.5m) (blown-up): due to their limited height they provide no shadow effect, resulting in a fairly uniform area.
- Moderately high drift-sand dunes (1.5 – 10m) (blown-up): as a result of their shadow effect they show a greater variation in vegetation and soil organic matter than the low drift-sand dunes do.
- Plateau-dunes (blown over): steep-sided dunes with a more or less level top with a buried profile (cover sand with podzol profile covered by drift-sand), located within blown-out areas. The buried profile is often impermeable.
- High drift-sand dunes: these often contain a short, steep SW slope and a long, moderately steep NE slope.
- Bordering (dune) ridges: long, winding or straight ridges with either symmetrical or asymmetrical cross-profiles, located at the edge of (former) active drift-sand areas. Their height varies from 1 to 20 m.

- Drift-sand plains: relatively flat areas that consist of a layer of drift-sand (blown over) or of remaining cover sand (blowing out area).

It is generally accepted that the drift-sands in the Netherlands have been transported predominantly by westerly winds (Koster, 1978; Castel, 1991). This can be deduced from the shape and orientation of the drift-sand dunes and drift-sand plains, the location of the blow-outs, and the location of the blown-up and blown-over areas. Today these landscape elements are often difficult to distinguish because most remnants of drift-sands have become covered by forest. The remaining open areas, especially the smaller ones, do not show all of these characteristic elements.

Drift-sands succession stages

The differences within the landscape units listed in the previous section are determined by the stage of natural regeneration from bare drift-sand to natural forest. The different succession stages of the vegetation in this process are shown in Table 1. The bare sand is first colonised by pioneer grasses, mosses and algae. The surface soil changes slowly: it becomes richer in nutrients and lower in pH value (Table 2). The extreme microclimate, which is due to large differences in temperature at the soil surface on the bare sand, also changes with the increasing soil cover. Due to these changes, the water availability in the surface soil improves. Under the improved conditions higher plant species can grow. When undisturbed, the drift-sand slowly changes into a natural forest.

Table 1: Succession stages of inland drift-sand vegetation.

Succ. stage	Process	Composition of the vegetation (main species)
0	Bare sand	No vegetation
1	Colonisation of drifting sand with pioneer grasses mainly *Corynephorus canescens*	Patches of pioneer grasses: *C. canescens, Ammophila arenaria, Festuca rubra* sp. *commutate and Carex arenaria*
2	Stabilization by algae and *C. canescens*	Mix of *C. canescens* and green algae
3	Colonisation by the moss *Polytrichum piliferum*	Mix of pioneer grasses, algae crust and *P. piliferum* and *Spergularia morisonii*
4	Dying moss because of algae development and decay and development of lichens on partly dead moss and/or colonisation by *Campylopus introflexus**	Carpet of *P. piliferum* covered by algae and lichens, and patches of *C. canescens*
5	Further decay of moss carpet and colonisation by *Festuca ovina* and/or *Agrostis vinealis* and *Calluna vulgaris*	Mix of *C. canescens*, mosses, grasses, lichens and *C. vulgaris*
6	Further colonisation by *F. ovina* and/or *A. vinealis, C. vulgaris* and seedlings of some trees (*Juniperus communis, Pinus sylvestris* and deciduous trees)	Mosaic vegetation of grass, mosses, lichen and *C. vulgaris* with seedlings of some trees
7	Development into a closed forest	Forest with grasses, mosses and some heather

** The moss C. introflexus is an exotic moss species that has invaded inland drift-sands since the 1980s (Typology after: Masselink, 1994; Ketner-Oostra and Huijsman, 1998)*

Table 2: Description of the soil for the drift-sand succession stages at Kootwijkerzand.

Succession stage	Vegetation cover (%)	Soil profile	OM top soil (%)	pH KCl
0	0	C	0.30	4.7
1	< 5	C	0.30	4.7
2	50 – 80*	C	0.34	4.6
3	40 – 75*	C	0.58	4.5
4	70 - 100*	AC	0.79	3.5
5	90 - 100	AC	0.88	3.5
6	100	AC	1.37	3.5
7	100	A(B)C	-	-

*) *Source: Ketner-Oostra, 1994*

-) *no data available*

Landscape Differentiating Processes

In a drift-sand landscape, soil erosion and natural regeneration are defined as the landscape differentiating processes. Morgan (1995) defines soil erosion as a two-phase process consisting of the detachment of individual particles from the soil mass and their transport by erosive agents such as running water and wind. When sufficient energy is no longer available to transport the particles, a third phase, deposition, occurs.

The force that causes the detachment is the resultant of drag, lift, gravity, friction and cohesive forces working on the soil particle. Once a soil particle, which can be a single grain or an aggregate, is detached from the surface, it goes into transport. The agent delivering the energy needed to keep the soil particle in transport is often a fluid such as water or air. On slopes, gravity can also serve as the main agent (mass movement) or influence the energy level of the fluid agent. When the energy level that keeps a specific soil particle in transport drops below a threshold value the soil particle will be deposited on the surface. The energy level of the fluid, which determines the transport capacity, depends on the flow velocity and on weather conditions. The energy level of the agent can drop below the threshold needed for transport: in time, due to a change in weather conditions, and in space, due to a change in surface roughness or slope, which causes losses due to friction.

Erosion results in a redistribution of soil material in space. In the detachment and transport zone soil erosion leads to degradation of the soil due to loss of the top soil including nutrients and soil organic matter and damage to vegetation from abrasion, exposure of plant roots and loss of seedlings. In the deposition zone the results are either local enrichment with nutrients from the deposition of organic matter and fine soil particles or soil degradation due to the burial of the soil profile with poor fine sand.

In an inland drift-sand landscape, erosion generally leads to soil degradation. In the present drift-sands, the balance between the landscape differentiating processes (Fig. 2), soil degradation from erosion and regeneration caused by vegetation, is leaning towards regeneration as the most dominant process, resulting in a rapid stabilisation of the drift-sands.

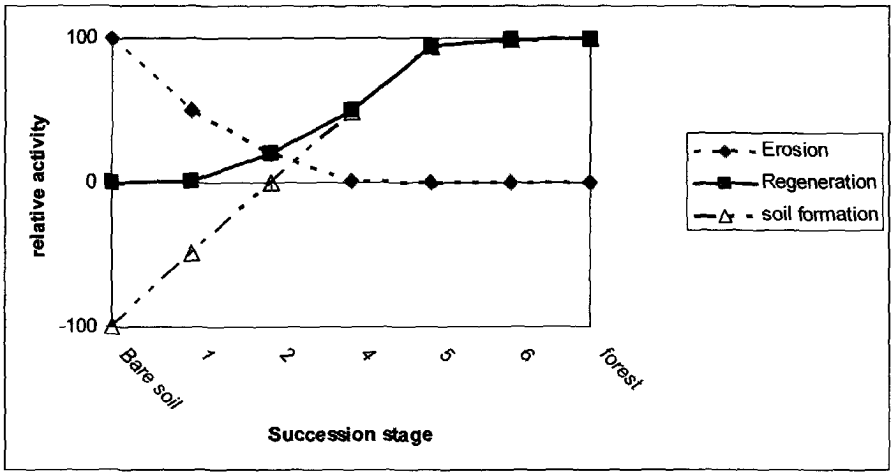

Figure 2. Schematic presentation of the interaction between soil degradation from erosion and soil regeneration caused by vegetation development on inland drift sands. Up to succession stage 2 the soil is degraded (negative soil formation); from succession stage 3 onwards the soil profile grows (positive soil formation).

Erosion Processes in Inland Drift-Sand Landscapes

In an inland drift-sand landscape, the following erosion processes occur: wind erosion (Fig. 3A, 3B), water erosion by splash (Fig. 3C, 3D) and wash and rill erosion by overland water flow (Fig. 3E, 3F) and mass movement (Fig. 3F).

Wind Erosion

Wind erosion can become a significant process whenever the soil is dry, loose and has a sandy texture, when the surface is bare or nearly bare, when the wind velocity regularly exceeds the threshold for initiation of soil particle movement, and when the susceptible area is sufficiently large (Fryrear and Skidmore, 1985; Lyles, 1988). By definition, wind erosion is the removal of soil material by wind, whereas sedimentation is the deposition of wind-blown material. Between detachment and sedimentation, transport takes place.

Detachment

In wind erosion, the air flowing over the soil surface provides the energy for the detachment and transport of the soil particles. The wind creates a vertical (lift) force and a horizontal (drag) force that act on the particles.

The lift is responsible for the initiation of the erosion process at the leading edge of the deflation zone. Lifted sand particles rapidly fall back to the surface after having accomplished their (strongly asymmetrical) saltation trajectory. From this point, most particles will become detached through the impact of these falling grains. This process is also known as bombardment.

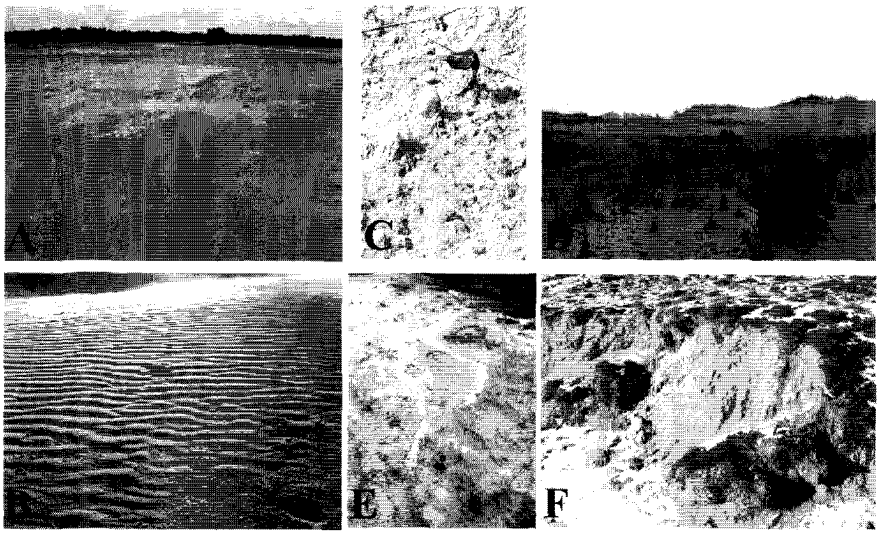

Figure 3. Erosion processes on an inland drift-sand landscape. A and B: wind erosion (saltation); C and D: pedestals formed by splash erosion; E: slope wash; F: mass movement and sloping sides by water erosion (see the rills in the lower half of the slope).

The drag force is caused by friction between the grain's surface and the air. This force is largest on the upper half of the grain and causes the grain to spin. Apart from this first component, the drag force also contains a second component caused by the difference in pressure between the windward side and leeside of the grain. The resultant drag force causes the grains to roll or slide over the surface.

Transport

Aeolian transport of particles can occur in three different modes: saltation, creep and suspension (Fig. 4). There is no sharp demarcation line between these three modes of particle transport but rather a gradual transition. The largest particles (>500μm) roll or slide over the surface without loosing contact with the latter, a process known as surface creep or surface traction (Pye and Tsoar, 1990). Smaller particles, between 500 and approximately 50-100 μm, are transported in saltation. Saltating particles jump and bounce over the surface, reaching a maximum height of approximately 1 m. However, the main particle mass moves just above the soil surface. When saltating particles fall back to the surface they not only ricochet or eject other saltation-size grains but also induce surface creep, reptation (some small-scale saltation with only a limited displacement of grains near the points of impact) and surface deformation. Saltating sand grains can also raise dust particles, which are transported in suspension. Suspended particles are kept aloft by the turbulent nature of the airflow. We speak of short-term and long-term suspension depending on whether the particles will stay airborne for only a short time (normally a few hours) or longer (days or weeks).

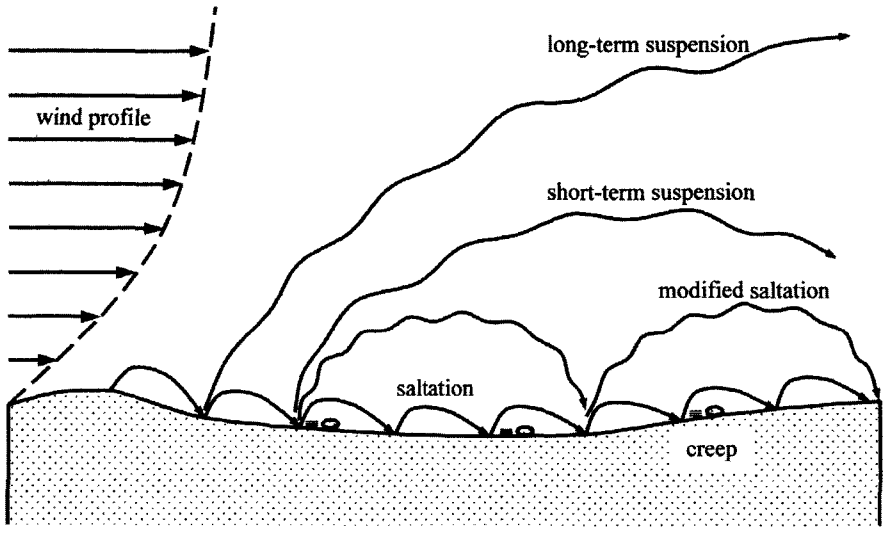

Figure 4. Wind erosion process: modes of transport (After Sterk et al., 2001).

The transition mode between saltation and suspension is known as modified saltation. Trajectories of particles transported in this way show similarities with typical saltation jumps but are significantly affected by turbulence. No clear particle size boundaries exist between saltation, modified saltation and suspension, although typical saltating particles are normally >100 μm whereas suspended particles are usually <50 μm. The lack of clear boundaries indicates that certain particles may be moved by different transport modes, depending on particle density, wind speed and the level of turbulence in the airflow.

The soils of the inland drift-sands in the Netherlands consist mainly of the fraction between 50 and 500 μm (Koster, 1978; Riksen and Sweeris, 2003; Bakker *et al.*, 2003). Thus, saltation is the main transport mode for these drift-sands. As said previously, concentrations of fine gravel can occur in or close to the blown-out areas. De Ploey (1977) found that during heavy winter storms gravel (2-5 mm) is transported by saltation up to a height of 0.5 m. He also showed that the interstratification of fine gravel in dune sand and coversands should not be considered an exceptional phenomenon. The presence of intercalated fine gravel requires nothing more than a local source of gravel prone to deflation. At Kootwijkerzand, concentrations of fine gravel are often noticed on spots with steep slopes (Fig. 5) or where transport zones change into sedimentation zones. Grain size analyses of drift-sands from the Veluwe and Drenthe areas (Koster, 1978; Castel, 1991; Riksen and Sweeris, 2003) showed that the fraction < 50 μm is smaller than 3 %. Therefore, suspension is of no significance in the Dutch inland drift-sand areas.

Sedimentation

When the wind speed drops, its capacity to keep the grains in transport also drops. More grains are falling to the surface than are emitting from it, which results in a net accretion of particles on the surface. This accretion may cause sand accumulation structures to form.

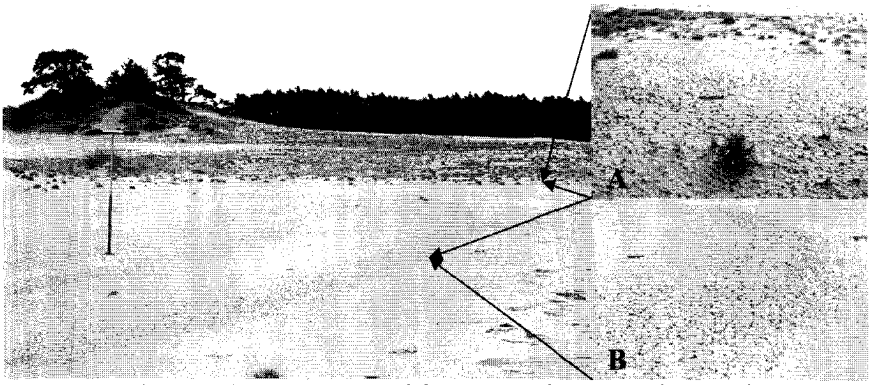

Figure 5. Wind erosion features. A: In the deflation zone of blow-outs ,fine gravel appears on the surface. B: At sufficiently high wind speeds, this fine gravel can go into transport and may be deposited at the crest of small hills or ridges.

Factors Determining the Extent and Impact of Wind Erosion

The extent of wind erosion is determined by the erosivity of the wind on one hand and the erodibility of the soil on the other. Erosion only occurs when the wind's velocity exceeds the threshold velocity required for detaching and transporting the soil particles.

Wind Erosivity

When blowing, near-surface winds provide the shear force that can be expressed in terms of shear velocity (or drag velocity, or friction velocity), u_*. u_* is proportional to the slope of the wind velocity profile (when the latter is plotted with a logarithmic height scale) and is related to the shear stress at the bed (τ_0) and the air density (ρ_a) (Cooke *et al.*, 1993; Nickling, 1994):

$$u_* = \sqrt{\tau_0 / \rho_a} \qquad (\text{m s}^{-1}) \qquad \text{[Eq. 1]}$$

where τ_0 is the shear stress per unit area on the soil surface (g cm^{-1} sec^{-2}) and ρ_a is the density of the air (g cm^{-3}).

Under neutral stability conditions, wind velocity increases logarithmically with height and the velocity profile above the viscous sub-layer (for aerodynamically rough surfaces) can be characterized by the Prandtl – von Karman equation:

$$u_z / u_* = \frac{1}{K} \ln \frac{z}{z_0} \qquad \text{[Eq. 2]}$$

u_z (m s^{-1}) is the wind velocity at height z above the surface, z_0 is the roughness height (m), and K is von Karman's constant, usually 0.4. The roughness height is defined as the layer above the surface where the wind velocity is zero (Cooke *et al.*, 1993).

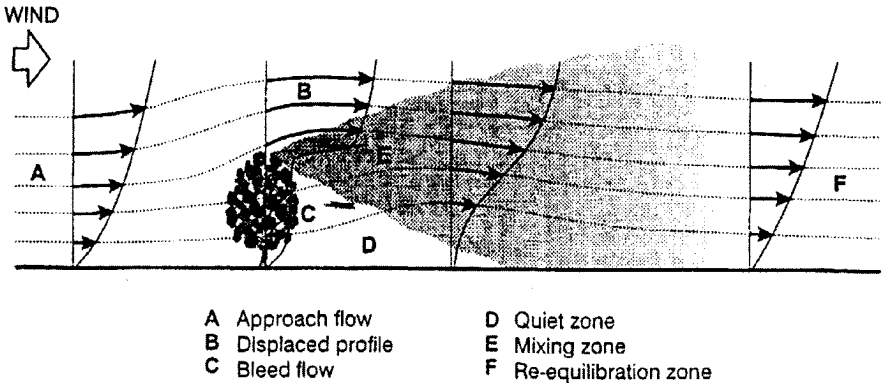

Figure 6. Schematic presentation of airflow regimes around a single windbreak oriented normal to the flow, in neutral atmospheric conditions (After: Cleugh, 1998).

Upper winds act fairly uniformly over wide areas. Within a particular area, the average wind profile depends on the landscape roughness. This roughness is based on the height, size, shape and arrangement of the landscape elements causing the roughness. These elements influence the vertical wind profile and the mean horizontal wind speed as shown in Figure 6 for a single windbreak. Large-scale changes in a landscape will influence the average vertical wind profile and, therefore, the mean horizontal wind speed near the surface. The mean horizontal wind speed near the surface is higher in an open landscape. Given the reforestation and the natural regeneration into forest of most drift-sand areas in the Netherlands in the 20th century, the remaining drift-sand areas have become relatively small in size. The ongoing regeneration further reduces their open character, thereby diminishing the mean average horizontal wind speed in these areas.

In the Dutch drift-sand areas, the elements causing the surface roughness are texture and fine surface gravel (on the bare terrain units) and vegetation (on all other units). Especially in the first succession stages, z_0 may show significant variations in space and time as a result of the interaction of vegetation development and erosion and sedimentation. Values of z_0 over sandy level terrain, without saltation, are of the order of 0.0003 to 0.005 m (Cooke *et al.*, 1993, Nickling, 1994). Under most natural field conditions, however, the z_0 value will be higher.

On nearly uniform, vegetated surfaces, the z_0 plain is displaced to a few cm above the surface (Cooke *et al.*, 1993). Under these conditions the vegetation protects the soil against the erosive winds. In situations where the vegetation does not act as a uniform (or near-uniform) surface, such as during low soil coverage and/or irregular spacing, with relatively large bare spots, the bunched vegetation and individual plants act as isolated elements. A transition zone between bare sand and a 30% vegetation cover can be noted in most drift-sand areas. In this zone, wind erosion is highly variable in space and time. Much of the airborne sediment will be deposited in this zone, thereby covering the existing vegetation. During very strong and long-lasting events, this sediment may be carried further into the vegetated areas.

Terrain topography and single elements like dunes and trees affect the local wind speed, creating zones of higher wind speeds, wind shadows (Fig. 6), and areas

with enhanced turbulence. In general, wind speed increases over windward slopes and decreases over lee slopes.

Closely spaced obstacles may also induce funnelling effects. The curtain of wind-transported sand will concentrate near the funnel of high wind velocity and diffuse at the other side, thereby creating sand-drift structures downwind of the funnel.

It is believed that westerly winds were the predominant influence on drift-sand areas in the Netherlands. Field records of wind erosion activity and wind direction at Kootwijkerzand (Fig. 7) show that under the present conditions the south-westerly winds prevail, although their effect is partly counteracted by erosive winds coming from the east. The easterly winds represent approximately 40% of the periods with high saltation activity.

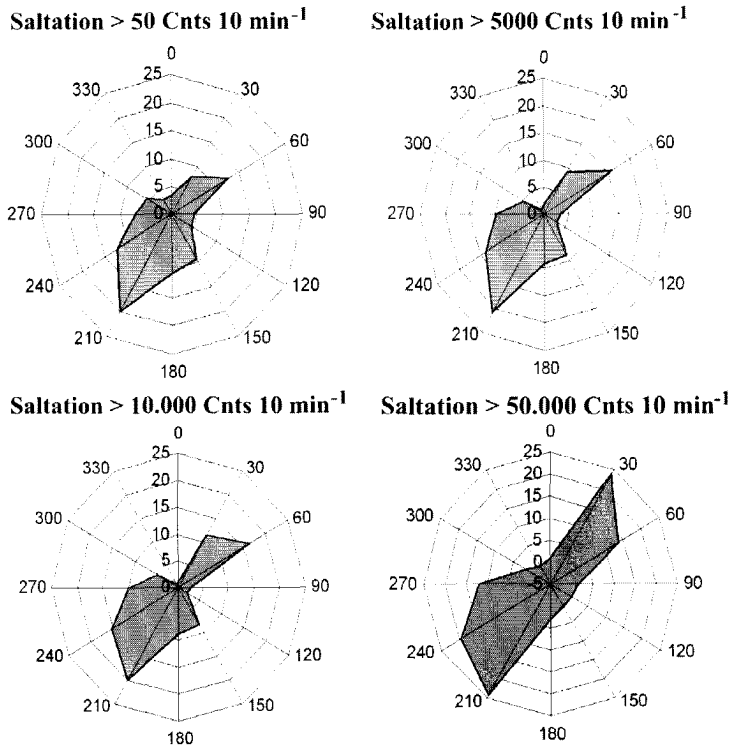

Figure 7. Saltation activity per wind direction at Kootwijkerzand, the Netherlands.

Deflation Threshold and Soil Erodibility

Winds of a given velocity can only carry particles of a maximum size. The threshold shear velocity (u_{*_t}) for any size of particle is the shear velocity at which these grains start to move. Once the bombardment mechanism starts, grain transport may continue even during lower overall wind velocity conditions (Fig. 8).

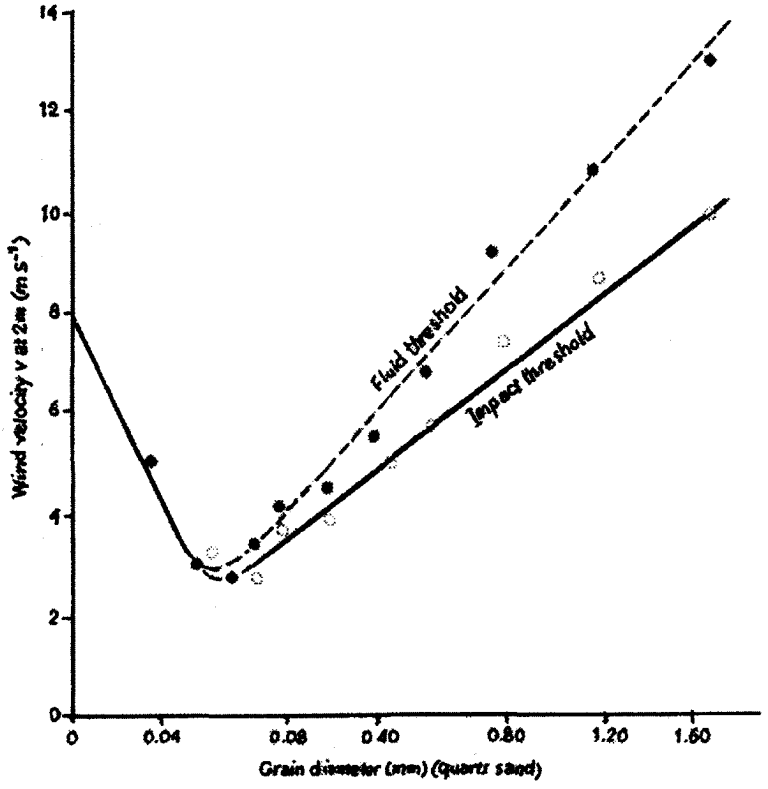

Figure 8. Fluid and impact threshold (Cooke et al., 1993).

Table 3 shows the grain size distribution of the soil at Kootwijkerzand. From Figure 8 it follows that, under dry conditions, the wind velocity (at 2 m) at which wind erosion starts lies between 4 and 7 m s^{-1}. Saltation transport has been recorded at Kootwijkerzand since March 2002, using 3 saltiphones (Spaan and van den Abeele, 1991) at a height of 10 cm above a bare surface. Simultaneously, wind speed has been measured with a cup anemometer at 2 m height. The records show that when saltation starts, the wind speed is between 4 and 9 m s^{-1} (10-min average at 2 m). The data also indicate that wind gusts play a dominant role in the detachment and transport of soil particles.

Table 3: Grain size distribution at Kootwijkerzand.

	n									
Fraction (µm)	**1**	**2**	**3**	**4**	**5**	**6**	**7**	**8**	**Average**	**St. dev**
< 50 (%)	1,4	2,3	3	1,9	3,3	3,1	1,4	1,9	2,3	0,8
50 – 500 (%)	84	91,3	91,8	85,3	84,2	81,4	86	86,2	86,3	3,6
> 500 (%)	14,6	6,4	5,2	12,8	12,5	15,5	12,6	11,9	11,4	3,7
Median (µm)	274	257	238	259	232	257	294	241	256,5	20,4

Grain size distribution was determined for the upper 5 cm on 8 randomly chosen locations. The samples were composed of 10 randomly taken sub-samples. Each sample was first sieved at 1 mm to exclude possible vegetation residue, and then analysed with a Malvern Mastersizer (type: S). As the samples showed nearly no aggregation, all analyses were done in water.

The packing density of the grains influences the susceptibility of the soil to wind erosion, probably because of its effect on soil moisture. Loosely packed fine sand dries more rapidly than compact fine sand. Aggregation is another factor influencing soil erodibility. Most drift-sand soils, however, lack structure due to the low clay and organic matter content.

Factors Controlling Wind Erosion Activity

Wind erosion is controlled by many factors. In inland drift-sand areas, the most important of these are vegetation, soil moisture and crust formation.

In areas covered by vegetation the soil is protected against the wind. The cover determines which areas are susceptible to wind erosion. It is generally assumed that areas are no longer susceptible to wind erosion from a vegetation cover percentage of 70%. Under undisturbed conditions, vegetation slowly changes the soil properties by producing organic matter as shown in Table 2. This process will reduce the erodibility of the soil surface. The effect is probably only minimal, however. More important is the increase in fertility of a soil that contains seeds. Removing the vegetation to re-activate wind erosion in areas with a minimum level of soil development is rarely successful because of the rapid regeneration of the vegetation. Only when sufficient wind erosion occurs in the period immediately after the removal, can the effect have a more permanent character.

On bare drift-sand the moisture content of the top layer is the dominant factor controlling wind erosion. Under wet conditions, entrainment of soil particles is only possible during high wind speeds. When the pores between the loose particles are saturated, the particles are only partly exposed to the wind. The grains are held together tightly by the surface tension in the meniscuses. This form of cohesion disappears when the meniscuses are broken during the drying process. Drying is a more rapid process at those locations that rise above the surrounding terrain. These locations often contain fresh deposits from the last event (Fig. 9). As soon as u_{*_l} drops below u_*, particle entrainment starts. Entrainment will continue until a soil layer has been reached where soil moisture is too high to maintain deflation. Wind erosion will stop in areas where the soil surface has reached the water table. The gradual lowering of the water table in Europe since 1400 AD has contributed to the formation of many drift-sand areas, e.g. near Bremervorde in Germany, Lheebroekerzand, Drouwenerzand and Mantingerzand in the Province of Drenthe in the Netherlands, and Marchfeld near Vienna in Austria (Slicher van Bath, 1960).

On wet surfaces, particle movement by wind is mainly restricted to transport. Scouring of the soil surface is observed near obstacles (Fig. 9). Under wet soil conditions the particle transport rate may increase due to splash drift (De Ploey, 1977; Cooke *et al.*, 1993). This process will be discussed later in this paper.

The relative humidity of the air influences the moisture condition of the topsoil and, therefore, the soil's erodibility. The rate of exchange of moisture between the soil surface and the lowest air layer depends on wind velocity, soil and air temperature, and the difference in moisture content between soil and air.

Knottnerus (1985) found that, for cover sand, the critical wind velocity increased from approximately 7.5 m s-1 to approximately 12.5 m s-1 (at 10 m height) when the relative air humidity increased from 45% to 75%. In Europe, the easterly winds are generally drier than the more dominant south-westerly winds. Although easterly sand storms are less frequent than westerly sand storms, the easterly storms can thus generate considerable sediment transport.

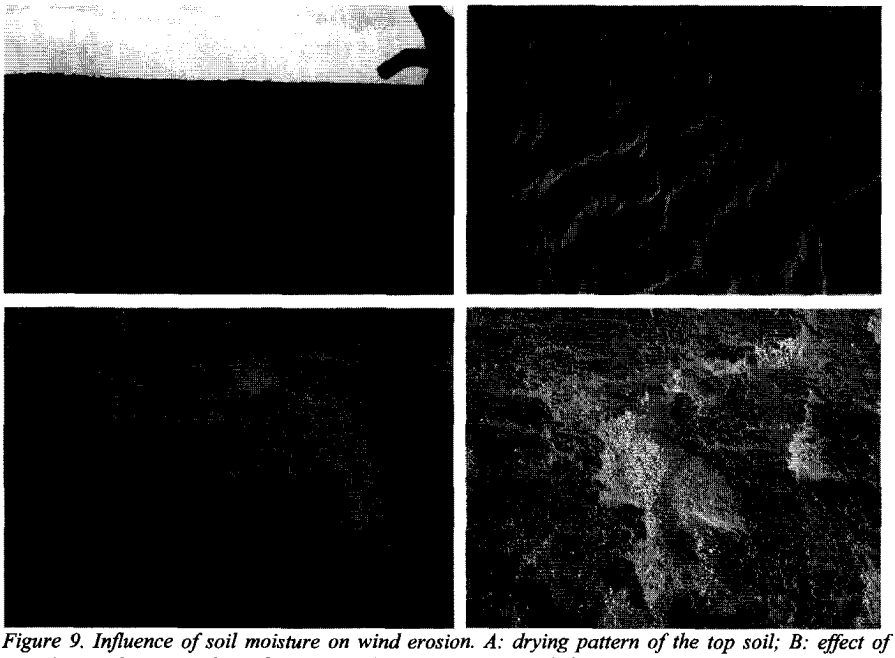

Figure 9. Influence of soil moisture on wind erosion. A: drying pattern of the top soil; B: effect of scouring on the wet surface of a windward dune slope; C: eroded sand knoll; D: a wetted mechanical crust is partly eroded away.

Two main types of surface crusts occur in drift-sand areas: physical crusts, which develop after rainfall, and biological crusts (Fig. 10). Physical crusts (Fig. 10A) play an important role on bare drift-sand and the first succession stage. They result from the drying of the soil, as discussed above, but are not very strong. Biological crusts, on the other hand, consist of algae. The algae are present in the bare soil as well as in the first four succession stages. Pluis (1993) found that only low amounts of algae occur on active drift-sands at any given point in the year. However, a strong algae crust can develop between the first succession stage and the full development of a *Polytrichum* carpet (Fig. 10B).

Pluis (1993) describes a sequential development from an algal community dominated by the filamentous *cyanobacterium Oscillatoria* through a crust in which initially the filamentous green algae Klebsormidium and later the unicellular *cyanobacterium Synechococcus* predominates. This crust is eventually succeeded by a *Zygogonium ericetorum* crust.

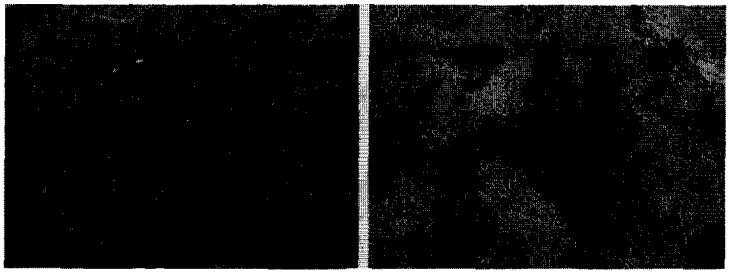

Figure 10. Surface crusts at inland drift-sand area Kootwijkerzand. A: Physical crust; B: Algae crust dominated by Zygogonium ericetorum

Algae crusts develop mainly under conditions of high moisture and low wind erosion activity. The development rate increases once the surface is more or less protected by pioneer vegetation, often *C. canescens*. Biological crusts range from 1 to 6 mm thick. Once a crust has been developed, the soil under it is protected against erosion. Only the loose particles on the crust are available for entrainment. Crusts developed near the bare active drift-sand zones may become covered by blown-in sediment. When this happens, the subsequent development of the crust will become retarded. At greater distances from the active zones the loose soil material on top of the crust is mainly moved by rain splash or by overland flow. The crust formed by *Z. ericetorum* is water repellent. Overland flow occurs in areas covered by this type of crust, especially during rainfall after an extreme dry period.

The Role of Wind Erosion in Drift-Sand Areas

The effects of wind erosion vary highly in time and space and they largely depend on the amount of sand available for wind erosion, on the local field conditions and on the weather. Three different zones can be distinguished: a deflation zone, a transport zone and a deposition zone. On an active sand dune, the location of these zones changes with the wind direction. In more or less flat and uniform drift-sand areas, on the other hand, deposition mainly occurs at the transition zone (first succession stage), and transport mainly in the unvegetated area.

The Deflation Zone

The erosional surfaces can be recognized from their abundance of coarse grains, which are absent on depositional surfaces. In the deflation zone the soil will further degrade as a result of the loss of fine particles, soil organic matter, seedlings and seeds. Roots can even outcrop (Fig. 1F). In some cases deflation may lead to a complete elimination of the scarce vegetation.

The Transport Zone

Ripples (Fig. 11A, B) and ephemeral shadow dunes (Fig. 11C) are the most common signs of recent wind erosion activity in the transport zone. Ripples are formed by grains in saltation. They migrate downwind quite rapidly, and usually have a rather short life span. Ripples are absent 1) at locations with very coarse sand; 2) at conditions of high friction velocity; 3) where there is grain-fall into local areas of low wind velocity (Cooke *et al.*, 1993). The ripple pattern is variable. It is strongly related to the degree of maturity of the ripples, to the wind velocity, to the texture of the sand, to the slope and the moisture condition of the underlying surface, and to the orientation of the field slope relative to the wind direction (Fig. 11A and 11B).

Single obstacles in the transport zone will have only a local effect. Sand is deposited in the shadow zone downwind of the obstacle. This zone is characterised by swirls and vortices of air whose average forward velocity is less than that of the air stream outside (Bagnold, 1973). Obstacles may create shadow dunes or lee dunes, depending on the rate and amount of sand supply, the friction velocity u_* and the geometry of the obstacle (Bagnold, 1973, Cooke *et al.*, 1993). The shadow dunes downwind of small obstacles in the transport zone can be classified as ephemeral dunes. They may form quickly, in less than an hour, and disappear when the wind direction changes. Their orientation thus makes it possible to reconstruct the prevailing wind direction during the last event (Fig. 11C).

Within the transport zone, fine sand, seeds and organic matter may settle in the wind shadow of obstacles, in footprints and in wheel tracks, where a sudden drop in

u_* occurs. Under favourable conditions the settled seeds (mainly *C. canescens*) will germinate. Once the new vegetation has become well established, it forms a new barrier in the transport zone, causing further accumulation of sand. In wheel tracks this can even lead to the formation of ridges (Fig. 11D), which have a more permanent character.

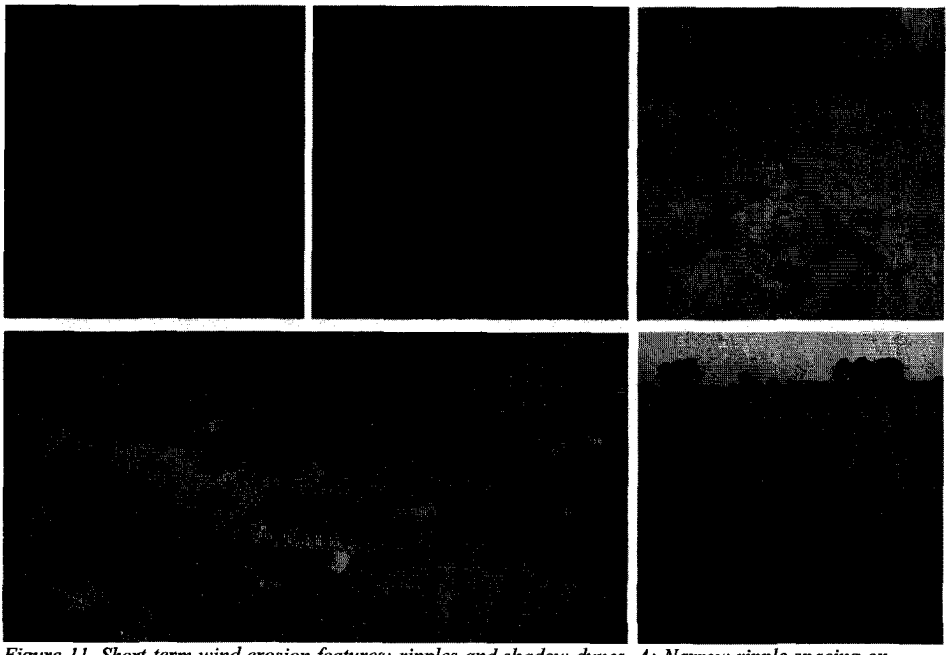

Figure 11. Short-term wind erosion features: ripples and shadow dunes. A: Narrow ripple spacing on downwind slope of a dune; B: Wide ripple spacing in coarse sand on a windward dune slope; C: Shadow dunes formed behind clumps of grass; D: Establishment of Corynephorus canescens in car tracks, Kootwijkerzand, September 2001; E: Accumulation of sand in the vegetation bunds creates ridges, Kootwijkerzand November 2002.

The Deposition Zone

Deposition takes place in the transition zone between the bare sand and the vegetated area where it can form ridges, and on dunes. A field experiment at Kootwijkerzand showed that the pioneer grass *C. canescens* profits from sedimentation by showing a strong rejuvenation, whereas algae more or less disappear from the surface. Regular deposition of fine sand can help maintain the poor soil conditions that are required for pioneer vegetation like the moss *P. piliferum* to survive. Without this mechanism, soil fertility will slowly increase, and higher plant species will take over the succession.

The zones with deposition can become very vulnerable to wind erosion when the vegetation cover drops below a critical level, usually around 30%. Freshly deposited fine sand is highly erodible because of its texture and because it is only loosely packed. Its water holding capacity is low, and it dries much faster than the soil surface in a transport zone does.

Main problems in present inland drift-sands affecting wind erosion activity

The effect of wind erosion in a landscape mainly depends on the extent and the intensity of the erosion. Without sufficient transport, no important changes will occur in the deposition zone. Wind erosion can be stimulated by maintaining the open character of the landscape, for example by regularly removing the seedlings of *P. sylvestris*. In the wind shadow of a forest, erosion can be stimulated by cutting a wind lane in the forest upwind of the locations where an increase in wind activity is preferred.

To guarantee a high level of wind erosion, a sufficiently large area, with enough material to blow away, is also required. Lack of erodible material in a drift-sand area may have various causes; 1) the drift-sand area is located in an erosion zone, where most of the erodible sand has already been blown away or 2) the source areas have become too small due to colonisation by algae and other vegetation.

Where only little sand is available for wind erosion, sand transport and deposition will also be minimal. This will have another consequence than a further stabilisation of the drift-sand by vegetation. Typical wind erosion features, such as dunes, can no longer form. On the inland drift-sand area Kootwijkerzand, wind erosion activity has been monitored on two locations: a more or less flat drift-sand plain and an active dune. On the first location the size of the source area contributing to sand transport is limited to less than 1 ha. The second site is located on an active dune, which is situated in the centre of a much larger active complex covering more than 10 ha. The raising (due to aeolian accumulation) or lowering (due to aeolian erosion) of the surface at each location was measured with erosion pins (De Ploey and Gabriëls, 1980). On both sites erosion pins were installed along a SW-NE transect, along the prevailing wind direction. The pins were 50 cm long and had a diameter of 5 mm. All pins were checked weekly. They were read with a precision of 1 mm. Table 4 shows the erosion and sedimentation rates for three intervals (one with easterly winds and two with south-westerly winds), during the period 13 March 2003 - 24 July 2003. On the dune, the spatial and temporal changes in surface level are more variable than on the erosion plain where the surface level is quite stable. The ongoing erosion and deposition on the plain have created a vegetated ridge at the plain's border. In the plain's centre, a modest lowering of the sand surface is observed (Table 4).

Analysis of the surface texture on the plain showed an increase in the coarse sand fraction compared to the surrounding regions. An increase in the amount of fine gravel on top of the surface was also visible.

Table 4: Statistics of the weekly accumulation flux (cm) in the period 22 March 2003 - 12 June 2003 on a drift-sand dune and a drift-sand plain, Kootwijkerzand, the Netherlands.

		Dune						Plain				
Week	Main wind Dir.	foot NE	slope NE	top NE	top SW	Slope SW	foot SW	Veg. NE border	NE	cente r	SW	Veg. SW border
5	E	-6	-9.5	-7.7	-2	-1.7	11.3	-0.2	0	-0.5	0.7	0.2
7	SW	0.3	3.4	0.5	0.1	-2.2	-1.9	0	-0.9	-1.4	-1.7	-0.4
11	SW	0.2	0.5	0.4	-2.7	1.2	-1.7	0.3	0	-0.1	-0.2	0
Net effect total period		-3.6	-10.6	-5.3	4.2	2.8	4.3	-0.1	-0.2	-1.7	1.9	-0.3
Weekly average		-0.3	-0.9	-0.4	0.4	0.2	0.4	0.0	0.0	-0.1	0.2	0.0
stdev.		2.0	3.6	2.5	2.3	2.0	3.7	0.3	0.4	0.8	0.8	0.2

More detailed information on the erosion activity and the actual sediment transport was obtained via sediment transport measurements on the two described locations. Sediment transport by wind was measured with MWAC (Kuntze *et al.*, 1990) catchers. Five catchers were installed along the erosion pin transect on the drift-sand plain, and nine catchers were installed on the dune. The horizontal sediment flux was calculated for all catchers using the combined mass flux model of Vories and Fryrear (1991) and Fryrear and Saleh (1993). Table 5 shows the sediment transport for three different periods. During the first two periods, particle transport was mainly caused by wind whereas the last period was characterised by heavy rainfall in combination with strong winds. In periods with only wind erosion the transport ratio dune: plain varies between 1:0.02 and 1:0.04. Under wet conditions, the ratio changed to 1:0.3.

The first period (18 Sep - 2 Oct 2003) showed only moderate wind erosion. Sediment transport in the vegetated border zone was too small to reduce vegetation development effectively. Only high transport rates, such as in the period 24 Oct - 14 Nov 2003, led to a reduction of the vegetation cover and transport the sand further into the vegetation. Notice that transport in the vegetated NE border of the plain is still about 50% of the transport in the centre of the plain. In the wet period (15 Jan - 19 Jan 2004), sediment transport was almost equal all over the plain, indicating that splash and splash-drift were the main mechanisms responsible for the sediment transport. On the dune, spatial variations in sediment transport remained prominent due to the effect the dune exerts on wind velocity. The mechanism and the significance of splash and splash-drift in inland drift-sands will be discussed below.

Table 5: Total mass transport values (kg m^{-1}) on a drift-sand dune and a drift-sand plain at Kootwijkerzand, the Netherlands.

	Dune			Plain				
period	NE slope	W slope	S slope	Veg. NE border	NE border	Centre	SW border	Veg. SW border
18 Sep. - 2 Oct. 2003	35.1	17.5	9.7	0.1	0.2	0.7	0.0	0.2
24 Oct. - 14 Nov. 2003	288.4	357.6	196.0	11.9	11.7	22.0	4.1	0.1
15 Jan. - 19 Jan. 2004	4.3	10.9	7.6	2.4	2.8	2.3	1.7	2.0

Splash Erosion

During the impact of raindrops the energy of the drops is transferred to the surface. Raindrop impacts initiate substantial changes in the state of the surface at and near the point of impact. On bare surfaces of sufficiently fine and un-cemented particles, the following effects are prominent:

- detachment, followed by emission, lateral transportation and subsequent deposition of several tens to several hundreds of particles near each point of impact;
- disintegration (partial or entire) of aggregates into smaller aggregates, or into individual grains;
- temporal and local increase, followed by sudden decrease, of pore water pressure in the upper sediment layer, which may affect the fabric of the top layer;
- remodelling of the micro-topographic structure and roughness of the surface.

All these effects result in a new surface structure, which may substantially deviate from the one before the rain shower. On unvegetated dunes and drift-sands,

which are characterized by low aggregation and a high permeability (and, thus, a dry surface layer), displacement of sediment and changes in micro-topography are the major effects of rain splash.

Displacement of the Sediment

On homogeneous, horizontal surfaces and under vertical impact conditions (no wind), splash erosion can be roughly approximated as a spatially symmetric process, in which both the displacement flux and the displacement distance (more correctly: the spectrum of displacement distances) are identical in all directions. Minor deviations in symmetry may be observed for individual impacts, but for sufficiently large impact areas, with many impacts, the sediment transport pattern initiated by splash is symmetric. This is no longer true when the angle between the impacting drops and the sedimentary surface deviates from 90 degrees. Such deviations may result from slope inclination (non-horizontal terrain), from oblique rainfall due to wind, or from a combination of these factors. The vertical impact of raindrops on a tilted surface results in a net displacement of grains in the down slope direction. Grains emitted downslope move a longer distance along their aerial trajectory compared to grains emitted upslope, hence they will travel a longer distance along the slope. In the case of oblique, wind-driven impacts, the extra energy supplied by the wind is an important additional factor. Although oblique rains transfer less energy to the soil than vertical rains do (Goossens *et al.*, 2000), they stimulate the downwind displacement of particles because the emitted grains receive an additional velocity component in the downwind direction. Although sediment will be emitted in all directions upon impact, most transport will occur downwind when the effect of the wind (on splash) is not counteracted by the effect exerted by slope inclination. At a constant energy of impact, oblique impacts will result in a decrease (compared to vertical impacts) of the average splash flux on the rain-facing slopes and in an increase of that flux on the opposite slopes, but the higher energy of impact on the former slopes (which correspond to the windward slopes) counteracts the process. The final splash picture will thus depend on the balance of all sub-processes, and also on the local characteristics (texture as well as structure) of the surface.

The airborne displacement (by wind) of sediment originally detached by splash has been defined in the literature as splash drift. It is an important transport mechanism on bare sand surfaces: heavy wind may result in horizontal displacement distances of the order of meters, whereas particles are rarely displaced more than a meter in the case of vertical rains.

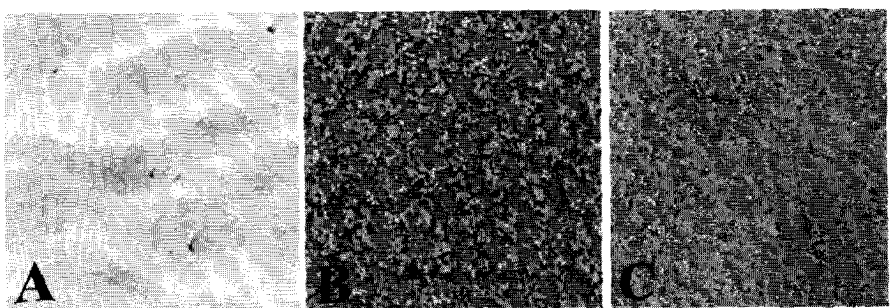

Figure 12. Sand surface prior to a rain event; 12B: Surface after first impacting raindrops; C: Surface after heavy and long-lasting rainfall.

Changes in the Topsoil's Micro Topography

On loamy soils rain splash generally leads to a smoothening of the top layer. The aggregates are partially or completely destroyed by the impacts, and the temporarily enhanced soil water pressure re-organizes the packing, which results in surface sealing. On dune sands, which are characterized by a high permeability and a low to very low degree of aggregation, impact by raindrops leads to an increase of the surface roughness. This is illustrated in Figure 12. Figure 12A shows a dune surface prior to a rain event. Apart from a few ripples created during the latest episode of wind erosion, the surface is relatively smooth. The first impacting raindrops change the micro-relief radically (Figure 12B). Each impact creates a shallow crater surrounded by an irregular, roughly circular pile of sand grains ejected during the impact.

The life span of the new topography depends on the intensity of the rain and the duration of the rain shower. Heavy and long-lasting rainfall will finally destroy the topographic structure and transform it into a new structure like the one shown in Figure 12C. The impact craters are still prominent, but the sand piles have been destroyed by the continuing rainfall. However, in the case of sufficiently gentle and sufficiently short showers the structure shown in Figure 12B may persist for a long time provided no new rain occurs. The new micro-relief may affect the onset of deflation during the next period of high winds, either positively or negatively, and it will also affect the heat economy in the top layer as long as it persists.

Role of Splash Erosion in Drift-Sand Areas

Splash erosion is an important mechanism of sediment displacement on drift-sand that has become largely colonized by vegetation. The plant cover effectively shelters the sand from the wind and there is no, or nearly no, wind erosion on these soils. Apart from biological activity, splash erosion is the only substantial mechanism that is still able to initiate horizontal movement of sediment on these surfaces. Splash moves not only sand grains, but also organic (and other) material present on the ground.

Table 6: Deposition by splash at different succession stages at Kootwijkerzand, the Netherlands.

Succession stage	Vegetation cover (%)	Sediment (g m^{-2})
0	0	2868
2	50	286
4	70	109
5	99	4

Measurements carried out on plots installed at locations in a different state of succession in the Kootwijkerzand area clearly show that even on surfaces nearly completely covered by vegetation, a measurable amount of sediment is displaced by splash (Table 6). Displacement of sediment by wind heavily dominates in the succession stages No. 0-2, but from succession stage No. 4 onward there is no further wind transport due to the vegetative shelter.

The drift-sand vegetation may substantially benefit from grain transport by splash. The horizontally and/or vertically transported sand particles may be caught by species with a vegetative structure that conducts the water to the plant centre. Particles caught by the leaves are also washed towards the plant centre and accumulate underneath the plant. Due to the progressive accumulation small, dome-like pedestals (often misinterpreted as micro-dunes) are created underneath the plants. These pedestals are of considerable ecological significance because they hold more rainwater than undisturbed drift-sand does. Especially *C. canescens* and *P. piliferum*

benefits from the accumulation, as this species requires a minimum rate of sand encroachment to survive.

Up to the present, the contribution of sediment transported by wind-driven rain to the total sediment transport budget in drift-sand areas is unknown. One reason is that drift-sands dry very quickly so that they may already re-deflate shortly after a rain-shower. This hampers an accurate measurement of the distinct transport mechanisms. The spatial and temporal variability in the rainfall and wind regime during a rain-shower are an additional handicap. Discontinuities in the episodes of sediment transport further complicate the analysis.

Measurements and observations executed on the Kootwijkerzand drift-sand revealed, however, that sediment transport by splash can be detected by means of acoustic sensors. The use of such sensors for detecting sediment transport by wind has become a routine operation since the early 1990s. Various instruments have been developed since then, such as the saltiphone (Spaan and van den Abeele, 1991) and the SENSIT (Stockton and Gillette, 1990). Careful analysis of saltiphone data collected at Kootwijkerzand showed that, in addition to aeolian transport, the saltiphone also records splash-induced transport. The distinction between the two transport processes is easily recognisable in the data output. Grain transport by wind always results in a high impact rate on the microphone (which has a diameter or 10 mm), usually of the order of a few tens of impacts per second. Grain transport by splash is characterized by a significantly lower impact rate, of the order of 0.5 - 2 impacts per second. The two types of impact are clearly recognizable in the data since no transition exists between the two types of signals.

Figure 13 shows saltiphone and rain data recorded on bare dune sand during a rainy day (3 July 2003) at Kootwijkerzand. No wind erosion occurred on that day because of the rains.

Rainfall amounts and saltiphone counts were recorded during an 8-h time interval, running from 10:30 h local time until 18:30 h local time. Rainfall was measured with a tipping bucket (tipping over after 0.2 mm rain). Three saltiphones, less than 10 m from the tipping bucket, counted the sediment impacts at a height of 10 cm above the surface. Rain and saltation data were stored as 10-second totals. In addition, sediment transport by splash was measured with 26 MWAC (Kuntze *et al.*, 1990) catchers in the direct vicinity of the saltiphones between 16:23 h and 17:26 h local time. The horizontal sediment flux (due to splash) was calculated for all catchers using the method described in Goossens *et al.* (2000).

Figure 13 shows the close-to-perfect agreement between the periods of rain and the periods of splash-induced sediment transport as recorded by the saltiphone. The total saltiphone count (recorded impacts) for the 63-minute period (between 16:23 h and 17:26 h) during which the horizontal sediment flux was measured was 67. The corresponding average horizontal sediment transport (between 0 and 100 cm height) in the downwind direction as measured by the MWAC catchers was 1.30 g cm^{-1}. The effective rain time during the 63-minute period was 610 s; thus, the horizontal sediment flux in the downwind direction due to splash was 2.13 10^{-3} g cm^{-1} s^{-1}. Extrapolating these data to the 8-hour long experimental period, during which 2501 counts were recorded by the saltiphone and 16.8 mm rain were registered by the tipping bucket, the horizontal sediment transport by splash (in the downwind direction) was 48.5 g cm^{-1}.

Although these numbers are preliminary, and should thus be regarded with some caution, they are of the same order of magnitude as those that are commonly measured on bare agricultural fields (see Goossens *et al.*, 2000 for a few examples).

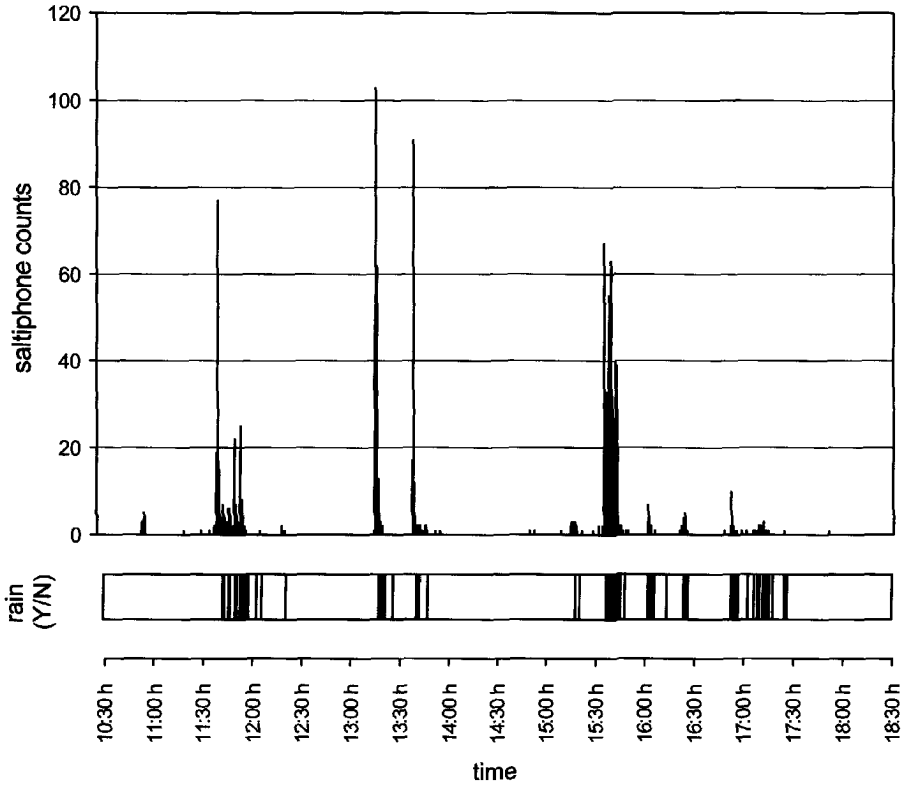

Figure 13. Rainfall and saltiphone data for the 3 July 2003 splash erosion experiment at Kootwijkerzand.

Erosion by Overland Flow

Geomorphologic processes in drift-sand areas are commonly regarded as belonging to the domain of the wind. This is accurate for dunes that are actively formed, but not for dunes that have been stabilized (Jungerius and Dekker, 1990). Dune slopes steeper than about 6° are subject to water erosion just like any other sloping terrain in the humid climates of the world. They are subject to the same processes, such as splash erosion and slope wash by overland flow. Also, the same factors as used in the Universal Soil Loss Equation apply: characteristics of the rainfall, nature of the vegetation, and length and steepness of the slope (Wischmeier and Smith, 1965). Only the properties of the soil are rather complex: conditions for overland flow include water repellency and impeded infiltration shown by the surface sand when dry.

Water Repellence

Water repellence of surface horizons is an often unobserved, but extensive property of sandy soils that dry out. It can be recognized by adding a drop of water to the surface of a dry soil. If the water upon contact with the soil 'balls up' into a sphere instead of being quickly absorbed, the soil is water repellent. Clean, dry sand readily absorbs water due to the strong attraction between the mineral particles and water. The affinity for water can be reduced by a range of hydrophobic organic materials including fungal hyphae (Bond and Harris, 1964), humic acids (Roberts and Carbon, 1972) and decomposing plant material (McGhie, 1987). They are either mixed with the sand or form a coating on the sand particles. Mashum and Farmer (1985) provided evidence that molecular orientation of organic matter determines whether or not a soil is water repellent. The ensuing water repellency is therefore explained by reference to the nature of the outer surface of the organic material that water encounters when attempting to infiltrate (Horne and McIntosh, 2000). Once the soil is moist throughout, its hydraulic conductivity is so high that no overland flow will develop. This may explain the observed larger-percent runoff from initial rainstorms as compared to later, comparable storms.

Water repellence can be found all over the world under a variety of climatic conditions (DeBano 1981) and under a variety of vegetation types including forests, brush fields, and agricultural lands. Dekker (1998) investigated the phenomenon in most soils of the Netherlands. He found that 75% of the agricultural surface soils and 95% of the surface soils in nature reserves, including dunes, exhibit strong to extreme water repellency. Dekker and Jungerius (1990) examined the water repellency of the coastal dunes, which in many ways are comparable to drift-sands. Grey dune and drift-sands are particularly water repellent when they dry out. Vegetation also plays a role, sands under *Ammophila arenaria* being less water repellent than those under *C. canescens*. Burning of vegetation is conducive to water repellency (DeBano, 1979).

Water repellency is commonly measured with the water drop penetration time test (WDPT). This is the length of time needed for drops of distilled water placed on a smoothed air-dry surface of soil to be completely absorbed by the soil. Generally, a soil is considered water repellent when the WDPT exceeds 5 seconds. It is an arbitrarily chosen period, which has no physical meaning.

Slope Wash

Overland flow under water repellent conditions is essentially of the Hortonian type because it is a function of rainfall intensity, infiltration capacity and slope position (Jungerius and Dekker, 1990). Erosion of the sand by overland flow occurs as either dispersed or concentrated surface wash (Carson and Kirkby, 1972). In the latter case, rills are formed on the slope (Fig. 14A). The mass of sand and water transported downslope gradually turns into a waterlogged slurry, much resembling a mudflow. This is actually a mass movement process because the ratio of solid material to water is very high. The tongues of the flow loose their water by percolation into the surface they pass, and this will bring them to a halt. First the sand is deposited, then, lower down, the organic material that has been washed out (Fig. 14B). The sand, which eventually reaches the base of the slope, is laid down as a fan of colluvium. The fan has a characteristic slope angle of 6°.

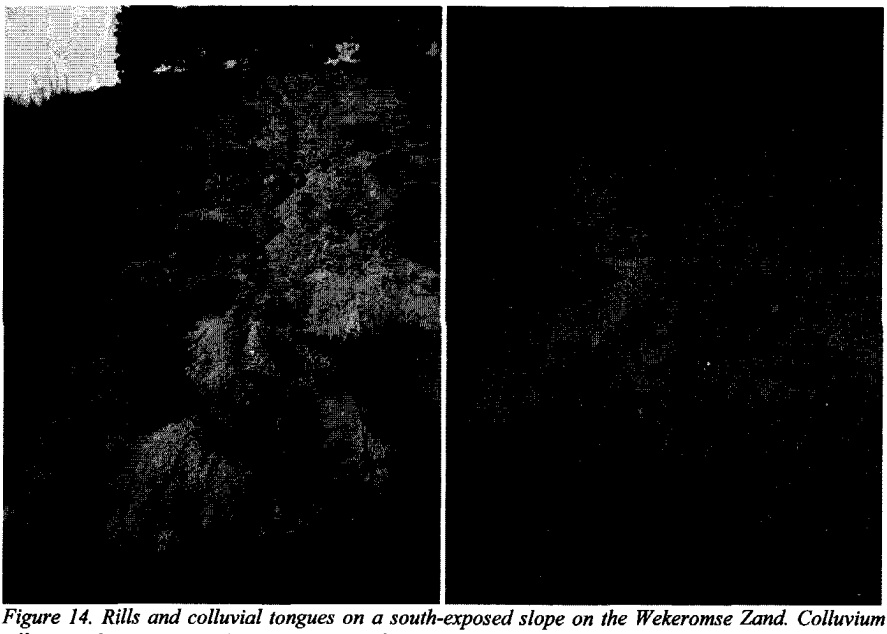

Figure 14. Rills and colluvial tongues on a south-exposed slope on the Wekeromse Zand. Colluvium offers good growing conditions because it has a relatively high organic matter content and remains moist when the surrounding slopes are already dry; 14B: Immobilized mudflow tongues. The sand is laid down first; the organic material is washed out and laid down as a rim around the sand.

The Role of Water Erosion in Drift-Sand Areas

Slope wash is particularly active on sparsely vegetated south-oriented slopes where bare sand at the surface is exposed to the sun and dries out quickly. The rills and the tongues disintegrate within a few days after the rain, which makes it difficult to assess the extent of water erosion on slopes. The colluvial fans at the base are more stable. Water erosion processes in drift-sand areas have important geomorphologic consequences. In contrast to wind erosion processes, they lead to a gradual leveling of the sand dune relief: the slopes are worn down in the upper sections and are covered by colluvium in the lower sections.

Although, in some drift-sand areas, water erosion processes are more widespread than wind processes, no research has as yet been done on the ecological consequences. The entrained seeds germinate easily in colluvium because this material has a relatively high organic matter content and remains moist when the surrounding slopes are already dry. It is favoured by the pioneer moss *P. piliferum* and various types of soil fauna. On the other hand, *Campylopus introflexus* avoids sites with water erosion and colluvium, because it is not resistant to many geomorphologic dynamics (Kooijman *et al.*, 2000).

Mass movement

Besides mud flows (see previous section), two additional types of mass movement can be distinguished in inland drift-sand areas: side wall failure and sand flow (avalanching) down the slip faces of an active dune.

Sidewall Failure

Sidewall failure is a common feature on steep slopes of plateau dunes and stabilised drift-sand dunes. Undermining by wind and/or water erosion is often the main cause, but wall failure may also be caused by human activities. Wall failure occurs when the resultant downward force caused by the weight of the soil exceeds the upward resistance force produced by the internal friction. When this happens, for instance due to an increase of the soil's weight as a result of an increase in soil moisture, or due to human activity, wind and water erosion may be stimulated due to the loss of the protective vegetation cover. Where the soil clumps are deposited (Fig. 15 A and B), erosion may be observed around the clumps due to the influence the clumps exert on the air and/or water flow. The effect of this process on ecology and landscape remains very local, however, and is more or less similar to that of slope wash. Over time, it leads to a gradual levelling of the sand dune relief.

Sand Flow

Sand flows down the slip face when the latter exceeds a critical angle, which is 33° for typical drift-sand (van der Meulen and van Rooijen, 1981). The point at which the flow starts is known as the pivot point. At this point, failure reduces the slip face from the angle of initial yield to the residual angle after shearing (angle of repose). The difference between these two angles is on average about 2.5° (Cooke *et al.*, 1993). After failure, a 5-10 cm scarp cuts back upslope from the pivot point to the brink and remains active for many minutes, feeding a sand flow avalanche. Avalanche deposits have a very low bulk density. The sand flow will come to rest at the gentler slope at the base of the dune. Avalanches affect only a relatively small area at the base of the slip face, where they can locally cover the vegetation (Fig. 15C). The frequency of sand flows on slip faces depends on the wind erosion activity in the upwind area. Sand flows mainly occur when sand transport rates are sufficiently high.

Conclusions

To preserve inland drift-sands as a nature reserve for the future, it is necessary to understand the landscape characteristics and the landscape differentiating processes. Active inland drift-sands are characterized by their:

- Relief: blow-outs, plateau dunes, drift-sand dunes and ridges.
- Distinct stages in the natural succession, with typical pioneers like *C. canescens*, *S. morisonii, P. piliferum*, lichen like *Cladonia sp.*, and *Cladina sp.*
- High dynamics: the landscape is changing constantly in time and space by the high intensity of the landscape differentiating processes: soil erosion, and regeneration (starting by colonisation of the bare drift-sand surfaces by pioneer vegetation, followed by the natural succession of the vegetation into forest).

To preserve the inland drift-sand areas and their characteristics, the degradation and regeneration processes should be in balance over time. However, since the 1960s the remaining drift-sand areas in the Netherlands showed a rapid decline in size due to a rapid colonisation by pioneer vegetation followed by the natural succession. This is attributed to:

- the reduced size of the remaining active drift-sand areas after the reforestation in the first half of the 20th century;
- the change in land use in these regions: from agricultural or military use into nature (only high recreation pressure can produce the same effect);

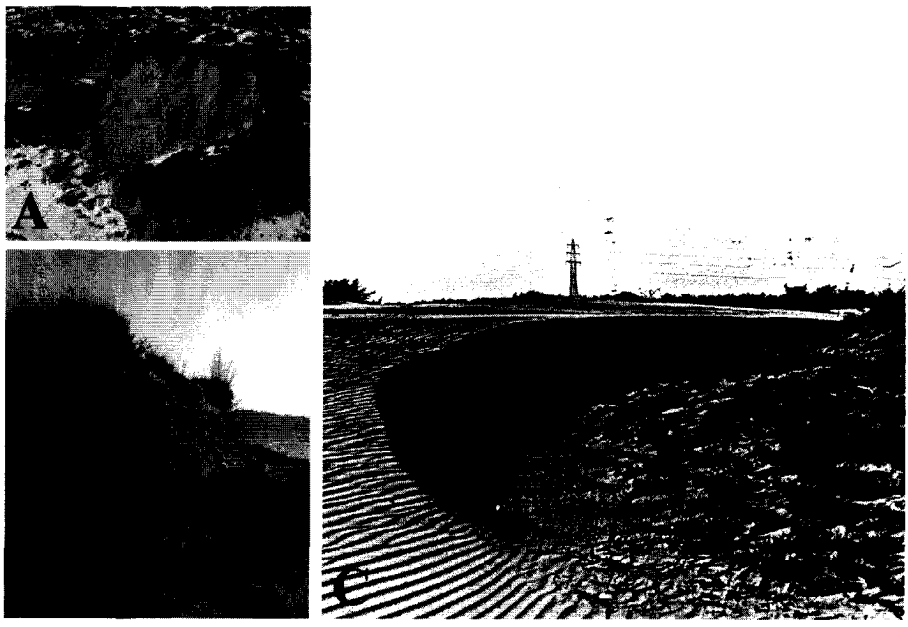

Figure 15A, B. Mass movement due to undermining by wind and/or water erosion; 15C: Sand flow down a slip face at Kootwijkerzand (photo van der Meulen and van Rooijen, 1981).

- the increased atmospheric nitrogen deposition caused by the intensive bio-industry in the Netherlands;
- the introduction of exotic plant species like *C. introflexus* and *P. sylvestris* .

In the development of the inland drift-sand areas, wind erosion has been the major process in landscape formation. In the inland drift-sand areas in the Netherlands the reforestation and the colonisation of the bare sands by vegetation have tempered the influence of wind erosion. Other erosion processes like rain splash, rain-wash, rill formation and mass movement have also become important. Wind erosion, and to a lesser extent splash drift, can generate sediment transport over relatively long distances. Splash, rain-wash, rill formation and mass movements have only a local effect, but can contribute to slowing down or setting back the natural succession. However, where wind erosion has created dunes, the latter processes lead to a gradual levelling of the landscape.
To preserve the typical drift-sand landscape, dune formation is needed. Field measurements showed that this could only happen when sand transport by wind takes place at regular intervals and in sufficiently high amounts. To obtain enough wind erosion activity with adequate sediment transport, the following preconditions should be met:

- a sufficiently large source area: at least 10 ha of highly erodible cover sand or drift-sand;
- a high wind speed at the soil surface inside the source area: no obstacles reducing the wind speed should appear in or near the source area.

Human interventions should focus first on slowing down the natural succession, and then on stimulating erosion. These interventions can reinforce each other. On one

hand, slowing down or setting back the natural succession by removing vegetation and trees will stimulate the erosion. A high erosion activity, on the other hand, can help slow down the natural succession in the zones influenced by wind erosion or sedimentation.

Acknowledgements

This study was carried out as part of the research project "Making use of Wind and Water Erosion Processes in Dutch Landscape Development", carried out by the Erosion and Soil & Water Conservation Group of Wageningen University, and was funded by the Dr. Ir. Cornelis Lely Foundation, the C.T. de Wit graduate school of Product Ecology and Resource Management (Wageningen University). The field experiments were realized in co-operation with the Dutch Forestry Foundation (Staatsbosbeheer), who provided the experimental terrain and assisted with the preparation of the experimental plots. Special thanks are expressed to Huiberdien Sweeris and Piet Peters for their assistance during the field measurements and the laboratory work. We also thank Rita Ketner-Oostra for sharing expertise on drift-sand vegetation.

References

Ancker, J.A.M. Van den and Jungerius P.D., 2003. *De ontwikkelingsmogelijkheden van stuifzanden op de Weerterheide/Boshoverheide.* Rapport Bureau G&L in opdracht van DGW&T, ministerie van Defensie.

Bakker, T., Everts, H., Jungerius, P.D., Ketner-Oostra, R., Kooijman, A., Turnhout, C. and Esselink, H., 2003. *Preadvies Stuifzanden.* Report EC-LNV No. 2003/228-0. Expertisecentrum LNV, Ministerie van Landbouw, Natuur en Voedselkwaliteit, Ede/Wageningen, the Netherlands, 114 pp.

Bagnold, R.A., 1973. *The physics of blown sand and desert dunes.* 5th ed., Chapman and Hall, London, UK, 265 pp.

Bond, R.D. and Harris, J.R., 1964. The influence of microflora on physical properties of soils. I. Effects associated with filamentous algae and fungi. *Austr. J. Soil Res.* 2: 111-122.

Carson, M.A. and Kirkby, M.J., 1972. *Hillslope form and process.* Cambridge University Press, Cambridge.

Castel, I.I.Y., 1991. *Late Holocene eolian drift sands in Drenthe* (the Netherlands). PhD thesis, Department of Geography, University of Utrecht, 157 pp.

Cleugh, H.A., 1998. Effects of windbreaks on airflow, microclimates and crop yields. *Agroforestry Systems* 41: 55-84.

Cooke, R., Warren, A. and Goudie, A., 1993. *Desert Geomorphology.* UCL Press, London, UK, 526 pp.

DeBano, L.F., 1979. Effects of fire on soil properties. Univ. Calif. Div. *Agric. Sci.* 4094, Berkeley: 109-118.

DeBano, L.F., 1981. Water-*repellent soils: a state of the art. Pacific SW Forest and Range Exp. Station.* General Tech. Rep. PSW-46.

Dekker, J.W.,1998. *Moisture variability resulting from water repellency in Dutch soils.* Doctoral Thesis. Wageningen Agricultural University, Netherlands.

Dekker, J.W. and Jungerius, P.D., 1990. Water repellency in the dunes with special reference to the Netherlands. In: Bakker, Th.W.M., Jungerius, P.D. and Klijn, J.A. (eds), Dunes of the European coast. Geomorphology, hydrology, soils. *Catena Supplement* 18, 173-183.

De Ploey, J., 1977. Some experimental data on slopewash and wind action with reference to Quaternary morphogenesis in Belgium. *Earth Surface processes* 2, 101-15.

De Ploey, J., and Gabriëls, D., 1980. Measuring soil loss and experimental studies. In: Kirkby, M.J., Morgan, R.P.C. (Eds.), *Soil Erosion.* Wiley, Chichester, pp. 63-108.

Deuzeman, S.B., 2003. *Broedvogels van het Kootwijkerzand en Kootwijk-Oost in 2002.* SOVON Vogelonderzoek Nederland, inventarisatierapport 03/04, ISSN 1382-6255, 45 pp.

Fryrear, D.W. and Skidmore, E.L., 1985. Methods for controlling wind erosion. In: Follet, R.F. and Stewart B.A. (Eds), *Soil Erosion and Crop Productivity*, pp. 443-457. Madison (WI): ASA-CSSA-SSSA.

Fryrear, D.W. and Saleh, A., 1993. Field wind erosion: Vertical distribution. *Soil Science* 60:305-320.

Goede, R.G.M. de, Georgieva, S.S., Verschoor, B.C. and Kamerman, J.W., 1993. Changes in nematode community structure in primary succession of blown-out areas in a drift sand landscape. *Fundamental and Applied Nematology* 16, 6: 501-513.

Goossens, D., Poesen, J., Gross, J. and Spaan, W., 2000. Splash drift on light sandy soils: a field experiment. *Agronomie* 20: 271-282.

Horne, D.J. and McIntosh, J.C., 2000. Hydrophobic compounds in sands in New Zealand – extraction, characterisation and proposed mechanism for repellency expression. *Journal of Hydrology* 231-232: 35-46.

Jungerius, P.D., and Dekker, L.W., 1990. Water erosion in the dunes. In: Bakker, Th.W., P.D. Jungerius and Klijn, J.A. (eds). *Dunes of the European coast. Geomorphology - hydrology – soils*. Catena Suppl. 18: 185-194.

Jungerius, P.D., 2003. De rol van de beheerder bij het behoud van actieve stuifzanden. *Vakblad Natuurbeheer LNV* 42, 43-45.

Ketner-Oostra, R., 1994. *De korstmos-vegetatie van het Kootwijkerzand: vegetatie- en bodemkundig onderzoek bij de aanleg van permanente kwaadranten in het stuifzandgebied.* S.B.B., Driebergen, Rapport 94/1. 148 pp.

Ketner-Oostra, R., 1996. *Stuifzandvegetatie van het Kootwijkerzand. De invloed van beheersmaatregelen en andere ingrepen in de periode 1960 – 1985.* Staatsbosbeheer Regio Gelderland, Rapport 96/5, 27 pp.

Ketner-Oostra, R. and Huijsman, W., 1998. Heeft het stuiflandschap in Nederland toekomst? *De Levende Natuur* 99/7, 272-277.

Knottnerus, D.J.C., *1985. Verstuiving van grond. Beschouwingen over te nemen maatregelen, rapportering van gedaan onderzoek.* Haren, Instituut voor bodemvruchtbaarheid. Nota 144, 57 pp.

Kooijman, A.M., Besse, M. and Haak, R., 2000. *Effectgerichte maatregelen tegen verzuring en eutrofiëring in open droge duinen.* Eindrapport fase 2. 1996-1999. Fysisch Geografisch en Bodemkundig Laboratorium, Universiteit van Amsterdam. Rapport.

Koster, E.A., 1978. *The eolien drift sands of the Veluwe (Central Netherlands): a physical geographical study* (De stuifzanden van de Veluwe; een fysisch-geografische studie). Thesis, University of Amsterdam, 195 pp.

Koster, E.A., Castel, I.I.Y. and Nap, R.L., 1993. Genesis and sedimentary structures of late Holocene aeolian drift sands in northwest Europe. In: Pye, K. (Ed.), *The Dynamics and Environmental Context of Aeolian Sedimentary Systems*. Geological Society Special Publications 72: 247-267.

Kuntze, H., Beinhauer, R. and Tetzlaff, G., 1990. *Quantification of Soil Erosion by Wind, I. Final Report of the BMFT project.* Project No. 0339058 A, B, C. Institute of Meteorology and Climatology, University of Hannover, Germany. (in German)

Lyles, L., 1988. Basic wind erosion processes. *Agriculture, Ecosystems and Environment*, 22/23: 91-101.

Mashum, M. and Farmer, V.C., 1985. Origin and assessment of water repellency of a sandy South Australian soil. *Austr. J. Soil Res.* 23: 623-626.

Masselink, A.K., 1994. Pionier- en lichenrijke begroeiingen op stuifzanden benoorden de grote rivieren: typologie en syntaxonomie. *Stratiotes* 8 :32-62.

McGhie, D.A., 1987. Non-wetting soils in western Australia. *New Zealand Turf Management Journal*, Nov.: 13-16.

Meulen, L. Van der and Rooijen, J. van, 1981. *De zandverstuivingen bij Kootwijk in woord en beeld: verslag van een doctoraalonderzoek geomorfologie.* Msc. Thesis, Wageningen university, the Netherlands, 64 pp.

Morgan, R.P.C., 1995. *Soil erosion and Conservation.* Second edition. Longman, London, 198 pp.

Mourik, J.M. van, 1988a. De ontwikkeling van een stuifzandgebied. *Netherlands Geographical Studies* 74: 5 - 42; KNAG, Amsterdam.

Mourik, J.M. van, (ed.), 1988b. *Landschap in beweging.* Nederlandse geografische studies 74, 191 pp.

Nickling, W.G., 1994. Aeolian sediment transport and deposition. In: Pye, K. (Ed.), 1994. *Sediment Transport and Depositional Processes*. Blackwell Scientific Publications, pp. 293-349.

Ommering, G. Van, 2002. *Handleiding Subsidie Effectgerichte Maatregelen 2003*. Rapport EC-LNV 2002/160-O, Ministerie LNV, Ede-Wageningen, the Netherlands.

Pluis, J.L.A., 1993. *The role of algae in the spontaneous stabilization of blowouts*. PhD thesis, University of Amsterdam, 167 pp.

Pye, K. and Tsoar, H., 1990. *Aeolian Sand and Sand Dunes*. London, UK: Unwin Hyman.

Riksen, M.J.P.M. and Sweeris, H., 2003. *Voortgangsrapport Erosieonderzoek Kootwijkerzand.* Erosion and Soil and Water Conservation Group, Wageningen University, Wageningen, 23 pp.

Roberts, F.J. and Carbon, B.A., 1972. Water repellence in sandy soils of SW Australia. II. Some chemical characteristics of the hydrophobic skin. *Aust. J. Soil Res.* 10: 35-42.

Schimmel, H., 1975. Atlantische woestijnen. De Veluwse zandverstuivingen. *Natuur en landschap* 29: 11-44.

Slicher van Bath, B., 1977. *De agrarische geschiedenis van West-Europa 500-1850.* Aula 565, Het Spectrum, Utrecht/Antwerpen, 416 pp.

Spaan, W.P. and Abeele, G.D. van den, 1991. Wind borne particle measurements with acoustic sensors. *Soil Technology* 4: 51-63.

Sterk, G., Riksen, M.J.P.M. and Goossens, D., 2001. Dryland degradation by wind erosion and its control. In: *Annals of arid Zone* 40 (3): 1-17.

Stiboka, 1979. Bodemkaart van Nederland, Blad 33, West Apeldoorn. Toelichting bij kaartblad 33. Stiboka, Wageningen.

Stockton, P. and Gillette, D.A., 1990. Field measurements of the sheltering effect of vegetation on erodible land surfaces. *Land Degradation and Rehabilitation* 2: 77-85.

Vories, E.D. and Fryrear, D.W., 1991. Vertical Distribution of Wind-eroded Soil over a Smooth, Bare Field. *Transactions of the ASAE*, 34: 1763-1768.

Wischmeier, W.H. and Smith, D.D., 1965. *Predicting rainfall-erosion losses from cropland east of the Rocky Mountains.* U.S. Dept. Agric. Handbook 282. Washington D.C.

Chapter 8

The Effect of Wind-Driven Rain on Transport of Sand by Splash-Saltation

W. Cornelis & D. Gabriels
Dept. Soil Management and Soil Care, International Centre for Eremology, Ghent University, Coupure Links 653, B-9000 Gent, Belgium; Email: Wim.Cornelis@UGent.be

The Effect of Wind-Driven Rain on Transport of Sand by Splash-Saltation

Introduction

An understanding of sediment transport systems is indispensable to predict the on site and off site effects associated with wind erosion. This is not only important in soil conservation and land use studies related to agricultural, ecological, coastal and environmental issues, but also in modern geomorphology. Many attempts to investigate sediment transport as induced by wind have been reported in literature. A review of sediment transport models relating the sediment transport rate to a wind-power index is given in Greeley and Iversen (1985) and Shao (2000). Most of this research was carried out under rainless conditions above a dry surface. Many researchers showed, however, that near-surface water can substantially affect the threshold conditions at which deflation or dislodgement of particles is initiated by wind shear near the surface. A critical review of such studies is given in Cornelis and Gabriels (2003). Wind-tunnel experiments of Cornelis et al. (2004a,b) further show that deflation will only occur once the near-surface water content drops below 75% of its value at a soil-water potential of -1.5 MPa. It is obvious that during rainfall events, the near-surface water content will be too high for particles to be dislodged by wind shear. However, as will be shown in this chapter, substantial sediment transport can occur on dunes and beaches during rainy days, though it is often not considered in sediment transport models.

Field observations of splash-saltation of sand by wind-driven rain

In his field study carried out from 1973 to 1977 on a crescent dune at Kalmthout-Wilgenduinen, Kempenland, Belgium, De Ploey (1980) observed severe sandstorms during heavy winter rainstorms when the dune was completely wet. Sediment transport was measured using sand catchers consisting of 25 cake pans and a psammograph. The annual removal and redeposition of dune sand was observed to occur mainly in a lapse time of 3 to 4 hours, particularly during rainy periods in autumn and winter. He concluded that the drifts of wet sand partly originated from sand splashing by raindrop impact. This process in which particles are dislodged by raindrop impact rather than by wind shear, and subsequently transported in saltation with the wind acting as a transporting agent only, can be defined as splash-saltation.

In the coastal dune area of De Blink, Noordwijkerhout, the Netherlands, Jungerius et al. (1981) used a network of wind erosion pins to assess weekly changes in surface from 1976 to 1978. When excluding rainy days, i.e. days with a daily precipitation of at least 0.1 mm, from their data set, they observed a decrease in the number of significant correlations between pin readings and wind velocity. Also, the actual values of the correlation coefficient between pin readings and wind velocity did not increase, when excluding rainy days. The high correlations that hence were noted when including rainy days were not only observed during strong winds which are usually accompagnied by rain, but also at relatively low wind velocities. The latter was attributed to the accumulation of splashed sand.

De Lima et al. (1992) and Van Dijk et al. (1996) used a saltiphone (Spaan and van den Abeele, 1991) to investigate the effect of rainfall on the movement of sand particles by wind at a flat coastal plain on the island of Schiermonnikoog, the Netherlands. Nine rainfall events were analysed during the year 1990. They observed that peaks in the saltiphone count rate coincided with peaks in rainfall. The duration of sediment transport and the saltiphone count rate increased strongly with rainfall intensity (De Lima et al., 1992). During rainfall, sediment was transported under conditions where no sediment transport was predicted by aeolian processes (Van Dijk et al., 1996). Once rainfall stopped, a sudden drop in recorded count rates became apparent, due to the

increased resistance of the wet soil to deflation (De Lima et al., 1992). It should, however, be noted that over longer periods, sediment transport by wind will primarily take place under dry weather conditions and the relative importance of splash-saltation is rather limited, though significant at higher rainfall intensities (Van Dijk et al., 1996).

Wind-tunnel observations of splash-saltation of sand by wind-driven rain

The field studies described above clearly show that transport of sand is very likely to occur during rainfall events based on observed correlations and trends between wind velocity, sediment transport and rainfall related parameters. In order to have a better understanding of the process of splash-saltation by wind-driven rain, including its distribution with downwind distance and with height, and its transport rate, Cornelis et al. (2004c,d) performed wind-tunnel experiments at the International Centre for Eremology (I.C.E.), Ghent University, Belgium. The I.C.E. wind tunnel with its rainfall-simulation facility is described in detail in Chapter 13.

Detachment of their 250-μm sized dune sand by raindrop impact was induced from a ca. 1-m long sample tray, and vertical deposition fluxes and horizontal fluxes of the detached sand were measured (Fig. 1). The study hence focused on the smallest and earliest space and time scale subprocess elements of erosion, being detachment, and subsequent transport and deposition, rather than on the overall sediment transport from a given area, as in the previously described field studies. The vertical deposition flux, which is the mass of particles that settle down at a given distance from the source of detachment per unit of area at the horizontal plane within a time unit, was measured with a horizontal array of 23 troughs located downwind of the sample tray. The horizontal flux, defined as the mass of particles passing at a given height per unit time through a unit area perpendicular to the wind, was measured using a vertical array of four to eight Wilson and Cooke catchers (Wilson and Cooke, 1980) located above the sample tray. Experiments were performed at different kinetic energy or momentum of the rain, including rainless conditions, and at different wind velocities. Sediment transport rates, defined as the quantity passing through a plane of unit width and infinite height above the surface perpendicular to the wind per unit of time, were then deduced from integration of the vertical deposition flux over the distance of deposition, and from integration of the horizontal fluxes over the transport height. Kinetic energy and momentum of the raindrops were determined using splash cups (Ellison, 1947). The calibration curve we applied was derived from vertical rain (rather than inclined rain) with known mass and fall velocity, and the kinetic energy or momentum hence obtained are their normal components only. For more details about the experimental setup, we refer to Cornelis et al. (2004c,d).

Vertical Deposition Flux

Cornelis et al. (2004c) found that the distribution of sediment with distance from the source of particle detachment could be well described by a double exponential equation, relating the vertical deposition flux q_x to the distance from the source Δx as:

$$q_x = a_1 e^{-b_1 \Delta x} + c_1 e^{-d_1 \Delta x} \qquad \text{[Eq. 1]}$$

where a_1, b_1, c_1 and d_1 are regression coefficients. The regression coefficients and the R^2 values are summarized in Table 1. In Table 1, the highest standard deviation σ_{max} that

A

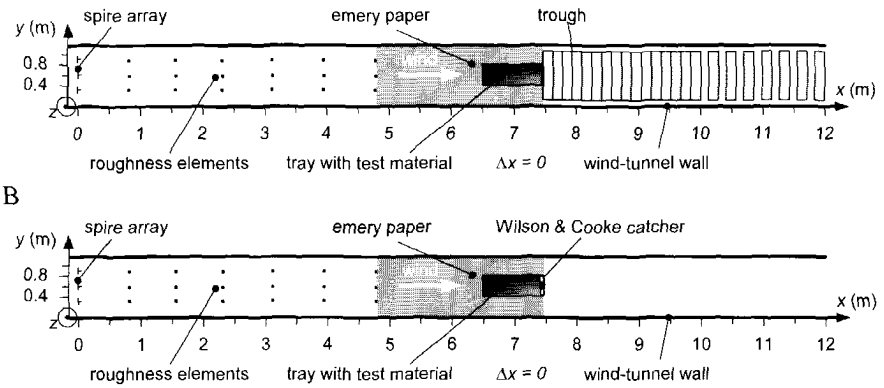

Figure 1. Top view of the experimental set-up to determine the vertical deposition flux (A) and the horizontal flux (B)

was observed for the 23 vertical deposition flux values is given as well. This parameter is an indication for the degree of replicability of the experiments, which were conducted in three replicates. Figure 2 shows the variation in vertical deposition flux q over the distance Δx windward of the sand tray for different wind shear velocities u_* and the normal component of kinetic energies KE_z (or momentum M_z) for the wind-driven rain case (Fig. 2a-c) and the rainless wind case (Fig. 2d).

A simple exponential equation as proposed by Savat and Poesen (1981) for windless conditions does not hold when considering the complete traveling length of the particles, but is only valid close to the sample tray. The particles that are splashed to a limited height above the soil surface, experience a relatively low impulse, as wind velocity is relatively low at low heights. The impulse force the particles hence receive does not exceed particle weight, and as a result, the effect of the wind is minimal.

Table 1. Best-fitted values of the regression coefficients from Eq. (1), σ_{max}, and R^2 at different wind shear velocities u_* and different kinetic energies KE_z or momentum M_z

u_*	KE_z	M_z	σ_{max}	a_1	b_1	c_1	d_1	R^2
m s^{-1}	J m^2 s^{-1}	kg m^{-1} s^{-2}	g m^2 s^{-1}	g m^2 s^{-1}	m^{-1}	g m^2 s^{-1}	m^{-1}	-
0.27	0.288	0.086	0.004	3.33 (0.17) †	10.18 (0.69)	0.58 (0.06)	1.92 (0.12)	1.000
0.27	0.250	0.074	0.039	3.12 (0.16)	9.95 (0.78)	0.53 (0.08)	2.04 (0.17)	0.999
0.27	0.185	0.055	0.011	2.21 (0.05)	11.06 (0.37)	0.66 (0.03)	2.74 (0.05)	1.000
0.39	0.496	0.148	0.006	3.80 (0.19)	7.64 (0.66)	1.32 (0.10)	1.23 (0.07)	0.999
0.39	0.455	0.136	0.026	3.85 (0.05)	5.56 (0.15)	0.68 (0.05)	1.04 (0.05)	1.000
0.39	0.426	0.127	0.015	4.93 (0.20)	9.91 (0.44)	1.21 (0.04)	1.28 (0.03)	1.000
0.50	0.653	0.194	0.005	4.42 (0.14)	6.15 (0.34)	0.95 (0.06)	0.70 (0.04)	0.998
0.50	0.591	0.176	0.025	4.43 (0.07)	5.09 (0.14)	0.44 (0.03)	0.46 (0.04)	0.999
0.50	0.460	0.137	0.011	4.25 (0.23)	7.18 (0.54)	0.82 (0.07)	0.71 (0.05)	0.997
0.33	0.000	0.000	0.000	0.05 (0.01)	9.09 (1.34)	0.01 (0.00)	1.21 (0.13)	0.995
0.36	0.000	0.000	0.014	0.77 (0.01)	5.54 (0.11)	0.02 (0.01)	0.83 (0.20)	1.000
0.39	0.000	0.000	0.089	53.06 (3.61)	13.31 (0.70)	3.81‡ (0.30)	1.74‡ (0.10)	1.000
0.50	0.000	0.000	2.254	612.20 (8.15)	7.60 (0.14)	21.55 (2.17)	0.77 (0.07)	1.000

† The values in parentheses are standard errors. All regression coefficients are significant at P<0.0001, except when indicated.
‡ Significant at P<0.004.

Particles that are lifted by raindrop impact to greater heights encounter higher impulses, and their trajectory is substantially influenced by the wind velocity. This phenomenon explains why a second exponential term is needed when expressing the vertical deposition flux as a function of distance.

When considering the flux values at different wind shear velocities and kinetic energies (or momentum) in Table 1, it seems that the intercept $a_1 + c_1$, which is the vertical deposition flux at zero distance from the tray, increases with increasing KE_z (or momentum M_z) as could be expected. Because u_* and KE_z act simultaneously, the effect of u_* as such could not be clearly distinguished. When considering the exponent values b_1 and d_1, the effect of the wind is more apparent. Both appear to decrease with increasing KE_z, which implies that more particles are splashed to greater heights, and with increasing u_*. Furthermore, as KE_z and u_* are increasing from their lowest to their highest value, d_1 is decreasing with a factor 5, whereas b_1 is only reduced with a factor 2. Since it is the second term in equation 1 that describes the vertical deposition flux at higher distances, this shows once more that the effect of the wind is highest on particles that splash into the zone of highest horizontal wind velocity. This could also indicate that the amount of splashed droplets containing a larger number of particles and hence become heavier, increases as KE_z increases.

With regard to the rainless wind-driven vertical deposition flux, the effect of an increasing wind shear velocity on both b_1 and d_1 is less pronounced (Table 1). On the other hand, the intercept $a_1 + c_1$ is clearly increasing with the wind shear velocity. This intercept determines to a high degree the deposition flux.

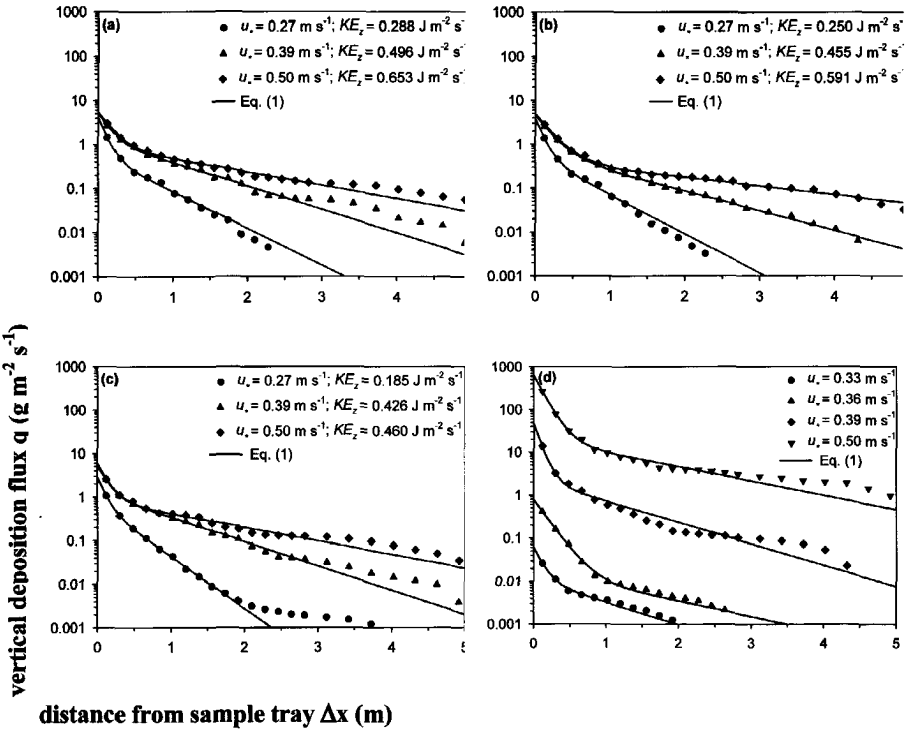

Figure 2. Vertical deposition flux q vs. distance from the sample tray Δx for different combinations of wind shear velocity u_* and kinetic energy KE_z. The symbols denote the observations.

Horizontal Flux

Cornelis et al. (2004d) found that the distribution of sediment with height above the surface could be well described by a single exponential equation, relating the horizontal flux q_z to the height above the surface z as:

$$q = a_2 \, e^{-b_2 z} \qquad \text{[Eq. 2]}$$

where a_2 and b_2 are regression coefficients. The results of fitting equation 2 to the data and the associated R^2 values are presented in Table 2. In Table 2, the highest standard deviation σ_{max} that was observed for the different horizontal flux values is given as well. This parameter is an indication for the degree of replicability of the experiments, which were conducted in three replicates.

Table 2. Best-fitted values of the regression coefficients from equation 2, σ_{max}, and R^2 at different wind shear velocities u_* and different kinetic energies KE_z or momentum M_z

u_*	KE_z	M_z	σ_{max}	a_2	b_2	R^2
m s^{-1}	J m^2 s^{-1}	kg m^1 s^{-2}	g m^2 s^{-1}	g m^2 s^{-1}	m^{-1}	-
0.27	0.288	0.086	0.066	7.98 (0.10)†	11.79 (0.23)	1.000
0.27	0.250	0.074	0.087	7.81 (0.67)	15.31 (1.71)	0.988
0.27	0.185	0.055	0.137	5.73 (0.31)	16.93 (1.14)	0.996
0.39	0.496	0.148	0.075	15.35 (1.03)	11.79‡ (1.18)	0.990
0.39	0.455	0.136	0.153	13.72 (0.87)	12.68 (1.16)	0.992
0.39	0.426	0.127	0.087	14.01‡ (0.04)	16.75‡ (0.06)	1.000
0.50	0.653	0.194	0.087	25.07 (1.50)	13.02 (1.10)	0.993
0.50	0.591	0.176	0.086	21.02 (2.46)	13.23 (2.18)	0.976
0.50	0.460	0.137	0.076	19.23 (0.85)	17.85 (0.96)	0.998
0.33	0.000	0.000	0.031	0.79 (0.10)	39.42 (6.10)	0.954
0.36	0.000	0.000	0.031	2.87 (0.44)	35.92 (6.95)	0.929
0.39	0.000	0.000	0.076	132.20 (8.59)	28.99 (2.53)	0.983
0.50	0.000	0.000	20.635	3621.72 (133.20)	33.29 (1.59)	0.995

† The values in parentheses are standard errors. All regression coefficients are significant at P<0.01, except when indicated.
‡ Significant at P<0.03.

A single exponential equation such as equation 2 is generally accepted to describe vertical distribution of saltation of sand under rainless conditions (Horikawa and Chen, 1960; Williams, 1964; Nalpanis, 1985; Fryrear and Saleh, 1993; Van Dijk et al., 1996). That such expression is also valid under wind-driven rain conditions means that most of the particles that are lifted off due to raindrop impact are splashed over a limited height. The variation of transport flux q with height z above the sand surface for different wind shear velocities u_* and kinetic energies KE_z (or momentum M_z) is illustrated in Figure 3a-c for the wind-driven rain case and Figure 3d for the rainless wind case.

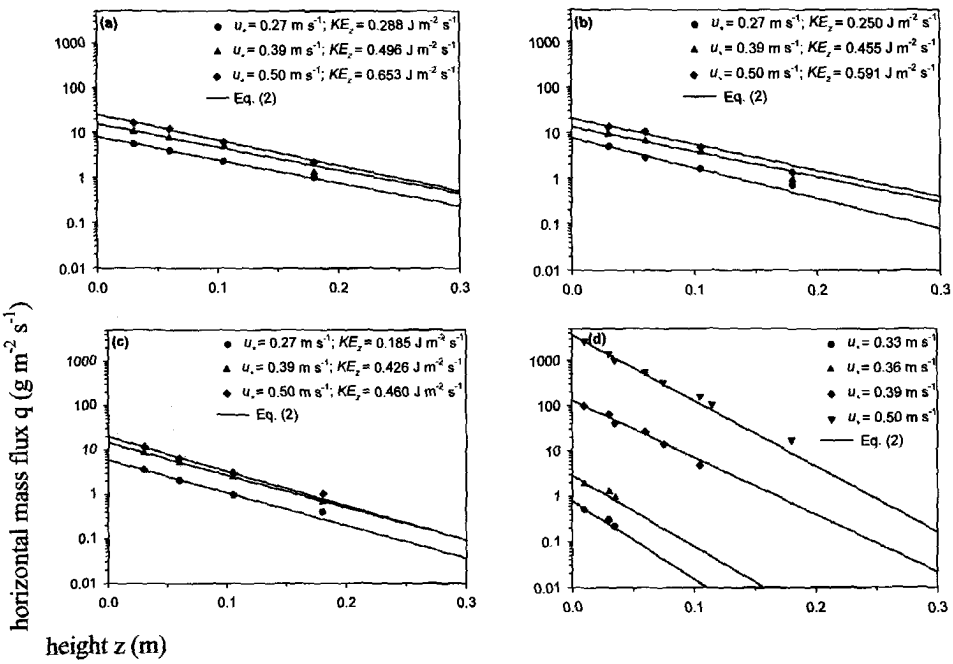

Figure 3. Horizontal mass flux q vs. height above the surface z for different combinations of wind shear velocity u_* and kinetic energy KE_z. The symbols denote the observations.

The role of u_* was not very clear, apart from its strong effect on KE_z (or M_z). The b_2 coefficient of equation 2 remained more or less constant with increasing KE_z or u_* and no trend could be observed (Table 2). This means that at each height, the flux is increasing with a more or less constant factor as KE_z increases. This is in contrast with the observations made under rainless wind conditions. In the latter case, b_2 decreases with increasing destabilizing force, which is expressed in terms of u_*. This in agreement with findings of Spaan et al. (1991), although Williams (1964) reported that particle shape plays a much more consistent role in changing b_2 than does u_*. According to Williams (1964), the average of b_2 at different wind shear velocity for a given particle shape and type is a reasonably good estimate.

When comparing wind-driven rain conditions with rainless wind conditions, the mean of the exponent b_2 is about a factor 2 larger for the rainless wind case (Table 2). This means that relatively speaking much more sediment will be transported at lower heights in the rainless case, or in other words, the mass distribution of sediment with height is more homogeneous in the case of wind-driven rain. The decay coefficients observed under wind-driven rain are somewhat lower than those reported by Van Dijk et al. (1996) who measured vertical mass fluxes of fine beach sand over wet surfaces.

Sediment Transport Rates

In their wind-tunnel study, Cornelis et al. (2004c) found good fits between sediment transport rate Q_x (computed from integrating vertical deposition flux data) and the normal component of rain erosivity (being kinetic energy or momentum of the rain drops), using an equation similar to the detachment model of Sharma and Gupta (1989):

$$Q = a_3 (E_z - E_{zt})^{b_3} \qquad \text{[Eq. 3]}$$

where a_3 and b_3 are regression coefficients, z denotes the normal direction and t denotes the threshold value. The results of fitting equation 3 to the transport rate data are compiled in Table 3. The high R^2 values indicate that the rain erosivity explains to a high extent the observed variation. Note that the exponent b_3 is very close to the value as observed by Sharma and Gupta (1989), who found b_3 to converge to 1 for windless rain. Refitting equation 3 with $b_3 = 1$, reduced R^2 only slightly. It should further be noted that the fitting coefficients given in Table 3 are based on integration of vertical deposition flux data only, i.e. on Q_x data.

Table 3. Coefficient values of equations 3 and 4 where the erosivity index is the normal component of kinetic energy KE_n or momentum M_n

	KE_n				M_n			
Eq.	a_3	b_3	c_3	R^2	a_3	b_3	c_3	R^2
	10^{-3} kg^{1-b} m^{-1-c} s$^{-3b+c-1}$				10^{-3} kg^{1-b} m^{-1-b-c} s^{-1-b+c}			
(3)	3.65 (0.40)†	1.18 (0.15)	-	0.935	15.34 (4.45)	1.18 (0.15)	-	0.935
(3)	3.21 (0.38)	1.00 (0.15)	-	0.920	10.77 (3.26)	1.00 (0.16)	-	0.920
(4)	4.52 (0.85)	-	0.41‡ (0.39)	0.956	15.23 (4.39)	-	0.42‡ (0.39)	0.956

† The values in parentheses are standard errors. All regression coefficients are significant at $P<0.05$, except when indicated.
‡ Not significant at $P<0.05$.

To explore whether u_* had an additional effect on Q, apart from its influence on the impact velocity of the raindrops, Cornelis et al. (2004c) expressed Q also as a function of both E_z and u_*, by using following model with an equal number of parameters as equation 3:

$$Q = a_3 (E_z - E_{zt}) u_*^{c_3} \qquad \text{[Eq. 4]}$$

where c_3 is a regression coefficient. The results of fitting equation 4 to the observed data (which again are based on integration of vertical deposition flux data only, i.e. on Q_x data) are presented in Table 3 as well. Including the wind shear velocity u_* into the transport rate model, resulted in a somewhat higher model performance ($R^2 = 0.956$), although the exponent c_3 is not significant at the 0.05 level. To examine the model performance graphically, the behavior of equation 4 is illustrated in Figure 4. The linearized relationship for a wide range of kinetic energy or momentum and wind shear velocity suggests that equation 4 adequately describes the transport rate of sand particles under wind-driven rain conditions. This is further supported by the Q_z data (Cornelis et al., 2004d), which, though determined on an independent set of measurements that was based on determining a different erosion parameter (i.e. horizontal flux instead of vertical deposition flux), follow equation 4 very well. The good agreement is also well illustrated in the scatter plot shown in Figure 5, in which the observed Q_z data (based on horizontal flux data) are plotted against Q values predicted from equation 4 (in which the coefficients were obtained from curve fitting against Q_x data, i.e. based on independently determined vertical deposition flux data).

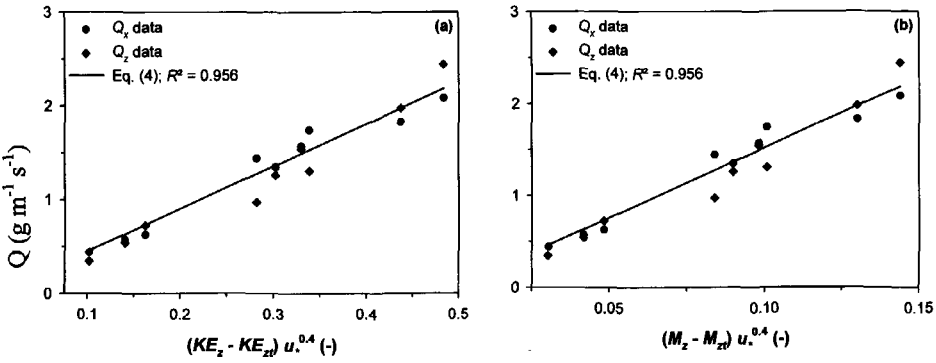

Figure 4. The mass transport rate Q_x and Q_z as determined from integration of vertical deposition flux and horizontal flux data respectively vs. the scaling factor of Eq. (4). The data are derived from wind-driven rain experiments. Equation (4) was curve fitted against Q_x data only.

As was expected, the effect of the wind shear velocity on the sediment transport rate apart from its influence on kinetic energy or momentum, is rather limited. Wind as such cannot detach the sand due to its high water content and the threshold wind shear velocity for deflation is hence not exceeded under rainy conditions. The additional effect of wind that, however, can be observed, could be due to an extra bombardment of the sand surface by rainsplash-saltating particles which are entrained in the droplets. As the erosivity of the raindrops increases, the number of particles that are transported per raindrop increases drastically. This is illustrated in Figure 6, showing that rainsplash-saltating particles are entrained into splash droplets, and that the number of entrained particles within one droplet, and hence the droplet weight, increases with increasing kinetic energy or momentum. Since an increase of erosivity is, in our study, mainly associated with an increase in wind shear velocity, the impact energy or momentum of a splash droplet will rise accordingly. On the other hand, this phenomenon will be hampered to some extent as the impact angle of the droplets decreases with increasing wind velocity. Furthermore, in sediment-laden flow, part of the energy of motion of the fluid is carried by the grains in order to sustain their movement. As a result, the shear stress exerted by the wind will be reduced somewhat. Another effect of the wind could be an increase in the transport capacity. As the wind velocity increases, the above-described process will be accelerated. The above observations suggest that wind has an additional effect on transport of particles under wind-driven rains. However, the error caused by discarding the wind shear velocity or using equation 3 will be limited, as long as the normal component of kinetic energy or momentum is taken into account.

As a reference, Cornelis et al. (2004c,d) further computed sediment transport rates based on their rainless wind experiments. When considering the Q_x data, best fits were obtained with following model:

$$Q = 18.6\ 10^{-3}\ (u_* - u_{*_t})^3 \qquad \text{[Eq. 5]}$$

where Q was calculated similarly as for the wind-driven rain data. The threshold shear velocity u_{*t} was 0.30 m s^{-1}. Again, as depicted in Figure 7, the Q_z data follow the expression determined based on Q_x data, equation 5, very well. This is also illustrated in the scatter plot shown in Figure 5, in which the observed Q_z data are plotted against Q values predicted from equation 5.

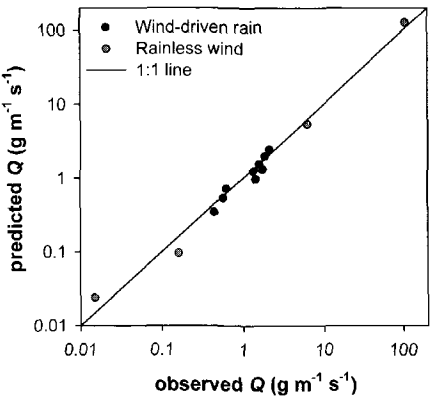

Figure 5. Observed sediment transport rate Q vs. predicted sediment transport rate Q for the wind-driven rain and rainless wind experiments. The observations refer to the Q_z data obtained from integration of horizontal flux data. The predicted Q values were computed from equation 4 and equation 5. Note that the coefficients of both equation 4 and equation 5 were obtained from curve fitting against Q_x data, i.e. based on independently determined vertical deposition flux data.

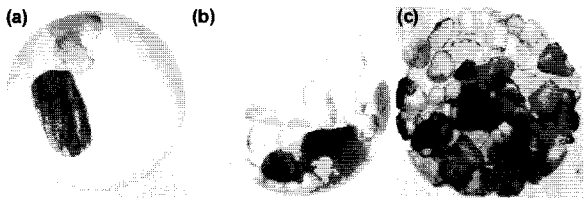

Figure 6. Splash droplets with entrapped sand grains as trapped on vaseline-rubbed glass plates when u_* was 0.27 m s^{-1} (a), 0.39 m s^{-1} (b), and 0.50 m s^{-1} (c)

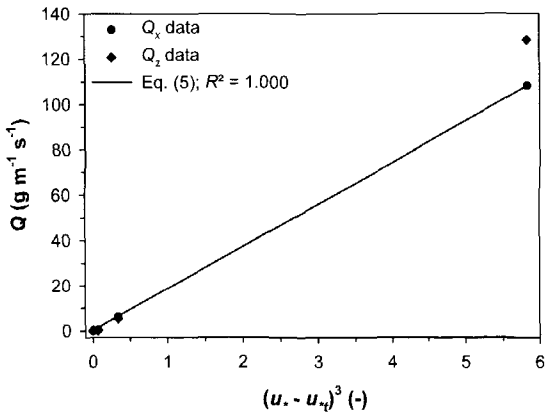

Figure 7. The mass transport rate Q_x and Q_z as determined from integration of vertical deposition flux and horizontal flux data respectively vs. the scaling factor of equation 5. The data are derived from rainless wind experiments. Equation 5 was curve fitted against Q_x data only.

Equation 5 shows that Q is a function of the third power of a wind-shear related parameter, as suggested by Bagnold (1941) who arbitrarily assumed that the initial velocity of ejection is linearly proportional to u_*. However, it should be noted that others such as Lettau and Lettau (1978) found Q to be related to $u_*^2\left(u_* - u_{*_t}\right)$, whereas e.g. Owen (1964) related Q to $u_*\left(u_*^2 - u_{*_t}^2\right)$, which illustrates once more the difficulty of establishing an appropriate model to fit to transport rate data. This was also concluded by Greeley and Iversen (1985) when reviewing the wide variety of equations that are reported in literature.

Sediment transport by rainless wind and wind-driven rain

When comparing the transport rates as observed under wind-driven rain circumstances with those from the rainless experiments, the much higher transport rates at high wind velocities above a dry surface when rain is absent, are notable. At wind velocities close to the deflation threshold, transport rates are in the latter case lower than those as induced by wind-driven raindrop impact, even if the wind shear velocities under wind-driven rain conditions were lower than the 'dry' deflation threshold. However, the transport rates that are observed during wind-driven rain events remain relatively low. The highest transport rate observed by Cornelis et al. (2004c) under wind-driven rain was 2.4 g m^{-1} s^{-1}, which occurred at KE_z = 0.6 J m^{-2} s^{-1} and u_* = 0.50 m s^{-1}. When applying Eq. (5) for dry conditions, the same transport rate would take place at u_* = 0.37 m s^{-1}. On the other hand, when the sand surface is too wet for deflation to occur, movement of sediment can occur once a rainfall event starts. Similarly, when the rain event stops, particle transport will cease, as has been observed on beaches by Van Dijk et al. (1996).

From the above results, it is apparent that in order to predict the total wind erosion budget over a given period, equation 5 should be combined with equation 3 or 4. This is also indirectly suggested by Sherman and Hotta (1990) arguing that "splash processes can move sediments in conditions where no motion is predicted by aeolian equations, and it may also be important during severe storms."

In general, a model that needs to predict sediment transport rate by wind (with or without being accompanied by rain), should be of the following form:

$$Q' = Q_{wr} + Q_w \qquad \text{[Eq. 6]}$$

where Q' is the total sediment transport rate (including periods with and without rain), Q_{wr} is the transport rate in the case of wind-driven rain conditions, and Q_w is the transport rate due to rainless wind. The 'rainless wind' transport can be calculated from Eq. (5) or similar, whereas 'wind-driven rain' transport should be predicted from equation 3 or 4. In the case that rain is accompanied by wind, $Q' = Q_{wr}$, and $Q_w = 0$ since u_{*_t} will not be exceeded. If rain ceases or its erosivity becomes lower than the threshold erosivity to cause detachment, transport will still occur if $u_* > u_{*_t}$. The latter will then greatly depend on the water content at the surface bed.

Summary and conclusions

Field observations on crescent dunes and on beaches in Belgium and the Netherlands have shown that sediment transport can be substantial during rainy days. This transport, in which particles are dislodged by raindrop impact rather than by wind shear, and subsequently transported in saltation with the wind acting as a transporting agent only, was attributed to splash-saltation.

These findings were supported by wind-tunnel experiments in which vertical deposition fluxes and horizontal fluxes of sand particles were measured under different rain and wind erosivity conditions, including wind-driven rain and rainless wind. The data were then used to compute sediment transport rates. The transport rate of rainsplash-saltating particles in the wind-driven rain experiments was to a high degree affected by the normal component of the kinetic energy or the momentum of the raindrops. The wind as such is not able to detach particles from the surface, due to the high threshold wind shear velocity associated with the higher near-surface water content that exists under rainfall events. However, the wind shear velocity could play an additional role as it can induce extra bombardment of the sand surface by rainsplash-saltating particles entrained in the droplets. This implies that impacting droplets exert additional impact energy. Furthermore, wind can increase the transport capacity, accelerating the rainsplash process. The observed variation in transport rate was to a very high degree predicted by a non-linear function of kinetic energy or momentum and wind shear velocity. Notwithstanding this, consideration of kinetic energy or momentum only, will not result in a substantial prediction error as long as the normal component of erosivity is accounted for.

In the absence of rain, the sediment transport rate was much lower at wind shear velocities close to the deflation threshold compared to the sediment transport rates determined from the wind-driven rain experiments at similar shear velocities. However, as wind shear velocity increased, the increase in transport rate was much more pronounced, compared to transport under wind-driven rain. This implies that when predicting transport of particles in general, not accounting for the transport that occurs during rainy periods will only result in minor errors, in the case that heavy winds occur frequently. When heavy winds are not expected to take place regularly, the contribution of rainsplash-saltation in the total soil loss budget will be considerable.

References

Bagnold, R.A.. 1941. The physics of blown sand and desert dunes. Chapman & Hall, London.

Cornelis, W.M. and D. Gabriels. 2003. The effect of surface moisture on the entrainment of dune sand by wind: an evaluation of selected models. *Sedimentology.* 50: 771-790.

Cornelis, W.M., D. Gabriels and R. Hartmann. 2004a. A conceptual model to predict the deflation threshold shear velocity as affected by near-surface water content: 1. *Theory. Soil Sci. Soc. Am. J.*, 68: 1154-1161.

Cornelis, W.M., D. Gabriels and R. Hartmann. 2004b. A conceptual model to predict the deflation threshold shear velocity as affected by near-surface water content: 2. Calibration and Verification. *Soil Sci. Soc. Am. J.* 68: 1162-1168.

Cornelis, W.M., G. Oltenfreiter, D. Gabriels and R. Hartmann. 2004c. Splash-Saltation of Sand due to Wind-Driven Rain: Vertical Deposition Flux and Sediment Transport Rate. *Soil Sci. Soc. Am. J.* 68: 32-40

Cornelis, W.M., G. Oltenfreiter, D. Gabriels and R. Hartmann. 2004d. Splash-Saltation of Sand due to Wind-Driven Rain: Horizontal Flux and Sediment Transport Rate. *Soil Sci. Soc. Am. J.* 68: 41-46.

De Lima, J.LM.P., P.M. Van Dijk, and W.P. Spaan. 1992. Splash-saltation transport under wind-driven rain. *Soil Tech.* 5:151-166.

De Ploey, J. 1980. Some field measurements and experimental data on wind-blown sands. p. 143-151. *In* M. De Boodt and D. Gabriels (ed.) *Assessment of erosion.* John Wiley & Sons, Chichester.

Ellison, W.D. 1947. Soil erosion studies, Part 1-7. *Agr. Eng.* 28:145-146;197-201;245-248;297-300;349-351;407-408;447-450.

Fryrear, D.W., and A. Saleh. 1993. Field wind erosion: vertical distribution. *Soil Sci.* 155:294-300.

Greeley, R., and J.D. Iversen. 1985. Wind as a geological process on Earth, Mars, Venus and Titan. Cambridge University Press, Cambridge.

Horikawa, K., and H.W. Shen. 1960. Sand movement by wind: on the characteristics of sand traps. Tech. Mem., vol. 119. Beach Erosion Board, US Army, Washington DC.

Jungerius, P.D., A.J.T. Verheggen, and A.J. Wiggers. 1981. The development of blowouts in 'De Blink', a coastal dune area near Noordwijkerhout, The Netherlands. *Earth Surf. Proc. Landf.* 6:375-396.

Lettau, K., and H. Lettau. 1978. Experimental and micro-meteorological field studies of dune migration. In : K. Lettau and H. Lettau (Eds.). Exploring the worlds driest climate. University of Wisconsin Press, Madison.

Nalpanis, P. 1985. Saltating and suspended particles over flat and sloping surfaces ii. Experiments and numerical simulations. Proc. of International Workshop on the Physics of Blown Sand. University of Aarhus.

Owen, P.R...1964. Saltation of uniform grains in air. *J. Fluid Mech.* 20:225-242.

Savat, J., and J. Poesen. 1981. Detachment and transportation of loose sediments by raindrop splash. Part I: The calculation of absolute data on detachability and transportability. *Catena* 8:1-18.

Shao, Y.. 2000. Physics and modelling of wind erosion. Atmospheric and oceanographic sciences library, 23, Kluwer Academic Publishers, Dordrecht.

Sharma, P.P., and S.C. Gupta. 1989. Sand detachment by single raindrops of varying kinetic energy and momentum. *Soil Sci. Soc. Am. J.* 53:1005-1010.

Sherman, D.J., and S. Hotta. 1990. Aeolian sediment transport: theory and measurement. Chapter 2. p. 17-37. *In* K.. Nordstrom et al. (ed.). *Coastal dunes: forms and process.* John Wiley & Sons, Chichester.

Spaan, W.P., and G.D. van den Abeele. 1991. Wind borne particle measurements with acoustic sensors, *Soil Technology*, 4, 51-63.

Spaan, W.P., P.M. Van Dijk, and L.A.A.J. Eppink. 1991. Wind erosion measurements on the island of Schiermonnikoog. Wageningen Agricultural University.

Van Dijk, P.M., L. Stroosnijder, and J.L.M.P. De Lima. 1996. The influence of rainfall on transport of beach sand by wind. *Earth Surf. Proc. Landf.* 21:341-352.

Williams, G..1964. Some aspects of the eolian saltation load. *Sedimentology* 3:257-287.

Wilson, S.J., and R.U. Cooke. 1980. Wind erosion. p. 217-251. In: M.J. Kirkby, and R.P.C. Morgan (ed.) *Soil Erosion.* John Wiley & Sons, Chichester.

Chapter 9

Effect of Slope Aspect on Sediment Transport

G. Erpul[1], D. Gabriels[2] & D. Norton[3]
[1] Faculty of Agriculture, Department of Soil Science, University of Ankara, 06110 Diskapi – Ankara, Turkey phone: + 90 (312) 317 0550; fax: + 90 (312) 317 8465; Email: erpul@agri.ankara.edu.tr
[2] Department of Soil Management and Soil Care, Ghent University, Coupure Links 653, B 9000 Ghent, Belgium.
[3] USDA – ARS National Soil Erosion Research Laboratory, 1196 SOIL Bldg., Purdue University, West Lafayette, IN, 47907 – 1196, USA.

Effect of Slope Aspect on Sediment Transport

Abstract
Aspect affects the raindrop trajectory and the distribution and intensity of rain on sloping surfaces due to variations in the angle of raindrop incidence. Slopes with windward facing aspects intercept more rain than slopes with leeward facing aspects, bringing about different erosion rates and processes. This article investigates the effect of slope aspect on sediment transport by wind-driven rainsplash and raindrop-impacted shallow flow. Windless rains and the rains driven by horizontal wind velocities of 6, 10, and 14 ms^{-1} were applied to three agricultural soils packed into a 20 by 55 cm soil pan placed both windward and leeward slopes of 7, 15, and 20%. Wind-driven rainsplash transport was measured by trapping the splashed particles at distances on a 7-m uniform slope segment in the upslope and downslope directions, respectively, for windward and leeward slopes. Sediment transport by rain-impacted shallow flow was measured by collecting sediment and runoff samples at 5-min intervals after runoff onset. We compared the rates of soil detachment and transport influenced by the aspect and concluded that it had such a significant effect on interrill erosion processes that it should be included in models for accurately estimating water erosion under wind-driven rain.

Introduction
The effect of aspect on variations in the raindrop trajectory and the distribution and intensity of rain has been long recognized by scientists. Sharon (1980) and De Lima (1990) introduced a model to calculate the actual amount of rain intercepted on a sloping surface with respect to the prevailing wind direction. Especially in wind driven rains, the effect of aspect becomes much more stronger, leading to differences in hydrological and erosional processes (Sharon, 1980; Erpul et al., 2003a, 2003b).

The impact frequency of raindrops is an important characteristic, which determines the rain erosivity together with the impact velocity of raindrops. An equation is given by Kinnell (1981) to calculate the rate of impact per unit area for raindrops hitting a horizontal surface provided the raindrops travel along a straight-line trajectory. However, wind-driven raindrops travel not vertically but strike the surface obliquely. Simply, the rain intensity will be greatest when rain falls normal to the surface, whereas, it decreases to zero when it falls parallel to the surface (Struzer, 1972). Additionally, since wind drives raindrops, they gain a degree of horizontal velocity and have the resultant impact velocity rather than the vertical velocity. Theses variations in the raindrop trajectory and frequency with wind velocity and direction suggest that erosion processes under wind-driven rain differ from those under windless rain.

On the other hand, the latest erosion models assume a maximum impact frequency measured on a horizontal plane and maximum normal impact velocity to assess the rain erosivity. Practically, this might sound a very cautious approach to take measures for preventing erosion with the conservatively predicted rain erosivity. However, Sharon (1980) reported that a windward facing slope received two times more rain than a leeward facing slope, or even exceeded it in extreme cases for rain inclination of 40 up to 70°. When the rain inclination and slope gradient increase, the discrepancies in the raindrop impact frequency become greater in connection with the slope aspect. Since the flow generation is very sensible to the differences in rain intensity, we expect a very important role of the slope aspect in the process dissimilarity, i.e. different erosion processes can take place in windward and leeward

slopes during a particular wind-driven rainstorm. For example, given that the interrill transport process under wind-driven rain is the work of both shallow flow-driven sediment transport and the rainsplash sediment transport (Erpul et al., 2002, 2003a), the reduced rain intensity in the leeward slopes might retard overland flow generation, and the wind-driven rainsplash process might last longer before runoff onset. Similarly, differential sediment delivery rates might occur depending on the change in raindrop trajectory and rain intensity with the wind velocity and direction. These kinds of variations and their effects on the processes are underestimated and overlooked in the recent models, and therefore, there is a need for a prediction technology to deal with the wind-driven rain events and the variability of the processes due to the slope aspect.

This study involves evaluating the effect of the slope aspect on the soil detachment and sediment transport with the objective of improving the understanding of interrill erosion processes under wind-driven rain, which is not uncommon in intense erosive storms.

Materials and methods

The study was conducted in a wind tunnel rainfall simulator facility at Ghent University, Belgium (Gabriels et al., 1997). The raindrop size distributions for windless and wind-driven rains described by Erpul et al. (1998, 2000) were used in this study. Rainfall intensity was directly measured with 5 small collectors on the inclined plane, and a kinetic energy sensor (Sensit™, 2000) measured the energy of simulated rainfalls.

Three loess derived agricultural soils, Kemmel1 sandy loam (57.6% sand, 31.1% silt, and 11.3% clay) and Kemmel2 loam (37.8% sand, 44.5% silt, and 17.7% clay) from the Kemmelbeek watershed (Heuvelland, West Flanders, Belgium) and Nukerke silt loam (32.1% sand, 52.3% silt, and 15.6% clay) from the Maarkebeek watershed (Flemish Ardennes, East Flanders, Belgium) were used in this study. The soil samples were collected from the A_p horizon and air-dried prior to the experiment. Soil was sieved into three aggregate fractions: 1.00 - 2.75, 2.75-4.80, and 4.80-8.00 mm and recombined to give a mixture with 28, 32, and 40%, respectively of each size fraction. A 5-kg soil sample was then packed loosely into a 55-cm-long and 20-cm-wide pan after three fractions of aggregates were thoroughly mixed. Windless rains and the rains driven by horizontal wind velocities of 6, 10, and 14 ms^{-1} were applied to the soil pan placed at both windward and leeward slopes of 7, 15, and 20% (4.0, 8.5, and 11.3°, respectively). For each soil and slope aspect, there were three replicates, 36 runs (a total of 216 rainfall simulations) were performed.

Soil detachment rates were evaluated by the amount of the splashed particles trapped at set distances on a 7-m uniform slope segment. Troughs were placed in both upslope and downslope direction for windless rain, and in upslope and downslope direction, respectively, for windward and leeward slopes for wind-driven rain. For windless rain, splashboards were also positioned to collect side splash. The soil particles trapped in the collecting troughs were washed, oven-dried, and weighed. Mass distribution curves were then determined for windless and wind-driven rains, of which samples are given in Figure 1. Calculation of rainsplash detachment rate was based on the mathematical form of rainsplash erosion (Van Heerden, 1967; Savat and Poesen, 1981; Poesen, 1985):

$$D = \frac{1}{At_r} \int \frac{m_i}{x_i} \partial x \qquad \text{[Eq. 1]}$$

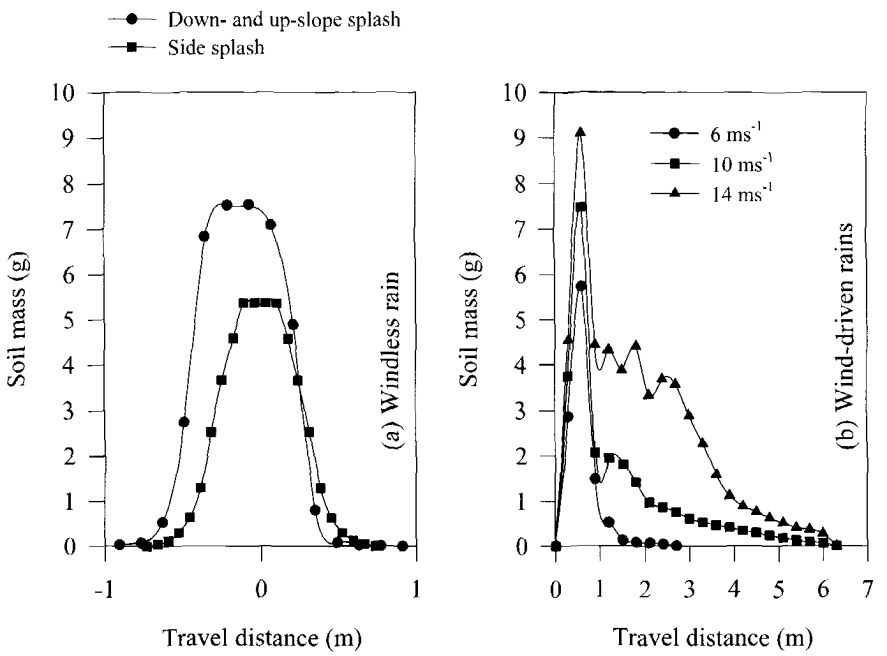

Figure 1. Mass distribution curves used for calculating rainsplash detachment rates. For windless rains (a) negative values stand for down-slope and left-side splash; while positive values for up-slope and right-side splash. For wind-driven rains (b) the particle movement is unidirectional and in the prevailing wind direction (Nukerke silt loam, windward slope of 11.3°).

where, D (g m^{-2} min^{-1}) is the rainsplash detachment rate, A is the surface area of soil pan $\left(0.55\text{m} \times 0.20\text{m} = 0.110\text{m}^2\right)$, t_r (min) is the time during which rainsplash process occurred, and m_i (g) is the mass of a particle, which is splashed over a distance x_i (m) measured along the x-axis. Flux of kinetic energy was used as rainfall parameter with the angle of incidence to statistically analyze the detachment rates with a power model (SAS, 1995):

$$KE = \Xi_a\left(\frac{1}{2}mV_R^2\right)\cos^2(\alpha \mp \theta) \qquad \text{[Eq. 2]}$$

where, KE (Wm^{-2}) is the kinetic energy flux, which is related to the normal component of resultant velocity, and Ξ_a is the actual number of raindrops and calculated by $\left(I_a/\forall\right)$ in # m^{-2} s^{-1}.

The wind-driven rainsplash transport rate was also evaluated by the mass distribution curves by:

$$Q_s = \frac{1}{At_r}\int m_i dx \qquad \text{[Eq. 3]}$$

where, Q_s is in g m^{-1} min^{-1}, and A is the collecting trough area $(1.20m \times 0.14m = 0.168m^2)$. The wind-driven rainsplash process was related to the rainfall parameter and the wind shear velocity and analyzed using a power model.

During each rainfall application and after runoff started sediment and runoff samples were collected at 5-min intervals at the bottom edge of the pan using wide-mouth bottles and were determined gravimetrically. Total sediment and runoff values, and the time during which the process occurred were used in calculation of sediment transport by rain-impacted shallow flow (q_s). The sediment transport by rain-impacted shallow flow was based on interrill erosion mechanics and related to the rainfall and flow parameters.

Results and discussion

Rainsplash detachment under wind-driven rain

Rainsplash detachment rates estimated from the mass distribution curves by equation 1 are given in Table 1 for the three soils. Also, the bar graphs of the detachment rate versus the horizontal wind velocity for windward and leeward slopes are presented in Figure 2.

The differential detachment rates occurred depending on the change in raindrop trajectory and rain intensity with the wind velocity and direction. For a particular wind velocity, the detachment rate gradually increased in windward slopes due to the greater raindrop impact frequency with greater impact angles as the slope gradient increased. Conversely, there were lesser raindrop impact frequencies with smaller impact angles in leeward slopes as the slope gradient increased, resulting in lesser detachment rates. Finally, differences in detachment rates between aspects increased as the slope gradient and the wind velocity increased. The detachment rate in windward slope was about 44 times greater than that in leeward slope for the rains driven by 14 m s^{-1} incident on slope of 11.3° for Nukerke silt loam. For the same runs, the rates were 37 and 28 times greater in the windward slopes than in the leeward slopes for Kemmel1 sandy loam and Kemmel2 loam, respectively.

A significant result of our findings was large differences between rainsplash detachment on wind- and leeward slopes. Pedersen and Hasholt (1995) stressed the necessity of studying slope aspect influence on energy levels under wind-driven rain. Our study indicated that there were dramatic differences in the parameter values between slope aspects, and these were in considerable agreement with variations in the rainsplash detachment rates.

Statistical analyses for the rainsplash detachment rate as a power function of E_{rn} were presented in Table 2 for three soils. Units of variables are as presented in Table 1. Statistical analyses were performed by log-linear regression technique, and the model parameters, K and a, in all equations were significant at the $P = 0.0001$ level of significance for the three soils and all data. The analyses also revealed that at the exponents a for all soils level of are not significantly different from 1.

Table 2. Statistical analyses for the relationship between the soil detachment rate and the selected rainfall parameter.

Soil	$D = K(KE^a)$		
	K	a	R^2
Nukerke	105.40	0.91	0.79
Kemmel1	108.64	1.05	0.78
Kemmel2	109.95	0.98	0.73
All data	108.05	0.98	0.76

Table 3. Statistical analyses for the equation of the wind-driven rainsplash transport (Q_s) for three soils and for the combined data from three soils.

Soil	$Q_s = k_1 KE^{a_1} u_*^{b_1}$			
	k_1	a_1	b_1	R^2
Nukerke	119.75	0.78	2.00	0.96
Kemmel1	144.43	0.86	2.32	0.95
Kemmel2	99.54	0.79	1.95	0.94
All data	119.95	0.81	2.09	0.94

Table 4. (†) Summary of the data for the measured rainsplash transport rates (Q_s) for three soils.

u m s^{-1}	θ (°)	u_* m s^{-1}	Rainsplash transport rate, Q_s (g m^{-1} min^{-1})						n
			Nukerke		Kemmel1		Kemmel2		
			Mean	Stdev.	Mean	Stdev.	Mean	Stdev.	
0 ww	4	-	0.64	0.14	1.02	0.89	0.49	0.02	3
	8.5		0.90	0.28	1.31	0.72	1.47	0.08	3
	11.3		1.59	0.35	1.47	0.31	1.25	0.33	3
6 ww	4	0.35	2.25	0.22	2.02	0.11	1.69	0.43	3
	8.5		2.81	0.35	3.11	0.31	2.24	0.33	3
	11.3		4.21	0.48	3.80	0.24	2.74	0.35	3
10 ww	4	0.53	11.03	0.48	9.02	1.43	8.91	1.60	3
	8.5		11.03	0.44	10.70	1.41	10.73	1.51	3
	11.3		16.03	1.60	20.83	2.22	12.90	3.23	3
14 ww	4	0.77	16.65	1.35	11.70	0.93	10.81	1.66	3
	8.5		29.41	3.13	23.64	3.01	25.76	5.59	3
	11.3		41.60	6.38	35.91	3.59	38.78	6.75	3
0 lw	4	-	0.60	0.15	0.54	0.12	0.71	0.30	3
	8.5		0.75	0.12	0.91	0.03	1.09	0.19	3
	11.3		1.19	0.05	1.31	0.26	1.18	0.05	3
6 lw	4	0.35	4.49	0.40	1.27	0.10	2.73	0.38	3
	8.5		1.54	0.06	0.86	0.05	2.78	0.44	3
	11.3		1.62	0.14	1.12	0.12	1.57	0.09	3
10 lw	4	0.53	4.31	0.30	3.72	0.23	3.21	0.16	3
	8.5		1.50	0.09	1.09	0.14	1.58	0.09	3
	11.3		1.58	0.26	0.96	0.10	1.07	0.04	3
14 lw	4	0.77	5.16	0.23	7.32	0.70	5.68	0.43	3
	8.5		2.74	0.26	1.56	0.22	2.00	0.26	3
	11.3		1.10	0.09	0.95	0.11	0.92	0.15	3

u: horizontal wind velocity (ww: windward; lw: leeward); θ: channel bottom slope; u_*: wind shear velocity.

† Mean values are given in the table, however, statistical analyses are performed with individual data points.

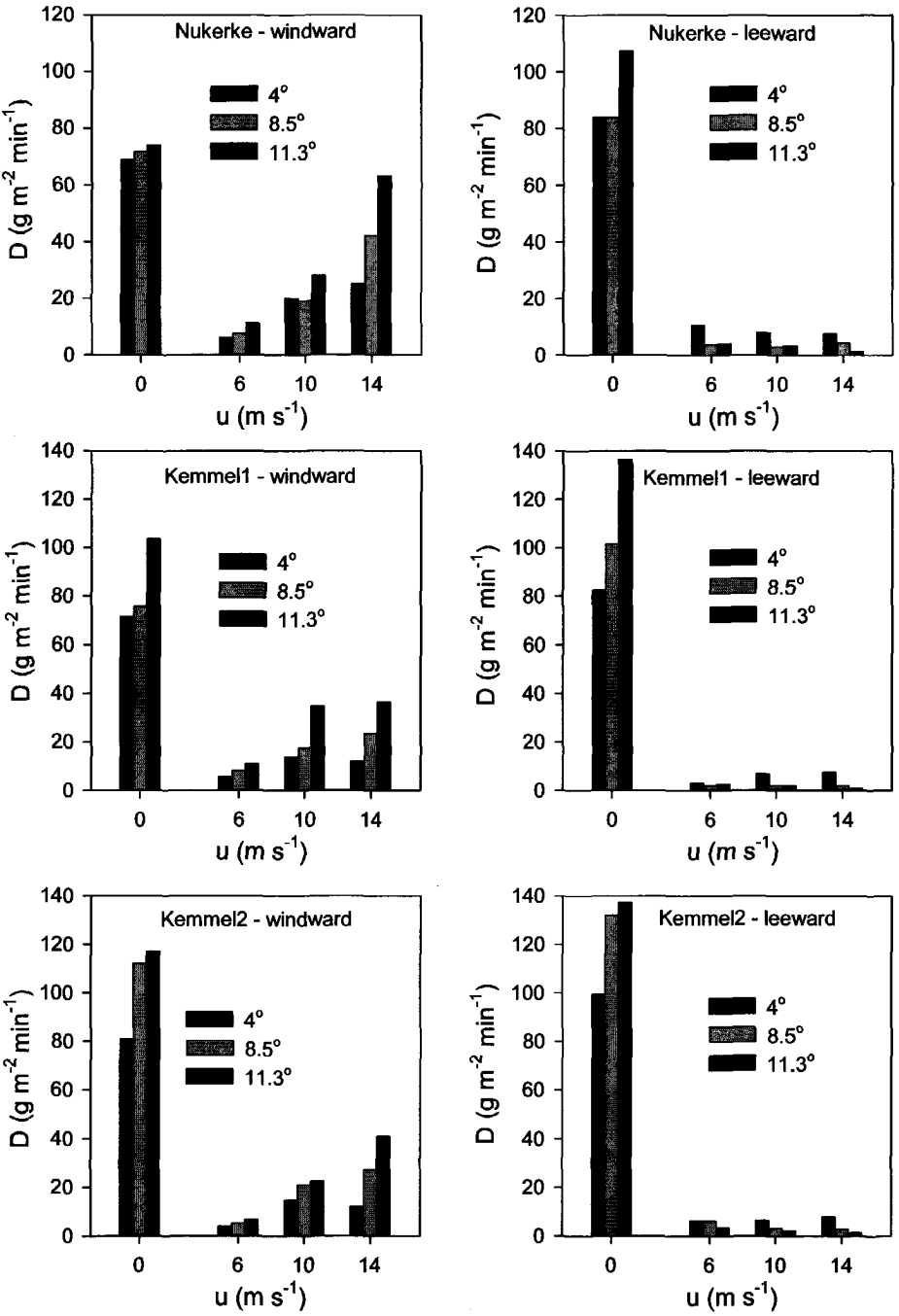

Figure 2. Measured rainsplash detachment rates of Nukerke silt loam, Kemmel1 sandy loam, and Kemmel2 loam.

Table 5. Summary of the data for the measured detachment rates (D, g m^{-2} s^{-1}) for three soils.

u $m\ s^{-1}$	θ (°)	I_a mm h^{-1}	KE W m^{-2}	Nukerke Mean	Nukerke Stdev.	Kemmel1 Mean	Kemmel1 Stdev.	Kemmel2 Mean	Kemmel2 Stdev.	n
0 ww	4	142	0.377	69.10	15.61	71.57	6.13	80.84	11.34	3
	8.5	140	0.365	71.73	5.99	75.68	12.23	112.15	10.50	3
	11.3	134	0.343	74.07	23.98	103.53	11.65	117.22	11.39	3
6 ww	4	90	0.116	6.13	0.59	5.59	0.37	3.98	0.86	3
	8.5	100	0.152	7.63	1.00	8.07	0.89	5.27	0.80	3
	11.3	106	0.177	11.28	1.52	10.06	0.80	6.72	1.29	3
10 ww	4	120	0.184	20.10	0.53	13.86	4.11	14.69	3.72	3
	8.5	130	0.268	19.04	1.90	17.46	0.40	21.02	3.64	3
	11.3	131	0.317	28.17	1.18	34.79	0.48	22.49	4.82	3
14 ww	4	90	0.168	25.14	5.04	11.96	1.93	11.98	2.35	3
	8.5	103	0.281	42.22	4.61	23.41	2.55	27.20	5.83	3
	11.3	112	0.372	63.49	8.16	36.50	4.17	40.96	5.90	3
0 lw	4	165	0.438	83.80	16.32	82.31	6.00	99.28	14.09	3
	8.5	172	0.448	83.82	20.42	101.48	6.24	131.99	26.60	3
	11.3	179	0.459	107.28	6.38	136.52	7.22	137.30	17.72	3
6 lw	4	126	0.112	10.61	0.91	3.03	0.38	6.34	0.81	3
	8.5	112	0.076	3.65	0.16	1.99	0.13	6.16	0.92	3
	11.3	94	0.053	3.96	0.36	2.54	0.30	3.50	0.33	3
10 lw	4	92	0.070	8.08	0.77	6.87	0.80	6.52	0.69	3
	8.5	61	0.027	2.99	0.30	2.08	0.44	3.11	0.11	3
	11.3	51	0.014	3.26	0.57	1.87	0.19	2.20	0.13	3
14 lw	4	66	0.047	7.64	0.44	7.56	1.05	8.07	1.04	3
	8.5	42	0.012	4.35	0.51	1.98	0.29	3.00	0.47	3
	11.3	34	0.004	1.43	0.13	0.98	0.17	1.44	0.16	3

u: horizontal wind velocity (ww: wind ward, lw: leeward), I_a: actual rainfall intensity. KE: flux of energy, which is related to the normal component of resultant impact velocity, calculated by equation 2.

Wind-driven rainsplash transport

The rainsplash process acted alone until runoff occurred, and net soil transport was affected by slope and wind, respectively for windless and wind-driven rains. The observed distance of particle travel was up to 0.40 m under windless rains and ranged from 3 to 7 m depending on the gradient of wind velocity profile under wind-driven rains. For example, the particle trajectories were complete at 3 m in the rains driven by 6 ms^{-1} wind velocity, and at 7 m in the rains driven by 10 and 14 ms^{-1} wind velocities. On the other hand, the rate at which soil particles were entrained into the air was a function of such physical raindrop parameters as velocity, frequency, and angle of impact. Values for the measured rainsplash rates are presented in Table 3, and also, the bar graphs of the transport rate versus the horizontal wind velocity for windward and leeward slopes are presented in Figure 3.

The statistical fit of the power law models is presented in Table 3, and units of the variables are presented in Table 1 and Table 4. The models performed equally well and provided similar R^2 values, which were ≥ 0.94 for the three soils. The analysis of variance also showed that k_1, a_1, and b_1 were significant at $P = 0.0001$ level of significance.

The form of the model developed above features an integration of wind effects on the physical raindrop impact, and hence detachment, and on the transport process. Because previous mathematical models of rainsplash erosion developed for windless rain did not include the roles of wind in both detachment and transport processes (Savat and Poesen, 1981; Poesen, 1985, 1986; Wright, 1986, 1987), they are unlikely to be suitable for modeling the process under wind-driven rains. In this experimental study, wind increased the raindrop resultant velocity and altered the angle of raindrop

incidence, which resulted in a variable raindrop impact frequency and impact angle. Therefore, differential delivery rates occurred depending on the variations in raindrop trajectory and frequency with wind velocity and direction. More significantly, the wind had a greater effect on transport than slope gradient.

Sediment transport by rain-impacted shallow flow

As soon as runoff started, the flow-driven process began to transport the detached soil particles. The rates of sediment transported by rain-impacted thin flow for three soils are presented in Table 5 and graphed in Figure 4. Time to runoff varied depending on the actual amount of rain intercepted by the soil surface, which was a function of rain inclination and slope gradient and aspect. The effect of slope aspect on rain interception and runoff generation was stronger for the higher wind velocities: the angle of rain incidence attained very high values as rain inclination and the slope gradient increased in leeward slopes, resulting in very low intensity values. For example, the overland flow generation was retarded approximately for 45 min under the rains driven by the wind velocities of 10 and 14 ms^{-1} on the leeward slopes of 7, 15, and 20%. When the rain intensity was less than 60 mm h^{-1}, the wind-driven rainsplash process lasted longer than the thin flow-driven process due to the retarded flow generation. Evidently, the wind effect was not only on the rainsplash detachment by changing velocity, frequency, and angle of the impinging raindrops but also on the flow generation, which demarcated the dominant transport process.

The statistical fit of the data, which is based on the interaction between raindrop impact and flow parameters (Julien and Simon, 1985; Gilley et al., 1985; Guy et al., 1987; Zhang et al., 1998), are shown in Table 6. The flux of rain energy adequately described the characteristics of wind-driven rains for the interrill sediment delivery to the shallow flow transport as well as to the rainsplash transport. The analysis of variance showed that a_2 was significant at the level of $\alpha = 0.05$ for each case. Compared to the impact of raindrops on bare soil, lesser a_2 values for flux of rain energy suggested the detaching power of raindrops was partially dispersed by the thin flow depth on the soil surface (Moss and Green, 1983; Torri et al., 1987; Kinnell, 1991). The relative soil transport parameter for shallow flow-driven process (k_2) and exponent values to which the unit discharge and slope were raised (b_2 and c_2, respectively) were also significant at the level of $\alpha = 0.05$ for all cases (Table 6).

The units of variables are as presented in Table 1 and Table 5. In general, the models performed reasonably well, accounted for $\geq 89\%$ of the variations in the shallow flow transport rates.

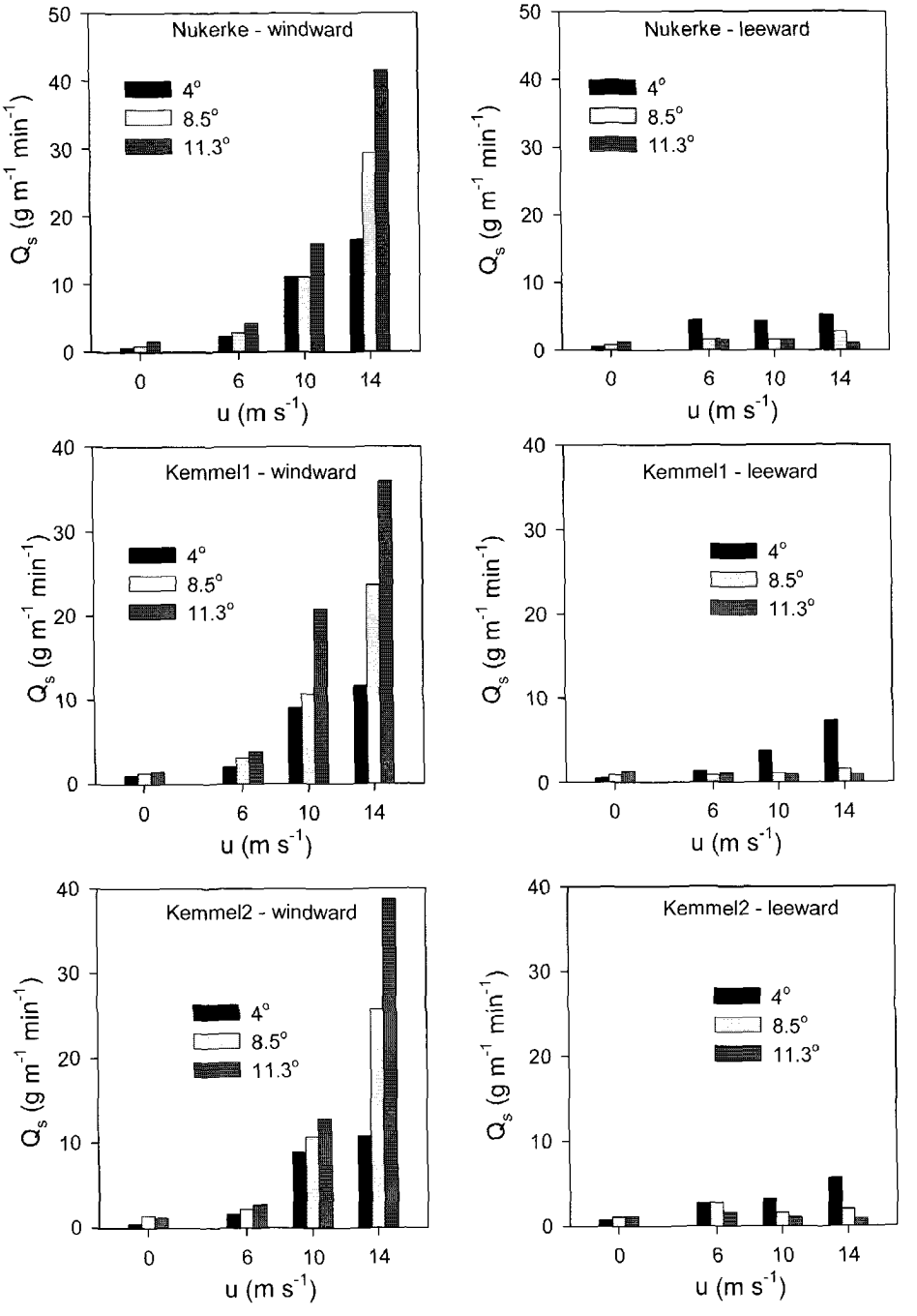

Figure 3. Measured wind-driven rainsplash transport rates of Nukerke silt loam, Kemmel1 sandy loam, and Kemmel2 loam.

Table 5. (†) Summary of the data used in evaluating sediment transport by the rain-impacted shallow flow (q_s) for three soils.

u	θ	Nukerke			Kemmel1			Kemmel2			n
m s^{-1}	(°)	q m^2 min^{-1}	q_s (g m^{-1} min^{-1}) Mean	Stdev.	q m^2 min^{-1}	q_s (g m^{-1} min^{-1}) Mean	Stdev.	q m^2 min^{-1}	q_s (g m^{-1} min^{-1}) Mean	Stdev.	
	4	3.878E-04††	23.98	2.41	4.935E-04	16.56	5.42	3.243E-04	20.13	0.84	3
0 - ww	8.5	4.888E-04	29.95	3.59	5.100E-04	38.39	5.94	3.540E-04	22.76	0.96	3
	11.3	4.938E-04	45.07	4.01	5.237E-04	37.50	1.83	3.831E-04	41.66	2.12	3
	4	4.308E-04	11.35	0.50	2.715E-04	5.35	0.12	2.348E-04	8.00	0.82	3
6 - ww	8.5	5.461E-04	29.93	3.14	3.769E-04	18.84	0.91	2.022E-04	12.59	2.04	3
	11.3	5.756E-04	45.39	3.49	4.755E-04	33.17	2.01	2.400E-04	22.34	4.78	3
	4	5.883E-04	26.28	1.22	5.497E-04	17.15	1.64	2.562E-04	20.65	4.53	3
10 - ww	8.5	7.367E-04	66.90	11.09	6.464E-04	61.92	8.48	3.429E-04	38.51	10.91	3
	11.3	7.926E-04	104.45	8.45	7.445E-04	121.95	5.98	3.468E-04	49.88	2.65	3
	4	4.788E-04	21.40	1.68	4.087E-04	14.98	3.84	2.380E-04	11.49	0.49	3
14 - ww	8.5	5.238E-04	54.41	15.25	5.169E-04	45.99	6.07	2.760E-04	36.29	5.74	3
	11.3	6.046E-04	81.08	22.17	5.867E-04	92.19	6.37	3.288E-04	55.75	3.43	3
	4	6.694E-04	34.77	2.87	6.087E-04	34.90	4.57	5.325E-04	30.89	1.28	3
0 - lw	8.5	6.673E-04	39.60	2.44	4.929E-04	49.48	2.12	4.642E-04	30.47	3.89	3
	11.3	8.286E-04	63.19	3.06	5.954E-04	59.95	5.76	6.555E-04	55.91	7.23	3
	4	5.516E-04	14.38	0.90	2.963E-04	9.81	0.51	4.073E-04	14.43	0.56	3
6 - lw	8.5	4.384E-04	17.01	0.79	2.218E-04	10.35	0.59	2.212E-04	8.22	0.28	3
	11.3	3.955E-04	19.70	0.97	1.801E-04	8.25	0.51	1.448E-04	5.59	0.41	3
	4	3.899E-04	14.75	0.33	1.899E-04	6.99	0.38	1.943E-04	11.68	0.68	3
10 - lw	8.5	1.644E-04	8.30	1.29	1.003E-04	3.23	0.21	8.110E-05	4.52	0.65	3
	11.3	1.363E-04	5.70	0.36	6.925E-05	1.89	0.13	4.554E-05	1.85	0.28	3
	4	1.756E-04	9.94	0.71	1.117E-04	5.76	0.30	9.650E-05	8.16	0.58	3
14 - lw	8.5	8.300E-05	6.81	1.00	5.328E-05	2.63	0.12	6.273E-05	3.00	0.25	3
	11.3	6.707E-05	4.98	0.19	4.137E-05	1.03	0.05	4.314E-05	1.80	0.20	3

u: horizontal wind velocity (ww: windward; lw: leeward); θ: channel bottom slope, which is given in degrees but is used in m m^{-1} in the statistical fit; q: unit discharge.

† Mean values are given in the table, however, statistical analyses are performed with individual data points.

†† The E notation means " times 10 to the power".

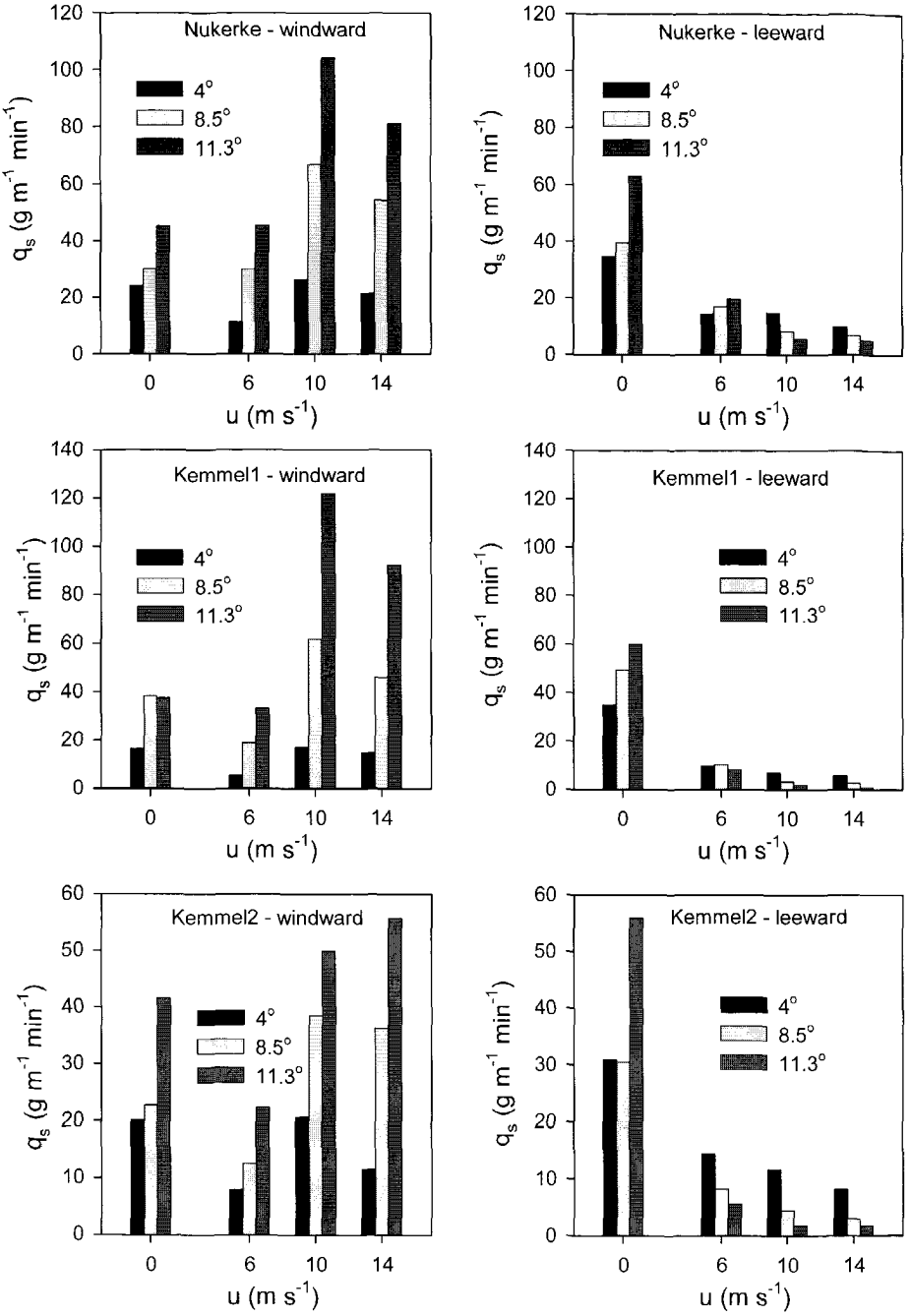

Figure 4. Measured sediment transport rates by raindrop-impacted shallow flow for Nukerke silt loam, Kemmel1 sandy loam, and Kemmel2 loam.

Conclusions

Only experimental data directly taken on the effect of the slope aspect on the soil detachment and sediment transport has been used in this study with the objective of improving the understanding of interrill erosion processes under wind-driven rain. Results showed that the differential detachment rates occurred depending on the slope aspect, and for a particular wind velocity, the detachment rate gradually increased and decreased in windward and leeward slopes, respectively as the slope gradient increased. At last, differences in detachment rates between aspects increased as the slope gradient and the wind velocity increased. The flux of rain energy calculated by Eq. [2], which integrates the effect of wind on the velocity, frequency, and angle of the raindrop impact, adequately described the characteristics of wind-driven rains for the interrill sediment delivery both to the shallow flow transport and to the rainsplash transport.

The slope factor currently used in the erosion models might be insensitive to changes possible to occur with the trajectory and frequency of raindrop impact with respect to the slope aspect. Therefore, there is a need for a prediction technology that could deal with the wind-driven rain events and the variability in the processes due to the slope aspect. These results can be used to improve the understanding of erosion processes and provide a better estimate of soil detachment and transport under wind-driven rain.

References

De Lima, J. L. M. P., 1990. The effect of oblique rain on inclined surfaces: A nomograph for the rain-gauge correction factor. *Journal of Hydrology*, 115: 407-412.

Erpul, G., D. Gabriels, and D. Janssens. 1998. Assessing the drop size distribution of simulated rainfall in a wind tunnel. *Soil and Tillage Research*, 45: 455-463.

Erpul, G., D. Gabriels, and D. Janssens. 2000. The effect of wind on size and energy of small simulated raindrops: a wind tunnel study. *International Agrophysics*, 14: 1-7.

Erpul, G., Norton, D. L., Gabriels, D., 2002. Raindrop-induced and wind-driven soil particle transport. *Catena*, 47, 227-243.

Erpul, G., Norton, D. L., Gabriels, D. 2003a. The effect of wind on raindrop impact and rainsplash detachment. *Transactions of ASAE*, 45: 51-62.

Erpul, G., Norton, D. L., Gabriels, D. 2003b. Sediment transport from interrill areas under wind-driven rain. *Journal of Hydrology*, 276: 184-197.

Gabriels, D., W. Cornelis, I. Pollet, T. Van Coillie and M. Quessar. 1997. The I.C.E. wind tunnel for wind and water erosion studies. *Soil Technology*, 10: 1-8.

Gilley, J. E., D. A. Woolhiser and D. B. McWhorter. 1985. Interrill soil erosion. Part I: Development of model equations. *Transactions of the ASAE* 28: 147-153 and 159.

Guy, B. T., W. T. Dickinson and R. P. Rudra. 1987. The roles of rainfall and runoff in the sediment transport capacity of interrill flow. *Transactions of the ASAE* 30: 1378-1386.

Julien, P. Y. and D. B. Simon. 1985. Sediment transport capacity of overland flow. *Transactions of the ASAE* 28: 755-762.

Kinnell, P. I. A., 1981. Rainfall intensity-kinetic energy relationship for soil loss prediction. *Soil Sci. Soc. Am. J.*, 45: 153-155.

Kinnell, P. I. A., 1991. The effect of flow depth on sediment transport induced by raindrops impacting shallow flows. *Transactions of the ASAE*, 34: 161-168.

Moss, A. J. and P. Green. 1983. Movement of solids in air and water by raindrop impact. Effects of drop-size and water-depth variations. *Aust. J. Soil Res.*, 21: 373-382.

Pedersen, H. S. and B. Hasholt. 1995. Influence of wind speed on rainsplash erosion. *Catena*,24: 39-54.

Poesen, J., 1985. An improved splash transport model. *Z. Geomorph. N. F.*, 29: 193-221.

Poesen, J., 1986. Field measurements of splash erosion to validate a splash transport model. *Z. Geomorph. N. F.*, Suppl. bd, 58: 81-91.

SAS, 1995. SAS System for Elementary Statistical Analysis. SAS Inst. Inc., Cary, NC, USA, pp. 280-285.

Savat, J. and J. Poesen. 1981. Detachment and transportation of loose sediments by raindrop splash. Part I: The calculation of absolute data on detachability and transportability. *Catena* 8: 1-18.

Sensit[TM], 2000. Model V04, Kinetic Energy of Rain Sensor. Sensit Company, Portland, ND 58274-9607.

Sharon, D. 1980. The distribution of hydrologically effective rainfall incident on sloping ground. *Journal of Hydrology* 46: 165-188.

Struzer, L. R. 1972. Problem of determining precipitation falling on mountain slopes. *Sov. Hydrol. Selected papers* 2: 129-142.

Torri, D., M. Sfalanga and M. Del Sette. 1987. Splash detachment: runoff depth and soil cohesion. *Catena*, 14: 149-155.

Van Heerden, W. M., 1967. An analysis of soil transportation by raindrop splash. *Transactions of the ASAE*, 10:166-169.

Wright, A. C., 1986. A physically-based model of the dispersion of splash droplets ejected from a water drop impact. *Earth Surf. Process. Landforms*, 11: 351-367.

Wright, A. C., 1987. A model of the redistribution of disaggregated soil particles by rainsplash. *Earth Surf. Process. Landforms*, 12: 583-596.

Zhang, X. C., M. A. Nearing, W. P. Miller, L. D. Norton and L. T. West. 1998. Modeling interrill sediment delivery. *Soil Sci. Soc. Am. J.* 62: 438-444.

Chapter 10

Seasonal interaction between water and wind erosion an example from the Ereri-Longonot area in the central Rift Valley of Kenya

G. R. Henneman
International Institute for Geo-information Science and Space Observation (ITC) ,Department of Earth Systems Analysis, P.O. Box 6, 7500 AA Enschede, The Netherlands; Email: Hennemann@itc.nl

Seasonal interaction between water and wind erosion
an example from the Ereri-Longonot area in the central Rift Valley of Kenya

Introduction

During the reconnaissance phase of a wind erosion research programme carried out in the central Rift Valley of Kenya from 1999 till 2001 a wide range of interesting erosion patterns was identified and described (Ataya 2000; Nagelhout 2001; Hennemann and Nagelhout 2004). In the southern part of the reconnaissance area, around Ereri and Longonot village, a peculiar erosion landscape was encountered that showed clear evidence of seasonal interaction between water and wind erosion. Although the area around Ereri was not included in the final research area, sufficient information was collected to obtain a broad overview and understanding of the erosion landscape. This chapter aims to give (1) a brief account of the erosion phenomena observed in the Ereri Longonot area, and (2) to discuss the synergistic relationship between the wind and water erosion and the key factors underlying this relationship.

General description of the reconnaissance area

The reconnaissance area is located in the central part of the Kenya Rift Valley, southeast of Lake Naivasha, along the old Nairobi-Nakuru Road, at approximately 70 km north-west of Nairobi. The area lies at an altitude of around 2,100 m a.s.l and is bounded by latitudes 0° 49' S to 0° 54' S and longitudes 36° 27' E to 36° 29' E. Administratively, it forms part of Nakuru District.

The area has a cool, relatively dry tropical highland climate (Cwik according to Köppen's classification). Mean annual rainfall ranges between 600-700 mm yr^{-1}. Mean minimum and maximum monthly temperatures vary between 15.9 °C to 18.5 °C and from 24.6 °C to 28.3 °C, respectively. The long rainy season lasts from March till May, with the short rainy season running from October till December.

Mean monthly wind velocity is highest in the period April-September (6-7 m s^{-1}) and lowest during November-February (3-4 m s^{-1}). Mean maximum wind speed, however, is considerably higher and may reach up to 15-20 m s^{-1} during May-August resulting in high erosivity levels of the predominantly easterly winds during this period. The natural vegetation mainly consists of low *Acacia* shrub grassland with *Acacia drepanolobium* ('Whistling Thorn') as main woody species and *Themeda triandra* as the dominant grass. Since the 1980s, however, most of the natural vegetation has been cleared or degraded into grassland. Current land use is mainly nomadic pastoralism with some marginal arable farming on small isolated farms. Most of these farms are remnants of the various wheat smallholder schemes that were developed mainly during the 1980s. Most of these schemes failed and were abandoned during the mid-1990s.

Differential development of erosion patterns

The wind erosion reconnaissance area can be broadly divided into three major zones as follows (going from north to south):

a) The Suswa area
b) The Magumu Junction area
c) The Ereri - Longonot area

The Suswa area
This northern part of the reconnaissance area is located just south of Suswa station and comprises a nearly level to very gently undulating volcanic plain (0-2%) just south Suswa railway station. Wind erosion features are virtually absent from this area due to the relatively favourable conditions prevailing here. These include the almost level topography and, most importantly, the absence of smallholder wheat cultivation during the 1980s and 1990s from the area as most of the wheat schemes were located further south, around Longonot and Mai Mahiu.

The Magumu Junction area
The Magumu Junction area occupies the central part of the reconnaissance area, which forms the watershed between the Lake Naivasha basin in the north and Ewaso Kedong catchment in the south. Its general landscape resembles that of the Suswa area except for the presence of low relic dune fields in the western part, along the railway line. A most conspicuous wind erosion pattern has developed in this area which has been extensively described, mapped and analysed by Ataya (2000), Nagelhout (2001) and Hennemann and Nagelhout (2004). This pattern consists of long east-west running grey strips following the prevailing wind direction in the area. At the windward side, deflation gullies of variable size occur which may be up to several tens of metres wide, up to 2 metres deep and over 200 metres long. At the leeward side of these gullies, broad sedimentation strips occur appearing as grey 'tails' of up to several hundreds of metres length. Such strips consist of deposited sandy ash material blown from the associated deflation trench. The above deflation areas are quite variable in size depending on their stage of development.

GIS-analysis revealed a distinct spatial relationship between the severity of wind erosion and the occurrence of the relic dune fields in the study area. This provided evidence that the presence of micro-relief forms a key factor in the prevailing wind erosion process in this area.

Severe wind erosion of above nature appeared to be a recent phenomenon to the area. In interviews all farmers emphasised that nearly all deflation trenches in the area developed after the mid-1990s and that some of the largest trenches only started to form 1-2 years before the interview. This was partly confirmed by systematic interpretation of aerial photographs available from the area taken in 1991 revealing just 1 deflation gully. Water erosion does not appear to play a key role in the Magumu Junction area, mainly as a result of the very gentle topography with slope gradients generally less than 2%.

The Ereri-Longonot area
Going across the watershed into the Ewaso Kedong catchment one enters the Ereri-Longonot area which occupies the southern most part of the reconnaissance area. A quite peculiar erosion pattern showing clear evidence of seasonal interaction between water and wind erosion was encountered here. The Ereri-Longonot area is described in more detail in the section below.

Erosion development in the Ereri-Longonot area

General soil-landscape conditions
The Ereri-Longonot area forms part of the Rift Valley floor and largely consists of a undulating (2-8%) somewhat dissected volcanic plain. The area is almost entirely

covered by young, poorly developed coarse-textured soils derived from stratified Longonot ash and Akira pumice deposits of Pleistocene age (Thompson et al., 1958). The predominant soil consists of very deep, excessively drained, very friable, brown loamy sands and sands (Ah and Bw horizons) overlying a succession of dark grey and whitish grey, loose fine, highly erodible ash layers (C-horizons) (Fig.1). The Bw horizon is susceptible to sealing but the C-horizon is not susceptible for erosion. The soils classify as *Areni-Vitric Andosols (Dystric)* according to the World Reference Base (FAO 1998) on account of their sandy texture, relatively high content of volcanic glass in the fine earth fraction, and low base saturation in the control section.

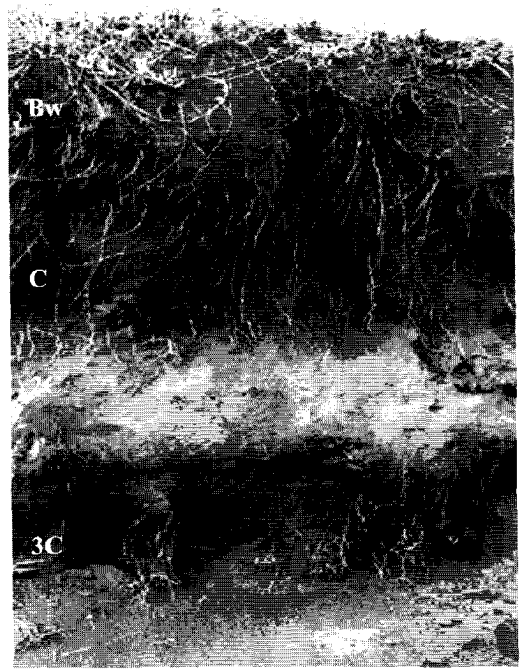

Figure 1. Young stratified volcanic soil with highly erodible subsoil (Areni-Vitric Andosols (Dystric) WRB 1998)

Successive phases in erosion pattern development

The distinct nature of the different erosion phenomena and patterns in the area clearly suggests the presence of a synergistic relationship between water erosion processes during the wet season and wind erosion processes during the dry season.Below the successive stages of erosion development are described and discussed. Three erosion formation phases have been distinguished:

1) Water erosion phase,
2) Water erosion - wind erosion synergy phase, and
3) Wind erosion phase.

Water erosion phase: development of rills and small gullies

Initial weakening and degradation of vegetation cover and topsoil result in surface sealing leading to excess runoff during rain storms. This will eventually initiate rill

erosion usually starting along old furrows and farm boundaries, which is subsequently followed by the formation of small gullies (Fig. 2). These gullies then rapidly extend upward along the slope through head-ward retreat until a substantial runoff catchment is developed.

Water & wind erosion synergy phase: development of deflation gullies
The second phase is started once the relatively coherent brown solum (Ah and Bw horizons) is breached and the underlying loose, largely unweathered ash layers of the C, 2C and 3C horizons become exposed at the surface (Fig. 3a and 3b).

Massive wind erosion sets in during the dry season, removing the fine to medium coarse and the coarse sand fractions of loose volcanic ash deposits in saltation and creep, respectively. These coarser fractions are deposited in- and outside or at short distance from the gully. The finer ash particles including the silt and fine sand fractions are carried off into suspension as dust polluting the areas around Lake Naivasha and Naivasha town.

The above described wind deflation process leads to rapid undercutting and subsequent collapse of gully sides (Fig. 3b). The combined effect of these processes is that the initially small 'water erosion' gullies are turned into huge deflation gullies, often at an astonishing rate.

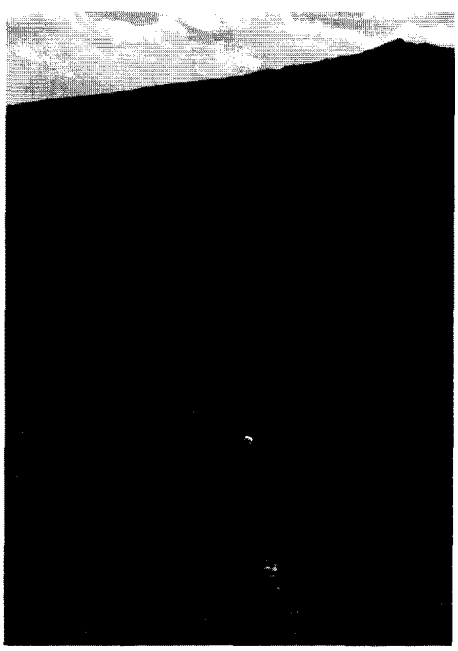

Figure 2.- Water erosion phase: formation of rills and small gullies along old farm boundaries and tracks caused by excess runoff

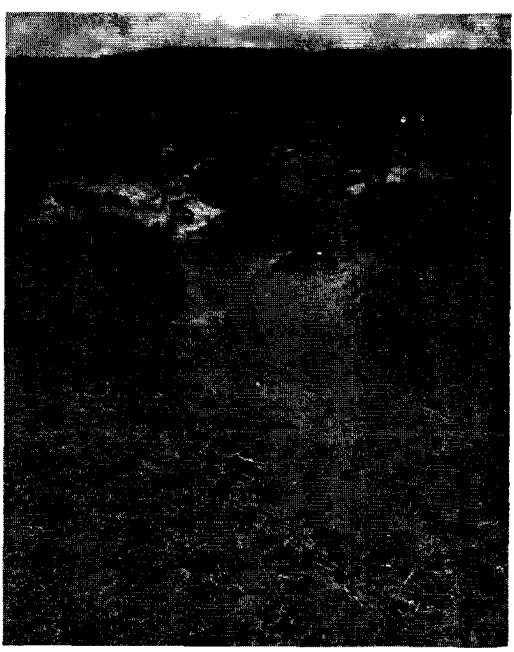

Figure 3a. Water & wind erosion synergy phase: rills and small gullies deepen further during the rainy season and expand into deflation gullies during the

Figure 3b. Water & wind erosion synergy phase: close-up of an active deflation gully. Note the distinct volcanic soil stratigraphy and associated collapse phenomena along the gully side.

Wind erosion phase: (a) coalescence of deflation gullies and (b) formation of a drift-sand plain

In the final phase of the wind and water erosion interaction, the influence of rill and gully erosion by water action is declining. Due to the widespread surface exposure of permeable ash layers of the subsoil, overland flow decreases; consequently, rill and gully development by water action comes to a standstill.

Wind erosion is now the dominant force controlling the further expansion of deflation and collapse processes in and along gullies. This is subsequently followed by a process of gully coalescence in which two or more deflation gullies merge into large blow-out areas. The final stage is the formation of a vast drift-sand plain on which deflation areas alternate with depositional areas consisting of low hummocks often developed centred around raised grass-tufts (Fig. 4).

Discussion

From above erosion observations it is clear that a specific combination of causative factors needs to be in place before the interactive erosion processes described can start and develop. This combination of key causative factors can be summarized as follows:

Climatic factors

Occurrence of high levels of both water and wind erosivity

No detailed information is available about rain erosivity in the area. However, with a mean annual rainfall of 600-700 mm, mostly falling in high-intensity rainstorms, erosivity levels can be assumed sufficiently high for substantial runoff and erosion to develop during the wet season. With respect to wind erosion, the wind erosivity index according to the Modified Chepil Equation was used (Chepil, Siddoway et al. 1962, Karanja 1997); this provided preliminary erosivity results around 250 $m^3 s^{-3}$; ranking

Figure 4. Wind erosion phase: coalescence of deflation gullies into vast drift-sand plains. Patches of the original, often somewhat abraded surface

among the highest levels found in Kenya (Karanja 1997). This high wind erosivity can be explained by the open, gentle topography in combination with the high elevation of the area (2100 m a.s.l.).

Topographic and soil-related factors

Open, treeless landscape with at least undulating topography

An open landscape is required to provide sufficient free range for the wind action to develop critical shear stress levels. For rill and gully development, slope gradients of over 1-2% are a prerequisite as below this level overland flow remains limited.

Stratified volcanic nature of the soils

The distict duplex nature of the young Andosols predominant in the area appears to be a key requirement for the interactive erosion processes described. At the surface, the coherent brown Bw-horizon is able to resist wind erosion thus acting as a protective cover for the erodible subsoil beneath during the dry season. Yet, at the same time, this surface horizon is quickly affected by rill and gully erosion due to its susceptibility to sealing during the rainy season[1]. In contrast, the very loose subsoil consisting of unweathered, stratified ash deposits forms - once exposed - an easy prey for wind erosion during the dry season[2]. During the wet season, however, the subsoil

[1] Another important erosion-enhancing soil factor might be the generally hydrophobic nature of the surface horizon due to the presence finely dispersed humus-coatings around sand grains in the Bw horizon thus further reducing initial infiltration capacity of the soil.

[2] The poor aggregate size distribution of the subsoil (high % dry aggregates with diameter < 0.84 mm) and its low specific density - probably due to the relatively high content of pumice in the fine earth fraction – are responsible for its high wind erodibility (Zobeck 1991; Nagelhout 2001).

due to its very permeable nature is able to quickly smother any runoff and water erosion.

It is this combination of strongly 'opposing' soil characteristics of both surface and subsurface horizons in these young Andosols that provides the specific conditions needed for the seasonal interaction between wind and water erosion in the area.

Landuse-related factors

Influence of past land management and land use changes

Rills and small gullies in the area generally have developed along boundaries of abandoned arable fields. In addition, GIS analysis of the erosion patterns in the adjacent Magumu Junction area revealed that almost all large deflation gullies are found on or along recent and old farm roads and farm boundaries (Nagelhout 2001). Careless land management, including not just poor conservational design of the old settlement schemes' farm-layout and neglect of old farm roads but also overgrazing by Maasai cattle can therefore be listed as a definite fourth key factor contributing to erosion development in the area.

References

Ataya, C.O., 2000. Wind erosion of volcanic soils. A reconnaissance study in the southern catchment of Lake Naivasha Region, Kenya. MSc thesis, ITC / Soil Science Division, Enschede, The Netherlands. pp.81.

Chepil, W.S.., F.H. Siddoway and D.V. Armbrust, 1962. Climatic factors for estimating wind erodibility of farm fields. *Journal of Soil and Water Conservation,* 17: 162-165.

FAO, 1998. World Reference base for soil resources. FAO, Rome.

Hennemann, G.R. and A. Nagelhout, 2004. Searching for effective, low-cost methods to detect and assess wind erosion damage: the promise of small-format aerial photography (SFAP). In: *Wind erosion and Dust Dynamics: Observations, Simulations, Modelling (Eds. D. Goossen and M.Riksen).* ESW Publications, Wageningen, pp. 123-137.

Karanja, F. K., 1997. Wind erosion and rainfall erosivity indicators. In : *National Land Degradation Assessment and Mapping in Kenya.* UNEP / Nairobi. pp. 62-71

Nagelhout, A., 2001. "Performance Analysis of Small-format Aerial Photography (SFAP) in Assessing Current Status and Trends in Wind Erosion, A Case study in the Longonot-Kijabe Hill area, Naivasha District, Kenya". MSc thesis, ITC / Soil Science Division, Enschede, The Netherlands. pp.100.

Thompson, A.O. and R.G. Dodson, 1958. Geology of the Naivasha Area.

Zobeck, T. M., 1991. Soil properties affecting wind erosion. *Journal of Soil and Water Conservation,* 46(2): 112-118.

Chapter 11

Farmers' Indicators for Water and Wind Erosion

O. Vigiak[1] & J.K. Leenders[1]
[1] Wageningen University, Erosion & Soil and Water Conservation Group
Nieuwe Kanaal 11, 6709PA Wageningen. Email: Olga.Vigiak@wur.nl

Farmers' Indicators for Water and Wind Erosion

Introduction

Land degradation, the decline in land quality caused by human activities, is a major global issue because of its impact on world food security and quality of the environment. The most important soil degradation processes are wind and water erosion (Oldeman, 1994). Through population growth, the demand for food, fodder and firewood increased, as well as the pressure on the land. In Africa the percentage of degraded area (73%) is the highest of the World (Dregne and Chou, 1994). In sub-saharan Africa, sustainable soil management at the current level of fertilizer and manure inputs, would be possible only if annually about 20% of the arable land would be cultivated and the remainder left fallow. Yet, this is about 60% at present (Drechsel and Penning de Vries, 2001). As farmers manage and cultivate natural resources, their role is crucial in the succeeding of Natural Resources Management (NRM) or Soil and Water Conservation (SWC) programs. Effective natural resource management can exist if 1) the resource user (individual farmer) recognizes the biophysical interdependencies and 2) if his resource management is coordinated with that of neighbouring farmers (Ravnborg, 2002; Howorth and O'Keefe, 1999).

Local knowledge has been described as experimental, rooted in place, empirical and dynamic (Ellen and Harris, 2000). In particular, farmers' perception and description of their environment are often linked to land management experience and land use history (e.g. Payton et al., 2003). Research has already shown the usefulness of employing farmers' knowledge to assess soil fertility (e.g. Murage et al., 2000). Among others, Habarurema and Steiner (1997), and Murage et al. (2000) documented extensive knowledge of farmers on landscape processes, and relations between soil productivity and relief position. Positive experiences have been reported also in the use of indigenous knowledge for erosion control (e.g. Warren et al., 2003).

The important contribution of local knowledge to ecological sciences is acknowledged (WinklerPrins and Sandor, 2003), but difficulties remains in how to effectively integrate local and scientific knowledge systems. Methodology studies that focus on integrating local and scientific knowledge are few (Payton et al., 2003). Niemeijer and Mazzuccato (2003) argued that the potential of farmers' knowledge is only partially exploited and they pleaded to move from the recognition of farmers' knowledge as a source of information to a more effective use of such knowledge for sustainable development. WinklerPrins (1999) stressed that the integration of local and scientific knowledge would be most beneficial in activities aimed to a more sustainable land management. Farmers' perceptions not necessarily concur with scientists' perceptions on the severity and extent of erosion problems, because farmers and scientists have a different objective and/or reference of frame (Kiome and Stocking, 1995; Ostberg, 1995). Van Dissel and de Graaff (1998) suggested that adoption and adaptation of farmers' knowledge into a scientific framework could only be achieved by thorough assessment of farmers' perceptions of ecological degradation.

In SWC planning activities, prompt and positive interventions are critical to establish a good co-operation between technicians and farmers. Soil and water conservation planning must take into account farmers' needs and priorities and requires information on the effectiveness of SWC measures to be selected. Data scarcity is, however, a common problem in tropical rural areas. In addition, capital and human resources are usually much below the demand, and extensionists must often cover large areas, that may comprise very different ecological and socio-

economic conditions and where their experience may be limited. Integration of the broader experience of the extensionists with the site-specific knowledge of the farmers may then become a key factor for successful interventions. To develop control measures that will actually fit into the local farming system, be adopted and last, it is inevitable to know the farmers' views and to gain insight in the local farming system. Given enough funds, any project can lay out erosion control measures on a large scale. The critical factor is the ability and the willingness of the people to carry out these measures, to maintain and extend them, without continued intervention (Rinaudo, 1994). Therefore farmers must be included from the outset if subsequent actions are to have any lasting effect.

This paper presents two case studies in which farmers' knowledge is used in the assessment of both wind and water erosion in Africa. The first case study focuses on farmers' perception of causes of erosion and the role of vegetation to prevent wind erosion in Sahelian Burkina Faso. The case study summarizes the main findings of an extensive research conducted in the area (Visser et al., 2003; Leenders et al., 2004). The second case study shows an example of exploiting farmers' knowledge to develop a field tool for erosion assessment for pre-intervention evaluation in the East African Highlands. A more extensive presentation of the research has been published elsewhere (Okoba et al., 2003; Tenge et al., 2004; Vigiak et al., 2004b). The case studies show that farmers are important protagonists in the struggle to conserve soil and water. Their active participation plays an essential role towards a sustainable management of the agricultural and natural land resources.

Case study 1: Farmers' perceptions of wind erosion and of the role of scattered vegetation in wind erosion control in Burkina Faso

The Sahelian zone of Africa forms a transitional zone between the arid Sahara to the North and the belt of humid savannas to the South. The farming systems and soil conditions in the Sahel are very favorable for wind erosion. The soils have a sandy texture and the soil surface is mostly bare, except for a few months in the growing season. At the start of the rainy season, rainfall comes with heavy thunderstorms. The downdrafts and outflow of these thunderstorms in combination with the bare soils can create severe dust storms. These events last usually 10-30 minutes, but can result in intense soil movement (Michels et al., 1995). The agricultural damage of these events can be soil degradation, crop damage and sedimentation at undesired places (Sterk, 2003). Until present, no adequate wind erosion control exists in the area due to poor socio-economic conditions, low biomass production, competition effects and management constraints (Sterk, 2003).

The studies done by Bielders et al. (2001), Rinaudo (1994) and Sterk and Haigis (1998) indicate that the use of woody natural vegetation present in the agro-forestry system of the area, the so-called parkland system might be a promising wind erosion control strategy in the Sahel. The presence of standing natural vegetation in between the crop increases the aerodynamic roughness, diminishing the net force of the wind on the soil surface. Competition between trees and crop for light, nutrients and water remains restricted, because the trees are scattered. A parkland system is a landscape in which mature trees occur scattered in cultivated or recently fallowed fields. The system allows the integration of cropping and livestock farming practices in combination with the management of trees (Petit, 2003). Additionally, the products of the trees are used as food, fodder, firewood or merchandise. Do farmers agree that the parkland system is a promising tool to diminish wind erosion? This case study

presents farmers' perceptions of wind erosion, the application of control measures and the role of scattered vegetation on wind erosion.

Material and Methods

The study was carried out in three villages of the Seno province, located in the Sahelian Zone of Burkina Faso (Figure 1). The climate in the area is characterized by a long dry season, lasting from October to May and a short rainy season from June to September. Average annual precipitation is 420 mm, but the variability from one year to another can be large (Fontès and Guinko, 1995). Average daily temperature changes from 28°C in December up to 45°C in April.

During the rainy season of 2001, 60 male farmers were interviewed: 20 in each village. The questionnaire consisted of a mixture of open-ended questions and questions with codified answers. The questionnaire was semi-structured: the central topics were covered in prescribed questions with the opportunity to expand interesting topics, depending on the course of the interview.

Results and Discussion

Wind erosion

The main problem the farmers encountered in cultivating their fields is the lack of rain (reported by 90% of the farmers). Lack of manure and lack of labour were seen as major constraints by 50% and 18% respectively. Only 4% of the farmers considered erosion by wind or water as a major problem. The figure of 4% does not mean that farmers do not experience erosion; it indicates that it is not the most important problem to them. When asked what farmers observe during periods of strong winds, 93% of the farmers noticed erosion on their fields and 85% reported also deposition. Of these farmers, 81% related erosion and deposition to the degree of vegetation or mulch cover. Crop damage, due to the strong winds was reported by 20% of the farmers. The farmers mentioned May to July, the beginning of the rainy season, as the period with the strongest wind. They believed that sediment transported by wind travels only limited distances from and to neighboring fields. None of the farmers thought that sand travels over longer distances.

Eighty two per cent of the farmers said to notice a difference in wind erosion intensities within and between fields. They related these differences to differences in tree and mulch cover, sand availability and topography. Ninety per cent of the farmers said that the fertility of their fields changes due to wind-blown sand particle transport. Of these farmers, 13% simply said that the fertility decreases. Most of the farmers relate deposition to an increase in fertility, and erosion to a decrease in fertility. Sterk et al. (1996) found that wind may transport considerable amounts of sediment and nutrients over short distances, resulting in an increase in soil productivity at places with deposition and a decrease in soil productivity at eroded areas.

All farmers reported observing plant losses during the first few weeks of the rainy season. In total 58% of the farmers said they loose seedlings because the moving sand damaged the plants. Furthermore, 76% of the farmers reported that when wind erosion events occur late in the rainy season the larger plants are broken by the wind causing a production loss. According to 88% of the farmers, the sand covered young seedlings. These plants often die because of lack of light for photosynthesis, the weight of the sand and the high soil temperatures during the day (Michels et al., 1995).

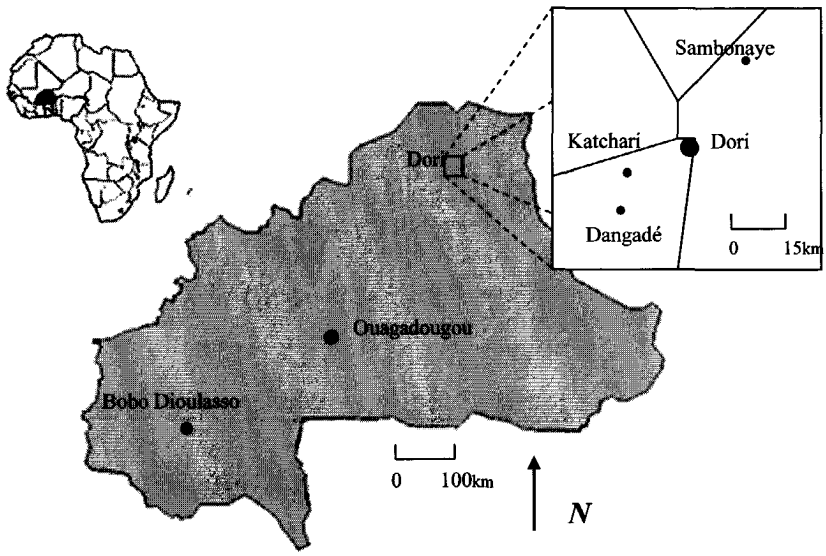

Figure 1. Location of study area of the case study in Burkina Faso (Leenders et al., 2004)

Conservation measures

Despite that wind and water erosion are not felt to be the most urgent problem, the farmers know and apply techniques to reduce their effects (Table 1). Mulching and applying manure, two indigenous techniques were known by all farmers. None of the farmers reported leaving crop residues on their fields as a protection. However, when visiting the fields, it was noticed that most farmers who said they applied mulch, simply left crop residues standing and lying. In approximately 25% of the fields of the farmers who applied mulch it was noticed that they had actively cut and brought branches and/or crop residues to the fields. According to 98% of the farmers, manure fertilizes the soil, prevents wind erosion and stimulates deposition.

Methods newly introduced by agricultural projects - stone rows, sand ridges, zaï and half moons - are not well known by the farmers in the area, except for stone rows. Only 20% of the farmers apply the 'new' techniques of stone rows and sand bunds and 6% of the farmers apply zaï and half moons. The farmers did not regard stone rows and sand ridges as an erosion control, but only as a water conservation measure: they said these measures diminish the velocity of runoff and stimulate infiltration. Zaï and half moons are not direct erosion control measures, but more practices to improve soil fertility. When zaï and/or half moons are applied, plants grow and develop better, and are more resistant to damage caused by soil erosion. The farmers in the study area are not much aware of the effects of these techniques. Tree planting as a control technique was only mentioned by 4% of the farmers.

As farmers apply methods for soil conservation, they are conscious that they can maintain the soil. The farmers, however, feel hampered in applying SWC techniques because of lack of labour and means to implement such measures. Besides, several measures were not applied because of a lack of knowledge (Table 1).

Table 1. Knowledge and application of erosion control measures by farmers in three villages in Northern Burkina Faso (n = 60, in each village 20 farmers were interviewed).

Control measure	In use (%)			Known, Not in use (%)			Unknown (%)		
	D	K	S	D	K	S	D	K	S
Application of manure by hand	30	34	25	3	0	8	0	0	0
Application of manure by grazing animals	24	30	28	10	3	5	0	0	0
Mulching	34	30	33	0	3	0	0	0	0
Stone rows	15	0	0	17	22	22	2	11	11
Sand ridges	2	3	0	0	0	0	32	30	33
Half moons	3	0	0	15	7	0	15	26	34
Zaï	3	0	0	20	8	2	10	25	32
Tree planting	0	0	0	0	2	2	34	31	31

D: Dangadé, K: Katchari, S: Sambonaye.

Table 2. Use of natural vegetation present in farmers' fields in the three villages (based on Leenders et al., 2004).

Use	Total n = 706 %
Fodder (cattle)	30.6
Food (people)	27.8
Erosion control	16.1
Medicinal	10.9
Domestic	9.5
Shade	4.2
Agriculture, general	0.8

n = Number of statements

The role of scattered vegetation on wind erosion

The main function of the parkland system is, according to the respondents in our research area, to supply food, for both cattle and humans. Erosion control was mentioned as the third most important use (Table 2).

The farmers appear to make a distinction between the characteristics of the species that cause high or low deposition and block the wind well, when the vegetation is small or large i.e. at different stage/shape of vegetation growth. Table 3 lists the most frequently mentioned characteristics that affect deposition and the blocking of wind, together with a classification of these reasons in four categories. According to the farmers, the most important characteristics of vegetation that promote deposition and block the wind are shape (32% of the statements), the openness of the vegetation stand (16% of the statements) and the capacity of vegetation to resist the forces of wind (15% of the statements). The arrangement of vegetation in the field was considered to be less important (5% of the statements). These factors, together with height, width and cover are also mentioned in literature as being important for the effect on wind velocity (Marshall, 1970; Musick and Gillette, 1990 and Wolfe and Nickling, 1993).

It appeared that the farmers had a good understanding of the effects of vegetation on wind erosion. Yet, they do not integrate this knowledge into the management of the natural woody vegetation. The application of this knowledge would not require much more labour nor additional means, two important constraints for a farmer to apply SWC measures. Therefore it is thought that scattered vegetation between the crops is a promising wind erosion control strategy.

Table 3. Characteristics of vegetation that cause high or low deposition and block the wind well, according to the 60 farmers (Leenders et al., 2004).

High Deposition (n = 87)	n	Low Deposition (n = 70)	n	Blocking wind (n = 68)	n
Branches fall on ground (R)	27	A single trunk (S)	15	Dense structure (O)	20
Low-hanging branches (S)	16	When species is large (S)	10	When species is small (S)	10
When species is small (S)	15	Open structure (O)	7	Species grows in groups (A)	8
Dense structure (O)	8	Branches do not fall on ground (R)	6	When species is large (S)	6

n = Number of statements. The letters in parenthesis indicates the class in which the reason is reclassified. R = Capacity of vegetation to resist force of the wind; S = shape; A = Arrangement; O = Openness

Case study 2: Using farmers indicators for water erosion assessment in East African Highlands

The East African Highlands constitute more than 76% of the Highland ecosystems of Tropical Africa (Pfeiffer, 1990). Thanks to a favourable climate and fertile soils, these areas have a high potential for crop production, and are very important sources of staple food, forest products and export crops (Lundgren, 1980). However, population densities are generally above 100 persons per km^2. Because of the heavy pressure on the land resources, soil erosion is a widespread phenomenon and a major cause of land degradation (Tiffen et al., 1994).

Soil and Water Conservation projects are active in these areas since the colonial period, experiencing various degrees of success. In the 1980s, a new SWC planning method was introduced by the Government of Kenya, the Catchment Approach (Admassie, 1992; Pretty et al., 1995). The method consists of a participatory community planning process, with actual planning of SWC measures at farm level. Since its introduction, the Catchment Approach gave positive results in the improvement of soil productivity together with reduced resource degradation and is now adopted by six East African Countries (Kamar, 1998; Kizunguto and Shelukindo, 2002). However, a critical review of the method lamented a low rate of SWC adoption and highlighted the lacking of proper tools for soil erosion assessment (Pretty et al., 1995). This case study describes a rapid field tool for qualitative water erosion assessment developed for the East African Highlands conditions using farmers' indicators of erosion.

Material and Methods

Participatory research on field indicators that farmers use to recognize and assess erosion in their fields was conducted on two pilot areas in the East African Highlands, Gikuuri catchment in Kenya and Kwalei catchment in Tanzania. Farmers of both areas listed the indicators they use. Both lists were in agreement with each other and with literature, indicating good potential for the use of these indicators for East African Highlands conditions (Okoba et al., 2003). This consensus list (Table 4) was further exploited to test the usefulness of farmers' indicators for water erosion assessment in Kwalei catchment.

Kwalei catchment (4048'S, 38026'E) is located in the West Usambara Mountains (Tanzania), at an average altitude of 1500 m a.s.l. Mean annual rainfall amount to 1100 mm and is distributed between the long rains season from March to May and the short rains season from September to November. The average temperature ranges between 18 and 23°C with maximum in March and minimum in July. The catchment is intensely inhabited, with a population density of around 412 persons per km^2 (Lyamchai et al., 1998). Over 90% of the catchment population depends on agriculture. The average household land size ranges from 1.2 to 1.6 ha (Tenge et al., 2004). Food crops, mainly maize inter-cropped with banana and beans, are cultivated on the upper slopes. The 2-layer cultivation of banana and coffee is

frequent on the steeper slopes along the stream incisions. Major cash crops are irrigated vegetables that are widespread in the valley bottoms and on the lower slopes. Soil erosion is one of the major constraints to agricultural production in the area (Meliyo et al., 2001), active especially at the on-set of the rainy season, when storms are intense and soil cover poor (Vigiak et al., 2004a).

Table 4. List of farmers' indicators of soil erosion in Kwalei (Tanzania) and Gikuuri (Kenya) catchments with their local names. Symbol √ means that the indicator was mentioned but the local name was not recorded (from Vigiak et al., 2004b).

Indicator	Local names	
	Kwalei (Kiswahili)	Gikuuri (Kiembu)
Soil color change	Udongo mwekundu[#]	Ithetu itune
Absence of topsoil	√	
Soil stoniness	Kokoto	Tumathiga
Rills	Michirizi	Tumivuko
Gullies	Makorongo	Mivuko minene
Sheetwash	Mmonyoko tandazo	Muguo
Bracken fern	Shiuu	
Poor crop development	Mazao ya rangi njano	
Root exposure	√	Kuicirurio tumiri
Washing crop / seeds	√	√
Deposition of soil downslope	Udongo mchanganyiko	Gukunikuo
Change in water colour	Rangi ya maji	√
Patches of bare land	Tambarare	√
Splash pedestals	Matone	Matata
Rock exposure	Mawe	Mathiga
Slope steepness	Mteremko mkali	
Breakage of SWC	Kuvunjka kwa hifadhi	Kuomomoka kwa mitaro
Wind-blown soils		Muthetu muvuthu
White-soft stones	Mashuhee	
Poor seed germination	√	

[#] *Farmers' terms are reported as mentioned, but translated taking into account their practical meanings. For instance, udongo mwekundu literally means 'red soil': in Kwalei soil changes to reddish when topsoil is removed by erosion; with this term farmers therefore refer to soil colour change.*

After the compilation of farmers' indicators consensus list, a combined team of scientists and farmers crossed the study area along two transects walks to get acquainted with what farmers considered as erosion indicator and eroded field. Then, an extensive erosion assessment survey at field scale was conducted with the Assessment of Current Erosion Damage method (ACED; Herweg, 1996). ACED requires observations of presence and intensity or erosion features, and factors causing erosion. The method allows semi-quantification of soil erosion. However, in order to cover the whole catchment, in this study less emphasis was applied in measuring erosion features and the method was applied to assess erosion qualitatively. Fields were classified into 5 qualitative erosion classes, from very low (class 1) to very high (class 5). At the same time, the surveyor annotated type and number of the farmers' indicators observed in the field.

Results and discussion

The survey comprised 336 fields, equally distributed among the five erosion classes. According to the frequency of observations, i.e. the number of fields where an indicator was present divided by the total number of fields, the farmers' indicators

could be classified into 4 groups (Table 5): most frequent (observed in more than 25 % of the fields); frequent (observed on the 15-25 % of the fields), occasional (observed on the 5-15% of the fields) or sparsely occurring, observed on less than 5% of the fields.

The number of farmers' indicators per field increased with erosion intensity: no field belonging to very low or low erosion classes showed more than 4 farmers' indicators at once, whereas more than eight indicators per field occurred only on very eroded fields (class 5, with a maxim of 13 indicators per field). Cases of highly and severely eroded fields where no or few farmers' indicators could be observed also occurred, even though sporadically.

A measure of the strength of a farmers' indicator i in terms of erosion assessment was defined as the empirical probability $p_{i,j}$ that an indicator i occurred in an erosion class equal or larger than j:

$$p_{i,j} = 1 - \frac{\sum_{0}^{j-1} n_{i,j}}{n_i} \qquad \text{[Eq.1]}$$

where $n_{i,j}$ was the number of presence of the indicator i in erosion class j, and n_i was the total number of presences observed for the indicator i. The higher the probability of occurrence in a high erosion class, the stronger was the farmers' indicator in terms of erosion assessment. The probabilities are displayed in table 5. According to our approach, two types of indicators could be defined:

1) Strong indicators; $p_{i,4} \geq 0.70$, i.e. the probability of presence of this indicator in highly or very eroded fields was at least 70 %. Examples are: rills, absence of topsoil, gullies, washing of crop and seeds, and poor seed germination (which could be considered very strong indicators, for their probability $p_{i,4}$ were higher than 0.95); and poor crop development, patches of bare land, soil color change, deposition of soil downslope, rock exposure, and white-soft stones.

2) Weak indicators, $p_{i,4} < 0.70$. Examples are: bracken fern, root exposure, slope steepness, and soil stoniness.

The presence of strong indicators increased monotonically from low to highly eroded fields, whereas weak indicators were more equally distributed among low or moderately eroded fields. Farmers' concept of soil erosion is broader than extension workers and experts usually refer to. Farmers comprehend land degradation and land fertility decline issues when speaking of soil erosion (Murage et al., 2000). Weak indicators probably indicate conditions of soil degradation or soil erosion hazard more than of soil erosion sensu strictu.

Number of indicators and presence of 'strong' erosion indicators were exploited to develop a simple, infield erosion assessment tool in the form of a classification tree. The sample of 336 fields was randomly split in two, one half was used for creating the classification tree; the other for validating it. The data set to build the classification tree comprised ten inputs. The first eight inputs referred to the presence (=1) or absence (=0) of strong indicators. The ninth input indicated the presence (=1) or absence (=0) of any of the sparsely occurring indicators. The tenth input was the number of indicators observed in the field (= sum of the previous entries). The classification tree is shown in Figure 2. The tree consists of a hierarchic sequence of questions: the uppermost question must be answered first, then the next

Table 5. Probabilities $p_{i,j}$ that an indicator i occurred in a field with erosion class equal or higher than j and total number of presences n_i observed per farmers' indicator (Kwalei, Tanzania).

Indicator i		p_{ij} per erosion class j				n_i
		2	3	4	5	
Most frequent	Slope steepness	0.94	0.79	0.60	0.39	126
	Bracken fern	0.94	0.77	0.56	0.35	124
	Withe-soft stones	0.99	0.91	0.72	0.40	92
Frequent	Poor crop development	1.00	0.97	0.87	0.58	67
	Rills	1.00	1.00	0.97	0.86	66
	Soil color change	0.98	0.95	0.79	0.52	66
	Absence of topsoil	1.00	1.00	0.95	0.62	60
Occasional	Patches of bare land	1.00	0.95	0.88	0.59	59
	Root exposure	0.96	0.76	0.60	0.38	45
	Rock exposure	0.95	0.92	0.76	0.58	38
	Deposition soil downslope	1.00	0.97	0.79	0.45	33
	Soil stoniness	0.94	0.84	0.68	0.52	31
Sparsely occurring	Washing crop / seeds	1.00	1.00	1.00	0.78	9
	Poor seed germination	1.00	1.00	1.00	1.00	4
	Gullies	1.00	1.00	1.00	1.00	2

question follows the branch stemming from the previous answer. The presence of rills dominates the classification tree: whenever rills are spotted, the field is classified as subject to very high erosion. This is valid for the Kwalei catchment, where most erosion occurs in the form of interrill erosion, and where rills are not frequent and gullies are rare (Vigiak et al., 2004a). However, it is doubtful whether such rules may be applied in other areas, where other erosion processes can be active. Rill presence is anyway an important feature of erosion assessment survey methods (e.g. Herweg, 1996). The dominant role of rills represents therefore a point of good agreement between farmers and scientific knowledge.

The application of the classification tree to the validation set yielded 49 % of correctly classified fields. Spearman rho correlation coefficient was high (0.81) and significant (at α= 0.01). Most of the misclassified fields were fields classified by the ACED survey as "low" erosion fields, which were mainly identified as "very low". Figure 2 shows that the classification tree never reaches the erosion class "low", i.e. the farmers' indicator classification tree mainly merged the two lower classes and can not discriminate among the two. This agrees with the way farmers perceive erosion in the area: when asked to classify fields into qualitative erosion classes, farmers defined only three classes of erosion (low, moderate or high; Okoba et al., 2003). Misclassifications also occurred among the moderately eroded fields, where 12 of the 41 fields were classified into "high" erosion class. However, the very eroded fields were mainly classified correctly, with only six out of 36 cases misclassified.

We envisage two ways of employing the classification tree of Figure 2 in practice. Extensionists could use it during their field visits to directly assess erosion; or, within the participatory framework of their interventions, they may ask farmers to map the key indicators, and rely on farmers figures to assess erosion over the area. The latter use may offer the advantage that farmers recall the presence of indicators in

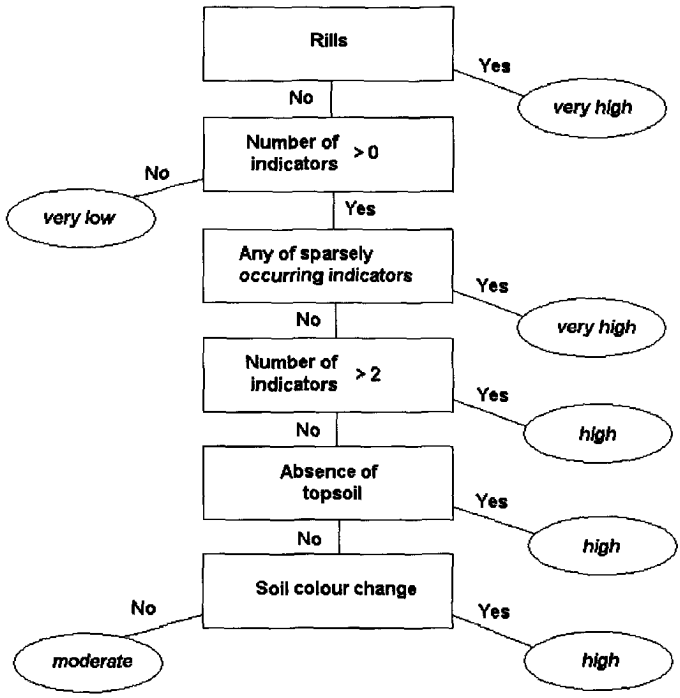

Figure 2. Classification tree for water erosion assessment using farmers' indicators of soil erosion (Sparsely occurring indicator = any of washing away of crops and seeds, poor seed germination or gullies).

their fields even if cultivation has already obliterated them, making the timing of the survey less critical. This may eventually lead to a considerable saving of time, better communication between experts and farmers, and, hopefully, a larger consensus on sustainable SWC activities.

Conclusions

The first case study indicates the possibility to use the knowledge of local farmers to develop a SWC measure that actually fits into the local farming system. It shows that local farmers in the Seno province of Burkina Faso, have insight in and an understanding of the process of wind erosion, that they recognize wind erosion as being a problem and see themselves as actors to prevent the negative agricultural effects of the process. However, due to a lack of knowledge on certain SWC measures and a lack of labour and means to apply the known SWC measures, currently no adequate wind erosion control strategy exists.

In the second case study, farmers' erosion indicators were successfully used to assess water erosion in the East African Highlands. Local knowledge was exploited to assess erosion in a fast and efficient way, and proved to be an important resource, especially valuable where other capital and human resources are limited. In both examples, the combination of the knowledge of farmers and scientists provided

information and insights on the processes and may eventually lead to the development of innovative but acceptable tools for a more sustainable use of land resources.

The two case studies presented here are but two examples of positive co-operations among farmers and scientist working towards a common aim. Crossing the psychological, social and cultural barriers require efforts from both sides. It is difficult to dismiss the skeptical position of the scientist who needs confirmation of how much trust concede to farmers, but it is also true that farmers often look at the newly come scientist with suspicion. Fortunately, awareness of cultural differences is rising among all the practitioners, and techniques are developed that help finding common ground for discussions (e.g. Oudwater and Martin, 2003).

The two examples offered here demonstrate, together with many others (e.g. WinklerPrins and Sandor, 2003) the usefulness of the farmers' knowledge within a scientific framework. In the near future' research and development of SWC measures, steps should be taken to make this co-operation even more fruitful.

References

Admassie, Y. 1992. The Catchment Approach to soil conservation in Kenya. Regional Soil Conservation Unit, Swedish International development Authority: Nairobi

Bielders, C.L., Alvey, S. and Cronyn, N. 2001. Wind erosion: The perspective of grass-roots communities in the Sahel. *Land Degradation & Development* 12: 57 - 70

Drechsel, P. and Penning de Vries, F.W.T. 2001. Land pressure and soil nutrient depletion in sub-saharan Africa. In S. Sombatpanit (Ed.), *Response to Land Degradation*: 507 pp. Science Publishers, Inc

Dregne, H.E. and Chou N.T. 1994. Global desertification dimensions and costs. In H.E. Dregne (Ed.), *Degradation and Restoration of Arid Lands*. Texas Technical University: Lubbock

Ellen R., Harris H. 2000: Introduction. Indigenous knowledge and its transformations: critical anthropological Perspectives, R. Ellen, P. Parkers, and A. Bicker, Eds., Harwood Academic, 1-33.

Fontès, J. and Guinko, S. 1995. Burkina Faso: Carte de la végétation naturelle et de l'occupation du sol - Notice explicative. Institut de la carte internationale de la végétation, Toulouse Cedex

Habarurema, E. and Steiner, K.G. 1997: Soil suitability classification by farmers in southern Rwanda. *Geoderma* 75: 75-87.

Herrweg, K. 1996: Assessment of Current Erosion damage. Centre for Development and Environment Institute of Geography. University of Berne.

Howorth, C. and O'Keefe, P. 1999. Farmers do it better: Local management of change in southern Burkina Faso. *Land Degradation & Development* 10: 93-109

Kamar, M.J. 1998. Soil conservation implementation approaches in Kenya. *Advances in geoecology* 31: 1057-1064

Kiome, R. and Stocking, M. 1995: Rationality of farmers' perception of soil erosion - The effectiveness of soil conservation in semi-arid Kenya. *Global environmental change* 5: 281-295.

Kizunguto, T.M. and Shelukindo, H.B. 2002. Guidelines to mobilize and support community-based Catchment Approach-Watershed management. SECAP: Lushoto

Leenders J.K., Visser S.M., and Stroosnijder L. 2004 Farmers' perceptions of the role of scattered vegetation in wind erosion control in Burkina Faso. *Land Degradation & Development* in press

Lundgren, L. 1980. Comparison of surface runoff and soil loss from runoff plots in the forest and small scale agriculture in the Usambara Mts., Tanzania. *Geografiska Annaler* 62A: 113-148

Lyamchai, C.J., Limo, S.D., Ndondi, R.V., Owenya, M.Z., Ndakidemi, P.A. and Massawe N.F. 1998. Participatory Rural Appraisal in Kwalei catchment, Lushoto district, Tanzania. SARI: Arusha

Marshall, JK. 1970. Assesing the protective role of shrub-dominated rangeland vegetation against soil erosion by wind. Proceedings of the 11th International Grassland Congress: 19-23

Meliyo, J.L., Kabushemera, J.W. and Tenge A.J. 2001: Characterization and mapping soils of Kwalei subcatchment, Lushoto District.

Michels, K., Sivakumar, M.V.K. and Allison, B.E. 1995. Wind erosion control using crop residue I. Effects on soil flux and soil properties. *Field Crops Res.* 40: 101-110

Murage, E.W., Karanja, N.K., Smithson, P.C. and Woomer, P.L. 2000: Diagnostic indicators of soil quality in productive and non-productive small holders' fields of Kenya's Central highlands. *Agriculture, Ecosystems and Environments* 79: 1-8.

Musick, H.B. and Gillette, D.A. 1990. Field evaluation of relationships between a vegetation structural parameter and sheltering against wind erosion. *Land Degradation and Rehabilitation* 2: 87-94

Niemeijer D. and Mazzuccato, V. 2003: Moving beyond indigenous soil taxonomies: local theories of soils for sustainable development. *Geoderma* 111: 403-424.

Okoba, B.O., Tenge, A.J. and Vigiak O. 2003. Farmers' indicators for semi-quantitative erosion assessment in the East African Highlands. In W. Cornelis (Ed.), *25 Years of Assessment of Erosion*: 555. University Gent: Ghent

Oldeman, L.R. 1994. Global extent of soil degradation. In I. Szabolcs (Ed.), *Resilience and Sustainable Land Use*: 99-118: Wallingford, UK: CAB International

Ostberg, W. 1995: Land is coming up. The Burunge of Central Tanzania and their environments. Stockolm studies in social Antropology.

Oudwater, N. and Martin, A. 2003. Methods and issues in exploring local knowledge of soils. *Geoderma* 111: 387-401

Payton, R.W., Barr, J.J.F., Martin, A., Sillitoe, P., Deckers, J.F., Gowing, J.W., Hatibu, N., Naseem, S.B., Tenywa, M. and Zuberi, M.I. 2003: Contrasting approaches to integrating indigenous knowledge about soils and scientific soil survey in East Africa and Bangladesh. *Geoderma* 111: 355-386.

Petit, S. 2003. Parklands with fodder trees: a Fulbe response to environment and social changes. *Applied Geography* 23: 205-225

Pfeiffer, R. 1990. Sustainable agriculture in practice - The production potential and environmental effects of macro-contour lines in West Usambara Mountains, Tanzania. Hohenheim University: *Hohenheim*

Pretty, J.N., Thompson, J., and Kiara, J.K. 1995. Agricultural regeneration in Kenya: the catchment approach to soil and water conservation. Ambio 24: 7-15

Ravnborg, H.M.W.O. and Westerman, O. 2002. Understanding interdependencies: Stakeholder identification and negotiation for collective natural resource management. Agric-syst. Oxford : Elsevier Science Ltd. July 2002. v. 73 (1) p. 41-56.(ISSN: 0308-521X)

Rinaudo,T. 1994. Tailoring wind erosion control methods to farmers' specific needs. In M. Oppen (Ed.), *'Wind Erosion in West Africa: The Problem and its Control'*: 161-171. University of Hohenheim: Germany, 5-7 December 1994

Sterk, G. 2003. Causes, consequences and control of wind erosion in Sahelian Africa: A review. *Land Degradation & Development* 14: 95 - 108

Sterk, G. and Haigis, J. 1998. Farmers' knowledge of wind erosion processes and control methods in Niger. *Land Degradation & Development* 9: 107 - 114

Sterk, G., Hermann, L. and Bationo, A. 1996. Wind-blown nutrient transport and soil productivity changes in southwest Niger. *Land Degradation & Development* 7: 325-335

Tenge, A.J., De Graaff, J. and Hella, J.P. 2004. Social and economic factors for adoption of soil and water conservation in West Usambara highlands, Tanzania. *Land Degradation & Development* 15: 99-114

Tiffen, M., Mortimer, M. and Gichuki ,F. 1994. More people, less erosion: environmental recovery in Kenya. Wiley: Chichester

Van Dissel, S.C. and De Graaff, J. 1998: Differences between farmers and scientists in the perception of soil erosion: South African case study. *Indigenous Knowledge and Development Monitor* 6.

Vigiak, O., Okoba ,B.O., Sterk, G. and Groenenberg, S. 2004a. Modelling of catchment-scale erosion patterns in the East African Highlands. *Earth Surface Processes and Landforms* in press

Vigiak, O., Okoba, B.O., Sterk, G. and Stroosnijder, L. 2004b Water erosion assessment using farmers' indicators inthe West Usambara Mountains, Tanzania *Catena* Submitted

Visser, S.M., Leenders, J.K. and Leeuwis, M. 2003. Farmers' perceptions of erosion by wind and water in northern Burkina Faso. *Land Degradation & Development* 14: 123-132

Warren, A., Osbahr, H.S.B. and Chappell, A. 2003: Indigenous views of soil erosion at Fandou Beri, southwestern Niger. Geoderma 111: 439-456.

WinklerPrins, A.M.G.A. 1999: Local soil knowledge: a tool for sustainable land management. *Society and Natural Resources* 12: 151-161.

WinklerPrins , A.M.G.A. and Sandor J.A. 2003. Local soil knowledge: insights, applications, and challenges. Geoderma 111: 165-170

Wolfe, S.A. and Nickling, W.G. 1993. The protective role of sparse vegetation in wind erosion. *Progress in Physical Geography* 17(1): 50-68

Chapter 12

Measurement Options for Water and Wind Erosion

L. Stroosnijder
Wageningen University, Erosion and Soil & Water Conservation Group, Nieuwe Kanaal 11, 6709 PA Wageningen, e-mail: Leo.Stroosnijder@wur.nl

Measurement Options for Water and Wind Erosion

Abstract
Reasons for erosion measurements are: (1) to determine the environmental impact of erosion and conservation practices, (2) scientific erosion research, (3) development and evaluation of erosion control technology, (4) development of erosion prediction technology and (5) allocation of conservation resources and development of conservation regulations, policies and programs. A handicap for the control of the insidious erosion process is the difficulty of determining its magnitude. Four causes are often mentioned in the literature: the large temporal and spatial variation of erosion, the paucity of accurate erosion measurements, the problem of extrapolating data from small plots to higher scales and the conversion of erosion into production and monetary units (impact). It is an illusion to think that the role of measurements can be taken over by the application of erosion prediction technology. Measurements are needed to develop, calibrate and validate that technology. Measurement techniques differ in accuracy, equipment and personnel cost. The most accurate (and often most expensive) techniques do not always serve the measurement purpose. This paper gives a critical overview of current measurements techniques for erosion at different spatial and temporal scales. Examples are presented of techniques for direct measurements as well as for indirect measurements, i.e. measurements of soil properties that serve as input for models. The paper is concluded with a critical evaluation.

Why measuring erosion?

Reasons for erosion measurements are (Toy *et al.*, 2002): (1) to determine the environmental impact of erosion and conservation practices, (2) scientific erosion research, (3) development and evaluation of erosion control technology, (4) development of erosion prediction technology and (5) allocation of conservation resources and development of conservation regulations, policies and programs.

Assessments are often carried out for the planning of erosion control at the watershed scale (Herweg, 1996; Stocking and Murnaghan, 2001). An erosion inventory often uses a mix of two technologies: direct measurements and the use of erosion prediction technology. Characteristics of measurement techniques for erosion inventory are: (1) they are not so accurate and (2) they are cheap and fast so that many spots (e.g. along transects) can be measured. An erosion inventory gives, at best, insight in the state of erosion. That is the effect that erosion in the past had on the landscape. Inventories hardly give a clue on the rate of erosion, i.e. the erosion processes in a time frame. An observed gully may be formed the previous years but can also be stable for over 100 years. The impact that erosion has on productivity and the environment is another weak point of inventories.

In order to understand the ongoing erosion processes (causes and effects) scientific research is needed. Erosion measurement techniques for scientific research are more accurate and aim at causes and effects of erosion. In erosion cause-effect studies one looks for relationships between erosion processes and variables. When expressed in an equation this implies a dependent variable can be estimated from values of one or more independent variables. Erosion research can be done in a laboratory or in the field. Advantages of erosion measurements in the laboratory are that they allow better control of the range of dependent variables as well as the use of advanced (automated) equipment and the possibility to conduct replicated

measurements. Advantages of research in the field are the possibility to conduct measurements at the proper scale, with realistic soil and plant characteristics and temporal changes in environmental variables.

Measurements are needed for the design of technology as well as for its evaluation. There are two broad categories of erosion control techniques; those applied over the whole surface and those that form barriers at regular intervals. Areal measures prevent the detachment of soil and control erosion at its source. Line interventions, mostly laid along contours, correct symptoms of erosion.

Erosion prediction technologies are condemned to measurements and visa versa. Measurements alone would only provide empirical evidence that is difficult to extrapolate in time and space. Predicting erosion using erosion models needs calibration and validation using measurements. Most erosion measurements nowadays are used for the development, calibration and validation of some form of erosion model.

Erosion can be controlled in many ways: (1) by moral persuasion in combination with regulations (e.g. with respect to land use), (2) by cultural, supporting or structural measures which are expensive or (3) by subsidies and other incentives. Scarce resources should be allocated for maximum results. Proper targeting to hot spots (on-site or off-site) and stakeholders is needed and for this measurements are indispensable.

Erosion indicators are sometimes used instead of direct measurements (Ciesiolka and Rose, 1998). Vigiak *et al.* (2005) distinguish two groups of indicators: strong indicators, which can be observed in more than 70 % of cases in severely eroded fields, and weak indicators, which are observed more frequently in slightly and moderately eroded fields. Strong indicators show current erosion while weak indicators are indicative of other land degradation phenomena, such as fertility decline.

Defining suitable techniques to measure erosion at variable scales is needed. Without this either, much expense, time and equipment will be wasted collecting superfluous data, or insufficient information will be available to draw conclusions (Swete Kelly and Gomez, 1998).

The purpose of this paper is to present a critical review of the most commonly used field measurement techniques. Given the importance to consider different scales a systematic hierarchy is used. No comprehensive review of all available techniques is given in order to remain informative for different kind of researchers and students. Due to this selection the paper reflects the author's own ideas and experiences about the usefulness of measuring erosion and the preferred techniques.

Measurements and scales

There are many different erosion processes. These processes operate at different scales, spatially and temporally. Measurements must be proper to the scale. There are five relevant spatial scales for water erosion: (1) the point (1 m^2) scale for interrill (splash) erosion, (2) the plot (< 100 m^2) for rill erosion, (3) the hillslope (< 500 m) for sediment deposition, (4) the field (< 1 ha) for channels and (5) the small watershed (< 50 ha) for spatial interaction effects.

A fundamental difference between water and wind erosion is that for water the flow direction and the boundaries of the sediment source area known while for wind erosion the sediment source area is not easily known and the wind direction can vary. This makes that in water erosion, at least at the point and plot scale, rate measurements can be used to calculate soil loss. At larger scales where soil loss and

sedimentation occur simultaneously in the considered spatial unit, one can define 'sediment yield' (sediment passing a point in the landscape with known source area) and 'sediment delivery ratio' (sediment yield expressed in t ha^{-1} source area divided by the hillslope soil loss (interrill + rill) in t ha^{-1}).

Due to the difference between water and wind erosion there are only three viable scales for wind erosion measurement: (1) the point (1 m^2) scale for creep, (2) the field (< 1 ha) scale for saltation and (3) the (supra)regional scale for suspension. For both water and wind erosion there are two relevant temporal scales: (1) the single rain- or windstorm for the design (strength) of erosion control technology and (2) the annual average for conservation planning. Different aims require different scales as can be illustrated for water erosion in Table 1.

Table 1. Matrix of scales and aims of water erosion measurements

Aim/ Scale	Assessment	Scientific research	Areal conservation	Line conservation	Prediction technology	Policies
Point		x	x		x	
Plot		x	x		x	
Hillslope	x	x	x	x	x	
Field	x	x	x	x	x	
Watershed	x	x	x	x	x	x

A special discussion deserves the use of remote sensing (RS) for measuring erosion. High resolution RS data (1 m-scale) such as aerial photos are mostly used for the 2000-10000 ha scale while low resolution RS data (15-m scale) are used for areas > 10000 ha. RS can provide direct measurements as well as measurements of inputs for erosion models. Four types of direct observations can be done. The first is visual interpretation of gullies and of eroded surfaces based on deviating spectral properties. A second application is similar to the first but identification is done automatically with for instance the maximum likelihood technique. A third application uses an empirical relation between erosion and reflection. Thereby a relation between vegetation cover and erosion is assumed. The last application uses repeated pass SAR interferometry. This has been successfully applied in semi-arid areas in case of large scale phenomena. This technique still needs further research. Another category of direct applications deals with off-site (downstream) effects, mainly on water quality because with RS the amount of dissolved sediment can be detected.

Most RS studies deal with the measurement of inputs for erosion models like the RUSLE. Land use (cover) is an example. It can be concluded that erosion can only be directly measured with RS under very specific conditions. Extent and development of gullies is in fact the only success story. An extended review of current literature is given by Vrieling (2004).

Direct erosion measurements

A measurement technique consists of the equipment to be used and the procedure to be followed. An advantage of carrying out erosion measurements during natural rain and wind events is that the characteristics of the erosive agents (rain/water/wind) are 'natural'. A disadvantage is that the natural erosive agents are unpredictable (they occur at night or very rarely) and are uncontrolled. For artificial rain (in lab or field) one needs a rainfall simulator that produces rain with the correct: (1) rainfall intensity, (2) raindrop-size distribution, (3) raindrop-impact energy, (4) spatial variability over the plot and (5) temporal variability over the plot. For artificial wind (in lab or field)

one needs a wind tunnel with similar requirements. These can be found in Cornelis (2002) and at www.soilman.ugent.be.
There are four fundamental ways to measure erosion: (1) change in weight, (2) change in surface elevation, (3) change in channel cross section and (4) sediment collection from erosion plots and watersheds.

The point (1 m^2) scale for interrill (splash) water erosion
The 'change in weight' method is best suited for measurements at the point scale. Detachment by rainsplash erosion can be collected (and later weighted) by splash cups and funnels (Morgan, 1995). Precautions to be taken are the prevention of runoff entering the device and the prevention of outsplash from the device.
Interrill erosion can be measured by: (1) trays under a rainfall simulator and (2) small (< 1 m^2) field plots. All sediment from the trays or the plots is collected and weighted after drying.
Interrill erosion is the combination of detachment by splash, entrainment and transport by runoff. After 1-5 m of sheet flow water may concentrate in rivulets due to variations in micro-topography. This may cause detachment by the flow of water. In order to avoid this, the size of plots for measuring interrill erosion is limited.

The point (1 m^2) scale for transport by creep in wind erosion.
Buried bottles (used PET mineral water bottles are ideal) are simple catchers of creep. Given their low cost many bottles can be installed.

The plot (< 100 m^2) scale for rill (+ interrill) water erosion
The 'sediment collection' method is best suited for measurements at the plot scale. Either the total flow with sediment is collected during a limited period of time or only a known fraction of the flow with sediment is collected. For the latter method a variety of 'dividers' exist. Rill erosion can be measured using: (1) long plots (4-10 m), (2) an artificial furrow with rain and (3) the same as 2 with supplementary upstream flow. Precautions need to be taken to measure correctly since rill erosion is the sediment measured at the bottom-end of the rill (furrow) minus the interrill erosion!
When conservation practices that control interrill and rill erosion are evaluated the 'normal' width and length of a plot should be respectively 3 – 25 m and 10 – 25 m and the number of replicated plots should be at least 3 (with the same soil type and slope steepness).

There is always the question whether to bound plots or leave them unbounded. The drawback of bounded plots is that there is no inflow at the top-end of the plot and the drawback of unbounded plot is that the source area from where the runoff and sediment comes from is not known.

The hillslope (< 500 m) scale for erosion and sediment deposition.
The 'change in surface elevation' method is best suited for this scale. Erosion pins are widely used (even by farmers) and can be implanted in the soil; soil removal or sediment deposit can then be determined by frequently measuring the distance from the top of the pin to surface. A decrease in distance corresponds to sedimentation whereas an increase means erosion. This method is used for water as well as for wind erosion or in the case that both processes occur at the same location; the method measures the total effect of wind and water erosion.

The field (< 1 ha) scale for channel (water) erosion.
The 'change in channel cross section' method is best suited for measurement of channel erosion at the field scale. Channel erosion can be measured by measuring cross sections at space intervals, repeating this after some time and comparing and determining the volume disappeared. This can be done either manually or using scanning techniques using laser beams.

The field (< 1 ha) scale for saltation transport in wind erosion.
There are two basis ways to determine saltation. Saltating material can be captured (for later laboratory analysis) or sensed with an electronic device. In wind erosion one should measure the flux (magnitude and direction) at different heights. Since the measured transport cannot be related to the source area single point measurements are not very meaningful. At least 20 points are needed for geostatistical analysis and to be able to determine whether a piece of land looses soil or gains soil due to wind erosion (Sterk and Stein, 1997).

Wind erosion can be collected at various heights with modified Wilson & Cooke (Sterk and Raats, 1996) catchers. For correct measurements the catcher must rotate with changing wind direction and should be isokinetic (i.e. it should not disturb wind flow and hence wind speed; and the pressure inside and outside the orifice must be the same).

Intensity of saltation transport can be detected with electronic sensors like the saltiphone. In a saltiphone the saltating particles hit a microphone by which the impact is detected and stored. Impacts are discriminated from noise and counted and using a calibration the flux is calculated (Spaan and Abeele, 1991).

For all catchers and sensors their trapping efficiency should be known at different wind speeds. For an excellent review of wind erosion measurement techniques, see Zobeck (2002) and Zobeck *et al.* (2003).

The small watershed (< 50 ha) scale for spatial interaction effects of water erosion.
Both the 'sediment collection' and the 'change in surface elevation' method are suited for measurements at watershed scale. Since runoff and sediment volumes are too large to be collected (even after division) runoff from small watersheds is often measured with flumes (Clemmens *et al.*, 2001). Flumes are calibrated devices that can calculate the volume of passing water by measuring the water height. While this runoff with the dissolved sediment passes you can take samples and measure the sediment content of these samples later on.

If there is a dam and reservoir at the outlet of a watershed, this reservoir can be used to determine the erosion rate (averaged over a number of years) by determining the water depth in the reservoir and comparing this with the original depth at the time of construction. The difference is the sediment that has filled the reservoir over the period between two measurements moments.

Soil erosion and sedimentation can also be assessed using environmental radio nuclides as tracers (Zapata, 2002; Faure and Mensing, 2004). This technique is more suitable for natural (geological) erosion studies in landscape ecology and geomorphology than for human induced accelerated erosion. In radio nuclide studies the time scale of interest is usually much longer than in agronomy or environmental studies.

Several radio nuclides in the environment can be used of which Cesium 137 is the most well know (Bai, personal communication). Wide spread global distribution of this radio nuclide stems from the nuclear tests of the 1950s and 1960s. The Cs137

technique is based on the comparison of Cs137 decay activity in the entire soil profile per unit surface area (expressed in Bq m^{-2}) with the activity of an undisturbed plot. For quantitative estimates of rates of erosion and deposition it is necessary to establish a relationship between the magnitude of this deviation and the extent of soil loss or gain. Because empirical calibration data are rarely available, many researchers use theoretical relationships or models to provide for the necessary calibration function. There are a number of drawbacks and limitations: First; all measurements are referred to an 'undisturbed' plot where neither erosion nor deposition has taken place. In some cases (e.g. sacred forest spots, graveyards) these places can be identified but in many cases this condition creates a severe limitation of the technique. This makes the method quite uncertain and inaccurate. Second; the Chernobyl accident in April 1986 has added new fallout to ecosystems around the world. On undisturbed plots this contribution will be added to the reference activity while on eroded soils this new input can be eroded away since 1986. Thirty; the cost of about 200 € per sample for those who have no 'in-house' analytical facilities but have to send samples to specialized laboratories, limits the number of samples that can be analyzed. Finally; Cs is strongly absorbed to the finer soil particles. Erosion is selective (in favor of finer soil particles) but values for texture enrichment are rarely available.

The Cs-method has been applied with variable success in a great number of countries for water erosion, i.e. Turkey (Haciyakupoglu *et al.*, 2003), China (Bai *et al.*, 2002), England (Walling *et al.*, 2003) and in a limited number of countries for wind erosion, i.e. China (Yan Ping and Dong Guang-rong, 2004). For an extended overview of publications see:
http://hydrolab.arsusda.gov/cesium137bib.htm.

The (supra)regional scale for measurement of air- suspended sediment (<100μm).
For measurements of air-suspended sediment two type of equipment are available; passive and active equipment. In passive equipment suspended particles move through a device with the natural wind. In active systems a vacuum pump draws a known volume of air in a known time interval into a device. An example of a passive device is the Vaseline-slide sampler (Cornelis and Hartmann, 1998). Another passive device is a box (or circular pan) full of glass marbles (Riksen *et al.*, 2003). Suspended sediment falls in the holes between the marbles and periodically the material is collected through washing after which it is dried and weighted.

Many types of active equipment exist, in particular for measurement of the hazardous particles < 10 μm (PM10). An extended review is given in Zobeck *et al.*, 2003. Simplest is the collection of dust in some filter material and weighing this on a micro-balance in the laboratory. Obviously this does not provide on-line continuous data. Automatic data are most commonly obtained using β–attenuation (www.lml.rivm.nl).

Measurements for erosion models
A large number of time variant and time-invariant soil properties needs to be determined as input for various erosion models (Table 2). For most of these, standard soil physical methods are available (Dane and Topp, 2001).
A 'flying erosion plot system' was designed for the validation of erosion models (Romero and Stroosnijder, 2002). Flying plots consist of a set of portable low cost materials to delineate and monitor a series of 'Wischmeier' type of plots. With flying plots only a few measurements are used to validate prediction technology. This technology is then used to make predictions over longer time scales. Flying plots can

be re-installed several times during one rainy season for instance to measure the effect of different land cover. This approach is contrary to a traditional plot set-up, which contains a large number of plots and a long duration of measurements to cover sufficient variation in rain shower and is designed to obtain a large data base for regression or index-based prediction.

Table 2. Soil properties needed for each mapping unit as input for the water erosion model WEPP (Alberts, 1995)

TIME VARIANT *for hydraulic model*	TIME VARIANT *for detachment model*	TIME INVARIANT
Random roughness	Interrill erodibility	Organic matter content
Ridge height	Rill erodibility	Clay content
Bulk density	Critical shear stress	Sand content
Effective hydraulic conductivity		Cation exchange capacity (CEC)
		Fraction coarse (> 2 mm) particles

Problems with measurements

Measurements should be frequently taken over sufficient long duration (Lal, 1994). Frequency is the number of times measurements are taken during the measuring campaign and duration is the length of time that measurements are taken. However, since erosion measurements are expensive the duration of measurement and their spatial coverage are often limited. This may cause a bias in the measurements since: (1) there is often large inter-annual variation and large intra-seasonal variation due to different erodibility of the soil, crust formation, vegetation cover, etc. (2) there is large spatial variation: upland erosion sometimes never show up in a stream because of sedimentation or large sediment load in a stream may primarily be due to bank erosion and (3) changing wind may return sediment where it came from in a previous storm.

Equipment used for erosion measurements should be: (1) properly constructed and delivered with a clearly written manual, (2) calibrated, (3) installed, (4) operated, (5) maintained and (6) handled by trained operators. However, most equipment is not available at the commercial market but locally made by researchers (Hudson, 1993). This implies little standardization. In addition, hands-on training in methods and equipment falls short in formal education programs. For erosion equipment a world wide web site should be developed as is available for soil moisture measurement: www.sowacs.com.

Beven (2001) is of the opinion that it is impossible to build a catchment level hydrological (and hence an erosion) model because of the lack of adequate measuring techniques. Instead of trying to improve models he advocates the use of collective intelligence gained from years of laboratory and field experiments in order to develop an approach based on collective induction rather than on deduction.

Conclusion

One may conclude that there is a crisis in erosion measurements because there are insufficient empirical data of adequate quality, there is a lack of funds to improve that situation, there is a lack of development of new technologies and equipment and a lack of skilled personnel. Due to their high data demand and the chronicle lack of good data erosion prediction models often use input data which are estimated or derived from (empirical) pedotransfer functions. Hence, although many erosion models are classified as deterministic they may be called empirical as well.

References

Alberts, E.E. (Editor), 1995. Chapter 7: Soil Component. *Technical documentation WEPP.*

Bai, Z.G., Wan, G.J., Huang, R.G. and Liu, T.S., 2002. A comparison on the accumulation characteristics of Be-7 and CS-137 in lake sediments and surface soils in western Yunnan and central Guizhou, China. *Catena* 49: 253-270.

Beven, K. 2001. On Modeling as Collective Intelligence. *Hydrological Processes* 15: 2205-2207.

Ciesiolka, C.A.A., Rose, C.W., 1998. The measurement of soil erosion. In: Penning de Vries, F., Agus, F.F. and Kerr, J., (Editors), *Soil erosion at multiple scales*. CABI Publishing, New York, U.S.A., pp. 287-302.

Clemmens, A.J., Wahl, T.L. and Bos, M.G., Replogle, J.A., 2001. Water Measurements with Flumes and Weirs. ILRI Publication 58, Wageningen.

Cornelis, W.M., 2002. Erosion processes of dry and wet sediment induced by wind and wind-driven rain: a wind-tunnel study. Ph.D. Thesis Gent University, Belgium.

Cornelis, W.M.and Hartmann, R., 1998. Assessment and control of dust problems, with special reference to industrial sites. Proceedings of the First European Conference and Trade Exposition on Erosion Control, Sitges-Barcelona, Spain.

Dane, J.H. and Topp, G.C., (Editors), 2001. Methods of Soil Analysis. Part 4: Physical Methods. SSSA Book Series: 5.

Faure, G. and Mensing, T.M., 2004. Isotopes: principles and applications; 3rd edition. John Wiley & Sons.

Haciyakupoglu, S., Ahmet Ertek, T., Walling, D., Ozturk, Z.F., Karahan, G., Erginal, A. and Celebi, N., 2003. Interpretation of the erosion effect with Caesium-137 profiles measurements in western side of Istanbul (NW Turkey). In: Gabriels, D., Cornelis, W., (Editors). *25 Years of Assessment of Erosion,* pp 239-240.

Herweg K, 1996. Field manual for the assessment of current erosion damage (ACED). SCRP, Ethiopia.

Hudson, N.W., 1993. Field measurement of soil erosion and runoff. FAO Soils Bulletin 68, Rome, Italy.

Lal, R. 1994. Soil Erosion Research Methods (second edition). SWSC.

Morgan, R.P.C. 1995. Soil Erosion & Conservation (second edition). Longman.

Riksen, M., Brouwer, F. and Graaff, J.de, 2003. Soil conservation policy measures to control wind erosion in northwestern Europe. *Catena* 52: 309-326.

Romero, C.C. and Stroosnijder, L., 2002. A multi-scale approach for erosion impact assessment for ecoregional research in the Andes. Paper IV-0-2 in: Proceedings SAAD-III, Lima, Peru.

Spaan, W.P. and Abeele, G.D. Van de, 1991. Wind born particle measurements with acoustic sensors. *Soil Technology* 4: 51-63.

Sterk, G. and Raats, P.A.C., 1996. Comparison of models describing the vertical distribution of wind-eroded sediment. *Soil Science Society of America Journal* 60: 1914-1919.

Sterk, G. and Stein, A., 1997. Mapping wind-blown mass transport by modeling variability in space and time. *Soil Science Society of America Journal*, 61: 232-239.

Stocking, M.A. and Murnaghan, N., 2001. Field Assessment of Land Degradation. EARTHSCAN.

Swete Kelly, D.E. and Gomez, A.A., 1998. Measuring erosion as a component of sustainability. In: F. Penning de Vries, F., Agus, F., Kerr, J., (Editors), *Soil erosion at multiple scales*. CABI Publishing, New York, U.S.A., pp. 133-148.

Toy, T.J., Foster, G.R. and Renard,K.G.. 2002. Soil Erosion: processes, prediction, measurement and control. Wiley & Sons, USA.

Vigiak, O., Okoba, B.O., Sterk, G. and Stroosnijder, L., 2004. Water erosion assessment using farmers' indicators in the West Usambara Mountains, Tanziania. *Catena,* (submitted)

Vrieling, A., 2004. Satellite remote sensing for water erosion assessment: a review. *Remote Sensing of Environment*, (submitted).

Walling, D.E., He, Q. and Whelan, P.A., 2003. Using 137Cs measurements to validate the application of the AGNPS and ANSWERS erosion and sedimentation yield models in two small Devon catchments. *Soil & Tillage Research* 69: 27-43.

Yan Ping and Dong Guang-rong, 2004. Application of the Caesium-137 technique on wind erosion in the Gonghe basis, Qinghai province. *Acta Pedologica Sinica* 40: 497-503.

Zapata, F. 2002. Handbook for the assessment of soil erosion and sedimentation using environmental radionuclides. Kluwer Academic Press, Boston, USA.

Zobeck, T.M., 2002. Field measurement of wind erosion. In: Lal, R., (Editor), *Encyclopedia of Soil Science*, Marcel Dekker, NY, USA., pp. 503-507

Zobeck, T.M., Sterk, G., Funk, R., Rajot, J.L., Stout, J.E. and Scott van Pelt, R., 2003. Measurements and data analysis methods for field-scale wind erosion studies and model validation. *Earth Surf. Process Landforms* 28: 1163-1188.

Chapter 13

The I.C.E. Wind Tunnel for Wind and Water Interaction Research

W. Cornelis[1], G. Erpul[2] & D. Gabriels[1]
Dept. Soil Management and Soil Care, International Centre for Eremology, Ghent University, Coupure links 653, B-9000 Gent, Belgium; Email: Wim.Cornelis@UGent.be
Department of Soil Science, Faculty of Agriculture, Ankara University, Diskapi, Ankara 06110, Turkey; Email: erpul@agri.ankara.edu.tr

The I.C.E. Wind Tunnel for Wind and Water Interaction Research

Introduction

The measurement and prediction of soil-erosion processes as influenced by wind and water has been of major interest to many research workers all over the world. A large variety of laboratory as well as field devices have been developed for that purpose. Pioneers as Bagnold (1941) in England and Chepil and Zingg (Chepil and Milne, 1939, 1941a, 1941b; Zingg and Chepil, 1950; Zingg, 1953) in the United States developed the first portable field and stationary laboratory wind tunnels for the simulation of physical processes and phenomena related to the study of wind erosion and its control. Pioneer work on the use of rainfall simulators to simulate natural rainfall for many types of water-erosion and hydrologic experiments was done in the USA by Meyer and McCune (Meyer and McCune, 1957, 1958; Meyer, 1958, 1960).

The use of wind tunnels and rainfall simulators for soil-erosion research offers many advantages as compared to field experiments under natural conditions. The main advantage is the better control of the factors that influence soil erosion such as the erosivity (of the wind or the rain), the erodibility of the soil and land-surface properties. The erosivity factors influencing soil erosion by wind include wind velocity, turbulence, wind direction, relative humidity and rainfall, the latter generally being equal to zero in wind-tunnel studies. The erosivity parameters that determine soil erosion by water are raindrop-size distribution, impact velocity of raindrops (and hence rain kinetic energy), rainfall intensity, and wind velocity, where the latter is generally considered or set as equal to zero in rainfall-simulation experiments. The erodibility factors effecting both wind and water erosion include static soil characteristics such as particle size distribution and particle shape, and dynamic soil characteristics including soil-water content, aggregate-size distribution, organic matter, and salt content. Important land-surface properties are roughness, coverage of vegetation and other non-erodible elements, crust formation, and fetch or field length. Another important advantage of wind tunnels and rainfall simulators is the absence of undesirable influences such as shelter effects from buildings or trees, turbulences due to traffic, etc.. As a consequence, wind-tunnel and rainfall-simulator experiments are to a relative high degree well replicable. Furthermore, they allow producing experimental results in relatively short time.

However, one should realise that wind tunnels and rainfall simulators also have their limitations. The cost and time needed to construct wind tunnels and rainfall simulators with related equipment and personnel to operate them is generally relatively high. The area considered in wind-tunnel and rainfall-simulation experiments is often limited compared to the full scale problem. Furthermore, the results obtained in wind tunnels and rainfall simulators can mostly not simply be transferred to field situations and need to be properly interpreted. Notwithstanding this, one of the most important merits of wind tunnels and rainfall simulators is that they allow studying the basic parameters that influence the soil erosion processes induced by wind and water, and that they enable to test whether theoretically derived functional relationships are acceptable. Those functions should always be calibrated and validated under field conditions.

The research on soil erosion conducted under controlled circumstances reported in literature has generally focused on the effects of wind or water separately. However, in nature, strong wind events are often accompanied by heavy rains, and vice versa. In field studies, it has been observed that wind erosion can be induced by raindrop splash (De Ploey, 1980; Jungerius et al., 1981; Jungerius and Dekker, 1990;

de Lima et al., 1992; van Dijk et al., 1996) or that the wind can significantly influence water erosion (Moeyersons, 1983; Moss and Green, 1983; Moss, 1988). There exist only very few facilities that allow the study of the combined effect of wind and water or rain on soil-erosion processes under controlled laboratory conditions. In calculating the raindrop trajectories in the presence of the air flow around buildings, Hangan (1999) used the windtunnel of the Boundary Layer Wind Tunnel Laboratory, University of Western Ontario, Canada. Gabriels et al. (1997) give a brief description of the wind tunnel of the International Centre for Eremomogy, I.C.E.. In the current paper, a detailed description is given of the I.C.E. wind tunnel and its rainfall facility, and the results of a series of tests to determine the different parameters related to its wind and rain erosivity are reported, including respectively vertical and transversal wind-velocity distribution and wind direction on the one hand and the effect of wind on raindrop-size distribution, rain intensity, and rain kinetic energy on the other hand. Special attention is given to the aerodynamic criteria that need to be fulfilled for appropriate research on soil-erosion induced by wind or wind-driven rain.

Description of the I.C.E. wind tunnel

The I.C.E. wind tunnel is a closed-circuit low-speed blowing-type tunnel made of sheet metal (Figure 1 and Figure 2). Air flow is generated by an axial fan, 1.5 m in diameter, with 16 adjustable blades (Fig. 2 A) driven by a 200 h.p. electric motor which is mounted in the fan nacelle. The wind velocity is controlled by adjusting the pitch angle of the blades by means of a compressor. At the entrance of the working area, the minimum free-stream wind velocity hence obtained is 5.6 m s^{-1}. Wind velocity can be reduced by placing obstacles and screens between the fan and the working area.

Fixed air-straightener vanes are placed in front of the fan to remove the swirl induced by the rotation of the blades. Further downstream, the cross section of the wind-tunnel channel changes from a circular into a rectangular shape. The air current is streamlined as it passes through a screen and a 2.6 m long cross-shaped splitter. Corner vanes suppress the generation of large-scale eddies that normally occur at sharp bends.

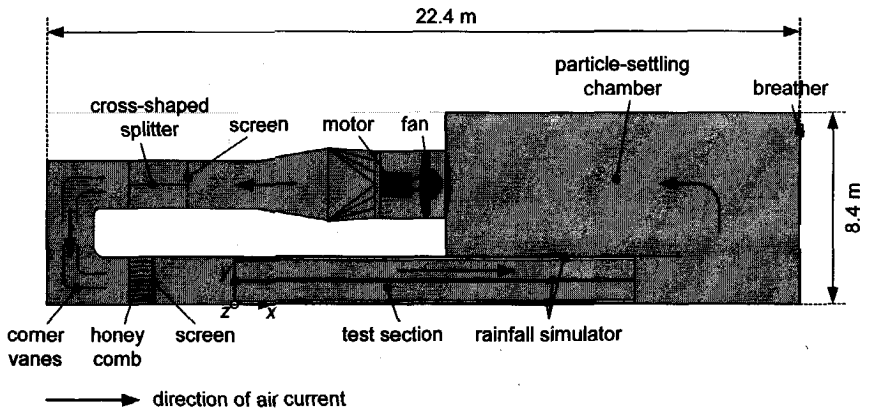

Figure 1. Top view of the closed-circuit low-speed blowing-type wind tunnel of the International Centre for Eremology, Ghent University, Belgium (on scale).

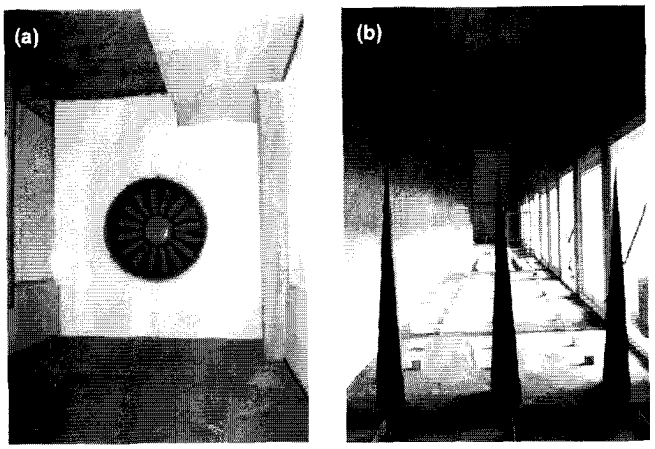

Figure 2. a) The axial fan with 16 adjustable blades and b) cross-sectional view of the test section with an array of spires and roughness elements.

After leaving the bend, the air stream passes through a honey-comb system and a screen, and arrives into a rectangular shaped working area (Figure 2B), 1.2 m wide, 12.0 m long and with the ceiling adjustable in height from 1.8 m to 3.2 m. Doors at the entry and exit of the working area enable to close the working area completely as to serve as a growth chamber.

In the test section, a rainfall-simulation facility is installed. It consists of three parallel pipes, two of which are fixed at the left and right tunnel wall, whereas the other pipe is fixed at the tunnel roof along the centreline of the test section. Nozzles are used rather than drop formers. The advantage of using nozzles is (*i*) the wide range of drop sizes produced, which can be selected by controlling the discharge in function of the nozzle type, and (*ii*) the existence of an initial velocity at the nozzle outlet, which depends on the operating pressure of the water. An appropriate initial raindrop velocity is very important to ensure the drops to reach the soil surface with a fall velocity close to their terminal velocity. Drop size further depends on the overlapping of spray cones, and the wind velocity. Different nozzle types have been tested and a Teejet TG SS 14 W nozzle from Spraying Systems Co[2], Weeton IL, USA, was finally selected as it produces an axial-flow, wide-angle, full spray cone. Water is supplied from a water tank to the pipes and accordingly to the nozzles by a pumping unit. The operating pressure on the water varies from 50 kPa to 1000 kPa.

Downstream of the working area, a particle-settling chamber with a volume of 284 m^3 allows sedimentation of the air load. The particle-settling chamber is vented to the atmosphere by means of a breather in order to prevent drifting of the static pressure in the tunnel.

Aerodynamic criteria for the air flow in test section

According to Raupach and Leys (1990) and Pye and Tsoar (1990), the flow in the test section of a wind tunnel for wind-erosion research should fulfil several criteria:

(*i*) in order to ensure realistic aerodynamic forces on the particles, the flow must reproduce the mean wind-velocity profile in the natural atmosphere, which is

[2] Mention of company names throughout this study is for the convenience of the reader and does not constitute any endorsement in whatever sense from the author.

logarithmic with height, and the surface shear stress must scale correctly with the wind velocity above the surface;

(*ii*) to avoid local scouring by anomalous regions of high surface stress, the flow must be spatially uniform;

(*iii*) to ensure correct modelling of the vertical turbulent dispersion of particles in suspension, the vertical turbulence intensity and scale in the region close to the surface must be realistic.

Further, the dimensionless Reynolds number Re_L for open and closed channels such as wind tunnels must be > 1,400, and the dimensionless Froude number Fr for saltation must be < 20. The Reynolds number for open and closed channels can be defined as:

$$Re_L = \frac{uL}{\nu} \qquad \text{[Eq. 1]}$$

where u is the fluid velocity (m s^{-1}), ν is the kinematic viscosity (m^2 s^{-1}) and L is a characteristic length (m). For circular pipes, L is equal to their diameter, while for square ducts the mean of base Y and height Z $((Y+Z)/2)$ is taken. The Froude number can be given by (Wang et al., 1996):

$$Fr = \frac{u_\delta^2}{Zg} \qquad \text{[Eq. 2]}$$

where u_δ is the free-stream wind velocity (m s^{-1}), δ denotes the boundary layer thickness (m), Z is the height of the wind tunnel (m), and g is the gravitational acceleration (m s^{-2}). These criteria are satisfied if an equilibrium boundary layer is developed in the wind tunnel's test section that is deep enough to contain the particle motion where the mean wind-velocity profile is logarithmic, according to the well-known Prandtl-von Kármán law (Prandtl, 1932):

$$u = \frac{u_*}{\kappa} \ln \frac{z}{z_0} \qquad \text{[Eq. 3]}$$

where u_* is the shear velocity (m s^{-1}), κ is the von-Kármán constant (≈0.4), z is the height above the surface (m) , and z_0 is the aerodynamic roughness length (m).

In order to create such a deep boundary layer, so-called spires and roughness elements can be used. In this study, the vertical and transversal distribution of the wind velocity and the wind direction were determined in the absence and in the presence of such spires and roughness elements. The instruments and methods available only enabled to control if the aforementioned criterion (*i*) and (*ii*), and the criteria concerning the Reynolds number and the Froude number are fulfilled. However, the third criterion (*iii*) could not be checked as the measuring frequency of the available reading unit was 1 Hz only, which is much too low in order to determine velocity variations for turbulence-intensity calculations (Goossens, personal communication).

Vertical wind-velocity profiles and boundary layer thickness

To test whether the flow in the test section satisfies the aforementioned criteria, wind velocity was monitored with 16-mm vane probes mounted at different distances x from the entrance of the test section, at different widths y and at different heights z. These vane probes are used for most wind-velocity measurements in the I.C.E. wind tunnel. By connecting the probes to a digital reading unit, wind velocity was recorded at a frequency of 1 Hz. The reading unit was then connected to a PC for data storage and further processing (Fig. 3). All the probes and the reading unit were from Testo, Lenzkirch, Germany.

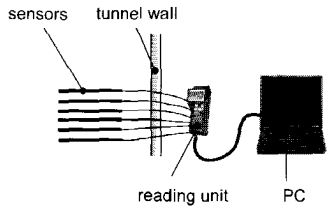

Figure 3. Set-up of the instrumentation used for wind-velocity measurements. A maximum of 6 sensors can be connected to the reading unit.

The measuring principle of the vane probe (Fig. 4) is based on the conversion of rotary motion into electric pulses. The air-flow current moves the vane. An inductive approximation switch 'counts' the rotations of the vane and transmits a series of impulses, which are converted in the digital reading unit and are displayed as a wind-velocity value. The error caused by the bearing friction or static friction at the instant of the measurement is corrected electronically. The measuring range of the vane probes used in this study is 0.4 to 60 m s^{-1} with a resolution of 0.1 m s^{-1} and an accuracy of ±0.2 m s^{-1}. In order to work most accurately, the vane probe has to be placed so that the direction of the flow is parallel to the vane axis (Fig. 4b). By slightly turning the probe in the air flow, the rotational speed of the vane will change, and hence the measured wind velocity value. Turning the probe by 10 degrees results in a mean deviation in the measured value of approximately 0.5%.

Since there exist small differences in measured wind velocity between the different vane probes used in this study, all recorded values were corrected with respect to a reference probe (vane probe No. 3). In Figure 5, the wind velocity as measured with the different probes at x = 6.0 m, y = 0.6 m and z = 0.6 m, is plotted against the wind velocity measured with vane probe No. 3. Linear regressions were drawn through the data. The values of the intercept, slope and R^2 are given in Table 1.

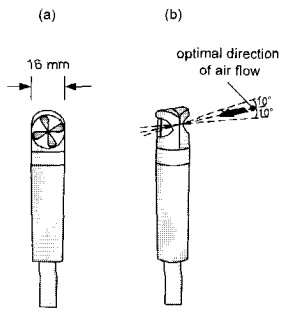

Figure 4 a) Design of the used vane probe and b) optimal position in the air current.

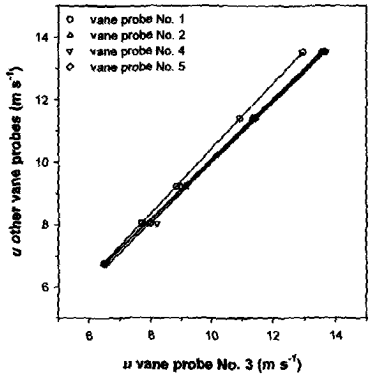

Figure 5. Wind velocity u measured with vane probe No. 3 vs. wind velocity u measured with the other vane probes.

Table 1. Intercept, slope and R^2 of linear regressions of u measured with vane probe No. 3 vs. u measured with the other vane probes.

probe No.	intercept	slope	R^2
1	-0.0177	0.9604	1.000
2	-0.4780	1.0372	1.000
4	-0.3528	1.0378	0.998
5	-0.5857	1.0526	0.999

Further corrections were introduced due to the limited number of sensors available, which was in our case 6. In many cases, it was necessary to conduct wind-velocity measurements in several series (of 6 measurements), but at one and the same reference wind velocity u_{ref}. Because wind velocity is adjusted by blades, obtaining exactly the same reference wind velocity during different experiments is not possible. Corrections are therefore needed to convert actual wind velocities with regards to the reference wind velocity. A vane probe located at $x = 2.0$ m, $y = 0.6$ m and $z = 1.0$ m was used for that purpose, viz. to measure the reference wind velocity. When analysing different series, the measured wind velocity at location i, $u_{i,m}$ (m s^{-1}), is corrected with:

$$u_{i,c} = u_{i,m} \frac{\overline{u}_{ref}}{u_{ref,m}} \qquad \text{[Eq. 4]}$$

where $u_{i,c}$ is the corrected wind velocity at location i (m s^{-1}), $u_{ref,m}$ is the wind velocity measured simultaneously with $u_{i,m}$ with the reference probe (m s^{-1}), and $\overline{u}_{ref}$ is the mean of N measured reference wind velocities, with N the number of series.

In Figure 6, vertical wind-velocity profiles measured at $x = 6.0$ m and $y = 0.6$ m and at different free-stream wind velocities are given for the case that spires and roughness elements were absent. The test section floor was covered with commercial emery paper with a roughness equal to that of dune sand with a mean diameter of 250 μm. The ceiling was set at $z = 2.5$ m. According to Eq. 3, a plot of u against z on a semi-logarithmic scale should produce a straight line with a slope equal to u_*/κ in the inner region of the boundary layer. Figure 6A clearly illustrates that the relation between u and $\ln(z)$ is linear over a height of about 0.16 m. Above this height, u remains constant (and the u-$\ln(z)$ relation is actually linear as well). To check whether

equation 3 is satisfied properly, and is not 'false logarithmic' as defined by Raupach and Leys (1990), the slope u_*/κ should be compared to independently measured u_* values. This can be done directly with a drag plate as was e.g. done by Gillies and Nickling (1999), or indirectly by deducing u_* from $\overline{u' w_v'}$ measurements within the inner region of the boundary layer (e.g. Raupach and Leys, 1990), where u' and w_v' are the fluctuating parts of the longitudinal and vertical (instantaneous) wind velocity, and the overbar denotes the average over time. In the latter case, the Reynolds stress τ_R

$$\tau_R = \sqrt{-\overline{u' w_v'}} \qquad \text{[Eq. 5]}$$

should then be combined with the shear velocity equation:

$$u_* = \sqrt{\frac{\tau_0}{\rho_f}} \qquad \text{[Eq. 6]}$$

where τ_0 is the surface shear stress (N m^{-2}), and ρ_f is the fluid density (kg m^{-3}), in order to compute u_*. Measurement of the wind-velocity fluctuations requires an anemometer with a measuring frequency far beyond 1 Hz (Goossens, personal communication). Raupach and Leys (1990) e.g. used a 5-kHz hot-wire anemometer. If u_* deduced from equation 3 would differ substantially from the u_* value determined from the two other mentioned techniques, the observed straightness of the profile could be misleading and the profile is said to be 'false logarithmic'. However, according to Raupach and Leys (1990), an acceptable logarithmic wind-velocity profile may be expected in tunnels with a rectangular cross-section. Nevertheless, to provide evidence for correct u_* measurements, the (u,z) data pairs were plotted on a log-log scale as an alternative method since the wind-velocity profile is often represented by a power function of following form:

$$u = u_\delta \left(\frac{z}{\delta}\right)^a \qquad \text{[Eq. 7]}$$

where a is a dimensionless coefficient. If the u_* values derived from equation 3 scale correctly, the power in equation 7 should approach 1/7, a typical value for flat and open terrain, and in wind tunnels (Jensen, 1954). The log-log plotted wind-velocity profiles from Figure 6b show that the (u,z) data pairs follow the power law, Eq. 7, very well, with an a value close to 1/7 (or 0.143) (Table 7). Consequently, it can be concluded that u_* scales correctly, and that correct u_* (and z_0) values can be deduced from linear least-square regression of equation 3. The confidence intervals of u_* and z_0 as calculated from different wind profiles above the same surface become narrower if a single value for z_0 is applied (as intercept). This concept was first introduced by Ling and Untersteiner (1974). In Table 2, the shear velocity and the roughness length obtained with the conventional method and with the method of Ling and Untersteiner are given as an illustration. The difference in u_* and z_0 as calculated with both methods is very small. This provides further evidence that the wind-velocity measurements with the vane-probes are reliable. Notice also the very high R^2 values associated with the three approaches to describe the wind-velocity profile. The

roughness length is of the order of magnitude of 4 10^{-5} m. This is slightly higher than the value obtained by using the empirical expression of Nikuradse (1933) for rough surfaces:

$$z_0 = \frac{1}{30} d_{65} \qquad \text{[Eq. 8]}$$

where d_{65} is the particle size (m) for which 65% of the material is finer. The hence calculated z_0 value is 10^{-5} m if d_{65} is 300 μm. Although, strictly speaking, the logarithmic law applies only to areas near the fluid boundary, where Eq. (3) is valid, the results reveal that the wind velocity is logarithmic with height within the complete boundary layer. This was also suggested by Rouse (1959), Carson (1971) and Raupach and Leys (1990).

Also given in Table 2 are the boundary-layer thickness δ and the power a that were obtained by curve-fitting equation 7. The boundary-layer thickness δ can also be calculated by solving Eq. 3 to z with u equal to the free stream wind velocity u_δ (i.e. the wind velocity above the boundary layer or within the zone where u is constant with height). This height corresponds to the intersection between Eq. 3 and $u = u_\delta$. It appears that $\delta \approx 0.16$ m when spires and roughness elements are absent, which is rather low compared to the height of the ceiling.

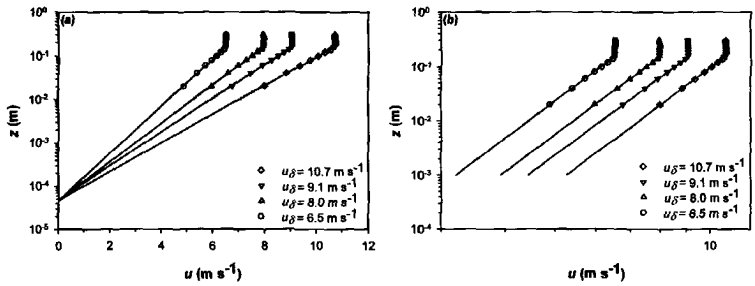

Figure 6. Vertical wind-velocity profiles measured at x = 6.0 m and y = 0.6 m at different free-stream wind velocities u_δ: wind velocity u as a function of height z. The logarithmic law (Eq. (3)) (a) and the power law (Eq. (4)) (b) were fitted to the within-boundary-layer data by linear regression. Note that (a) is on semi-log scale, whereas (b) is on log-log scale. Spires and roughness elements were absent.

Table 2. Shear velocity u_*, roughness length z_0, boundary-layer thickness δ, power a, and R^2 as determined from the conventional method, the method of Ling and Untersteiner (1974) and the power law. Spires and roughness elements were absent.

Method	u_* m s^{-1}	z_0 10^{-6} m	δ m	a -	R^2 -
Conventional log law Eq. 3	0.320	46.0	0.158	-	0.998
	0.392	46.4	0.158	-	0.998
	0.448	49.2	0.157	-	0.999
	0.525	46.6	0.159	-	0.998
Ling and Untersteiner log law Eq. 3	0.317	44.0	0.164	-	0.998
	0.387	44.0	0.165	-	0.998
	0.439	44.0	0.166	-	0.999
	0.519	44.0	0.166	-	0.998
Power law Eq. 7	-	-	0.153	0.140	0.999
	-	-	0.154	0.140	0.999
	-	-	0.153	0.142	1.000
	-	-	0.154	0.141	0.999

In order to determine the development of the boundary-layer thickness δ within the test section, vertical wind-velocity profiles were established along the centreline (y = 0.6 m) at several distances x. The boundary-layer thickness was calculated as described above, by solving Eq. 3 to z at u_δ. The growth of the boundary-layer thickness $\Delta\delta$ can also be estimated with following equation (Irwin, 1981):

$$\Delta\delta = 0.068a\frac{1+2a}{1+a}\Delta x F \qquad \text{[Eq. 9]}$$

where F is a correction factor to take account of the pressure drop in the test section due to the boundary-layer growth. If the pressure drop is not eliminated by adjusting the tunnel roof, then:

$$F = \frac{1}{1+\frac{\delta}{Z}\frac{a(3+2a)}{1+a\left(1-\frac{\delta}{Z}\right)}} \qquad \text{[Eq. 10]}$$

In Figure 7, the boundary-layer thickness δ is given as a function of the distance x from the entrance of the test section. It seems that δ increases slightly and very gradually with x, meaning that the boundary layer is still in development within the test section. Note that equation 9 follows the measured data very well.

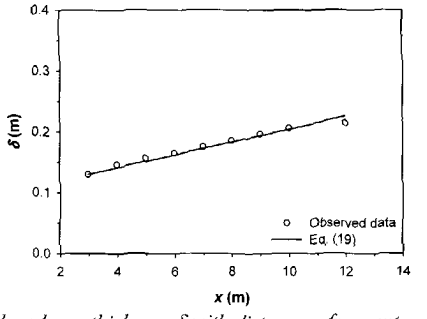

Figure 7. Growth of boundary-layer thickness δ with distance x from entrance of the test section when spires and roughness elements are absent.

Although the flow as described in the previous section obeys the logarithmic law, the surface shear stress scales correctly with the wind velocity above the surface, and the flow is spatially uniform within a confined region, the boundary-layer thickness was relatively low. In order to increase the boundary-layer depth, spires and roughness blocks can be employed and were tested in this study. The use of spire arrays combined with floor roughness was introduced in the late 1960's (Campbell and Standen, 1969; Counihan, 1979) in order to obtain velocity profiles of the correct shape and to produce large-scale turbulence with an intensity that matched planetary boundary-layer data (Irwin, 1981). Nowadays, the technique is widely used and several different shapes of spires are employed. According to Irwin (1981), a spire with a simple triangular front face and a triangular splitter plate on the downwind side

(Fig. 8) works very well. Non-triangular front faces have not been found to have any obvious advantage. Typical floor-roughness elements include cubic blocks (Fig. 8). The size of the spires and roughness blocks to create a given boundary layer can be determined by solving the momentum balance of a rectangular test section, assuming that uniform flow exists upwind of the spire array and that the velocity profile downwind of the array follows the power law, equation 7.

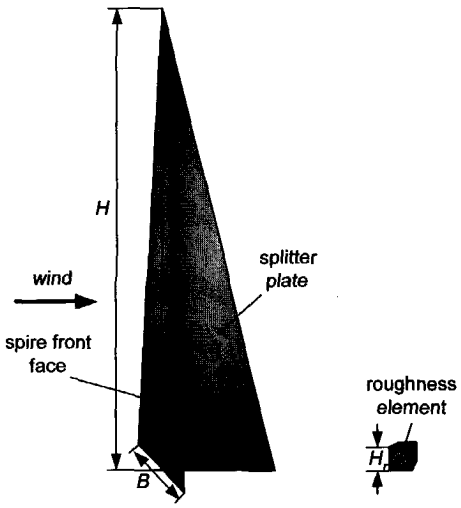

Figure 8. Design of triangular spire with splitter and cubic roughness element (on scale).

The deficit of momentum flux in the boundary layer and the pressure drop along the test section is balanced against the spire drag, including blockage effects, and the drag of the floor roughness. Having chosen the required values of boundary-layer thickness δ (m) and the dimensionless power a in equation 7, the spire height H (m) and spire base B (m) can be calculated empirically (Irwin, 1981):

$$H = \frac{1.39\delta}{1+\frac{a}{2}} \qquad \text{[Eq. 11]}$$

$$B = H\frac{1}{2}\left(\xi\frac{\frac{Z}{\delta}}{1+\xi}\right)\left(1+\frac{a}{2}\right) \qquad \text{[Eq. 12]}$$

where:

$$\xi = \zeta\frac{\frac{2}{1+2a}+\zeta-\frac{1.13a}{(1+a)\left(1+\frac{a}{2}\right)}}{(1-\zeta)^2} \quad \text{and} \quad \zeta = \frac{\delta}{Z}\frac{a}{1+a}.$$

Equations 11 and 12 will produce the required boundary layer at a distance of 6 H downstream of the spire array, which is a sufficient distance to ensure lateral uniformity of the air flow when the spires are laterally spaced with their centrelines at intervals of $H/2$ (Campbell and Standen, 1969; Irwin, 1979). Equation 12 includes the drag coefficient of the spire array based on its frontal area and the effect of a triangular splitter-plate with a base length of $H/4$. Also incorporated in Eq. 12 is the effect of aerodynamic drag of the floor roughness. Although the contribution of the floor friction to the overall momentum deficit in the boundary layer is not dominant within a distance of 6 H downstream of the spire arrays, it cannot be ignored completely. Assuming that the average floor drag per unit area τ_f (N m^{-2}) within 6 H is:

$$\tau_f = \frac{1}{2}\rho_f u_\delta^2 C_f \qquad \text{[Eq. 13]}$$

and with the skin friction coefficient C_f at 6 H (Gartshore, 1973):

$$C_f = 0.136\left(\frac{a}{1+a}\right)^2 \qquad \text{[Eq. 14]}$$

where ρ_f is the fluid density (kg m^{-3}), the term $(-1.13a) / [(1 + a) (1 + a/2)]$ was introduced in the expression for ξ.

The effect of the floor friction is most easily seen in the simplified case where $\delta/Z << 1$, implying the spire blockage effect is negligible. Equation 12 then reduces to:

$$B = H\,\frac{\left(1+\frac{a}{2}\right)a}{(1+a)(1+2a)}\left[1-0.56\frac{a(1+2a)}{(1+a)\left(1+\frac{a}{2}\right)}\right] \qquad \text{[Eq. 15]}$$

where the term $0.56\{a(1 + 2a) / [(1 + a) (1 + a/2)]\}$ represents the effect of floor friction. For $a = 1/7$, the contribution of the floor roughness to the overall momentum deficit is about 8.5%.

To determine the size of the roughness elements that will produce the required value of C_f, the empirical equations of Wooding et al. (1973) can be used. For cubic roughness elements, their height H_r (m) can be calculated as:

$$H_r = \delta \exp\left[\frac{2}{3}\ln\left(\frac{D}{\delta}\right) - 0.116\sqrt{\frac{2}{C_f}+2.05}\right] \qquad \text{[Eq. 16]}$$

where D is the spacing between the roughness elements. Equation 16 is valid in the range $30 < a\,D^2/h^3 < 2000$ (Irwin, 1981). It also allows calculating the spacing between the cubes for given cube heights.

The spires were placed at the entrance of the test section ($x = 0$ m). They were 0.75 m high and 0.10 m wide at the base. The splitter base length was 0.19 m. Height H and width B were calculated by applying Eq. 11 and Eq. 12. The splitter base length

was considered to be $H/4$. With a centreline spacing of $H/2$ and a tunnel width of 1.2 m, the number of spires used was 3, and spire spacing and first-spire distance from the wall was hence 0.37 m and 0.23 m respectively. The values for H and B were calculated for a desired boundary-layer thickness δ of 0.6 m.

Leeward of the spires, wooden cubic roughness elements were placed. Choosing a height H_r = 0.04 m, the spacing of the blocks was calculated from Eq. 16 as 0.36 m, and hence the lateral number of blocks was 3, with the first block at 0.24 m from the tunnel wall. Assuming a length of 6 H in order to create the desired floor drag, the total number of blocks was 36.

As for the case where spires and roughness elements were absent, vertical wind-velocity profiles were measured at x = 6.0 m and y = 0.6 m at different free-stream wind velocities above the same aforementioned emery paper. The test section roof was at z = 2.5 m. It appears that the logarithmic law (Eq. 3) and the power law (Eq. 7) are still applicable with a very close to 1/7 in all three cases. The R^2 values are very high, i.e. > 0.97, when applying the conventional method as well as the Ling and Untersteiner (1974) method to calculate the coefficients of the logarithmic law (Eq. 3) and > 0.99 when applying the power law (Eq. 7). The boundary-layer thickness was 0.61 m, which is almost equal to the postulated value of 0.60 m. This means that the equations used to calculate the spire and roughness-element dimensions and spacing perform very well. Nevertheless, there was a slight tendency for δ to increase with free-stream velocity. The roughness length z_0 deduced from the Ling and Untersteiner (1974) method was ca. 5.9 10^{-5} m. This value is only slightly higher than if no spires and roughness elements were present and hence criterion (*i*) is fulfilled.

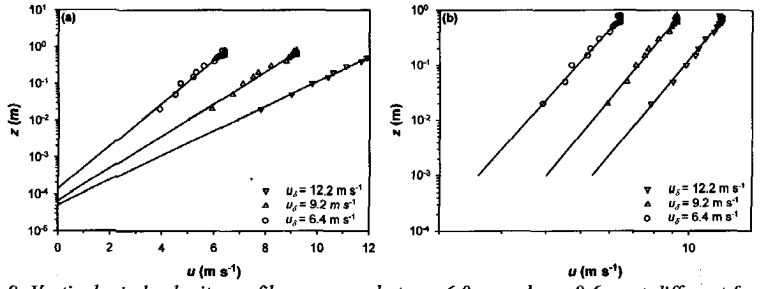

Figure 9. Vertical wind-velocity profiles measured at x = 6.0 m and y = 0.6 m at different free-stream wind velocities u_δ: wind velocity u as a function of height z. The logarithmic law (Eq. (3)) (a) and the power law (Eq. (4)) (b) were fitted to the within-boundary-layer data by linear regression. Note that (a) is on semi-log scale, whereas (b) is on log-log scale. Spires and roughness elements were present.

The growth of the boundary-layer thickness δ with distance from the entrance of the test section is given in Figure 10. A graduate increase in δ with x can be observed over the test section. Equation 9 appears also here to be valid. Since a stable boundary layer can be observed, it can be concluded that a friction floor of length 6 H is sufficiently long.

Transversal wind-velocity profiles

To allocate the regions in the test section where the air flow is uniform along the cross-section of the working area free of spires and roughness elements, transversal wind-velocity profiles were made at x = 6.0 m, which is the distance from the test-section entrance where most of the experiments take place. Wind velocity was measured at intervals of 0.1 m starting from y = 0.05 m from the tunnel wall and floor.

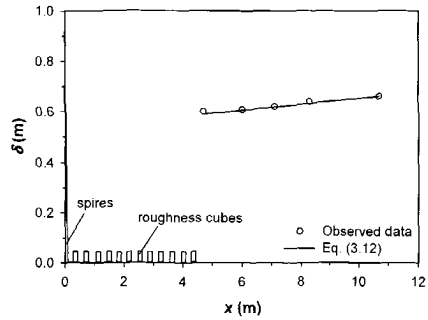

Figure 10. Growth of boundary-layer thickness δ with distance x from entrance of the test section when spires and roughness elements are present.

The floor of the test section was made of plywood (and not covered with emery paper or sand). Figure 11 shows that there is a tendency for the flow to exist in two jets (the dark colours in Figure 9). These jets are fortunately located above the boundary layer and will therefore not influence the experiments as they are supposed to be confined to the boundary layer. Further, the wind-velocity distribution across the test section is asymmetrical with regard to the centreline $y = 0.6$ m. The lowest-located nucleus with high wind velocity is oriented to the right-hand side of the working-area cross section. On the other hand, the lowest wind velocities can be observed at the left-hand side. These effects could be due to some residual axial swirl emanating from secondary flow induced at the 90° corners. However, the presence of the windows with PVC frame at the left-hand side of the cross section will induce an additional friction that will be higher than the friction due the right-hand wall, which is made of sheet metal. This difference in roughness is presumably more important than potential axial swirl. Also apparent are the lower wind velocities above the tunnel floor compared to those over the right-hand wall. Notwithstanding these observations, the wind velocity is uniform within the boundary layer between approximately $y = 0.5$ m and $y = 0.9$ m. This means that the wind-erosion or other experiments should be confined to this zone.

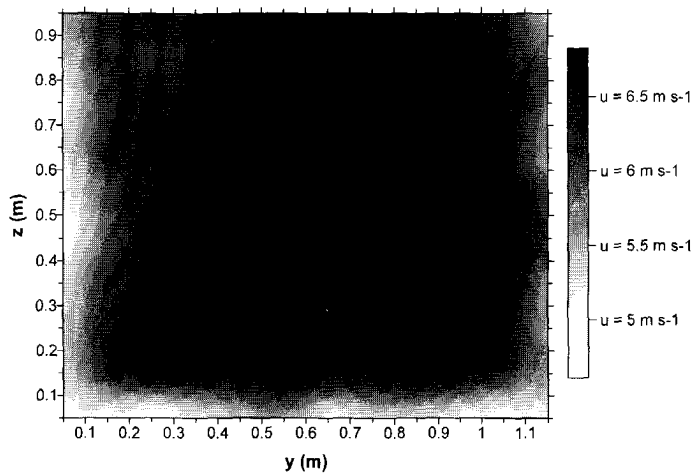

Figure 9. Transversal wind-velocity profiles: wind velocity u (in m s^{-1}) as a function of width y and height z. Wind velocity was measured at x = 6.0 m. The wind direction is towards the reader. Spires and roughness elements were absent.

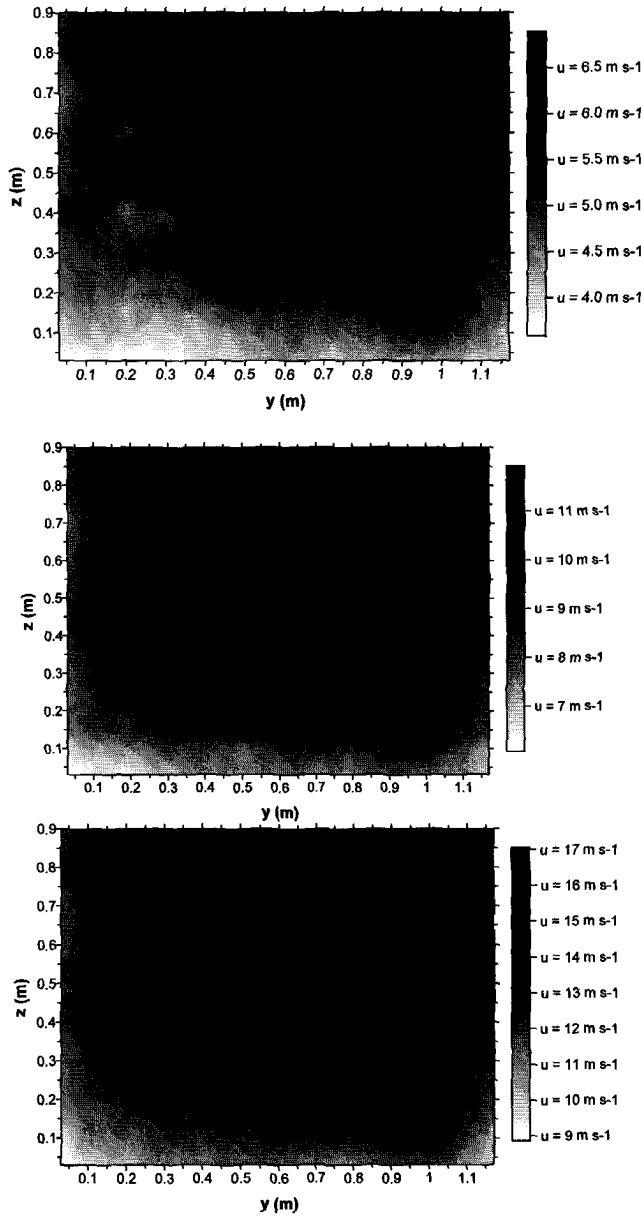

Figure 10. Transversal wind-velocity profiles: wind velocity u (in m s^{-1}) as a function of width y and height z. Wind velocity was measured at x = 6.0 m. The wind direction is towards the reader. Sspires and roughness elements were present. Three different free-stream wind velocities were applied: u_δ = 6.6 m s^{-1} (a), u_δ = 11.6 m s^{-1} (b), u_δ = 16.6 m s^{-1} (c).

As was done for the no-spire case, transversal wind-velocity profiles were made at x = 6.0 m in the presence of spires and roughness elements. Wind velocity was measured at intervals of 0.1 m starting from y = 0.03 m from the tunnel wall and floor. These measurements were carried out at three different free-stream wind velocities. The tunnel floor was more or less smooth (no emery paper or sand). Figure 12 shows that the wind velocity distribution across the test section is still asymmetrical with respect to the centreline y = 0.6 m. However, the distribution is more uniform than if no spires and cubes were present, and the number of jets is reduced to one. The nucleus with the highest wind velocity is situated above the boundary layer between y = 0.65 m and y = 0.90 m. The lowest wind velocities occur just above the test section's floor. The presence of the windows at the left-hand side is still apparent. However, their effect on the flow pattern diminishes with increasing free-stream wind velocity. The effect of the drag which is due to increased floor roughness within 6 H can be well observed: the difference in wind velocity measured above the tunnel floor and measured close to the side walls is more pronounced compared to the case where spires and cubes were absent. Most important is, however, that within the boundary layer the wind velocity is uniform between approximately y = 0.4 m and y = 1.0 m. This zone even extends far beyond the boundary-layer height.

Wind direction

To asses the direction of the flow, the tuft method was used (Bradshaw, 1970). Woollen wires, 20 cm in length, were tied on nails that were driven in the tunnel's false wooden floor. Several tests were done with wires of different length in order to see their flag-waving effect, as described by Pope and Harper (1966). Flag waving was observed only once the wire length exceeded 25 cm. The tunnel floor was covered with mm paper, in order to read the deviation of the wind direction from being parallel with the tunnel walls. The readings on the mm paper were done only after the wind tunnel motor was turned off, in order not to disturb the air current. A test run lasted for 1 minute and was repeated trice.

In Figure 11, the wind direction measured near the test section floor (z = 0 m) is given at several locations. Wind direction is parallel to the side walls between y = 0.2 m and y = 0.9 m, except for the last 3 m of the test section, where parallel air flow only occurs between y = 0.2 m and y = 0.8 m. At the left-hand side of the test section, the air flow deviates from being parallel by 5°, whereas the deviation at the right-hand side is only 2°. The wind direction was also determined at z = 0.2 m and 0.5 m, both at x = 6 m. There, the air current was found to be parallel over the complete width of the test section. These findings are important in that they enable to allocate the regions where the wind-tunnel experiments should be executed, i.e. in the zone where the air current is parallel to side walls of the test section. In combination with Figure 6 and Figure 9, it can be concluded that this zone should be confined to 0.0 m $\leq x \leq$ 12.0 m, 0.5 m $\leq y \leq$ 0.9 m and 0.0 m $\leq z \leq$ 0.2 m.

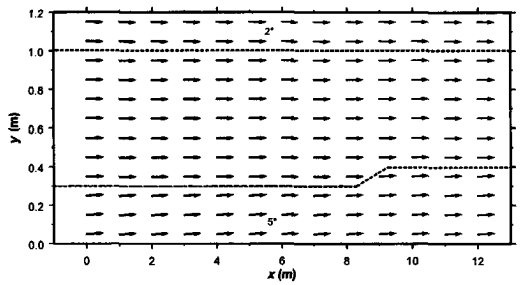

Figure 11. Wind direction along the test section as a function of distance x and width y, and at height z = 0 m. Wind direction is in ° respective to the tunnel wall and is equal to 0° in the area delineated by the dotted lines. Note that the angle of the vectors is not on scale. Spires and roughness elements were absent.

Figure 12 shows the wind direction near the test section floor (z = 0 m) as measured in the presence of spires and roughness elements. The zone where the air current is parallel with the side walls is still wide enough for proper experiments. The deviation at the right hand side is somewhat higher compared to the no-spires case. The measurements were carried out at different free-stream wind velocities, but this did not have a significant influence on the wind direction. The flow appears to be parallel with the side wall for 0.35 m $\leq y \leq$ 0.95 m. Combining now these observation with the conclusions drawn from Figure 9 and Figure 11, the region for correct measurements is confined to 5.0 m $\leq x \leq$ 12.0 m, 0.4 m $\leq y \leq$ 0.9 m, and 0.0 m $\leq z \leq$ 0.6 m.

Reynolds number and Froude number

As was outlined above, the flow properties can be quantified by means of the Reynolds number Re_L and Froude number Fr. For the flow to be fully turbulent or Re_L > 1400, the wind velocity u should exceed 1.38 10^{-2} m s^{-1} if the tunnel ceiling is at 1.8 m and 0.93 10^{-2} m s^{-1} if it is at 3.2 m (Eq. 1). If the free-stream wind velocity is 5.6 m s^{-1}, which is the minimum wind velocity that can be generated, the above velocities occur at a height z of 6.0 10^{-5} m and 5.9 10^{-5} m respectively if spires are employed. If the latter are not present, these heights become 4.1 10^{-5} m at both ceiling heights. Since all these heights are only within 1 10^{-5} m above the surface, flow can be considered as fully turbulent over the entire test section.

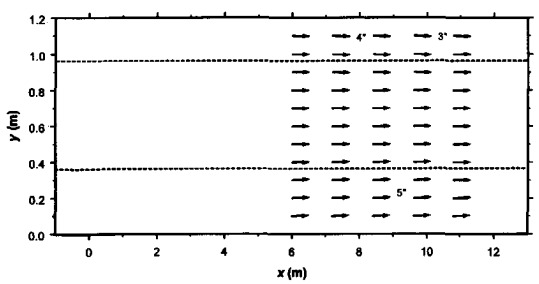

Figure 12. Wind direction along the test section as a function of distance x and width y, and at height z = 0 m. Wind direction is in ° respective to the tunnel wall and is equal to 0° in the area delineated by the dotted lines. Note that the angle of the vectors is not on scale Spires and roughness elements were present.

With regards to the Froude number for correct saltation, the wind velocity should not exceed 18.8 m s^{-1} if the tunnel ceiling is at 1.8 m and 25.1 m s^{-1} if it as at 3.2 m (Eq. 2). Since such velocities are above the operating wind velocities of the I.C.E. wind tunnel, the criterion for the Froude number will always be fulfilled as well. This is mainly attributed to the great height of the working section.

Raindrop Size Distribution

The drop size distribution was determined by the stain method (Hall, 1970). An absorbent paper was coloured with 1 M $CuSO_4$ and dried in order to obtain permanent stains after raindrop hits. Dyed absorbent paper was exposed to the simulated rainfall in the wind tunnel for such a short time that several drops were prevented from falling at the same spot. After formed, the light blue stains were carefully marked, measured and counted. To obtain equivalence between the size of drops and that of the stains, drops of known size were allowed to fall on the dyed absorbent paper, and the size of the resultant stains was determined. Hypothermic needles produced drops of known size and changing the fall height changed the vertical fall velocity of the drops. Laws nomograph (Laws, 1941) was used to determine the fall velocity.

Cumulative volume percentage of the drop size distributions for the simulated rainfall without wind and the wind-driven rains at different operating pressures are shown in Table 3 and Figure 13.

Data of Table 3 were also fitted to the logistic growth model to assess the drop size distributions ($R^2 \geq 0.99$):

$$N(d) = \frac{100}{1 + e^{-\beta d - \gamma}} \qquad \text{[Eq.17]}$$

where, $N(d)$ is the cumulative percentage of a given drop size by volume, d is drop diameter (mm), and β and γ are parameters of the logistic growth model.

Table 3. Cumulative volume percentage of the drop sizes at different operating pressures for windless rains and the rains driven by 6, 10, and 14 m s^{-1} wind.

d (mm)	0 m s^{-1}			6 m s^{-1}			10 m s^{-1}			14 m s^{-1}		
	P (kPa)											
	75	100	150	75	100	150	75	100	150	75	100	150
0.2	0.10	0.14	0.42	0.01	0.01	0.01	0.01	0.01	0.01	0.02	0.01	0.01
0.6	8.51	7.34	10.18	1.47	0.49	1.20	0.87	0.75	1.12	1.72	1.66	1.22
1.0	38.53	27.77	49.62	14.58	12.51	17.85	13.15	11.25	14.47	12.78	14.57	13.38
1.4	65.98	55.20	85.36	29.73	34.98	40.58	34.09	29.50	35.62	28.79	36.01	38.71
1.8	94.08	86.18	100.00	64.60	72.14	60.71	65.29	65.17	78.24	68.19	74.38	68.48
2.2	100.00	100.00	100.00	87.87	83.77	76.33	82.10	79.33	89.27	91.90	92.77	90.05
2.6	100.00	100.00	100.00	100.00	90.17	93.01	92.89	100.00	95.33	100.00	100.00	97.97
3.0	100.00	100.00	100.00	100.00	100.00	100.00	100.00	100.00	100.00	100.00	100.00	100.00

d: drop diameter; P: nozzle operating pressure

From Equation 17 calculated are d_{25}, d_{50}, and d_{75}, drop diameters of which 25, 50, and 75% of the simulated rainfall is smaller, respectively:

$$d_{25} = -\left(\frac{\ln(3) + \gamma}{\beta}\right) \qquad \text{[Eq. 18]}$$

$$d_{50} = -\left(\frac{\gamma}{\beta}\right) \qquad \text{[Eq. 19]}$$

$$d_{75} = -\left(\frac{\ln\left(\frac{1}{3}\right) + \gamma}{\beta}\right) \qquad \text{[Eq. 20]}$$

The 'spreading coefficient', (d_{75}/d_{25}), and the 'sorting coefficient', $[(d_{75} - d_{25})/d_{50}]$, were derived from equations 18, 19 and 20. Raindrop characteristics of windless rains and the rains driven by 6, 10, and 14 m s^{-1} wind, evaluated by d_{25}, d_{50} and d_{75}, and spreading and sorting coefficients, are given in Table 4.

It can be easily observed from Table 4 that the simulated rains in the wind tunnel consist of rather small drops, which range from 0.2 to 2.2 mm in diameter for rains without wind and up to 3 mm in diameter for wind-driven rains. Without wind, the rains have rather low d_{50} ranging between 1.01 and 1.31 mm (Table 4). The corresponding d_{25} and d_{75} also have the lowest values, which change from 0.79 to 1.00 mm and from 1.23 to 1.61 mm, respectively. However, 'spreading' and 'sorting' coefficients tend to be greater in the windless rains: mostly, there is a wider range between the interval during which distribution progressed from 25% to 75% of the limit 100% in the windless rains than in the wind-driven rains. When horizontal wind velocities are introduced, it was clear that a variation in raindrop characteristics occurs. At all wind velocities, the d_{25}, d_{50}, and d_{75} increase compared to the windless rains. This can be ascribed to the formation of larger drops since collisions between small drops happen more frequently as a result of their greater number per unit volume of air. This accordingly results in an increase in the median drop size.

There is, on the other hand, no significant difference in the median drop sizes for the different wind velocities, only ranged between 1.52 and 1.67 mm (Table 4). The lower 'spreading' and 'sorting' coefficients for wind-driven rains show that the raindrop size distributions have a narrow range around d_{50}, and accordingly that d_{50} can be used as a representative raindrop characteristic.

Evaluation of the drop size distribution of the simulated rains in the I. C. E. wind tunnel indicates that wind has a significant effect on raindrop size characteristics. The erosivity of wind-driven rain might differ from that of rain without wind depending on the size distribution. However, these results are limited to the drop size distributions observed and valid for the conditions existing in the tunnel. Indeed, the effects of wind on large drop sizes would not be as great as its effects on small drops. Large drops are less stable, and wind may cause some of them to break up into smaller drops. Consequently, disintegration of large drops depending on wind may actually lead to a reduction in drop size.

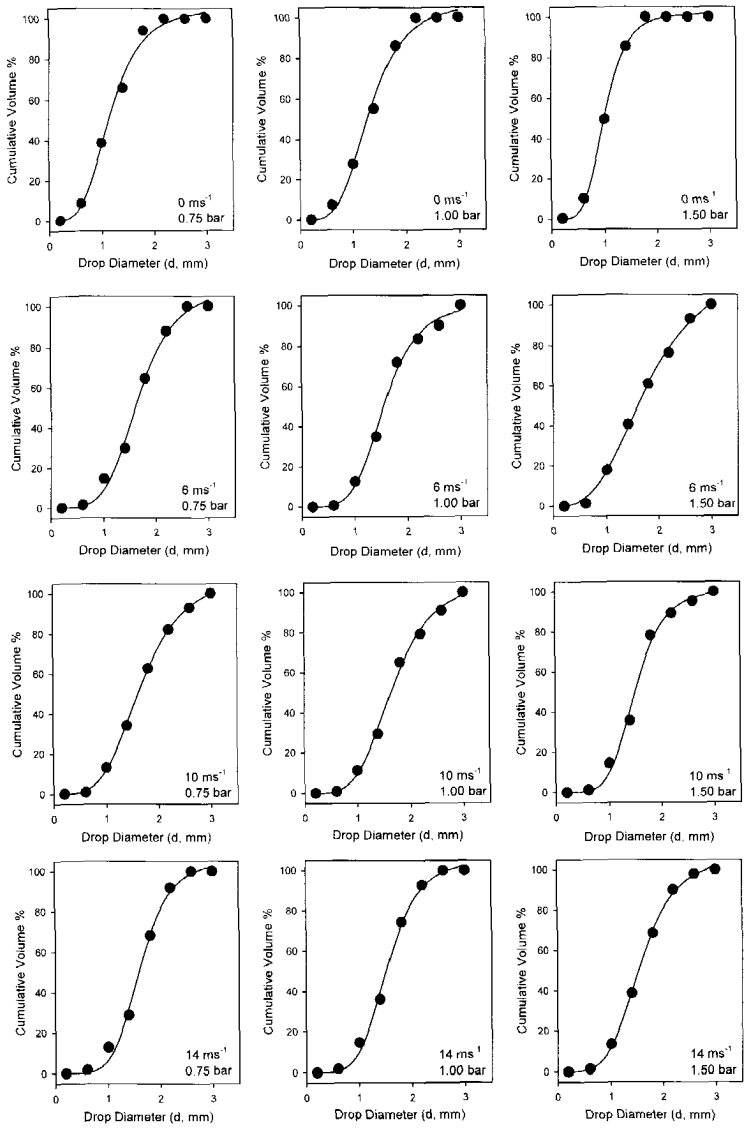

Figure 13. Cumulative volume percentage of drop sizes for windless rains and the rains driven by 6, 10, and 14 m s^{-1} wind velocities at 75, 100, and 150 kPa operating pressures.

Table 4. Raindrop characteristics of windless rains and the rains driven by 6, 10, and 14 m s^{-1} wind evaluated by d_{25}, d_{50} and d_{75}, and spreading and sorting coefficients.

u ($m\ s^{-1}$)	P (kPa)	β	CI_β Lower	CI_β Upper	γ	CI_γ Lower	CI_γ Upper	d_{25}	d_{50}	d_{75}	(d_{75}/d_{25})*	$[(d_{75}-d_{25})/d_{50}]$**
	75	3.74	3.00	4.48	- 4.38	- 5.27	- 3.48	0.88	1.17	1.46	1.66	0.50
0	100	3.58	3.02	4.14	- 4.68	- 5.44	- 3.92	1.00	1.31	1.61	1.61	0.47
	150	5.00	4.45	5.56	- 5.07	- 5.64	- 4.49	0.79	1.01	1.23	1.56	0.44
	75	3.45	2.93	3.97	- 5.60	- 6.45	- 4.74	1.30	1.62	1.94	1.49	0.40
6	100	3.23	2.44	4.03	- 5.11	- 6.39	- 3.82	1.24	1.58	1.92	1.55	0.43
	150	2.51	1.98	3.04	- 4.08	- 4.97	- 3.19	1.19	1.63	2.06	1.73	0.53
	75	2.95	2.60	3.30	- 4.83	- 5.42	- 4.24	1.27	1.64	2.01	1.58	0.45
10	100	3. 02	2.42	3.63	- 5.03	- 6.06	- 4.00	1.30	1.67	2.03	1.56	0.44
	150	3.81	3.04	4.58	- 5.80	- 6.99	- 4.61	1.23	1.52	1.81	1.47	0.38
	75	3.89	3.35	4.43	- 6.25	- 7.14	-5.36	1.32	1.61	1.89	1.43	0.35
14	100	3.81	3.40	4.23	- 5.84	- 6.48	- 5.19	1.24	1.53	1.82	1.47	0.38
	150	3.40	3.10	3.70	- 5.28	- 5.76	- 4.80	1.23	1.55	1.88	1.53	0.42

u: reference horizontal wind velocity; P: nozzle operating pressure; β and γ: parameters of the logistic growth model fitted to cumulative volume percentage of drop size distribution; CI_β and CI_γ: 95% confidence interval on β and γ, respectively; d_{25}, d_{50}, and d_{75}: drop diameter of which 25, 50, and 75% of the simulated rainfall by volume is smaller, respectively.

** spreading coefficient; ** sorting coefficient*

Rain Intensity

The number of raindrops varies with the rain amount and drop size distribution. The number is a significant rainfall characteristic, which distinguishes the rain from the same amount of water (Park et al., 1983). The number of raindrops Ξ per unit sampling area A and time t can be calculated from the rainfall intensity I (Kinnell, 1981):

$$I = \left[\sum_{i=1}^{n} \forall_i \Xi_i\right] A^{-1} t^{-1} \qquad \text{[Eq. 21]}$$

where I is the rainfall intensity with respect to a plane normal to the rain vector ($m^3\ m^{-2}\ s^{-1}$), and $\forall_i$ is the volume of the raindrop of diameter i (m^3). In fact, Eq.21 gives the rate of impact per unit area per unit time impacting the horizontal surface provided the raindrops travel along a straight-line trajectory. However, in wind-driven rains, raindrops are deviated from vertical and strike a surface with an angle because of their horizontal and vertical velocities. On sloped surfaces, the intensity will be greatest when rain falls normal to the surface, whereas, it decreases to zero when rain falls parallel to it (Struzer, 1972). Therefore, the frequency of wind-driven raindrops on a sloping surface differs depending on the free stream wind-velocity and the direction and raindrop size. Accordingly, there is a need to specify the angle of incidence of each raindrop, which is a function of raindrop inclination, slope aspect and degree. The resultant angle of incidence between the wind vector and the plane of the surface is measured from the normal to the plane of incidence (Figure.) and given by the cosine law of spherical trigonometry (Sellers, 1965; Sharon, 1980):

$$\cos(\alpha \mp \theta) = \cos\alpha\cos\theta \pm \sin\alpha\sin\theta\cos(z_\alpha \mp z_\theta) \qquad \text{[Eq. 22]}$$

where α is the raindrop inclination from vertical, θ is the slope degree, z_α is the azimuth from which rain is falling, and z_θ is the azimuth towards which the plane of surface is inclined (the slope aspect). In the second term of equation 22, the positive sign indicates the windward-facing slope and the negative sign corresponds to the

leeward-facing slope, implying the raindrop impact deficit with the same values of the slope degree and the raindrop inclination. In order to include the effect of the angle of incidence on the rain intensity, the impact efficiency ϕ can be defined by:

$$\phi = \frac{I_a}{I} = \frac{\Xi_a}{\Xi} = \cos(\alpha \mp \theta) \qquad \text{[Eq. 23]}$$

where I_a and Ξ_a are, respectively, the actual intensity intercepted by a sloping surface and number of raindrops actually arriving at the surface under wind-driven rain. Equation 23 indicates that the actual number of raindrops arriving at the surface varies with the raindrop inclination, slope degree and aspect.

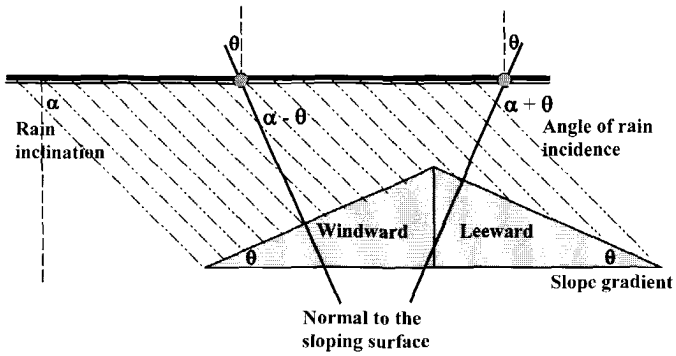

Windward:

$$\cos(\alpha - \theta) = \cos\alpha\cos\theta + \sin\alpha\sin\theta$$

Leeward:

$$\cos(\alpha + \theta) = \cos\alpha\cos\theta - \sin\alpha\sin\theta$$

Figure.12. Angle of raindrop incidence measured from the normal to the plane of incidence.

The spatial distribution of the rain intensity in the wind tunnel was measured with small collectors (rain gauges), 11 cm in diameter and 13.5 cm in depth (and a hence collecting surface of 95.03 cm^2). 240 collectors, placed in the specified surface, were exposed to 15 min of rain on the horizontal plane. The spatial distribution of the rain intensity was obtained by mapping the pattern of iso-lines and locating the most available working area in the tunnel (Fig. 13), and the uniformity coefficients *Cv* representative of the described areas were determined.

The correction factor is defined by $F_c = I_a / I_o$ and from Eq. 22 and 25, F_c is given by:

$$F_c = 1 \mp \tan\alpha \tan\theta \qquad \text{[Eq. 26]}$$

Calculated corrections factors by equation 26 are given in Table 5, and the calculated wind-driven rain intensity from I_o is given by:

$$I_{cal} = I_o F_c \qquad \text{[Eq. 27]}$$

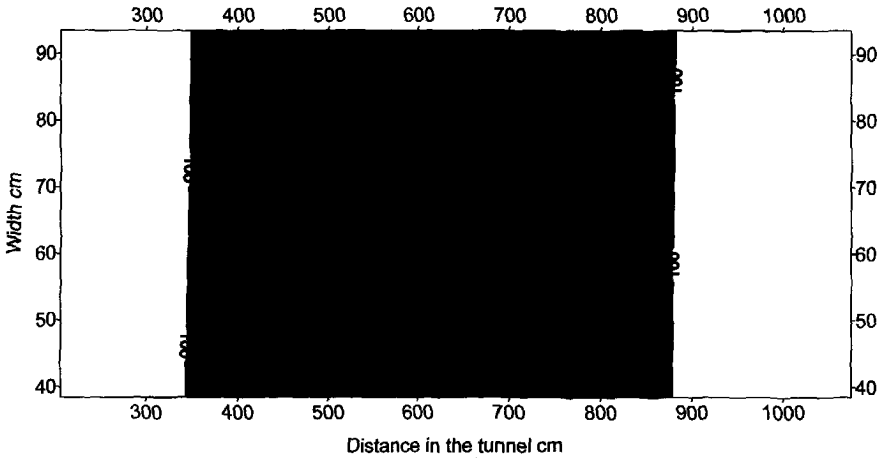

Figure 12. The iso-intensity lines to locate the working area (rectangle), which was the basis for the calculations of Cv and the determination of the drop size distribution in the wind tunnel.

where I_{cal} is the calculated wind-driven rain intensity, which is actual amount incident on the inclined surface with respect to the prevailing wind direction (mm h^{-1}).

Measured windless and wind-driven rain intensities on the horizontal plane equation 24 are reported in Table 6.The calculated wind-driven rain intensities by equation 27 for windward and leeward slopes of 7, 15, and 20% (4, 8.53, and 11.31°, respectively) are shown in Table 7.

Table 5. Calculated correction factors using rain inclination, slope gradient, and slope aspect.

u ($m\ s^{-1}$)	α (°)	θ (°)	$F_c = 1 + \tan\alpha \tan\theta$ for windward
		4.00	1.09
6	53.0 ± 11.5*	8.53	1.20
		11.31	1.27
		4.00	1.17
10	68.2 ± 7.6	8.53	1.37
		11.31	1.50
		4.00	1.24
14	73.5 ± 6.6	8.53	1.51
		11.31	1.68
u ($m\ s^{-1}$)	α (°)	θ (°)	$F_c = 1 - \tan\alpha \tan\theta$ for leeward
		4.00	0.91
6	53.0 ± 11.5	8.53	0.80
		11.31	0.73
		4.00	0.83
10	68.2 ± 7.6	8.53	0.63
		11.31	0.50
		4.00	0.76
14	73.5 ± 6.6	8.53	0.49
		11.31	0.32

u: reference horizontal wind velocity; α: rain inclination from vertical (the angle of rain inclination was approximately 53, 68, and 74° for the wind-driven rain with 6, 10, and 14 ms^{-1}, respectively, Erpul et al., 2003); θ: slope gradient; F_c: correction factor;

**Standard deviation of the average rainfall inclination is given next to the mean value with ± sign.*

Table 6 shows that the rain intensity varies widely with wind velocity and direction, leading to different rain fluxes on different facing and sloping surfaces. The rain intensities calculated for the windward slopes were significantly greater than those for leeward slopes. Particularly, differences in the rain intensity between aspects were extremely large for the rains driven by 10 and 14 m s^{-1} wind and incident on 15 and 20% slopes. This examination indicates that different rainsplash rates and different erosion processes can be anticipated to take place in windward and leeward slopes during a wind-driven rainstorm. For instance, when overland flow generation retarded due to the decreased rainfall interception by a leeward sloping surface, wind-driven soil particle transport (Erpul et al., 2002) might be the dominant erosion process.

Table 6. Uniformity coefficients and intensity ranges of the windless rains and the rains driven by 6, 10, and 14 m s^{-1} wind.

u (m s^{-1})	P (kPa)	I_o (mm h^{-1})	S	Cv
0	75	97.2	19.54	0.80
	100	98.5	24.86	0.75
	150	143.0	10.07	0.93
6	75	113.3	18.41	0.84
	100	116.4	10.82	0.91
	150	124.0	10.22	0.92
10	75	108.0	21.55	0.80
	100	110.9	10.73	0.90
	150	136.6	19.55	0.86
14	75	110.0	20.13	0.82
	100	115.4	8.73	0.92
	150	139.1	13.02	0.91

u: reference horizontal wind velocity; P: nozzle operating pressure; I_o: rain intensity measured in horizontal plane, depends only on rain inclination α for wind-driven rains; S: standard deviation of I_o; Cv: uniformity coefficient of I_o.

Table 7. Calculated wind-driven rain intensities (I^*_{cal}, mm h^{-1}) for windward and leeward slopes of 4, 8.53, and 11.31°.

θ (°)	u (m s^{-1})								
	6			10			14		
	P (kPa)								
	75	100	150	75	100	150	75	100	150
	windward								
4	123.5	126.9	135.2	126.4	129.8	159.8	136.4	143.1	172.5
8.53	136.0	139.7	148.8	148.0	151.9	187.1	166.1	174.3	210.0
11.31	143.9	147.8	157.5	162.0	166.4	204.9	184.8	193.9	233.7
θ (°)	u (m s^{-1})								
	6			10			14		
	P (kPa)								
	75	100	150	75	100	150	075	100	150
	leeward								
4	103.1	105.9	112.8	89.6	92.0	113.4	83.6	87.7	105.7
8.53	90.6	93.1	99.2	68.0	69.9	86.1	53.9	56.5	68.2
11.31	82.7	85.0	90.5	54	55.5	68.3	35.2	36.9	44.5

u: reference horizontal wind velocity; P: nozzle operating pressure; θ: slope gradient;
** I_{cal} is calculated by Eq.27 using wind-driven intensity measured in horizontal plane I_o and the correction factor F_c.*

Rain Energy

Wind-driven raindrops gain some degree of horizontal velocity, which increases their resultant impact velocity. The kinetic energy load of the rain is expected to change as a result of increased velocity and altered size of the raindrops.

The energy of the simulated rains of the tunnel was measured by a Sensit kinetic energy sensor (Sensit, 2000). The kinetic energy sensor is a 5-cm ceramic piezoelectric disk. The Sensit works on the piezoelectric effect of a ceramic disk, which produces electric charges proportional to the kinetic energy of impacting raindrops, and essentially has two outputs, kinetic energy units and number of raindrop impacts. The response of Sensit (voltage output) was calibrated for kinetic energy with vertically falling water drops of known size and known fall velocity. Table 8 shows kinetic energies of windless and wind-driven rains measured by the kinetic energy sensor. Figure 18 also illustrates the kinetic energy as a function of the horizontal wind velocity.

Table 8. The kinetic energies *KE* and the resultant impact velocities V_R of windless and wind-driven rains measured by the kinetic energy sensor.

u (m s^{-1})	d_{50} (mm)	KE (J)	V_R (m s^{-1})	$KE = f(u)$*	R^2
0	1.00	5.11E-06[†] (1.25E-06)[‡]	4.38 (0.58)		
6	1.63	2.47E-05 (5.99E-06)	4.64 (0.56)	$KE = 6E\text{-}06e^{0.2184u}$	0.9887
10	1.53	5.51E-05 (8.50E-06)	7.64 (0.60)		
14	1.54	1.07E-04 (1.15E-05)	10.48 (0.57)		

u: reference horizontal wind velocity; d_{50}: median drop size.

** This illustrates a functional relationship which exists between the impact energy and the horizontal wind velocity obtained by the corresponding method in the form of $KE = a\ e^{b\ u}$ with a and b showing the model parameters.*

[†] The E notation means "times 10 to the power".

[‡] Standard deviation is given inside the parentheses for the kinetic energy and the resultant impact velocity.

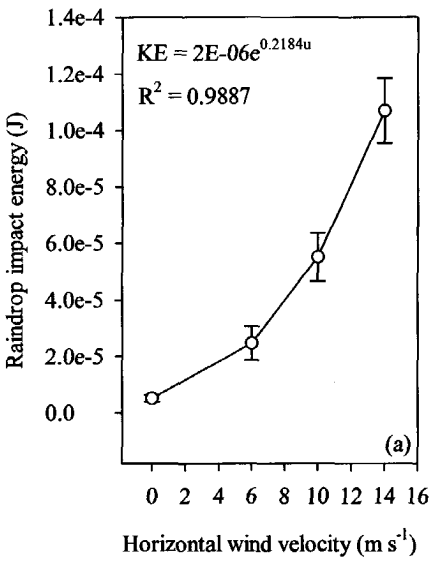

Figure 13. Kinetic energy (KE, J) of simulated rains as a function of the horizontal wind velocity (u, m s^{-1}) evaluated by the kinetic energy sensor.

Sensit measurements revealed that an exponential relationship existed between the rain energy and the horizontal wind velocity (Table 8). The increase in rain energy was attributed to the increase in the resultant raindrop impact velocity since the raindrop size distribution did not change significantly in the rains driven by 6, 10, and 14 m s^{-1} in the facility. The following expression was obtained for kinetic energy as a function of wind velocity:

$$KE = a e^{bu} \qquad \text{[Eq. 28]}$$

where a and b are the parameters of regression. Pedersen and Hasholt (1995) found a similar expression with smaller exponent value (b = 0.12) for natural rainfalls. The effect of wind on large raindrops would not be as great as the effect on small raindrops (Sharon, 1980). Therefore, the exponent values were greater in our equation obtained by the small raindrops of the facility than that by the natural rainfalls. The exponent was approximately 0.22 for the relationship found by the kinetic energy sensor (Table 8).

Summary and Conclusions

In this paper, the wind tunnel of the International Centre for Eremology is described in detail. In brief, the wind-tunnel is a closed-circuit low-speed blowing-type wind tunnel with a 12-m long and 1.2-m wide test section. The height is adjustable from 1.8 m to 3.2 m. A unique feature of the I.C.E. wind tunnel is the presence of a rainfall-simulation facility in the working area.

Measurements were performed to test whether the flow criteria for correct wind-erosion simulations are fulfilled. Since the criteria are normally followed if a deep stable boundary layer is developed, spires and roughness elements were constructed in that respect. This was based on the consideration of momentum balance equations according to Irwin (1981). The vertical and transversal wind-velocity and wind-direction measurements enabled to draw several conclusions with respect to the aerodynamic characteristics of the I.C.E. wind tunnel. First, the flow in the tunnel's test section is acceptable and satisfied the logarithmic law well enough to permit the shear velocity to be deduced from a measured wind-velocity profile using the Prandtl-von Kármán law and the Ling and Untersteiner (1974) method. This was verified by fitting the power law to the wind-velocity profile data. The curve-fitted exponent was close to 1/7, which is a typical value for flat and open terrain, and in wind tunnels (Jensen, 1954). These conclusions refer to both the no-spire and spire case. The flow thus reproduces the wind-velocity profiles commonly observed in atmospheric boundary layers.

Second, from cross-sectional wind-velocity profiles it was concluded that within the boundary layer, there exist a zone that extents from y = 0.5 m to y = 0.9 m where the wind velocity is constant with height. When spires and roughness elements are present this region is even greater. Wind-direction measurements showed that, within this zone, the flow is parallel to the tunnel wall along the entire test section length. When spires and roughness elements are absent, the boundary layer thickness is rather limited and grows gradually from about δ = 0.13 m to δ = 0.21 m. The spires produce a much deeper boundary layer growing from δ = 0.6 m as the flow leaves the roughness floor to δ = 0.66 m at the end of the test section. Such a deep boundary layer is preferable.

Third, both the criterion for the Reynolds and Froude number are satisfied under the operating conditions of the I.C.E. wind tunnel.

Finally, it was not possible to verify if the intensity and scale of turbulence was realistic. Instrumentation to measure wind-velocity fluctuations at a very high measuring frequency is not available at I.C.E.. The reading units presently available had a measuring frequency of maximum 1 Hz. This equipment is limited to record mean values of e.g. velocity only. Rapid changes can not be detected. Notwithstanding this, the anemometers as such appeared to give reliable results.

By the description of the drop size distribution of the simulated rains in the tunnel, it was found that the rains have rather small drops, whose diameters range from 0.2 mm to 2.2 mm for windless rains and up to 3 mm for wind-driven rains. However, the wind has noticeable effect within this drop size range, and leads to the formation of larger drops since impacts between small drops occur more often as a result of their greater number per unit volume of air. While d_{50} ranges between 1.01 mm and 1.31 mm in the windless rains, it changes from 1.52 mm to 1.67 mm in the wind-driven rains.

Concerning the spatial distribution of the rain intensity, based on the calculation of the uniformity coefficients *Cv* and mean intensity values, quite satisfactory workable places with $Cv \geq 75\%$ were determined in the tunnel. Rain intensities measured in the horizontal plane are between 97.2 mm $h^{-1}$and 143 mm h^{-1}. Since the rain intensity varies widely with the wind velocity and direction in the tunnel, depending on the rain inclination, slope gradient and aspect, it is also possible to work with both lower and greater intensity levels than those determined in the horizontal plane. For example, the rainfall intensities calculated for the rains driven by a 14 m s^{-1} wind at 150 kPa nozzle operating pressure and incident on the windward and leeward slopes of 11.3° are 233.7 mm h^{-1} and 44.5 mm h^{-1}, respectively.
Additionally, measuring the kinetic energy of wind-driven raindrops by the kinetic energy sensor showed that there is an exponential relationship between the rain energy and the horizontal wind velocity. This exponential increase in the energy is ascribed to the increase in the resultant raindrop impact velocity, which are 4.64 m s^{-1}, 7.64 m s^{-1}, and 10.48 m s^{-1} for the rains driven by free-stream wind velocities of 6 m s^{-1}, 10 m s^{-1}, and 14 m s^{-1}, respectively. This is 4.38 m s^{-1} for the windless rains.

References

Bradshaw, P. 1970. Experimental fluid mechanics, 2nd Ed.. Pergamon Press Ltd., Oxford.

Bagnold, R.A. 1941. The physics of blown sand and desert dunes. Chapman & Hall, London.

Banzhaf, J., D.E. Leihner, A. Buerkert, and P.G. Serafini. 1992. Soil tillage and wind break effects on millet and cowpea: I. Wind speed, evaporation, and wind erosion. *Agron. J.* 84: 1056-1060.

Campbell, G.C., and N.M. Standen. 1969. Simulation of earth's surface winds by artificially thickened wind tunnel boundary layers. Progress Report II. National Research Council of Canada. NAE Rep. LTR-LA-37.

Carson, M.A. 1971. The mechanics of erosion. Pion Ltd., London.

Chepil, W.S., and R.A. Milne. 1939. Comparative study of soil drifting in the field and in a wind tunnel. *Sci. Agric.* 19: 249-257.

Chepil, W.S., and R.A. Milne. 1941a. Wind erosion in relation to size and nature of the exposed area. *Sci. Agric.* 21: 479-487.

Chepil, W.S., and R.A. Milne. 1941b. Wind erosion of soil in relation to roughness of surface. *Soil Sci.* 52: 417-433.

Counihan, J. 1979. A method of simulating a neutral atmospheric boundary layer in a wind tunnel. Proc. Advisory Group for Aerospace Research and Development. Conf. on the Aerodynamics of Atmospheric Shear Flows, No. 48, Pap. 14.

de Lima, J.L.M.P., P.M. van Dijk, and W.P. Spaan. 1992. Splash-saltation transport under wind-driven rain. *Soil Tech.* 5: 151-166.

De Ploey, J. 1980. Some field measurements and experimental data on wind-blown sands. In: M. De Boodt and D. Gabriels (Eds.). Assessment of erosion. John Wiley & Sons, Chichester. pp. 143-151.

Erpul, G., D.L. Norton, and D. Gabriels. 2002. Raindrop-induced and wind-driven soil particle transport. *Catena*, 47: 227-243.

Erpul, G., D.L. Norton, and D. Gabriels. 2003. The effect of wind on raindrop impact and rainsplash detachment. *Transactions of ASAE* 45: 51-62.

Gabriels D., W.M. Cornelis, I. Pollet, T. Van Coillie, and M. Ouessar. 1997. The I.C.E. wind tunnel for wind and water erosion studies. *Soil Tech.* 10: 1-8.

Gartshore, I.S. 1973. A relationship between roughness geometry and velocity profile shape for turbulent boundary layers. National Research Council of Canada, NAE Rep. LTR-LA-140.

Gillies, J.A., and W.G. Nickling. 1999. Shear stress behavior on complex rough surfaces. Proceedings of Wind Erosion: An International Symposium/Workshop, Manhattan, KS. Manuscript on CD-Rom. 18 pp.

Hall, M.J. 1970. Use of stain method in determining the drop size distributions of coarse liquid sprays. Transactions of ASAE, 13: 33-41.

Hangan, H. 1999. Wind-driven rain studies. A C-FD-E approach. *Journal of Wind Engineering and Industrial Aerodynamics* 81: 323-331.

Irwin, H.P.A.H. 1979. Design and use of spires for natural wind simulation, National Research Council of Canada, NAE Rep. LTR-LA-233.

Irwin, H.P.A.H. 1981. The design of spires for wind simulation. J. Wind Eng. Ind. Aerodyn., 7: 361-366.

Jensen, M. 1954. Shelter effect: investigations into aerodynamics of shelter and its effects on climate and crops. *Danish Tech. Press*, Copenhagen.

Jungerius, P.D., A.J.T. Verheggen, and A.J. Wiggers. 1981. The development of blowouts in 'De Blink', a coastal dune area near Noordwijkerhout, The Netherlands. *Earth Surf. Proc. Landf.*, 6: 375-396.

Jungerius, P.D., and L.W. Dekker. 1990. Water erosion in the dunes. *Catena Suppl.*, 18: 185-193.

Kinnell, P.I.A. 1981. Rainfall intensity - kinetic energy relationship for soil loss prediction. *Soil Science Society of American Journal* 45: 153-155.

Laws, J.O. 1941. Measurements of the fall velocity of water drops and raindrops. *Trans. Amer. Geophys. Union* 22: 709-721.

Ling, C.H., and N. Untersteiner. 1974. On the calculation of the roughness parameter of sea ice. *J. Geophys. Res.* 79: 4112-4114.

Meyer, L. D. 1958. An investigation of methods for simulating rainfall on standard run-off plots, and a study of drop size, velocity and kinetic energy of selected spray nozzles. USDA ARS Div. E. S. and W Man. Branch, Special Report No. 81.

Meyer, L. D. 1960. Use of the rainulator for run-off plot research. *Soil Science Society of American Proceedings* 24: 319-322.

Meyer, L. D. and D. L. McCune. 1957. Development of a rainfall simulator for run-off plots. Paper to Amer. Soc. Agr. Eng. Dec. 15 – 18th. Journal series paper1197. Purdue Agric. Expt. Sta.

Meyer, L. D. and D. L. McCune. 1958. Rainfall simulator for run-off plots. *Agric. Engineering* 39: 644-648.

Moeyersons, J. 1983. Measurements of splash-saltation fluxes under oblique rain. *Catena Suppl.* 4: 19-31.

Moss, A.J. 1988. Effects of flow-velocity variation on rain-driven transportation and the role of rain impact in the movement of solids. *Aust. J. Soil Res.* 26: 443 - 450.

Moss, A.J., and P. Green. 1983. Movement of solids in air and water by raindrop impact. Effects of drop-size and water-depth variations. *Aust. J. Soil Res.* 21: 373 - 382.

Nikuradse, J. 1933. Strömungsgesetze in rauhen Rohren. Forschung auf dem Gebiete des Ingenieurswesens, Ausg. B, Band 4. 1-22.

Park, S.W., J.K. Mitchell, and G.D. Bubenzer. 1983. Rainfall characteristics and their relation to splash erosion. *Transactions of ASAE*, 26: 795-804.

Pedersen, H.S. and B. Hasholt. 1995. Influence of wind speed on rainsplash erosion. *Catena*, 24: 39-54.

Pope, A., and J.J. Harper. 1966. Low-speed windtunnel testing. John Wiley & Sons, New York.

Prandtl, H. 1932. Zur turbulenten Strömung in Rohren und längs Platten. Ergebn. Aerodyn. Versuchsanst. Göttingen, 4: 18-29.

Pye, K., and H. Tsoar. 1990. Aeolian sand and sand dunes. Unwin Hyman, London.

Raupach, M.R., and J.F. Leys. 1990. Aerodynamics of a portable wind erosion tunnel for measuring soil erodibility by wind. *Aust. J. Soil Res.*, 28 : 177-191.

Rouse, H. 1959. Advanced mechanics of fluids. John Wiley & Sons, New York.

Sellers, W.D. 1965. Physical Climatology. University of Chicago Press, Chicago, Ill. pp. 33-35.

Sensit™. 2000. Model V04, Kinetic Energy of Rain Sensor. Sensit Company, Portland, ND 58274-9607.

Sharon, D. 1980. The distribution of hydrologically effective rainfall incident on sloping ground. *Journal of Hydrology*, 46: 165-188.

Sharon, D. and A. Arazi. 1997. The distribution of wind-driven rainfall in a small valley: an emprical basis for numerical model verification. *Journal of Hydrology,* 201: 21-48.

Struzer, L.R. 1972. Problem of determining precipitation falling on mountain slopes. *Sov. Hydrol. Selected papers* 2: 129-142.

van Dijk, P.M., L. Stroosnijder, and J.L.M.P. de Lima. 1996. The influence of rainfall on transport of beach sand by wind. *Earth Surf. Proc. Landf.* 21: 341-352.

Wang , Z.Y., E.J. Plate, M. Rau, and R. Keiser. 1996. Scale effects in wind tunnel modelling. *J. Wind Eng. Ind. Aerodyn.*, 61: 113-130.

Wooding, R.A. 1968. A low-speed wind tunnel for model studies in micrometeorology. I. General design considerations. *Division of Plant Industry Tech. Paper No.* 25.

Wooding, R.A., E.F. Bradley, and J.. Marshall 1973. Drag due to regular arrays of roughness elements of varying geometry. *Bound.-Lay. Meteorol.*, 5, 285.

Zingg, A.W. 1953. Wind-tunnel studies of the movement of sedimentary materials. In: Proc. Fifth Hydraulic Conf., Iowa Institute of Hydraulics Res. Bul. 34., John Wiley & Sons, New York. pp. 111-135.

Zingg, A.W., and W.S. Chepil. 1950. Aerodynamics of wind erosion. *Agric. Engin.*, 31: 279-282, 284.

Chapter 14

Future Work on Wind and Water Interaction in Erosion Models

L.Stroosnijder[1] & D. Gabriels[2]
[1]Wageningen University, Erosion and Soil & Water Conservation Group, Nieuwe Kanaal 11, 6709 PA Wageningen, e-mail: Leo.Stroosnijder@wur.nl
[2]Dept. Soil Management and Soil Care, International Centre for Eremology, Ghent University, Coupure links 653, B-9000 Gent, Belgium; email:Donald.gabriels@Ugent.be

Future Work on Wind and Water Interaction in Erosion Models

At the end of the 2-week postgraduate course, the first topic discussed was the applicability outside the USA of WEPS and WEPP, two physically based models developed in the USA. The discussion ranged over the input parameters required by the models and the need to incorporate wind/water interaction in erosion models. Then, three aspects of future work were discussed in working groups and presented in the form of projects: (1) What will be the future of erosion modeling? (2) How will event-based erosion models develop? and (3) What new methods for water and wind erosion measurements are needed to provide input data for models and to calibrate and validate these models?

Are WEPS and WEPP applicable outside the USA?

One characteristic of a physically based model should be that it is applicable to a wide range of climates and environments, since this type of model describes erosion processes based on physical processes and mathematical equations. The philosophy underlying the physical approach is that given a good understanding of processes and how they respond to stresses, the system's response to any form of stress can be predicted, even when the magnitude of the new stress falls outside the test range of stresses.

One of the main problems arising when either WEPP or WEPS is used outside the USA is that the large amount of input data these physical models require is not always available. One of the most important parameters is the climate file. Both models make use of a stochastic climate simulator (CLIGEN) and, in addition, WEPS uses a stochastic wind-simulator (WINDGEN). WEPP comes with an option to create new CLIGEN files from your own data combined with data from the USA weather database. However, one of the disadvantages of this system is that climate data from several years is required to create the CLIGEN file. Given the wide range of climates present in the USA, WEPS users suggest finding climate files in the USA or elsewhere that closely match the one required for the climate of the study area. In order to generate the WINDGEN file, a large data set of wind records is necessary. The course participants recommend that CLIGEN be evaluated and validated at locations outside the USA and that additional ways of incorporating climate data be incorporated in both WEPP and WEPS. Until this is done, the participants recommend that for applications outside the USA, only the single-event mode of the models should be used. In this mode measured data can be used and this prevents errors related to input data.

Apart from climate data, both models require detailed information on soil, texture and vegetation/crop cover. Most of the input data can be obtained by various measurement methods, which result in different values for a single parameter; e.g. a value for soil roughness can be obtained by Saleh's chain, the pinboard, or optically. The participants recommend that in the future the model developers should append a description of procedures of measurement techniques to the manual. Furthermore, based on analysis of the models' and submodels' sensitivity to the various input parameters, the model builders should say which parameters it is most important to estimate accurately.

The participants also suggest a guide be written on the use and the misuse of the models. It should mention at which scale the model can be applied, which processes are simulated, and the range of stresses for which the model has been tested.

Finally, the participants recommend that the consequences of error propagation be studied in both models, including errors in measurements and empirical relations.

Should wind/water interaction be included in models?
One conclusion of the discussion on the need to incorporate interaction between wind and water was that the need depends on the type of the model and on the climate and scale (in space and time) at which the model is applied. There is no need for the incorporation of wind/water interaction in climates without strong winds or in areas where no wind erosion occurs and simulation is performed at a larger scale (grid size >> average rainsplash distance). In all other cases, wind/water interaction – and especially the wind-driven rain effects – should be incorporated into erosion models.

In physical and event-based models, mathematical equations of the wind effect on rainfall, kinetic energy of the rain, interrill detachment and the direction of the transport processes should be included in the model. Furthermore the wind/water interaction effect on seal and crust development should be simulated. The consequences for the model are: the grid size should be equal to or less than the average splash distance, the direction of sediment transport cannot solely be dependent on the Digital Elevation Model, and time steps should be small (< than 1 minute?) For empirically-based models the effect of wind-driven rains should be included in the climate factor.

What will be the future of erosion modeling?
The *rationale* for the further refinement of erosion models is that they are needed for the assessment of erosion risk in both the short and long term. Models are also needed to improve our scientific understanding of erosion processes because there are still a number of processes imperfectly understood and some parameters are still difficult to assess. Furthermore, with the ongoing development of agriculture and other ecosystems, more and more people (farmers, development advisors and policy makers, for example) will use and come to depend on erosion models and their outcomes. Finally, the development and transfer of conservation technology (via education) will benefit from adequate erosion models.

Our *vision* is that in the future there will be a few user-friendly models and databases that can be used to manage natural resources suffering from wind and water erosion.

The *goals* for the near future are to have erosion models with a modular structure whose components have been developed, tested and validated by leading erosion groups in different ecological zones of the world. There are a number of accessible international databases that can be used for validating and comparing different models. As well as having a modular structure, the models will also have a nested structure, so they suit different spatial scales. There is adequate model documentation that clearly states the limitations of each of the models.

Only a few examples of the *activities* needed in order to achieve these objectives are given here. One is that it would be helpful to recode certain models into a common computer language. It is also proposed to set up a center for model integration, in order to assure quality work.

How will event-based erosion models develop?
The *rationale* for event-based erosion models is that compared with continuous modeling they have more advantages than disadvantages. The advantages are that in some cases they are less data intensive and have a simpler structure, which allows for

more control over initial parameters and error propagation. Event-based erosion models are very suitable for worst-case scenarios of extreme events. And there is more focus on erosion processes during an event. The disadvantages are that event-based models are sensitive to initial boundary conditions, and it is often difficult and cumbersome to determine these initial parameters.

Our *vision* is that in the future there will be continuous models in which events are modeled with an event-based model and the intra-event periods are covered by simple automatic observations followed by data assimilation.

The *goal* for the near future is to build a continuous intra-event model that includes data assimilation techniques. This goal can only be achieved when we know enough about erosion processes to be able to reduce the sensitivity of the event part of the continuous model to the conditions prior to the event (the initial conditions).

The *activities* needed to attain our objectives are given include improving the identification of key parameters and processes for the event's initial conditions. Another necessary action is to increase flexibility, so that all available data can be used (e.g. information obtained via a data assimilation technique from remote sensing and farmers and other stakeholders). Finally, we need more laboratory and field experiments on combined water and wind erosion.

What new methods for water and wind erosion measurements are needed?

The *rationale* for the development of new methods is that model development is hampered by the lack of sufficient data of adequate quality. We need measurements not only to improve our understanding of the erosion processes but also for the calibration and validation of our models. Widely available Internet data lack quality and standardization. A method consists of a technique (for taking measurements) and the equipment required. The equipment used to collect data should be affordable; at present it is expensive because it is not mass produced. Many researchers use equipment they have created themselves, but this leads to a lack of international standardization.

Our *vision* is that in the future there will be a few clear standards worldwide that are used in water and wind erosion measurements. Methods will be ISO certified and there will be a limited number of ISO-certified institutes that calibrate equipment. Procedures (technique, equipment, data collection and handling) will be clear and widely known. This standardization will make it attractive for manufacturers to invest in technical developments and increase production; this will bring down the cost of equipment.

The *goals* for the near future in order to make our vision come true are manifold. The upcoming EU soil protection strategy with its important monitoring component is an ideal moment for the standardization of measurements. EU R&D funding should be used for the development of new methods and this should be done in collaboration with SMEs (Small and Medium Enterprises). Methods should be an integral part of university curricula and given due attention in professional societies concerned with soil erosion. Finally, one of the upcoming international conferences should be devoted to methods for measuring water and wind erosion.

Only a few examples of *activities* by which we can obtain our objectives are given here. One is that at each of the planned international meetings there should be an evening session devoted to methods for measuring water and wind erosion. Another is for interested partners to get together and submit an EU project. In the curricula of Ghent and Wageningen universities a 'project' and an 'open course'

devoted to methods for water and wind erosion measurements can be introduced in the short term.

As mentioned in the Introduction, this 50th publication in the TRMP series combines wind and water erosion. The basis of this special publication has been the long-standing collaboration between the universities of Ghent and Wageningen, plus the spin-off from a 2-week postgraduate course at which lecturers from Ghent and Wageningen were joined by lecturers from Purdue University and Kansas State.

List of previous volumes/Ont déjà paru dans cette série:
(out of order)*

1 L'Agroforesterie au Burkina Faso: bilan et analyse de la situation actuelle. J.J. Kessler & J. Boni (1991).
2 Aspects de l'aménagement intégré des ressources naturelles au Sahel. E. Bognetteau-Verlinden, S. van der Graaf & J.J. Kessler (1992).
3* Perspectives pour le développement soutenu des systèmes de production ag sylvopastorale au Sanmatenga, Burkina Faso. R. van der Hoek, A. Groot, F. Hottinga, J.J. Kessler & H. Peters (1993).
4 Le système d'élevage Peulh dans le sud du Burkina Faso: une étude agro-écologique du département de Tô (Province de la Sissili). W.F. de Boer & J.J. Kessler (1994).
5 L'Aménagement des terroirs villageois : une contribution à la gestion durable des ressources naturelles. Une étude de cas du projet Reboisement Rive Droite Téra, Niger. J. van den Briel, P. Schuthof & E. Topper (1994).
6 Indigenous management systems as a basis for community forestry in Tanzania: a case study of Dodoma urban and Lushoto Districts. G.C. Kajembe (1994).
7 La régénération de l'espace sylvo-pastoral au Sahel: Une étude de l'effet de mesures de conservation des eaux et des sols au Burkina Faso. F.G. Hien (1995).
8 Choix et modalités d'exécution des mesures de conservation des eaux et des sols au Sahel. C.A. Kessler, W.P. Spaan, W.F. van Driel & L. Stroosnijder (1995).
9 Sécurité foncière et gestion des ressources naturelles dans la Boucle du Mouhoun - Burkina Faso. F. de Zeeuw (1995).
10 No Runoff, No Soil Loss: soil and water conservation in hedgerow barrier systems. P. Kiepe (1995).
11* *Chromolaena odorata* fallow in food cropping systems: An agronomic assessment in South-West Ivory Coast. J.J.P. Slaats (1995).
12 Nutrient Management over Extended Cropping Periods in the Shifting Cultivation System of south-west Côte d'Ivoire. H. Van Reuler (1996).
13* On Park Design, looking beyond the wars. M. Oneka (1996).
14* The Price of Soil Erosion: an economic evaluation of soil conservation and watershed development. J. de Graaff (1996).
15 Wind Erosion in the Sahelian Zone of Niger: Processes, Models and Control Techniques. G. Sterk (1997).
16 The role of termites and mulch in the rehabilitation of crusted Sahelian soils. A. Mando (1997).
17 A Participatory Agroforestry Approach for Soil and Water Conservation in Ethiopia. A. Bekele-Tesemma (1997).
18* Conservation and Utilization of Natural Resources in the East Usambara Forest Reserves: Conventional Views and Local Perspectives. J.F. Kessy (1998).
19 Simulation of Maize Growth under Conservation Farming in Tropical Environments. L. Stroosnijder & P. Kiepe (1998).
20 Catastrophic vegetation dynamics and soil degradation in semi-arid grazing systems. M. Rietkerk (1998).
21 Millet growth in windbreak-shielded fields in the Sahel: Experiment and Model. M. Mayus (1998).
23 Et demain l'Agriculture? Options techniques et mesures politiques pour un développement agricole durable en Afrique subsaharienne. Cas du Cercle de Koutiala en zone sud du Mali. Keffing Sissoko (1998).
24 Tillage for soil and water conservation in the semi-arid tropics. W.B. Hoogmoed (1999).
25 Modelling the dynamics of agricultural development: a process approach. The case of Koutiala. T. Struif Bontkes (1999).
26 The phosphorous and nitrogen nutrition of bambara groundnut (*Vigna subterranea* (L.) Verdc.) in Botswana soils. An exploratory study. G. M. Ramolemana (1999).
27 Fire and Life in Tarangire: Effects of Burning and Herbivory on an East African Savanna System. C. van de Vijver (1999).
28 The vegetation of Manyara: Scale-dependent states and transitions in the African Rift Valley. P.E. Loth (1999).

29 Living with Wildlife: Coexistence of Wildlife and Livestock in an East African Savanna system. M.M. Voeten (1999).
30 Birds on fragmented islands: persistence in the forests of Java and Bali. B. van Balen (1999).
31 Crop Residue Management in relation to Sustainable Land Use. A case study in Burkina Faso. M. Savadogo (2000).
32 Rethinking soil and water conservation in a changing society: a case study in eastern Burkina Faso. V. Mazzucato and D. Niemeijer (2000).
33 Tropical Forest Resource Dynamics and Conservation: From Local to Global Issues. K.F. Wiersum (ed.) 2000).
34 Mixed Farming: Scope and Constraints in West African savanna. M. Slingerland (2000)
35* The distribution and regeneration of *Boswellia papyrifera* (Del.) Hochst. in Eritrea. Woldeselassie Ogbazghi (2001).
36 Soil and Water Management in Spate Irrigation Systems in Eritrea. Mehreteab Tesfai Hadera (2001).
37* Ecological and economic impacts of gorilla-based tourism in Dzanga-Sangha, central African republic. Allard Blom (2001)
38 Mise au point de Système d'Aide a la Décision en Matière de Gestion de la fertilité des Sols pour Différentes Catégories de Paysans. Salif Kanté (2001)
39 Tree-grass interaction on an East African Savanna : the effects of competition, facilitation and hydraulic lift. Fulco Ludwig (2001)
40 Water harvesting in Mediterranean zones: an impact assessment and economic evaluation. Jan de Graaff and Mohamed Ouessar (Eds.) (2002)
41 Understanding farmers: explaining soil and water conservation in Konso, Wolaita and Wello, Ethiopia. Tesfaye Beshah Asfaw (2003)
42 Consuming the Savings: Water Conservation in a vegetation barrier system at the Central Plateau in Burkina Faso. Wim Spaan (2003)
43 Working towards SEAN-ERA; a framework and principles for integrating environmental sustainability into planning. Jan Joost Kessler (2003)
44 Towards integrated watershed management in highland Ethiopia: the Chemoga watershed case study. Woldeamlak Bewket (2003)
45 Integrated water and nutrient management for sorghum production in semi-arid Burkina Faso. Robert Zougmoré (2003)
46 Soil quality and rice productivity problems in Sahelian irrigation schems. Piet J.A. van Asten (2003)
47 Integrated crop management strategies in Sahelian land use systems to improve agricultural productivity and sustainability: A case study in Mali. Odiaba Samaké (2003)
48 Habitats and spatial pattern of solitarious desert locusts (*Schistocerca gregaria* Forsk.) on the coastal plain of Sudan. Gebremedhin Woldewahid (2003)
49 Bridging the gap: computer model enhanced learning for natural resource management in Burkina Faso. Annemarie van Paassen (2004)
50 Water and Wind Interaction in Erosion. Saskia Visser and Wim Cornelis (eds.) (2004)
51 Soil Quality Improvement for Crop Production in semi-arid West Africa. Elisée Ouédraogo (2004)
52 Using Eucalyptus for Soil & Water Conservation on the highland Vertisols of Ethiopia. Selamyihun Kidanu (2004)
53 Modelling Nutrient Losses by Wind and Water Erosion in northern Burkino Faso. Saskia M. Visser (2004)
54 Maize-sesame intercropping in Southeast Tanzania: Farmers' practices and perceptions, and intercrop performance. Geoffrey S. Mkamilo (2004)
55 The tripartite interaction between sorghum, *Striga hermonthica*, and arbuscular mycorrhizal fungi. Venasius W. Lendzemo (2004)
56 Soil Macrofauna Community Structure along a Gradient of Land Use Intensification in the Humid Forest Zone of Southern Cameroon. Madong à Birang (2004)
57 Improving weed management and crop productivity in maize systems in Zimbabwe. Arnold B. Mahingaidze (2004)

Abstract
A growing group of researchers starts to realise that the classic paradigm - water and wind erosion have little in common and occur in different climates - is not suitable in all situations. On the contrary, wind and water erosion may occur almost simultaneously at the same location and a large interaction between the two processes may occur. Consequently, wind erosion models should account for water erosion and vice versa.
The idea for combining knowledge on wind and rain interaction was born during an international two-week course titled: Wind and Water Erosion; Modelling and Measurements, which was held in Ghent and Wageningen. This book bundles all experience and ideas of the course participants. The book starts with a discussion on modelling wind and water erosion, it continuous with a description of the various aspects of the interrelationship between wind and water, then farmers' perceptions on wind and water erosion are described. Furthermore the book contains a description of the various techniques for measuring wind and water erosion separately and a description of a wind tunnel in which the interaction between the two processes can be investigated. The book ends with an outlook for future research on wind and rain interaction.

Résumé
Un groupe grandissant des chercheurs commence à se rendre compte que le paradigme classique - l'érosion éolienne et l'érosion hydrique se trouve dans des climats différents et n'ont pas des caractéristiques communes - n'est pas toujours applicables à chaque situation. Au contraire, les deux processus d'érosion peuvent se passer simultanément et une grande interaction entre l'érosion hydrique et l'érosion éolienne peut arriver. Par conséquent les modèles d'érosion éolienne doivent tenir compte de l'érosion hydrique et vice versa.
L'idée de combiner la connaissance d'interaction entre le vent et la pluie était née pendant des cours internationaux titrés: L'Erosion Eolienne et Hydrique: Modélisation et Mesures. Ces cours étaient organisés par les universités de Gent et de Wageningen. Ce livre traite toutes les expériences et les idées des participants des cours. Le livre commence par une discussion sur la modélisation de l'érosion, ça continue avec une description des perspectives différentes de l'interaction entre le vent et la pluie, puis les perceptions des agriculteurs sur l'érosion éolienne et l'érosion hydrique sont décrites. En outre le livre comprend une description des mesures de l'érosion hydrique et de l'érosion éolienne séparément et une description d'un tunnel aérodynamique pour le mesurage de l'interaction entre les deux processus. Finalement, ce livre finit par une perspective sur l'avenir de recherche de l'interaction entre le vent et la pluie.

Wageningen University and Research Centre
Wageningen Université et Centre de Recherche